THE ISO HANDBOOK

Volume IV:

PHT –
The Imaging Photo-Polarimeter

Rene J. Laureijs[1], Ulrich Klaas[2], Phil J. Richards[3], Bernard Schulz[1], and Peter Ábrahám[2,4]

SAI-99-069/Dc, Version 2.0.1

June, 2003

[1] ISO Data Centre, Science Operations and Data Systems Division
Research and Scientific Support Department of ESA,
Villafranca del Castillo, P.O. Box 50727, E-28080 Madrid, Spain
[2] Max-Planck-Institut für Astronomie, ISOPHOT Data Centre,
Königstuhl 17, D-69117 Heidelberg, Germany
[3] CCLRC, Rutherford Appleton Laboratory,
Chilton, Didcot, Oxon OX11 0QX, United Kingdom
[4] Konkoly Observatory of the Hungarian Academy of Sciences,
P.O. Box 67, H-1525 Budapest, Hungary

Document Information

Document:	The ISO Handbook ESA SP-1262
Volume:	IV
Title:	PHT – The Imaging Photo-Polarimeter
Reference Number:	SAI-99-069/Dc
Issue:	Version 2.0.1
Issue Date:	June 2003
Authors:	R.J. Laureijs, U. Klaas, P.J. Richards et al.
Editors:	T. Müller, J. Blommaert & P. Garca-Lario
Web-Editor:	J. Matagne

Document History

The ISO Handbook, Volume IV: PHT – The Imaging Photo-Polarimeter, is based on the following documents:

- The *ISOPHOT Observer's Manual* (Version 3.1, April 1994), produced by the ISOPHOT consortium and edited by U. Klaas, H. Krüger, I. Heinrichsen, A. Heske and R. Laureijs.
- The *Addendum to the ISOPHOT Observer's Manual* (SAI/96-171/Dc, Version 1.0, 5 August 1996), R.J. Laureijs, U. Klaas, D. Lemke, U. Herbstmeier and P. Ábrahám.
- The *ISOPHOT Data Users Manual* (SAI/95-220/Dc, Version 4.1, November 1999), R. Laureijs, U. Klaas, P.J. Richards and B. Schulz.
- Earlier versions of *The ISO Handbook on PHT – The Imaging Photo-Polarimeter* (previously called Volume V), SAI-99-069/Dc.
- All other documents listed in the Bibliography.

Document Change Record

Date	**Revision**	**Comments**
Oct. 99	—	Observer's Manual and Addendum merged with the IDUM information
15/11/99	Draft 1.0	Initial Draft for comments
30/01/00	Version 1.0	First Version of the ISO Handbook, Volume V: PHT – The Imaging Photo-Polarimeter; related to OLP 7 data products with an OLP 8.4 update
01/11/00	Version 1.1	update, related to OLP 9.0
01/07/01	Version 1.2	update, related to OLP 10.0
08/07/02	Version 2.0	update, now Volume IV
23/06/03	Version 2.0.1	minor editorial changes, printed version

ISOPHOT Instrument Consortium

Principal Investigator

D. Lemke MPI Astronomie, Heidelberg, Germany

Co-Investigators

H. D. Denner	Freie Universität Berlin, Germany
L. Drury	DIAS, Dublin, Ireland
F. Garzón	IAC, La Laguna, Tenerife, Spain
E. Grün	MPI Kernphysik, Heidelberg, Germany
C. Hajduk	MPI Astronomie, Heidelberg, Germany
R. D. Joseph	IRTF-NASA, Hawaii, USA
U. Klaas	MPI Astronomie, Heidelberg, Germany
W. Krätschmer	MPI Kernphysik, Heidelberg, Germany
E. Kreysa	MPI Radioastronomie, Bonn, Germany
W. Martin	MPI Astronomie, Heidelberg, now Planetarium Wolfsburg, Germany
K. Mattila	Helsinki University Observatory, Helsinki, Finland
I. Rasmussen	DSRI, Lyngby, Denmark
B. Reipurth	Copenhagen Observatory, Denmark
J. Riedinger	MPI Astronomie, Heidelberg, Germany, now ESA/ESTEC
J. Rodríguez Espinosa	IAC, La Laguna, Tenerife, Spain
M. Rowan-Robinson	ICSTM, London, United Kingdom
H. Schnopper	DSRI, Lyngby, Denmark
M. Selby[1]	IAC, La Laguna, Tenerife, Spain
C. Telesco	MSFC – NASA, now Univ. Florida, USA
H. Völk	MPI Kernphysik, Heidelberg, Germany
H. Walker	RAL, Chilton, United Kingdom
J. Wolf	MPI Astronomie, Heidelberg, Germany

Scientific Associates

J. A. Abolins	RAL, Chilton, United Kingdom
S. Beckwith	MPI Astronomie, Heidelberg, Germany
S. Bogun	MPI Astronomie, Heidelberg, Germany
H. Campins	University of Florida, USA
R. Chini	MPI Radioastronomie, Bonn, Germany
J. Gürtler	Universitätssternwarte, Jena, Germany
I. Heinrichsen	MPI Astronomie/MPI Kernphysik, Heidelberg, Germany
T. Henning	Universitätssternwarte, Jena, Germany
H. Hippelein	MPI Astronomie, Heidelberg, Germany
H. Krüger	MPI Astronomie, Heidelberg, Germany
A. Leger	Univ. Paris VII, Paris, France
C. Leinert	MPI Astronomie, Heidelberg, Germany

[1] deceased 1993

P. Lützow-Wentzky	MPI Astronomie, Heidelberg, Germany
P. G. Mezger	MPI Radioastronomie, Bonn, Germany
H. Nørgaard-Nielsen	DSRI, Lyngby, Denmark
W. Pfau	Universitätssternwarte, Jena, Germany
T. Ray	DIAS, Dublin, Ireland
P. Richards	RAL, Chilton, United Kingdom
S. Russell	DIAS, Dublin, Ireland
J. Schubert	MPI Astronomie, Heidelberg, Germany
E. Sedlmayr	Technische Universität, Berlin, Germany
D. Skaley	MPI Kernphysik, Heidelberg, Germany
J. Staude	MPI Astronomie, Heidelberg, Germany
C. Tilgner	MPI Astronomie, Heidelberg, Germany
R. Tuffs	MPI Kernphysik, Heidelberg, Germany
M. Wells	University of Edinburgh, United Kingdom

Development

Members of PI Team

Peter Ábrahám (MPIA)	preparation of ISOPHOT Guaranteed Time programme
Erich Ackermann (MPIA)	sensitivity calculations and confusion noise estimates (diploma thesis)
Hans-Heinrich Altfeld (MPIA)	cryo mechanics development tests (Ph.D. thesis)
Steven Beckwith (MPIA)	director, preparation of ISOPHOT Guaranteed Time programme
Heinrich Bellemann (MPIA)	head of mechanics workshop, cryo mechanics development
Jürgen Blum (MPIA)	high energy radiation impacts on IR detectors (diploma thesis)
Stefan Bogun (MPIA)	requirements for ISOPHOT Serendipity mode operations
Matthias Botz (MPIA)	characterisation of internal calibration sources (diploma thesis)
Martin Burgdorf (MPIA)	detector tests (diploma thesis), Serendipity mode simulation (Ph.D. thesis)
Armin Böhm (MPIA)	manufacture of Fine Calibration Sources for ISOPHOT
Hans Elsässer (MPIA)	managing director of the institute (until 1994)
Edgar Fink (MPIA)	head of administration, industrial contracts
Franz Flock (MPIA)	manufacture of mechanical components
Ursula Flock (MPIA)	personnel administration
Peter Franke (MPIA)	design of ISOPHOT components
Wolfgang Fuhr (MPIA)	calibration measurements and time line planning
Carlos Gabriel (MPIA)	design of pipeline software
Ulrich Grözinger (MPIA)	electronic engineer, detector testing, electronic components
Christian Hajduk (MPIA)	definition of ground segment activities
Heidi Hajduk (MPIA)	optical components design
K. Haussecker[2] (MPIA)	electronic engineer, detector testing, electronic components
Ingolf Heinrichsen (MPIA)	commanding and processing software, Astronomical Observation Template (AOT) design
Hannelore Heissler (MPIA)	project administration
Uwe Herbstmeier (MPIA)	flight operation procedures, instrument end-to-end testing
Hans Hippelein (MPIA)	preparation of ISOPHOT Guaranteed Time programme
Diethelm Johannismann (MPIA)	FIR filter design (diploma thesis)
Ulrich Kinkel[3] (MPIA)	calibration measurements and time line planning
Stefan Kirches (MPIA)	instrument ground testing

[2]deceased 1989
[3]deceased 1997

Ulrich Klaas (MPIA)	preparation of ISOPHOT Guaranteed Time programme, ground segment development coordination, PIDT build-up
Harald Krüger (MPIA)	ISOPHOT Guaranteed Time programme coordination, documentation (Observer's Manual)
Christoph Leinert (MPIA)	preparation of ISOPHOT Guaranteed Time programme
Dietrich Lemke (MPIA)	Principal Investigator ISOPHOT
Dieter Lutz (MPIA)	detector tests (diploma thesis)
Peter Lützow-Wentzky (MPIA)	management of industrial contracts, PIDT build-up
Klaus Meisenheimer (MPIA)	preparation of ISOPHOT Guaranteed Time programme
Thomas Müller (MPIA)	asteroids as celestial FIR standards (Ph.D. thesis)
Tibor Pacher (MPIA)	computer system management, AOT logic testing
Guido Pelz (MPIA)	preparation of real time operations
Gabriele Roth (MPIA)	detector curing methods (diploma thesis)
Alison Rushworth (MPIA)	project secretary, documentation
Ulrich Schneider (MPIA)	detector curing methods (diploma thesis)
Joseph Schubert (MPIA)	optical components, instrument ground testing and detector transients (Ph.D. thesis)
Bernhard Schulz (MPIA)	instrument ground testing (Ph.D. thesis)
Jakob Staude (MPIA)	preparation of ISOPHOT Guaranteed Time programme
Clemens Tilgner (MPIA)	instrument and system tests
Karsten Wilke (MPIA)	investigation of signal transients (diploma thesis)
Lothar Weitzel (MPIA)	detector array tests (diploma thesis)
Lorenz Wiest (MPIA)	detector tests (diploma thesis)
Jürgen Wolf (MPIA)	detector design and testing, instrument ground testing coordination

Members of Co-I teams

Jack Abolins (RAL)	Real Time software development coordinator
Rolf Chini (MPIfR)	preparation of ISOPHOT Guaranteed Time programme
Linda Cornwall (RAL)	Quick Look Analysis (QLA) software development
Luke Drury (DIAS)	preparation of ISOPHOT Guaranteed Time programme
Francisco Garzón (IAC)	project manager ISOPHOT-S, preparation of ISOPHOT Guaranteed Time programme
Hans-Peter Gemünd (MPIfR)	FIR filter and polariser development
Eberhard Grün (MPIK)	preparation of ISOPHOT Guaranteed Time programme
Joachim Gürtler (FSJ)	preparation of ISOPHOT Guaranteed Time programme
Steve Guest (RAL)	Offline Processing Pipeline (OLP) design and development
Graham Hall (RAL)	Real Time Assessment (RTA) software development
Peter Hammersley (IAC)	celestial calibration standards, preparation of ISOPHOT Guaranteed Time programme
Thomas Henning (FSJ)	preparation of ISOPHOT Guaranteed Time programme

Reinhard Hofacker (MPIK)	electronic components development
Bob Joseph (ICSTM/IRTF)	ISOPHOT-S design, preparation of ISOPHOT Guaranteed Time programme
Carsten Kömpe (FSJ)	design of calibration meausurements and calibration time line planning
Ernst Kreysa (MPIfR)	FIR filter and polariser development
Wolfgang Krätschmer (MPIK)	NIR/MIR filter and polariser procurement and testing
Kalevi Mattila (Helsinki Observatory)	preparation of ISOPHOT Guaranteed Time programme
Peter Mezger (MPIfR)	preparation of ISOPHOT Guaranteed Time programme
Hans Ulrik Nørgaard-Nielsen (DSRI)	preparation of ISOPHOT Guaranteed Time programme
Werner Pfau (FSJ)	preparation of ISOPHOT Guaranteed Time programme
Emil Popow (AIP)	instrument ground testing
Ib Rasmussen (DSRI)	Electrical Ground Segment Equipment development
Tom Ray (DIAS)	preparation of ISOPHOT Guaranteed Time programme
Phil Richards (RAL)	Offline Processing Pipeline (OLP) design and development
Gotthard Richter (AIP)	preparation of ISOPHOT Guaranteed Time programme
José Miguel Rodríguez Espinosa (IAC)	ISOPHOT-S ground testing, preparation of ISOPHOT Guaranteed Time programme
Mike Selby[4] (ICSTM/IAC)	ISOPHOT-S design, stellar IR standards
Detlef Skaley (MPIK)	PHT Interactive Analysis (PIA) development
Charles Telesco (Univ. Florida)	FIR calibration standards, preparation of ISOPHOT Guaranteed Time programme
Wai Min Tai (DIAS)	PHT Interactive Analysis (PIA) development
Richard Tuffs (MPIK)	Astronomical Observation Template (AOT) design, preparation of ISOPHOT Guaranteed Time programme
Peter Vaughan (RAL)	project manager
Heinrich Völk (MPIK)	preparation of ISOPHOT Guaranteed Time programme
Helen Walker (RAL)	Astronomical Observation Template (AOT) design, preparation of ISOPHOT Guaranteed Time programme
Martyn Wells (ICSTM/ROE)	ISOPHOT-S design, preparation of ISOPHOT Guaranteed Time programme, design of calibration measurements
Robert Wagner (MPIK)	instrument ground testing analysis software development

[4] deceased 1993

Members of the German Space Agency and the Industrial Teams

Günter Albrecht (ZEISS)	cold focal plane unit; production manager
Jürgen Altmann (ZEISS)	cold focal plane unit; test engineer
Manfred Amann (Dornier)	industrial prime contractor; analogue electronics
Heiko Bäurle (ZEISS)	cold focal plane unit; assembly
Hans Peter Batroff (ZEISS)	cold focal plane unit; coating
Johann Bestler (Dornier)	industrial prime contractor; electric system engineering
Wolfgang Bollinger (ZEISS)	cold focal plane unit; project manager
Reinhold Bolz (ANTEC)	infrared detectors; assembly of P detectors
Walter Breitling (Dornier)	industrial prime contractor; system engineer
Kurt Brenner (ZEISS)	cold focal plane unit; mechanical design
Stefaan Cos (IMEC)	cold readout electronics; test engineer
Bart Dierickx (IMEC)	cold readout electronics; design engineer
Peter Dinges (ANTEC)	infrared detectors; C200 design, assembly
Stefan Dornheim (ZEISS)	cold focal plane unit; production
Albert Ebert (ZEISS)	cold focal plane unit; mechanical design
Rudolf Faymonville (ANTEC)	infrared detectors; project manager
Reiner Felten (ANTEC)	infrared detectors; electronics, software
Harald Feuer (Dornier)	industrial prime contractor; instrument assembly integration test
Vic Fonderie (IMEC)	cold readout electronics; QA manager
Jürgen Frank (Dornier)	industrial prime contractor; project controller
Danny Frederickx (IMEC)	cold readout electronics
Otto Frenzl (ANTEC)	infrared detectors; system engineer, QA
Wolfgang Fricke (Dornier)	industrial prime contractor; project manager
Hans Göhringer (ZEISS)	cold focal plane unit; quality assurance
Peter Hackel (ZEISS)	cold focal plane unit; quality assurance
Michael Harr (ANTEC)	infrared detectors; administration
Gernot Hartmann (DLR)	German Space Agency DLR; programme manager
Peter Henneberg (ZEISS)	cold focal plane unit; optics, straylight
Edgar Herbst (Dornier)	industrial prime contractor; FPU shadow engineering
Lou Hermans (IMEC)	cold readout electronics; project manager
Ottmar Hertel (ANTEC)	infrared detectors; documentation
Hermann Hohl (ZEISS)	cold focal plane unit; production
Joachim Junghans (ZEISS)	cold focal plane unit; electric design, testing
Hans Köppen (ZEISS)	cold focal plane unit; chopper assembly, FPU
Wolfgang Klück (ANTEC)	infrared detectors; C100 assembly
Axel Koppe (Dornier)	industrial prime contractor; detector shadow engineer
Heribert Krüger (ANTEC)	infrared detectors; spectral measurements
Hansjörg Lehle (ZEISS)	cold focal plane unit; electrical assembly manager
Werner Lenz (Dornier)	industrial prime contractor; analogue electronics
Klaus Lethaus (Dornier)	industrial prime contractor; electrical interface engineering
Reinhard Link (ZEISS)	cold focal plane unit; sales manager
Anne Litzelmann (ZEISS)	cold focal plane unit; test engineer
Reinhard Ludewig (ZEISS)	cold focal plane unit; design manager
Georg Luichtel (ZEISS)	cold focal plane unit; quality assurance, testing
Hans Jürgen Meier (ZEISS)	cold focal plane unit; FE analysis

Klaus Meyer (ANTEC)	infrared detectors; S arrays assembly/test
Roland Müller (Dornier)	industrial prime contractor; software
Manfred Otterbein (DLR)	German Space Agency DLR; programme manager
Reinhold Passenheim (ZEISS)	cold focal plane unit; electric design, testing
Christian Peschel (ZEISS)	cold focal plane unit; assembly of wheels FPU
Klaus Proetel (DLR)	German Space Agency DLR; funding manager
Michael Röser (ANTEC)	infrared detectors; C50 assembly
Rudolf Schlegelmilch (ZEISS)	cold focal plane unit; project manager
Günter Seger (ANTEC)	infrared detectors; administration
Axel W. Sohn (ANTEC)	infrared detectors; C100 detector, software
Götz Thieme (Dornier)	industrial prime contractor; software engineering, operations
Friedrich Trebstein (ZEISS)	cold focal plane unit; test engineer
Michael Trunz (ZEISS)	cold focal plane unit; mechanical design
Jan Vermeiren (IMEC)	cold readout electronics; technical project leader
Berthold Vogt (Dornier)	industrial prime contractor; test facilities
Erhard Wedel (Dornier)	industrial prime contractor; electronics coordination, digital electronics
Hans Willaczek (ZEISS)	cold focal plane unit; vibration test

Members of Operations Preparation Teams

Mauro Casale (ESA)	Uplink and satellite systems support
Carlos Gabriel (ESA)	PHT Interactive Analysis (PIA) development
René Laureijs (ESA)	AOT and pipeline processing design, design of calibration meausurements
Keith Morgan (ESA)	Performance Verification Phase timeline planning
Luciano Orsini (ESA)	AOT logic development
Johannes Riedinger (ESA)	Uplink design and development
Bernhard Schulz (ESA)	Calibration Uplink System (CUS) development, calibration meausurements and time line planning
Julian Sternberg (ESA)	Offline Processing Pipeline design and development
Rob Verschoor (ESA)	Pipeline processing development

Operations

Members of PHT Instrument Dedicated Team (PIDT)

José Acosta Pulido	(MPIA/IAC)	calibration planning and analysis, PIA development
Michael Braun	(MPIA)	calibration analysis
Héctor Castañeda	(MPIA/IAC)	instrument real time operations, trend analysis
Linda Cornwall	(RAL)	RTA/QLA development, data quality control, instrument real time operations
Carlos Gabriel	(ESA)	PIA management, development and documentation
Ingolf Heinrichsen	(MPIK)	AOT maintenance, OLP scientific validation, PIA development and documentation
Steffen Huth	(MPIA)	calibration analysis, data quality control
Ulrich Kinkel[5]	(MPIA)	calibration planning and analysis
Ulrich Klaas	(MPIA)	PIDT leader
René Laureijs	(ESA)	calibration coordination, observer support
Michael Linden-Vørnle	(MPIA)	calibration analysis
Thomas Müller	(MPIA)	calibration planning and analysis
Guido Pelz	(MPIA)	instrument real time operations, trend analysis
Mario Radovich	(MPIA)	OLP scientific validation
Pilar Román	(ESA)	data quality control, calibration analysis
Bernhard Schulz	(ESA)	PIDT deputy leader, calibration planning and analysis

Members of PI team

Peter Ábrahám	(MPIA)	optimisation of faint source observing strategies, calibration analysis
Stefan Bogun	(MPIA)	Serendipity Survey analysis software development and calibration
Ulrich Grözinger	(MPIA)	instrument commissioning
Martin Haas	(MPIA)	Guaranteed Time programme execution, calibration analysis
Hannelore Heissler	(MPIA)	project administration
Philippe Héraudeau	(MPIA)	ELAIS survey analysis, calibration analysis
Edgar Herbst	(Dornier)	instrument commissioning
Uwe Herbstmeier	(MPIA)	data centre build-up, calibration
Hans Hippelein	(MPIA)	scientific data analysis
Thilo Kranz	(MPIA)	straylight measurement analysis (diploma thesis)
Harald Krüger	(MPIA)	Guaranteed Time programme execution, calibration analysis
Michael Kunkel	(MPIA)	computer system manager
Christoph Leinert	(MPIA)	scientific data analysis
Dietrich Lemke	(MPIA)	Principal Investigator ISOPHOT
Klaus Meisenheimer	(MPIA)	scientific data analysis
Thomas Müller	(MPIA)	asteroids as celestial FIR standard sources (Ph.D. thesis)
Stephan Nicklas	(MPIK)	calibration analysis

[5] deceased 1997

Alison Rushworth	(MPIA)	project secretary, documentation
Manfred Stickel	(MPIA)	Serendipity Survey analysis, software development and calibration
Christian Surace	(MPIA)	ELAIS survey analysis, calibration analysis
Clemens Tilgner	(MPIA)	instrument commissioning
Victor Tóth	(MPIA)	Serendipity survey data analysis

Post Operations

Members of National Data Centres

Peter Ábrahám	(MPIA)	calibration and scientific data analysis, user support
José Acosta-Pulido	(IAC)	calibration analysis
Immo Appenzeller	(MPIA)	acting director, management support
Steven Beckwith	(MPIA)	director, Guaranteed Time science projects, support of ISOPHOT Data Centre
Simone Bianchi	(MPIA)	calibration analysis
Carlos Del Burgo Díaz	(MPIA)	calibration analysis
Martin Haas	(MPIA)	calibration and scientific data analysis, user support
Philippe Héraudeau	(MPIA)	ELAIS survey and calibration analysis
Stephan Hotzel	(MPIA)	Serendipity Survey data analysis
Ulrich Klaas	(MPIA)	ISOPHOT Data Centre manager, calibration coordinator and offline s/w activities
Dietrich Lemke	(MPIA)	ISOPHOT Principal Investigator and Head of ISOPHOT Data Centre
Huw Morris	(RAL)	OLP development
Mario Radovich	(MPIA)	OLP scientific validation, scientific and calibration analysis
Phil Richards	(RAL)	OLP design development and scientific validation
Hans-Walter Rix	(MPIA)	director, management support
Linda Schmidtobreick	(MPIA)	calibration and scientific data analysis
Manfred Stickel	(MPIA)	Serendipity Survey data analysis, scientific data analysis, user support
Victor Tóth	(MPIA)	Serendipity Survey data analysis
Richard Tuffs	(MPIK)	PIA development
Helen Walker	(RAL)	UKIDC user support coordination
Karsten Wilke	(MPIA)	OLP scientific validation, scientific and calibration analysis

Members of ISO Data Centre

Carlos Gabriel	(ESA)	PIA management, development and documentation
René Laureijs	(ESA)	PHT team leader, community support, calibration analysis, handbook documentation
Thomas Müller	(ESA)	calibration analysis, handbook documentation
Sybille Peschke	(ESA)	community support, calibration analysis
Pilar Román	(ESA)	calibration analysis
Bernhard Schulz	(ESA)	community support, calibration analysis, handbook documentation

Contents

List of Figures

List of Tables

Chapter 1

Introduction

1.1 Purpose

The PHT Handbook is one in a series of five[1] documents that explain the operations of the Infrared Space Observatory (ISO) and its four instruments, the data received from the instruments and the processing carried out on the data. Volume I gives an overview of the entire ISO mission and it explains the operations of the ISO satellite while the remaining four explain the individual instruments (CAM, LWS, PHT and SWS). The PHT document is intended to provide all information necessary to understand the offered ISOPHOT standard data products, as processed by version 10 of the Off-Line Processing (OLP) system, retrievable from the Legacy ISO Data Archive (IDA) at:

`http://www.iso.vilspa.esa.es/`

Besides OLP 10 software processing steps and product specific details, background information is provided about the ISOPHOT instrument itself, its observational modes and all aspects of calibration.

Although it tries to contain as completely as possible ISOPHOT related information, it should be stressed that this manual is not intended to support interactive data analysis. For specific algorithms to process and improve the results interactively we refer to the *ISOPHOT Interactive Analysis Users Manual*, [9] and to the ISOPHOT instrument page:

`http://www.iso.vilspa.esa.es/` → `ISO Explanatory Library` → `PHT`.

This volume of the ISO Handbook serves as the reference for both the processing as well as the correct interpretation of ISOPHOT data as available from the ISO Data Archive.

1.2 Structure

In this document we present information on:

- the ISOPHOT instrument and its observing modes,
- the processing steps carried out from raw data level to products in astrophysical flux units,
- the calibration of the instrument,
- the uncertainties of the data,
- the final ISOPHOT archive products.

[1] Originally six documents were planned with Volume I on the *ISO Mission* and II on the *ISO Satellite* but both have now been merged in Volume I in Version 2.0.

For guidance we present a brief description of the contents of the subsequent chapters:

Chapter 2: Instrument Description

This chapter contains a technical description of the ISOPHOT instrument in the light of data collection. The detector - electronics chain is described in detail as this determines the format of the raw data. Additional sections describe the features of optical/calibration systems like chopper, internal reference sources (FCSs), etc.

Chapter 3: Instrument Modes and Astronomical Observation Templates (AOT)

This chapter describes the individual instrument modes and all observing templates, including the operational steps performed by the AOTs during observations.

Chapter 4: Instrumental Characteristics

This chapter describes the known instrumental features and how these can affect the (raw) data. It is recommended to consider this chapter to become aware of the possible instrumental effects before an in-depth astronomical interpretation of the data is carried out.

Chapter 5: Photometric Calibration

This chapter gives the detailed overview of the photometric calibration of ISOPHOT, including also strategies and calibration files.

Chapters 6, 7, 8: Data Processing

The standard data-processing performed by the ISO Data Centre is referred to as Off-Line Processing (OLP). The OLP data processing is sub-divided into three processing levels which are described in detail in these 3 chapters. An overview of the development of the ISOPHOT pipeline can be found in Richards et al. 2001, [46].

Chapter 9: Photometric Calibration Accuracies

The best estimates of the photometric accuracies of the OLP products are presented in this chapter. For each ISOPHOT observing mode the status of the scientific validation is given.

Chapter 10: Caveats

This chapter describes current or final limitations in the documentation, processing and calibration. The observer should have read this chapter before drawing scientific conclusions from the ISOPHOT OLP data products.

Chapter 11: Getting started

In this chapter hints are given how to become familiar with the OLP data. Suggestions for further processing are included.

Chapter 12: Guide to Data Products

This chapter gives an overview of the ISOPHOT data products listed per processing level or per AOT. For each product, references to relevant descriptional sections elsewhere in this manual are given.

Chapter 13: Product descriptions

The descriptions of the ISOPHOT data products directly related to an AOT can be found in this chapter.

Chapter 14: Calibration-G Products

Detailed descriptions of the ISOPHOT general calibration files (or 'Cal-G' files) can be found in this chapter.

In the **Appendices** the following is presented:

Appendix A: Instrument Tables

Description and characterisation of the filters, apertures, and polarisers are given as well as their positions on the instrument change wheels.

Appendix B: Conversion Algorithms for ERD

This appendix gives details on conversion algorithms necessary to convert sensor readouts in the telemetry information to parameters with standard physical units like temperature in K, chopper amplitudes in *arcseconds*, internal reference sources' heating powers in mW, etc.

Appendix C: Colour Correction

Formulae are presented to derive colour corrections assuming different (modified) blackbody and power-law spectral energy distributions. These relations are used to construct the colour correction (Cal-G) products. Tables with colour correction factors for different spectral energy distributions are given.

Appendix D: Magnitude System in ISOPHOT

The zero magnitude flux densities of the ISOPHOT filters are listed.

Appendix F: Symbols

Lists the roman and greek symbols defined in this document.

Appendix E: Acronyms

This appendix gives a compilation of acronyms used in this document.

Appendix G: Glossary

This appendix gives a glossary of frequently used terms.

1.3 How to Contact Us

A broad set of information on ISOPHOT and its interactive analysis system is available on the instrument web page:

`http://www.iso.vilspa.esa.es/` → `ISO Explanatory Library` → `PHT`

Information on the ISO satellite and its pointing modes is available under:

`http://www.iso.vilspa.esa.es/` → `ISO Explanatory Library` → `ISO Satellite`

In addition you may contact us by sending an email to the ISO helpdesk:

`helpdesk@iso.vilspa.esa.es`

1.4 ISOPHOT Publications

1.4.1 Acknowledgements and guidelines

Any paper published based on **ISO data** should contain the following text, as a footnote to the title.

Based on observations with ISO, an ESA project with instruments funded by ESA Member States (especially the PI countries: France, Germany, the Netherlands and the United Kingdom) and with the participation of ISAS and NASA.

Should the journal in question not permit footnotes to the title, the above text should appear as a footnote the first time ISO is mentioned.

The preferred reference for the ISO mission is:

The Infrared Space Observatory (ISO) mission, Kessler, M.F. et al. 1996, A & A 315, L27

Any paper published based on **ISOPHOT data** should acknowledge the instrument with the following reference:

ISOPHOT - capabilities and performance, Lemke, D. et al. 1996, A & A 315, L64

If you used the **ISOPHOT Interactive Analysis** (PIA) to reduce your ISOPHOT data please write in the acknowledgments:

The ISOPHOT data presented in this paper were reduced using PIA, which is a joint development by the ESA Astrophysics Division and the ISOPHOT Consortium with the collaboration of the Infrared Processing and Analysis Centre (IPAC). Contributing ISOPHOT Consortium institutes are DIAS, RAL, AIP, MPIK, and MPIA.

The preferred reference to PIA is:

The ISOPHOT Interactive Analysis PIA, a calibration and scientific analysis tool, Gabriel, C. et al. 1997, in ASP Conf. Ser. Vol. 125, Astronomical Data Analysis Software and Systems (ADASS) VI, ed. G. Hunt & H.E. Payne (San Francisco: ASP), 108

1.4.2 Inventory of publications

In order to offer a complete bibliographic information to the ISO Data Archive users, we try to keep track of all publications involving ISO data, and of all observations used for these publications. As a result, in IDA next to any selected observation, the button 'Articles' provides the references of the publications involving this particular observation and a link to their Astrophysics Data System (ADS) entry[2]. Your contribution in this matter can greatly help keeping an information as comprehensive as possible and we therefore ask you to kindly provide the following information for each of your publications:
- complete reference of the article (or preprint)
- list of TDT numbers and instrument modes of the observations that you have exploited for the publication.

You can send the information either by e-mail to:
helpdesk@iso.vilspa.esa.es
or by normal mail to:
ISO Project Scientist
(ISO Preprints)
ESA Satellite Tracking Station
Villafranca del Castillo
P.O. Box 50727
28080 Madrid

[2] `http://adswww.harvard.edu/`

Chapter 2

Instrument Description

2.1 Introduction

ISOPHOT (PHT) was the imaging photo-polarimeter on board the Infrared Space Observatory ISO. Its four principal modes were single detector element aperture photometry (3 – 120 μm), array imaging (40 – 240 μm), polarimetry (25, 170 μm) and spectrophotometry (2.5 – 12 μm). The wavelength range that was covered by IRAS was extended by a factor of two towards longer wavelengths. This wavelength regime, which is dominated by the emission of very cool objects (15 – 30 K), is not accessible from the ground and only with considerably less sensitivity with airborne instruments.

Since ISO was a satellite observatory designed for pointed observations, the much longer dwell times allowed to measure with ISOPHOT objects significantly fainter (by a factor 10 to 100) than the IRAS survey detection limit. However, in the FIR the gain in sensitivity did not increase with the square root in integration time, but was limited either by detector noise or sky confusion. See Table 2.1 for typical sensitivity from faint source programmes. The table with further details is given in Klaas et al. 1997, [22].

Table 2.1: *ISOPHOT sensitivity limits: $S/N = 1$, 256 s on-source integration time, 1 reference background position. The numbers in parentheses in the 'Pre-flight' column give an estimate of the $1\,\sigma$ confusion noise at the corresponding background brightness. The confusion noise has to be added to the pure detector noise limit. The in-flight values include all possible noise sources.*

Det.	Filt.	Aper. [arcsec]	Sensitivity Pre-flight [mJy]	In-flight [mJy]	Bckgr. [MJy sr^{-1}]	Limiting Param.
P1	P_4.85	52 circ.	2	2.5	0.1	detector noise
P1	P_11.5	52 circ.	2	5	15	background noise (ZL)
P2	P_25	79 circ.	7	13	40	background noise (ZL)
P3	P_60	180 circ.	3.5(+5)	20	10	detector/cirrus noise
C100	C_90	45 (1 pix)	1(+5)	7.5	10	dark current 100× higher detector/cirrus noise
C200	C_160	90 (1 pix)	3(+21)	40	5	cirrus noise
S1(SL)		24 × 24	21	10	15	detector/background noise
S2(SS)		24 × 24	11	26	0.5	detector noise

Key features of the instrument were:

- The filter set allowed nearly simultaneous and therefore consistent measurements (with regards to variable sources) from the NIR to the FIR.
- A range of apertures ($5'' - 180''$) could be selected to match the point spread function of the selected filter and thus to optimise the source-to-background contrast.
- Because the cold space telescope contributed negligible emission, relatively wide beams could be used to detect faint extended emission and measure absolute surface brightness.
- A chopping mirror in the beam path permitted differential measurements to detect faint sources superposed on a much higher background level.
- The chopper mirror also allowed for oversampled scans on bright celestial objects at far infrared wavelengths.
- Internal reference sources provided a homogenous calibration relative to the best available sky standards.
- The PHT spectrometer sub-instrument was optimised in wavelength coverage and spectral resolution for the investigation of dust features.
- The high sensitivity and therefore relatively short observation times permitted differential measurements through different polariser settings.

2.2 Overview

ISOPHOT, or PHT, was composed of 3 subsystems, or sub-instruments, optimised for specific photometric modes. Only one sub-instrument could be used at a time. The sub-instruments were:

PHT-P, a multi-band, multi-aperture photometer with three single detectors covering the wavelength range 3 – 120 μm from the near-infrared (NIR) to the far-infrared (FIR).

PHT-C, two photometric far-infrared (FIR) cameras for the wavelength range 50 – 240 μm.

PHT-S, two grating spectrophotometers, operated simultaneously, for the wavelength ranges of about 2.5 – 5 μm and 6 – 12 μm.

The modular subsystem concept minimised the number of mechanisms and resulted in a compact and rigid instrument. By appropriately setting three ratchet wheels a certain observational set-up could be selected from a large choice of useful combinations of filters and apertures. Figure 2.1 shows a schematic view of the instrument. For a more detailed description of the cryo-mechanics see Lemke et al. 1993, [35].

A focal plane chopping mirror was included for beam switching and modulation within the field of view of the instrument (Lemke et al. 1993, [35]). For absolute photometric measurements, the fine calibration sources (FCSs) were used as standard reference sources.

In addition, PHT was equipped with two sets of three polarisers, one set for the PHT-P detector group and one for the PHT-C detectors, covering the whole wavelength region from 3 to 240 μm. During the mission polarisation observations were only done at 25 μm and 170 μm.

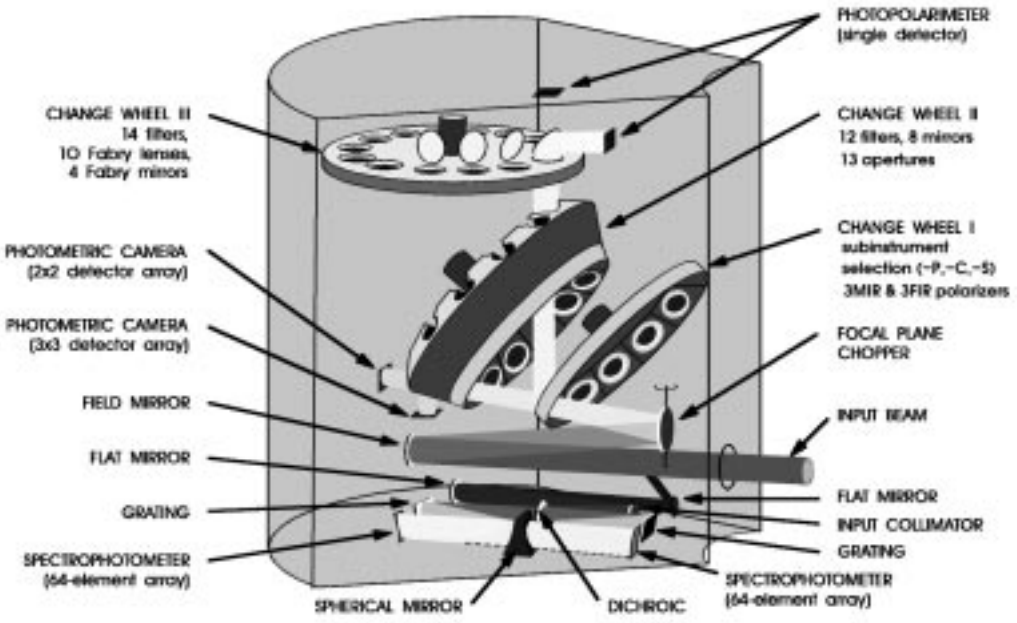

Figure 2.1: *Schematic view of the PHT instrument. After passing the field mirror and the focal plane chopper the light beam coming from the telescope reaches change wheel I, which allows for the choice of one of the various sub-instruments and the polarimetric observing mode. The dual channel design of the PHT-S sub-instrument is indicated in the lower part of the drawing by showing the dichroic element and the two PHT-S detector arrays. Both PHT-C detectors are illuminated via change wheel II, which contains the filters for these sub-instruments. This wheel also carries the apertures for the PHT-P photometers. Finally, change wheel III contains the filters for the PHT-P sub-instruments. The fine calibration sources and the third PHT-P detector have been omitted for clarity (see also Figure 2.2).*

2.3 Focal Plane Scale

Figure 2.3 shows the relative sizes of the PHT-P and -S apertures, and the PHT-C detector pixels. They were centred in the specified unvignetted field of view of 3′ inside the 20′ field of view of the ISO telescope. Note that the gaps between the individual PHT-C detector pixels are real. These gaps may have influenced the choice of the observing mode, in particular, if the flux of a source or its spatial flux distribution had to be measured accurately.

2.4 Data Collection with ISOPHOT

The analysis and reduction of ISOPHOT data require a basic knowledge of the instrument itself and the instrument procedures performed during an observation. The way ISOPHOT data were taken is given in the following section. This section is of importance to understand the structure of ERD products (Chapter 6).

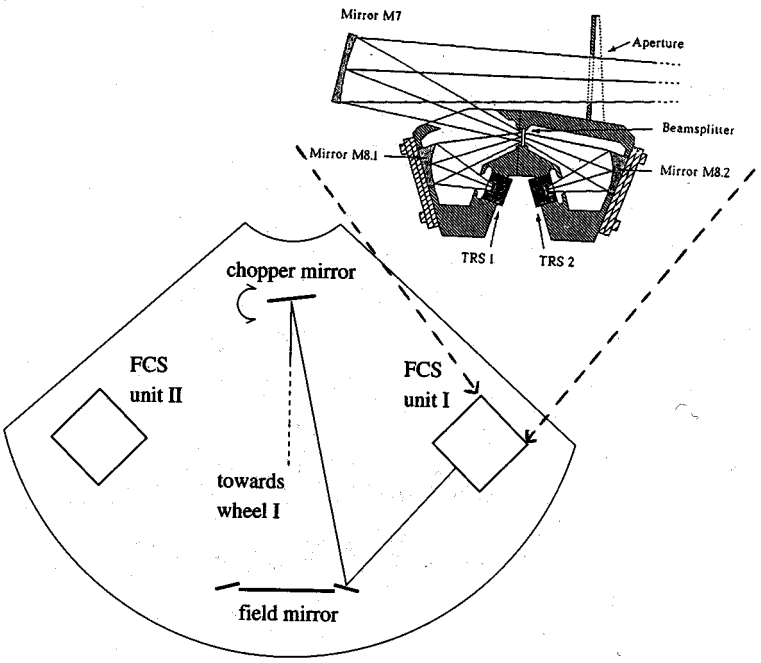

Figure 2.2: *Schematic view of the PHT instrument set-up for calibration measurements with the internal fine calibration sources (FCSs). Each FCS contained two thermal radiation sources (TRS). Tuning of the heating currents of the TRS elements in combination with the beam splitter allowed to match a wide range of calibration fluxes.*

2.4.1 Signal flow in ISOPHOT

In this section we introduce the elements related to the ISOPHOT signal flow. For the understanding of the instrument output related to an astronomical observation, systems on both the cold and warm side of the cryostat were of importance, see also Figure 2.4:

- The cold focal plane unit (FPU) inside the ISO cryostat (payload module) described in (Wolf 1994, [57]; Lemke et al. 1993, [35] and Lemke et al. 1994, [36]) containing
  - detector subsystems with the cold readout electronics (CRE),
  - the change wheel (CHW) system,
  - the focal plane chopper (FPC), and
  - the internal reference sources (FCSs).
- The warm external electronics unit (EEU) in ISO's service module containing
  - the central processing units,
  - the readout timing control and voltage supply units, and
  - the detector interface electronics (DIE) of the processing subsystem.

  Telecommands were processed by the central processing electronics. The electronics for the CHWs, temperature control, bias supplies, etc. were in the EEU. The central processing unit also generated the instrument telemetry. It combined the science data from the detector with relevant housekeeping

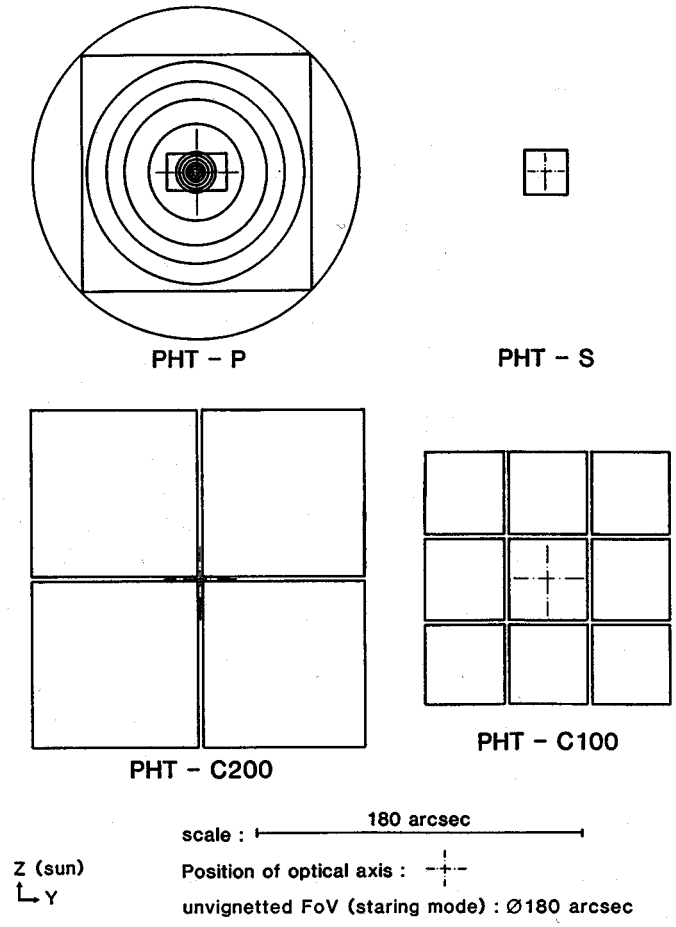

Figure 2.3: *Focal plane map of PHT apertures and detectors showing relative sizes of the pixels and apertures of the different sub-instruments. Note the gaps between the individual PHT-C pixels. The scale is indicated at the bottom. The 3 arcmin circle is the minimum required unvignetted field of view inside the ISO's 20 arcmin field of view. Z and Y denote the satellite axes as explained in the 'ISO Handbook, Vol. I: ISO – Mission & Satellite Overview', [20].*

information on the selected subunits. In case PHT was the prime instrument, but no exposure was ongoing, extended housekeeping telemetry was generated.

- The ISO on-board data handling system (OBDH) in ISO's service module which communicated with the instrument EEU. The instrument telemetry coming from the EEU was combined with the pointing data from the attitude and orbit control system (AOCS) and put in telemetry blocks. Each telemetry block or record covers a time period of 2 s. The telemetry of a whole revolution is stored in a TDF (Telemetry Distribution File).

2.4.2 Cold Readout Electronics (CRE)

The ISOPHOT detectors were either Silicon doped or Germanium doped photoconductors. The function of the Cold Readout Electronics (CRE) unit was to pre-amplify and sample the photo-currents generated in these detectors. To reach the maximum efficiency, the CRE was integrated on the chip containing the

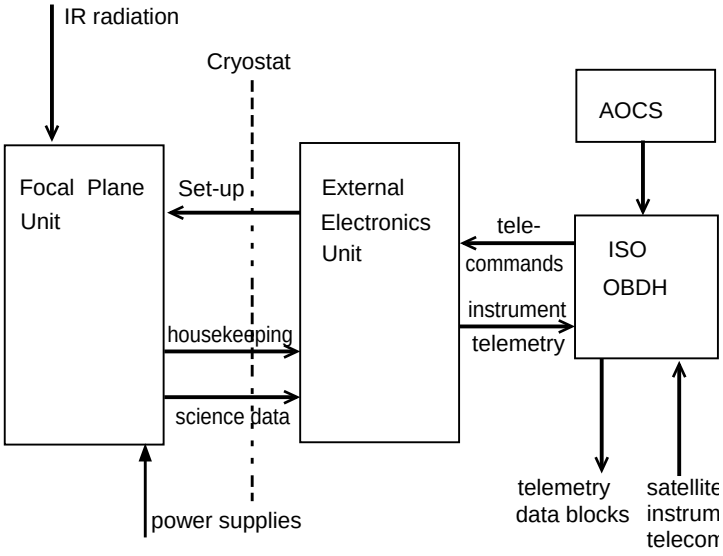

Figure 2.4: *Main systems for data collection.*

detector. For more details, see Wolf 1994, [57] and Wolf, Grözinger & Lemke 1995, [58].

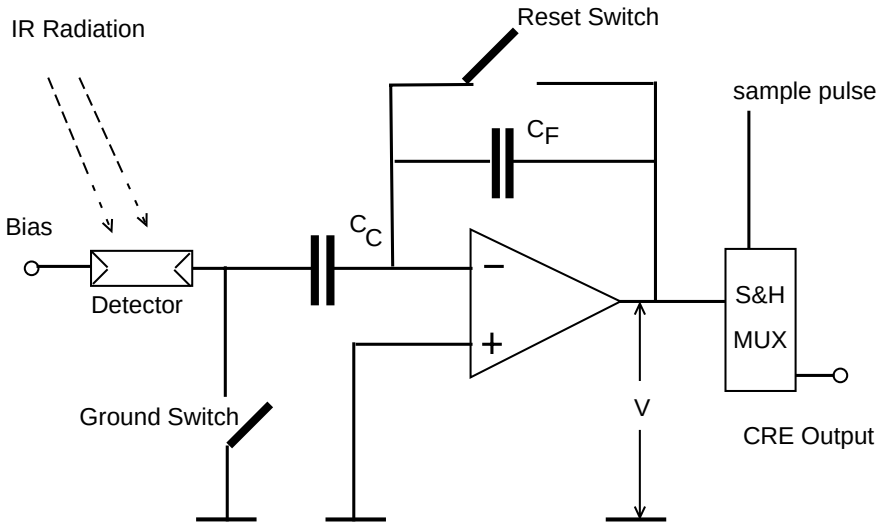

Figure 2.5: *Schematic diagram showing the detector - CRE amplifier chain, the capacitance C_F is also denoted by C_{int} in this document.*

The detector/CRE chain in Figure 2.5 represents an integrating amplifier with capacitive feedback. Each detector pixel was connected to one input channel of a CRE. In case the detector was receiving IR photons from an astronomical or internal source, the voltage V at the output of the CRE increased as

a function of time. The voltage increase per time interval was dependent on the amount of the current through the detector which is in turn dependent on the number of photons falling on the detector. In the remainder of this manual this voltage increase or slope (in V/s) will be referred to as photo-current or *signal*. For the observer the signal is a fundamental concept: once signals from calibration standards have been measured, it is possible to relate the signal to a power from the source in the filter band.

After the amplifier stage there was a sample & hold (S&H) stage. By applying a sample pulse the voltage was clamped and while the front-end continued to integrate, the clamped signal was read out through a multiplexer (MUX). In that way the readout did not disturb the integration.

Since the output voltage should stay within a limited range, the voltage was reset by short circuiting the capacitors using both the ground as well as the reset switch. A reset pulse was applied in addition to a sample pulse after a number of desired voltages had been sampled. The readout associated with this reset is called the *destructive readout*, the other sampled voltages are called *non-destructive readouts*. The time between two reset pulses (in seconds) is called the fundamental integration time or *reset interval* (RI). The duration of a reset interval is denoted by t_{RI}. All readouts collected during one reset interval are part of one integration ramp or simply *ramp*. In Figure 2.6, the readout data stream is shown schematically.

The voltage of the first readout after reset is not zero but starts at an arbitrary voltage level. This level is called the *reset level*, since it has more or less the same value during a measurement. Variations were caused by instabilities in the amplifier electronics.

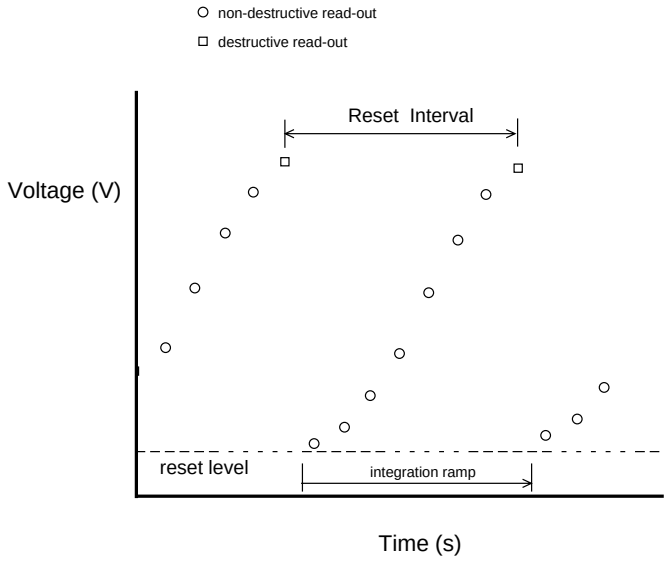

Figure 2.6: *Schematic diagram showing CRE output for a ramp of 7 non-destructive readouts (NDR=3).*

2.4.3 Detector Interface Electronics (DIE)

The detector interface electronics (DIE) acquired the output signals from the CREs and processed these for the telemetry transmission. It also served as a multiplexer thus reducing the number of output lines. For redundancy reasons there were two DIEs in the EEU, each interfacing with the following groups of detectors:

- DIE1: C200, P1, P2, and SL

- DIE2: C100, P3, and SS

The DIE subtracted a commandable offset from the CRE output voltage and amplified the difference with a commandable gain factor. Note that for PHT the gain was a constant unlike other instruments for which the gain was used to adjust the dynamical range. The dynamic range was adjusted by selection of the proper reset interval (see Section 2.4.4).

The DIE also converted the analogue signal from the CRE to a digital signal. This AD conversion produced a 12 bits value per readout which means that each readout has a digitalisation resolution of $2^{12} = 4096$. The fact that there are several readouts per ramp increases the resolution in the signal.

2.4.4 Readout timing control

To cover a dynamic range equivalent to the flux density range of astronomical sources (a few mJy to hundreds of Jy) within the available commanding bits in the telecommands, the design of the readout parameters was based on an exponential scale with base 2. Only a power of 2 readouts per reset interval was commanded, and the duration of a reset interval (in seconds) had also to be a power of 2. Since there were 4 bits available for commanding, the reset interval could have 16 values ranging from 1/256, 1/128, 1/64,...128 s. Per ramp there were 2^n readouts. The last one, the destructive readout, was generally not reliable, since it was disturbed by the reset. The number of non-destructive readouts per ramp was determined by the parameter *NDR*, it is equal to $2^{NDR} - 1$.

The parameter DR was defined to set the chopper plateau time. DR was defined such that 2^{DR} is equal to the number of destructive readouts (or number of ramps) per chopper plateau.

The *chopper dwell time* or duration of a chopper plateau t_{chop} can be derived from:

$$t_{chop} = 2^{DR} \times t_{RI}. \tag{2.1}$$

The commanding of PHT imposed at least 4 ramps per chopper plateau, thus DR$\geq$2 for chopped observations. The maximum plateau time is 128 s. The first ramp of a chopper plateau is affected by the chopper transition and therefore unreliable. DR was always commanded, both for staring and chopped observations. In case of staring observations, DR was commanded such that $2^{DR} \times t_{RI} = 128\,\mathrm{s}$. After 128 s a virtual chopper transition (with physical chopper throw = $0''$) occurred.

For high readout rates the amount of data to be transferred was too high to be matched into the ISO TM format. In order to avoid telemetry overflow, the parameter *data reduction* (DAT_RED) was introduced. The value of DAT_RED is an integer indicating that only the first ramp of a sequence of DAT_RED ramps should be transmitted. For example, DAT_RED = 4 means that only the first of every 4 ramps is transmitted. DAT_RED = 1 indicates no reduction. Observations of bright sources had a DAT_RED parameter larger than 1. The value of DAT_RED depended not only on NDR and RI, but also on the number of pixels per detector array.

2.5 ISOPHOT Measurement Concept

A PHT measurement comprises all detector readouts telemetered following a 'start measurement' command with the instrument in a fixed configuration. A change of instrument configuration can be a change of detector, a change of aperture, a change of filter, a change of polariser, or a switching-on or -off of the FCS. These changes can only occur *between* measurements and not *during* a measurement. The *measurement time* is the total time necessary to perform a measurement. This time is different from the on-source *integration time*, which excludes the time when the background is measured by the chopper in case of a chopped measurement.

Data collected while the spacecraft was performing a raster map belong to the same measurement. The integration time per raster point, or the *raster point dwell time* and the time for the microslews between the raster points are included in the measurement time.

Apart from the sky measurements, the observations provide a number of special internal measurements:

- FCS measurement. All AOTs except PHT40 include at least one FCS measurement, see also Chapter 5, Sections 5.2.4 and 5.7.2.
- Dark instrument configuration measurement. This measurement type is obtained with AOTs PHT05, PHT25, and PHT40 and is used to subtract dark signals (in case of PHT05 and PHT25) or to identify possible detector memory artifacts from a preceding measurement of a bright source (in case of PHT40).
- Cold FCS measurement. This measurement is used to assess the zero signal level of an accompanying FCS measurement by applying no heating power to the FCS. It is also referred to as 'FCS straylight' measurement because parasitic light from the sky into the instrument (ISOPHOT had no shutter) or from the instrument itself can be measured. The absolute photometry AOTs PHT05 and PHT25 can contain such a measurement.

2.6 Detector Subsystems

2.6.1 PHT-P

Subsystem PHT-P was a multi-filter, multi-aperture photopolarimeter with single element detectors and wide beam (up to 3 arcmin) capability for faint extended sources. The covered wavelength range was ≈3–130 μm. The PHT-P detectors were each located inside an integrating cavity and had a dimension of $1\times1\times1\,\mathrm{mm}^3$. This subsystem was designed for sensitive, high precision photometry and polarimetry, using three different detector types (in parenthesis the detector material is given):

- P1 (Si:Ga) 10 filters: 3.3–16 μm
- P2 (Si:B) 2 filters: 20 and 25 μm
- P3 (Ge:Ga) 2 filters: 60 and 100 μm

Any combination of apertures and filters was allowed. Polarisers were only used with the P2 25 μm filter and the 79″ aperture. At long wavelengths the Airy disc is significantly larger than the smallest aperture available. The diameter of the Airy disc is $\mathrm{d_{Airy}}[''] = 0.84 \cdot \lambda[\mu\mathrm{m}]$. The selection of apertures much smaller than $\mathrm{d_{Airy}}$ was not recommended (see Table 2.2). Section 2.9 gives more details about the calculation of λ_c, $\Delta\lambda$ and R_{mean}.

Polarisers: 0, 120 and 240 degrees
Apertures: 5.0, 7.6, 10, 13.8, 18, 20×32, 23, 52, 79, 99, 120, 127×127 and 180 arcsec. All apertures are circular except if noted.

The precision of the ISO pointing had implications on the achieved photometric accuracy. When observing with the smallest PHT-P apertures (5.0″ and 7.6″), the source might have been observed strongly off-centre, see 'ISO Handbook, Vol. I: ISO – Mission & Satellite Overview', [20] for details about the ISO pointing accuracy.

Table 2.2: *PHT-P filter characteristics. λ_{ref} is the PHT reference wavelength (Moneti, Metcalfe & Schulz 1997, [39]), to be used for colour corrected monochromatic fluxes, λ_c is the central wavelength, $\Delta\lambda$ is the width and R_{mean} the average relative system response derived from the bandpasses (see Section 2.9 and Appendix A.2). d_{Airy} is the diameter of the Airy disc taken at λ_c. The minimum aperture was the smallest one recommended; it was the minimum aperture which completely covered the Airy disc.*

No. #	Filter	λ_{ref} [μm]	λ_c [μm]	$\Delta\lambda$ [μm]	R_{mean}	d_{Airy} [$''$]	min. aper. [$''$]	scientific objective
	P1							
1	P3.29	3.3	3.30	0.22	0.10	2.8	5	PAH
2	P3.6	3.6	3.59	0.99	0.14	3.0	5	cosmological gap, common to ISOCAM
3	P4.85	4.8	4.86	1.55	0.16	4.1	5	continuum to #1, #4 and #5
4	P7.3	7.3	7.41	3.38	0.28	6.2	7.6	6.2, 7.7, 8.6 μm PAH complex
5	P7.7	7.7	7.66	0.82	0.25	6.4	7.6	PAH
6	P10	10.0	10.00	1.80	0.35	8.4	10	silicate feature
7	P11.3	11.3	11.36	0.81	0.29	9.5	10	PAH
8	P11.5	12.0	11.88	6.53	0.48	10.0	10	IRAS 12 μm band, common to ISOCAM
9	P12.8	12.8	12.82	2.31	0.52	10.8	10	continuum to #7
10	P16	15.0	15.16	2.84	0.35	12.7	13.8	general purpose
	P2							
11	P20	20.0	21.03	9.03	0.32	17.7	18	close to standard Q band
12	P25	25.0	23.80	9.12	0.38	20.0	23	IRAS 25 μm band
	P3							
13	P60	60.0	60.85	25.89	0.11	50.3	52	IRAS 60 μm band
14	P100	100.0	102.44	39.55	0.31	83.9	79	IRAS 100 μm band

2.6.2 PHT-C

PHT C100 was a 3×3 array of Ge:Ga with $0.7\times0.7\times1\,\mathrm{mm}^3$ elements. Increased photon absorption was achieved by total reflection of a 30° wedged pixel surface and an integrating cavity. The telescope beam was fed into these cavities by $1.9\times1.9\ \mathrm{mm}^2$ anti-reflection coated germanium fabry lenses mounted with 100 μm spacing which resulted in an optical fill factor of 93%. The effective size of the pixels on the sky was $43.5\times43.5\,\mathrm{arcsec}^2$, the distance between the pixel centers ('pitch') was 46.0 arcsec.

Throughout this manual the individual C100 pixels/detectors are labelled as in Table 2.4 where the +Z direction is upwards, and +Y is to the left. This corresponds to the projection of the array on the sky. The numbers (1...9) in Table 2.4 refer to the labelling and array counting in ERD, SPD and AAR products.

PHT C200 consisted of 4 pixels arranged in a 2×2 matrix. The telescope beam was concentrated on the four detector pixels by anti-reflection coated germanium Fabry lenses of $3.9\times3.9\,\mathrm{mm}^2$. The detector crystals were mounted in an integrating cavity and had prismatic shape to increase photon absorption. The sizes of the detector pixels themselves were approximately $1\,\mathrm{mm}^3$. The effective size of the pixels on the sky was $89.4\times89.4\,\mathrm{arcsec}^2$, the distance between the pixel centers was 92.0 arcsec.

The pixels were stressed by individual screws (Wolf, Grözinger & Lemke 1995, [58]); the stress was maximized in order to give a cut-off wavelength of 240 μm. The labelling of the individual C200 pixels is given in Tables 2.5 and 2.6 for the ERD and SPD/AAR convention.

Table 2.3: *Intensity fraction* f_{PSF} *of a point source entering the apertures of PHT-P. A theoretical monochromatic point spread function centred in the aperture has been adopted.*

	PHT-P apertures												
filter	5″	7.6″	10″	13.8″	18″	23″	20×32″	52″	79″	99″	120″	127×127″	180″
P1													
3.3	0.85	0.88	0.91	0.92	0.95	0.96	0.96	0.99	0.99	0.99	1.00	1.00	1.00
3.6	0.81	0.88	0.91	0.92	0.94	0.95	0.96	0.98	0.99	0.99	1.00	1.00	1.00
4.8	0.69	0.86	0.88	0.90	0.92	0.93	0.94	0.98	0.99	0.99	0.99	0.99	1.00
7.3	0.64	0.76	0.85	0.87	0.89	0.91	0.92	0.96	0.97	0.98	0.99	0.99	0.99
7.7	0.64	0.73	0.85	0.87	0.88	0.90	0.91	0.96	0.97	0.98	0.99	0.99	0.99
10	0.54	0.66	0.73	0.84	0.87	0.88	0.89	0.94	0.96	0.97	0.98	0.98	0.99
11.3	0.48	0.66	0.68	0.79	0.86	0.87	0.89	0.93	0.96	0.97	0.97	0.98	0.99
12	0.48	0.65	0.70	0.78	0.86	0.87	0.88	0.93	0.95	0.97	0.97	0.98	0.99
12.8	0.42	0.65	0.66	0.73	0.86	0.87	0.88	0.92	0.95	0.96	0.97	0.98	0.98
15	0.33	0.61	0.66	0.67	0.80	0.86	0.85	0.92	0.94	0.95	0.96	0.97	0.98
P2													
20	0.22	0.47	0.59	0.65	0.69	0.75	0.79	0.89	0.92	0.93	0.95	0.95	0.97
25	0.17	0.41	0.54	0.63	0.66	0.70	0.76	0.88	0.91	0.93	0.94	0.95	0.96
P3													
60	0.04	0.09	0.15	0.23	0.36	0.46	0.51	0.68	0.81	0.86	0.87	0.88	0.90
100	0.01	0.04	0.05	0.09	0.15	0.22	0.27	0.59	0.66	0.70	0.77	0.83	0.87

Table 2.4: *C100 ERD, SPD and AAR pixel labels, +Z is up, +Y is left.*

9	6	3
8	5	2
7	4	1

Table 2.5: *C200 ERD pixel labels, +Z is up, +Y is left.*

4	3
1	2

Table 2.6: *C200 SPD and AAR pixel labels, +Z is up, +Y is left.*

4	2
3	1

There were 6 filters for C100 and 5 for C200 available. Table 2.7 gives a list of these filters including the reference and central wavelength, the widths, their resolution and the transmission. Section 2.9 gives more details about the calculation of λ_c, $\Delta\lambda$ and R_{mean}.

Table 2.7: *PHT-C filter characteristics. λ_{ref} is the PHT reference wavelength (Moneti, Metcalfe & Schulz 1997, [39]), to be used for colour corrected monochromatic fluxes, λ_c is the central wavelength, $\Delta\lambda$ is the width and R_{mean} the average relative system response derived from the bandpasses (see Section 2.9). $d_{\rm Airy}$ is the diameter of the Airy disc at λ_c.*

Filter	λ_{ref} [μm]	λ_c [μm]	$\Delta\lambda$ [μm]	R_{mean}	$d_{\rm Airy}$ [$''$]
C100					
C50	65	68.7	60.8	0.04	42
C60	60	61.8	24.6	0.13	50
C70	80	80.7	48.4	0.12	59
C90	90	95.2	56.4	0.30	76
C100	100	102.6	47.1	0.27	84
C105	105	107.2	38.4	0.24	88
C200					
C120	120	118.7	49.5	0.13	101
C135	150	155.1	81.2	0.26	113
C160	170	174.3	89.9	0.43	134
C180	180	181.0	68.8	0.33	151
C200	200	202.1	56.9	0.22	168

Table 2.8: *Intensity fraction f_{PSF} of a point source falling on one pixel of the C100 or C200 detector, respectively. A theoretical point spread function centred on the pixel has been adopted.*

filter	f_{PSF}	filter	f_{PSF}
C100		**C200**	
C_50	0.656	C_120	0.678
C_60	0.667	C_135	0.641
C_70	0.629	C_160	0.620
C_90	0.586	C_180	0.609
C_100	0.558	C_200	0.568
C_105	0.540		

2.6.3 PHT-S

PHT-S consisted of a dual grating spectrometer with resolving power of order 90 in two wavelength bands. Band SS covered the wavelength range 2.5–4.9 μm and band SL covered the range 5.8–11.6 μm. Each spectrometer used a linear array of 64 element Si:Ga detectors with dimensions of $0.31\times0.37\times1.80\,{\rm mm}^3$ per element. The arrays, hence the dispersion direction, were oriented in the spacecraft Z-direction. PHT-S had one square entrance aperture with dimensions $24''\times24''$; this aperture was imaged onto each detector pixel.

In dispersion direction this resulted in a triangular spectral bandpass with a spectral range (Full Width at Half Maximum) for a single detector of 42.4 nm ($=3500$ km s^{-1}) for PHT-SS and 96.6 nm ($=3200$ km s^{-1}) for PHT-SL. The resolution was about 85 for PHT-SS and about 95 for PHT-SL, respectively. The spectra could be fully sampled at half of the resolution, i.e. with 89 nm (PHT-SS) and 189.8 nm (PHT-SL). PHT-S could be used with the chopper.

Both gratings were operated in first order. The wavelength scale was established in-orbit against celestial sources which emit narrow lines by fitting a 2nd order polynomial through the measured line centers.

2.7 Fine Calibration Sources (FCSs)

The internal fine calibration sources acted as stable reference sources and were used for photometric calibration of PHT-P or PHT-C observations, see Chapter 5. In terms of data collection, internal calibration measurements were similar to the celestial measurements except that they utilized one of the internal FCSs by imaging it via the chopper mirror, see also Section 2.8. All ISOPHOT AOTs except PHT40 contained one or more FCS measurements depending on the observing mode(s) requested.

There were two identical FCSs which could be operated independently. Each FCS consisted of two Thermal Radiation Sources (TRSs): TRS1 was operated in reflecting mode via a mirror, whereas TRS2 was operated in a transmitting mode via a beam splitter giving a factor of about 1000 lower flux level than for TRS1. The TRSs were diamond wafers, heated to temperatures up to 300 K. By controlling the source temperature between 5 K and 300 K with an accuracy of $\Delta T \approx 0.1$ K, different flux levels in the range 5×10^{-17} to $\geq 10^{-12}$ W on the detector could be applied to all detectors except PHT-S (see Chapter 5). The temperature was accomplished by tuning the electrical heating power of the FCSs.

During the entire ISO mission FCS1 was calibrated against astronomical standards. For standard astronomical observations only FCS1 was used as reference source, its emission was directly compared with the flux of celestial standards. For P1 and P2, FCS2/TRS1 was cross-calibrated against FCS1/TRS1. After the change of illumination behaviour of TRS2 in FCS1 on revolution 94, it was decided to independently calibrate FCS2/TRS2 by a set of measurements against celestial standards with P3, C100 and C200 detectors. The calibration against celestial standards was accomplished by determining the heating power (in mW) that should be commanded on the FCS in order to mimic the power on the detector from a celestial calibration source (in W). Details of the calibration procedure can be found in Chapter 5.

One FCS measurement was obtained at the end of a sequence of measurements with a given detector subsystem for single pointing photometric observations. In case of multi-filter observations using more than one detector subsystem, one FCS measurement per subsystem was collected, see Section 3.10. For observations using raster mode where the execution of the AOT could be relatively long, the actual measurement was bracketed by two internal calibration measurements.

In AOT PHT40 (spectrophotometry with PHT-S) no FCS measurements were taken, because the colour temperature of the FCS was too low to allow a homogeneous illumination of both PHT-SS and PHT-SL. In particular, in order to illuminate PHT-SS sufficiently, PHT-SL would have had to be heavily saturated which would have led to long term drifts of the PHT-SL detector afterwards.

2.8 Focal Plane Chopper (FPC)

The Focal Plane Chopper (FPC) deflected the beam onto adjacent fields on the sky, or, in case of internal reference measurements, onto the two FCSs (see Figure 2.2). The chopper could move the beam only along the spacecraft Y direction, positive chopper position commands yielded throws in +Y direction. FCS1 was seen by the detectors when the chopper moved the beam beyond the (+) field of view of the field mirror at $+460''$, FCS2 was seen at $-460''$. The maximum amplitude for the sky was $\pm 180''$. The chopper transition times are given in Table 2.9. The first column indicates the mode: either from the centre field of view (CFOV) to one of the FCSs (FCS mode) or to a sky offset (FOV mode):

Note: 1 ITK (instrumental time key) unit = 2^{-14} *sec*.

The chopper could be commanded to operate in staring mode (i.e. one position for the whole measurement) or in chopped mode whereby two or more viewing directions could be chosen during a measurement. In the AOTs three distinct chopper modulation functions could be selected (see also Figure 3.1):

Table 2.9: *Chopper transition times.*

Mode	Transition time in ITK units	Transition time $[s]$
FCS	832	0.051
FOV	224	0.014

- RECTANGULAR:
  chopping between two end positions, with an equal time spent on both positions.
- SAWTOOTH:
  chopper scan with the number of steps ranging from 3 to 301; minimum step size $1''$, maximum step size $150''$, and $(number\,of\,steps - 1) \times stepsize \leq 300''$.
- TRIANGULAR:
  chopper scan with the number of steps ranging from 3 to 301; step sizes and limitations as for sawtooth chopper scan.

The first chopper position of a chopper cycle was always the largest deflection in –Y direction. The chopper mode and amplitude is fixed per AOT and not per measurement. The parameters of the modulation function per AOT are described in detail in Section 3.1.

2.9 Filters

The filters available for PHT-P and PHT-C are listed in Tables 2.2 and 2.7. Let $R(\lambda)$ be the actual bandpass, which is the filter transmission function convolved with the relative spectral detector response[1]; then the central wavelength λ_c, the filter width $\Delta\lambda$, and the average relative system response $R_{\rm mean}$ are defined as:

$$\lambda_c = \frac{\int_0^\infty \lambda R(\lambda) d\,\lambda}{\int_0^\infty R(\lambda) d\,\lambda} \tag{2.2}$$

$$\Delta\lambda = 2\sqrt{3\frac{\int_0^\infty (\lambda - \lambda_c)^2 R(\lambda) d\,\lambda}{\int_0^\infty R(\lambda) d\,\lambda}} \tag{2.3}$$

$$R_{mean} = \frac{\int_0^\infty R(\lambda) d\,\lambda}{\Delta\lambda} \tag{2.4}$$

$\Delta\lambda$ is the width of a rectangular filter having the same integrated relative system response as the actual bandpass[2]. The relative response curves of all bandpasses are shown in Appendix A.2. Note that due to the large wings of especially the long wavelength filters, the rectangular widths (given in Tables 2.2 and 2.7) are significantly different from the full width at half maximum. Some useful filter combinations, including comparisons with IRAS filters, are illustrated in Appendix A.2.

[1] Relative spectral detector response means detector response normalised to its maximum value.

[2] The factor of $2\sqrt{3}$ is a normalising factor forcing the filter width to be equal to that of a rectangular filter with height $\rm R_{mean}$.

Chapter 3

Instrument Modes and Astronomical Observation Templates

The three main PHT observing modes are photometry, spectrophotometry and polarimetry. In the photometric mode PHT offered a number of possibilities to observe point-like and extended sources, in staring or in chopped observing mode.

In the following sections these modes are described in detail. Chopping is regarded here as a general procedure applicable to several modes.

- Chopping
- Photometry – Single pointing multi-filter/multi-aperture
- Photometry – Multi-filter rastering
- Photometry – Absolute photometry
- Photometry – Oversampled Scans and Maps
- Photometry – Sparse maps
- Polarimetry
- Spectrophotometry

3.1 Chopping

There were three different chopper modes available for single pointing photometry. The decision to chop or stare and the selection of the chopper mode depended on the structure of the source and the nearby sky background. The different chopper modes are illustrated in Figure 3.1.

Rectangular – In this mode, the satellite pointed to the position between the source and an off-source position, and the chopper moved alternately between these two positions. The source was always in the positive beam in spacecraft Y-direction[1]. Chopper throws (peak to peak) between 30″ and 330″ in steps of 30″ were possible. There was the additional constraint that the chopper throw had to be greater than or equal to the selected aperture

[1]In the PV phase the opposite scheme was implemented, with the source in the –Y axis beam; this was corrected from revolution 70 onwards

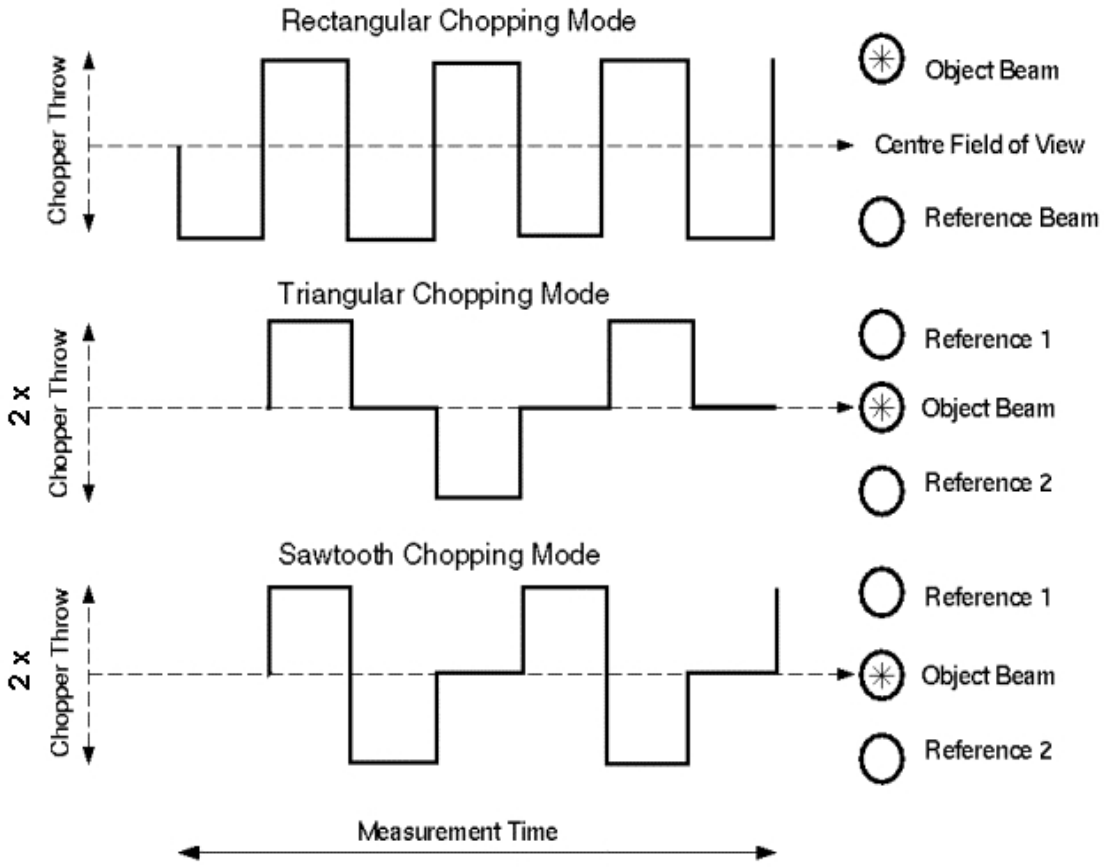

Figure 3.1: *Chopper modes. The curves represent the chopping cycles. To the right the projection on the sky is illustrated. The chopping starts in the $-y$ direction. For triangular and sawtooth chopper modes the peak-to-peak deflection is twice the chopper throw.*

diameter[2] or the array side length (to avoid overlap of the beams) and less or equal than 360″ minus the aperture diameter or array side length (to avoid beam vignetting). For instance, PHT-P observations with the 10″ aperture allowed the use of all possible throws, namely 30″, 60″, 90″, ..., 330″; observation with the 79″ aperture allowed the use of the following throws: 90″, 120″, 150″, 180″, 210″, 240″, 270″; any observation with the 180″ aperture allowed only the 180″ throw. For C100 the throws of 150″, 180″ and 210″ were allowed, and for C200 only a throw of 180″ was possible.

Triangular – Chopping occured to two positions on either side of the source. The satellite pointed to the source position, and the chopper moved from one off-source position to the source and then to the other off-source position and finally back to the source, and so forth. In this way, the source was observed twice during each cycle and each of the off-source positions once. Chopper throws (distance between on-source and off-source positions) between 15″ and 150″ in steps of 15″ were possible. There was the additional constraint that the chopper throw had to be greater or equal to the selected aperture diameter or the array side length (to avoid overlap of the beams) and less or equal than 180″ minus half the aperture diameter or half of the array side length (to avoid beam vignetting). For instance,

[2]For the 20″×32″ aperture the 32″ value had to be used.

observing with the 10″ aperture allowed the use of the full set of throws, namely 15″, 30″, ..., 150″; observing with the 79″ aperture allowed the use of the following throws: 90″, 105″, 120″, 135″ (to be compatible with the vignetting rule). The 120″ aperture was the largest one to be used for the triangular chopping mode. It was not allowed to use C200 with this chopper mode, and for C100 the only throw was the 150″ one.

Saw-Tooth – As in the triangular mode there were two off-source positions, and the satellite pointed to the source. However, after having moved from one off-source position to the source and then to the other off-source position, the chopper moved back to the first off-source position. During the transition between the two off-source positions the source was inside the beam for a very short time. Here the same chopper throw limitations applied as for triangular chopping.

In summary: for the C200 detector it was only possible to choose rectangular chopping mode with a single chop throw of 180″. For the C100 detector the only chopper throws were 150″, 180″, and 210″ for rectangular chopping. In case triangular and sawtooth chopping with C100 was selected, the only available throw was 150″.

The different chopper modes determined the number and locations of reference positions observed with respect to the on-source position (see Figure 3.1). Chopping was recommended, if the sky background was expected to be comparable to the source flux, or stronger.

By chopping, source and background were measured with one telescope pointing. Otherwise, an additional pointing had to be made, which meant an additional observation using the same AOT on the background position. Depending on the structure of the background, e.g. flat background, infrared cirrus, or with strong gradients, one of the different chopper modes had to be selected.

The fastest chopper frequency was constrained to 0.5 Hz. This occurred for the brightest sources. For fainter sources the frequency was lower due to the requirements to fit at least 4 ramps into one plateau; therefore the selected reset intervals (*times*4) determined the chopper frequency. In-flight it was found, that the fastest chopper frequencies meant significant signal losses of the differential signal with regard to the stabilised signal difference given by staring observations. Therefore, telescope nodding was recommended as a better alternative for slow signal modulation of very bright and intermediate sources against the sky background (see Section 3.3).

3.2 Single-Pointing Multi-Filter and Multi-Aperture Modes

With single-pointing photometry it was possible to measure the energy distribution of point-like or compact extended sources in broad-band filters. For the detection of dust features dedicated narrow band filters were available, and there were some very broad filters dedicated to the detection of faint sources. Figures 3.2, 3.3 and 3.4 give some typical combinations of filters for different scientific purposes, and the complete set of ISOPHOT bandpasses is displayed in Appendix A.2.

The large set of apertures in the PHT-P subinstrument offered the study of faint extended emission around point sources, by means of multi-aperture photometry. The largest apertures permitted detection of faint and extended emission, either in staring or chopped mode. For the chopped mode the restrictions in chopper throw described in Section 3.1 had to be applied to the largest selected aperture.

3.3 Raster Mode

The staring raster mode was a sequence of staring observations (i.e. chopping was not allowed) on a two-dimensional regular grid which consisted of a sequence of spacecraft pointings. The detector setting remained unchanged for all pointings. The orientation of the raster could be chosen either aligned with the spacecraft y-axis orientation and hence the detector array orientation, or with regard to the sky

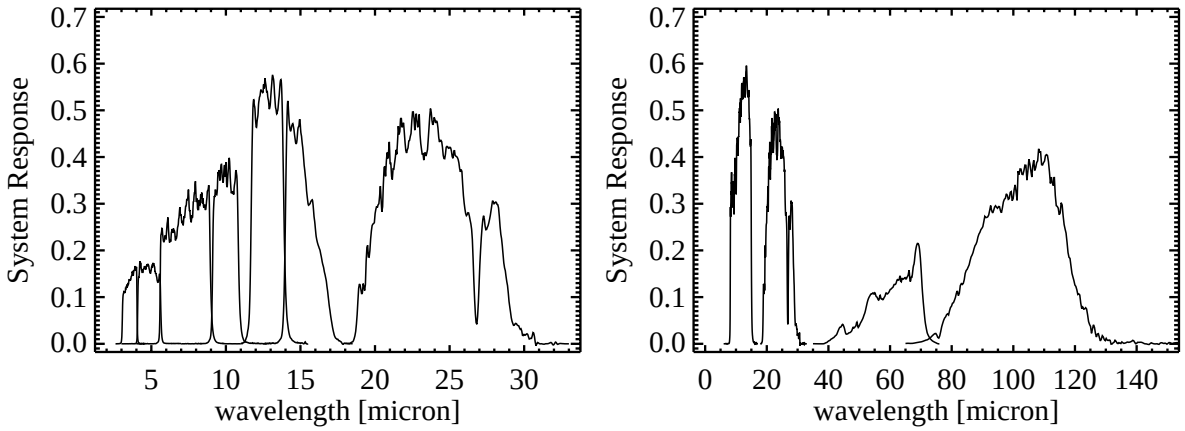

Figure 3.2: *Relative system response (i.e. detector response normalised to its maximum value) of PHT filter bandpasses: near and mid infrared PHT-P filter sequence 3.6 – 25 μm (left); and the corresponding IRAS filter sequence with PHT-P (right)*

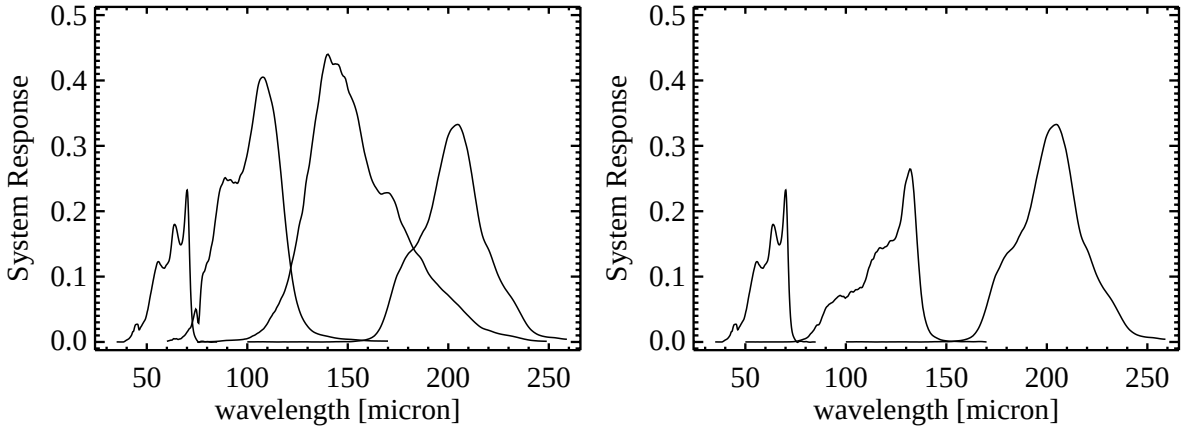

Figure 3.3: *PHT filter bandpasses: combination 1 of far infrared PHT-C filters (left); and combination 2 of far infrared PHT-C filters (right)*

N-direction, i.e. in general independently of the spacecraft orientation. However, in the latter case the observed sky region was not always completely sampled (for example see Figure 3.5).

Studies of point sources on complex backgrounds or extended sources (sizes of more than 3 arcmin) were possible with this observing mode. This mode was the only one for mapping with PHT-P.

The maximum number of raster points was 32×32. The maximum raster step size was 180″ Therefore, the maximum sampling area was 1.6°×1.6°.

In the beginning the minimum raster step size was half the aperture size and one quarter of the array size. Later in the mission (from 17-Oct-1996, revolution 336[3]) the minimum raster step size was reduced to 'On-target-flag threshold' plus 3″ in the case of PHT-P and -S and 15″ for both C-arrays. Since the 'On-target-flag threshold' was reduced to 2″ in the end, raster step sizes as small as 5″ were possible, which allowed highly oversampled PHT-P rasters (for example: Heinrichsen, Walker & Klaas 1998, [16]). A special raster mode was the so-called 'telescope nodding' allowing to perform a slow off-on-off-on-off-...

[3]PGA v5.3, AOT-Logic v3.4.0

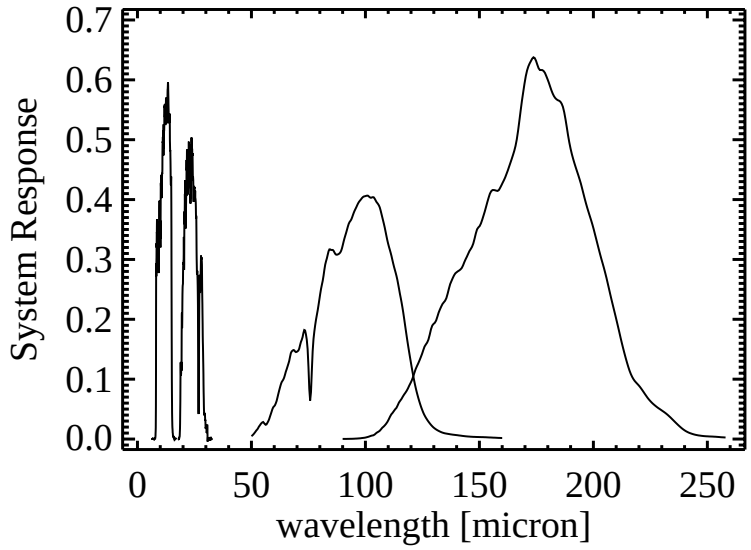

Figure 3.4: *PHT filter bandpasses: the very broad band filters for low flux detections.*

modulation similar to triangular (M= 3, 5, ...) and rectangular (M= 2) chopping. By selecting a raster step size of $0''$ in between raster legs ($\Delta N = 0'$) and more than 1 raster leg ($N > 1$) the telescope performed a nodding observation.

3.4 Absolute Photometry

This mode was mainly designed for the measurement of the absolute total sky brightness (e.g. Zodiacal Light, Galactic emission). For point sources a single measurement did not provide any information on the sky background for subtraction of the background contribution. In this case an extra measurement on the background had to be performed.

Absolute photometry was only possible in single filter mode. No chopped mode and no raster mode was possible.

Absolute fluxes were most accurately determined with a special procedure including additional control and calibration measurements not offered by the normal photometric mode. As an option the absolute photometry sequence could be started with a measurement in dark configuration in order to determine the actual dark current level and improve over the average dark current behaviour established from a set of special dark calibration measurements. Furthermore, a measurement against the cold FCS could be selected in order to determine external straylight contamination of the FCS measurement and subtract that to obtain the true zero level of the FCS calibration. The heated FCS measurement, performed after the sky measurement, was as long as the sky measurement and usually longer than 32 *sec* (in contrast to the normal mode for which a sensitivity criterion fixed the FCS exposure in most cases to 32 sec) which allowed a better stabilisation of the FCS measurement.

Note: Pre-flight the absolute mode was designed as chopping sky-FCS. The mode was completely revised during the mission, as this did not work properly.

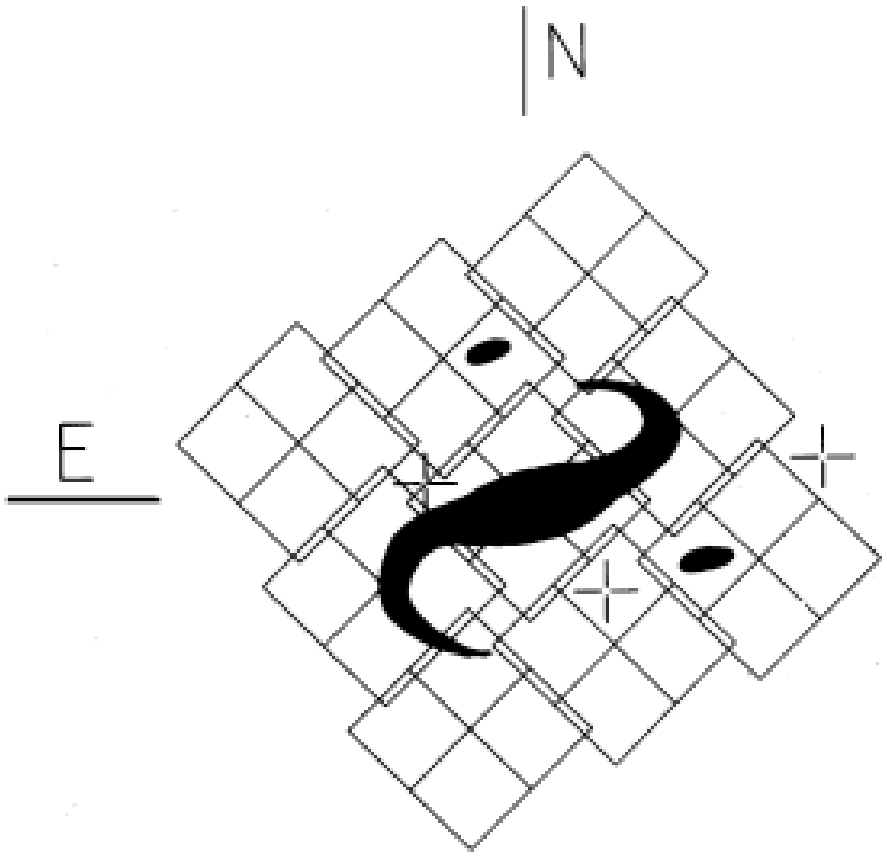

Figure 3.5: *Projection of PHT-C200 arrays, in the staring mode, on the sky for an orientation of the spacecraft y-axis non-parallel to R.A. or Dec. Note the gaps between the individual array pointings.*

3.5 Oversampled Linear Scans and Maps

These observing modes also performed observations on a regular one-dimensional grid, like rasters, but they were differential measurements. The chopper was used for oversampling between individual spacecraft positions, where chopping was performed along the scan line. This meant that all these observations were performed using the chopper and several spacecraft positions, which was in contrast to the staring raster mode. The same celestial position was observed during several raster pointings allowing for elimination of temporal changes in detector response (see Figure 3.6).

The scanning direction was parallel to the spacecraft y-axis. Its orientation with respect to equatorial coordinates depended on the date of observation and was not known before the observation was scheduled. As a fixed orientation of the scan line implied strong scheduling constraints due to a fixed observing time, a tolerance angle for the actual scan line as large as possible had to be provided.

Scans were used to obtain flux density profiles, or to observe bright sources with Nyquist sampling.

Maps were composed of a series of parallel scans which overlaped and were dedicated to observe extended sources or complex far infrared sources with the optimum spatial resolution. As in scans, chopping was only performed in scan direction, the sampling in the orthogonal direction was obtained by stepping the spacecraft in a fine mode so that the detector pixels were oversampled.

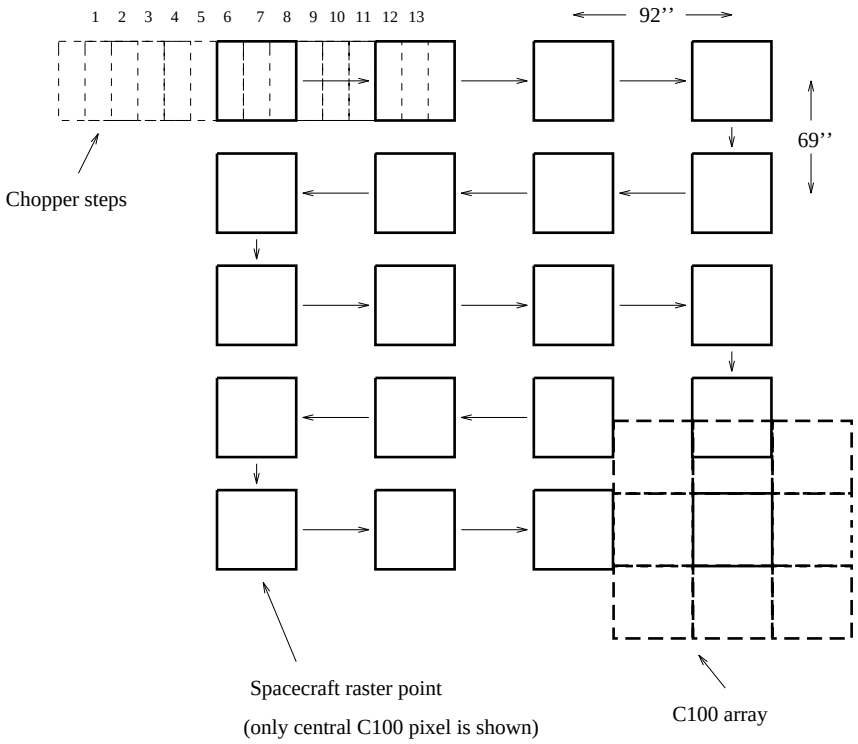

Figure 3.6: *Illustration of the PHT32 sampling procedure for the C100 array and an oversampling factor in Z direction of 2/3, i.e. a step of 3/2 pixels or half the array size. In the illustration the mapping starts at the upper-left raster point, and the sampling steps performed with the chopper (numbered 1 to 13) are indicated at that position. Note that at each spacecraft raster point only the central C100 pixel is shown.*

3.6 Sparse Maps

A special mode of mapping was sparse mapping. This was a sequence of irregularly spaced positions within an area of 3 degrees in diameter, with the first selected pointing determining the centre. Contrary to the normal mapping modes, multi-filter observations were carried out such that the complete set of requested filters was measured at each position before moving to the next position. This mode facilitated observations of a cluster of sources in a small area. As the detector remained switched-on all the time the signal stability was increased and the times for overheads were reduced. Additionally, the dynamic range of the detector was adjustable to the brightness at each individual position. It was recommended to perform the sequence such, that the total intensity increased in order to avoid strong, long lasting signal transients which usually occured when moving from a very bright spot to a faint patch.

3.7 Spectrophotometry

The spectrophotometric mode was dedicated to obtaining low resolution spectra of broad spectral features such as dust and polyaromatic hydrocarbon (PAH) features. This mode was also used for detection of faint atomic or ionic lines, but the intensity was contained in only 1 or 2 pixels, thus this did not allow the determination of the line profile. For this purpose the SWS instrument (see ISO Handbook Volume V on SWS, [34]) was recommended. For extended sources it was possible to perform spectrophotometry

in a spacecraft raster.

3.8 Polarimetry

Polarimetric observations were possible in one PHT-P (at 25 μm) and one PHT-C filter (at 170 μm). Measurements were always made for all three polarisers together with (1) a non-polarised measurement to determine the total intensity and (2) an FCS measurement for photometric calibration. At least two cycles of measurements in the three polarisers were collected in order to obtain sufficient redundancy for signal assessment. The PHT-C polarimetry was usually performed on a 2×2 raster with step size of one array pixel, so that the central map pixel of the resulting 3×3 map was seen by all 4 pixels.

3.9 Serendipity Mode

This was a specific photometric mode integrating with the C200 camera during slews in order to utilize the otherwise lost slew time between ISO's pointed observations and thus increase the overall observatory efficiency. It was not a generally selectable observation mode. Serendipity Mode was automatically activated by the Mission Planning software when a slew was longer than 30 s. For slews longer than 70 s an internal FCS measurement of 32 s was included. The filter used for Serendipity Mode was the 170 μm filter, the readout rate was fixed to a reset interval of 1/8 s.

3.10 ISOPHOT Modes of Operation

In this section summaries of the logic behind the ISOPHOT AOTs are given. Only those operations that may be relevant for data processing are mentioned. Details on the parameters to be entered by the observer are described in the *ISOPHOT Observers' Manual* by Klaas et al. 1994, [21]. For details on the filter wheel settings see Section A.1.

3.10.1 PHT-P: PHT03, PHT04, PHT05, PHT17/18/19

3.10.1.1 PHT03

PHT03 included the following operations:

1. Pointing procedure, pointing:

   - on source in case of single pointing observations except when rectangular chopped mode was requested;
   - in between the source position and the chopper position in case of rectangular chopper mode;
   - on the first raster point in case of raster maps (see below).

   PHT03 in single pointing mode:

   Repeat points 2 - 5 for all detector assemblies selected.

2. In case of detectors P2 and P3, switch on heating and wait for heating stabilisation. Activate detector.

   Repeat points 3 - 4 for each filter using the activated detector:

3. Rotate the filter and aperture wheels to the commanded configuration, optimised to instrument requirements. To minimize memory effects of the detectors the measurements with the different filter/aperture combinations were performed according to increasing power on the detector. A warning was given to the observer, if the ratio between the highest and the lowest flux on one detector for the selected filter/aperture combinations was higher than 1000. Such a flux combination within one AOT could lead to poor calibration. In order to minimize heating and cooling stabilisation times in multi-detector mode, the detectors were used in the order:

   ```
   P3 -> P1 -> P2
   ```

   The heater for P2 was switched on before measuring with P1. The start with the P3 detector was also to avoid thermal disturbances by the P2 heater on the P3 measurement.

4. Integrate on the source for the specified or calculated exposure time. A measurement was performed in staring mode or one of the three following chopped modes:

   ```
    (i) RECTANGULAR
   (ii) SAWTOOTH
  (iii) TRIANGULAR
   ```

   In staring mode the observer had to provide an appropriate reference field measurement for background subtraction, which was not part of this AOT.

5. The internal calibration was performed with the last filter/aperture combination used with the current detector. This meant that there was one FCS calibration per detector used. If the observation was in staring mode, a staring measurement on FCS1 was performed. If the sky was measured in any chopper mode, both FCS's were measured in rectangular chopped mode; FCS1 was tuned close to the [source+background] power, FCS2 close to the background power as calculated from the fluxes given by the user. After calibration, the FCSs were switched off.

6. After the last integration the heaters were switched off, the detector assemblies were set to standby and the instrument was reconfigured to the default mechanical state which was the C200 serendipity mode configuration.

PHT03 in raster mode:

For raster mode measurements, only one detector could be chosen per AOT. Filters were not changed during the raster, but rather a complete map was performed per filter. If more than one filter was selected, the map measurements were sorted according to increasing power on detector. While PHT was measuring, the spacecraft independently performed a raster map giving no feedback to PHT on the pointing progress in the raster. To synchronize the spacecraft rastering and the instrument data collection, the AOT logic calculated the total time necessary to perform a complete raster including the microslews. After the elapse of that time the integration was stopped by a 'pulse command' (a high priority interrupt to the PHT microprocessor) which also switched off all electronics including the detector heaters. After the pulse command a re-initialisation of the instrument was necessary, this was reflected in the AOT operations.

1. Pointing on the first raster point.

2. In case of a heated detector, switch on heating and wait for heating stabilisation. Activate detector.

   Repeat points 3 - 7 for each filter:

3. Rotate the filter and aperture wheels to the commanded configuration.

4. An internal calibration on FCS1 was performed in staring mode. After the calibration FCS1 was switched off.

5. Set the instrument integration time such that it covered the time needed to perform a full raster map with the specified raster point integrations requested by the user. The spacecraft was commanded to perform a raster according to the requested parameters. PHT was collecting data during the raster slews. The raster point ID and the on-target flag were recorded to reconstruct where the spacecraft was pointing.

6. After the raster had been completed the integration was halted by a pulse command. This pulse command also stopped the electronics. The detector was activated again and in case of a heated detector, a stabilisation heating time was included.

7. An internal calibration on FCS1 was performed in staring mode. After the calibration FCS1 was switched off.

8. From the last raster pointing the spacecraft moved back to the first raster pointing, in case the filter was not the last one in the selected sequence.

9. After the last integration, the heaters were switched off, the detector assemblies were set to standby and the instrument was reconfigured to the default mechanical state which was the serendipity mode configuration.

3.10.1.2 PHT04

PHT04 included the following operations:

1. Pointing procedure, pointing:

   - on source in case of single pointing observations except when rectangular chopped mode was requested;
   - in between the source position and the chopper off-position in case of rectangular chopper mode;

2. In case of a heated detector, switch on heating and wait for heating stabilisation. Activate detector.

3. Rotate filter wheel to the position of the required spectral bandpass.

   Repeat points 4 - 5 for each aperture:

4. Rotate the aperture wheel to the respective aperture configuration. Measurements were ordered with increasing power on the detector, i.e. with increasing aperture size.

5. Integrate on the source for the specified (or calculated) integration time. Measurement was performed in staring mode or one of the three following chopped modes:

   ```
     (i) RECTANGULAR
    (ii) SAWTOOTH
   (iii) TRIANGULAR
   ```

6. The internal calibration was performed with the last aperture used with the current detector. This meant that there was one FCS calibration per detector used. If the observation was in staring mode, a staring measurement on FCS1 was performed. If the sky was measured in any chopper mode, both FCSs were measured in rectangular chopped mode; FCS1 was tuned close to the [source+background] power, FCS2 close to the background power as calculated from the fluxes given by the user. After calibration, the FCSs were switched off.

7. After the last integration, the heaters were switched off, the detector assemblies were set to standby and the instrument was reconfigured to the default state.

3.10.1.3 PHT05

For the absolute photometry AOT PHT05 only one filter and one aperture could be selected. Chopped and/or raster mode was not possible.

1. Pointing on target.

2. In case of heated detector, switch on heating and wait for heating stabilisation. Activate detector.

3. If a dark measurement was requested then

   - rotate the filter and aperture wheels to the dark instrument configuration for the requested subsystem (see Table 3.1);
   - perform a dark measurement of 256 s.

4. Rotate the filter and aperture wheels to the commanded configuration.

5. If a cold FCS measurement was requested then

   - perform an internal calibration measurement of 256 s in staring mode on FCS1 with zero electrical power applied.

6. Perform the sky measurement.

7. Perform the calibration measurement in staring mode on the heated FCS1 with an measurement time equal to the sky measurement. After the calibration the FCS1 was switched off.

8. The heaters were switched off, the detector assembly was set to standby and the instrument is reconfigured to default mode.

Note that the dark instrument configuration was different for the different P detectors in order to ensure that no (stray-)light could reach the detector, see Table 3.1 for the selected filter wheel settings. The mnemonics given in the table are explained in Appendix A.1.

3.10.1.4 PHT17/18/19

PHT17 initiated the following operations:

1. Pointing on requested position.

2. In case of heated detector, switch on heating and wait for heating stabilisation. Activate detector.

   Repeat points 3 - 4 for each filter using the selected detector:

Table 3.1: *Filter wheel settings for dark measurements in AOTs.*

Detector	Wheel I mnemonic	Wheel II mnemonic	Wheel III mnemonic
P1	PHT_S	5_SEC	P3_100_UM
P2	PHT_S	5_SEC	P1_3P29_UM
P3	PHT_C_NO_POL	5_SEC	P1_11P5_UM
C100	PHT_S	C200_200_UM	P3_100_UM
C200	PHT_S	C100_50_UM	P3_100_UM
SS/SL	PHT_P_NO_POL	180_SEC	P1_7P3_UM

3. Rotate the filter and aperture wheels to the commanded configuration, optimised according to instrument requirements. To minimize memory effects of the detectors the measurements were sorted according to increasing power on the detector. The selected filters had to belong to the same detector.

4. Integrate on the source for the specified (or calculated) integration time. Measurement was performed in staring mode.

5. The internal calibration was performed in staring mode on FCS1 with the last filter of the selected detector. After the calibration, FCS1 was switched off.

6. When moving to the next pointing of the sparse map, the detector remained switched-on.

PHT18 modules were optional for a sparse map execution (a minimum combination was PHT17 and PHT19). Up to 28 PHT18 modules could be inserted into a sparse map sequence. A sequence up to 30 positions in total was measured, which could be irregularly distributed, to create a sparse map.

PHT18 initiated the following operations:

1. Pointing on requested position.

   Repeat points 2–3 for each filter using the activated detector:

2. Rotate the filter (and aperture) wheel(s) to the commanded configuration, optimised according to instrument requirements. The measurements were sorted according to increasing power on the detector.

3. Integrate on the source for the specified (or calculated) integration time.

4. The detector was not switched off in this module.

PHT19 initiated the following operations:

1. Pointing on requested position

   Repeat points 2–3 for each filter using the activated detector

2. Rotate the filter (and aperture) wheel(s) to the commanded configuration, optimised according to instrument requirements.

3. Integrate on the source for the specified (or calculated) integration time.

4. At the end of the filter sequence a calibration measurement was performed in the last filter in staring mode on FCS1.
5. The heater was switched off, detector assemblies were set to standby and the instrument was reset to the default configuration.

All measurements were performed in staring mode, thus the observer had to provide an appropriate reference field measurement for background subtraction, which was usually one or more measurements in the sequence.

Prior to PHT18, a PHT17 had to be performed in order to switch on the detector. After the last PHT18 had been done, a PHT19 was performed. Prior to a PHT19, a PHT17 had to be performed. During the whole sequence the detector remained activated, but measurements were only performed on the target positions.

3.10.2 PHT-C: PHT22, PHT25, PHT32, PHT37/38/39

3.10.2.1 PHT22

PHT22 initiated the following operations:

1. Pointing procedure, pointing:
   - on source in case of single pointing observations except when rectangular chopped mode is requested;
   - in between the source position and the chopper off-position in case of rectangular chopper mode;
   - on the first raster point in case of raster maps

   PHT22 in single pointing mode:

   Repeat points 2 - 5 for all detector assemblies selected:
2. Switch on heating and wait for heating stabilisation in case C100 was used. Activate detector.

   Repeat points 3 - 4 for each filter using the activated detector:
3. Rotate the filter wheel to the commanded configuration, optimised according to instrument requirements. If filters of both C100 and C200 were requested, detectors were operated in the following order:

   ```
   C200 -> C100
   ```

   To minimize memory effects of the detectors the measurements per detector were performed according to increasing power on the detector.
4. Integrate on the source for the specified (or calculated) integration time. The measurement was performed in staring mode or chopped mode. If only filters of the C100 filter set were selected, one of the three following chopped modes was possible:

   ```
     (i) RECTANGULAR
    (ii) SAWTOOTH
   (iii) TRIANGULAR
   ```

If at least one filter of the C200 filter set was selected, the chopper mode was automatically restricted to RECTANGULAR chopping with 180″ throw. In staring mode the observer had to provide an appropriate reference field measurement for background subtraction which was not part of this AOT.

5. The internal calibration was performed with the last filter used with the current detector. This meant that there was one FCS calibration per detector used. If the observation was in staring mode a staring measurement on FCS1 was performed. If the sky was measured in any chopper mode, both FCSs were measured in rectangular chopped mode; FCS1 was tuned close to the [source+background] power, FCS2 close to the background power as calculated from the fluxes given by the user. After calibration, the FCSs were switched off.

6. After the last integration, the heater was switched off, the detector assemblies were set to standby and the instrument was reconfigured to the default configuration.

PHT22 in raster mode (restricted to filter sets belonging to either C100 or C200):

The procedure was identical to the raster logic presented for PHT03.

3.10.2.2 PHT25

See description of PHT05. The available detectors were C100 and C200 for which C100 needed heating. The cold FCS measurement time in the case of C200 was 128 s instead of 256 s.

3.10.2.3 PHT32

PHT32 initiated the following operations:

1. Pointing on the first raster point

2. Activate either PHT C100 or C200 depending on selection of filters and wait for stabilisation of the detector in case C100 had been selected.

   Repeat steps 3-7 for all filters:

3. Rotate the filter wheel to the commanded filter position.

4. An FCS1 calibration measurement was performed in staring mode.

5. Set the instrument integration time such that it covered the time needed to perform a full raster map with the specified raster point integrations requested by the user. The spacecraft was commanded to perform a raster according to the requested parameters. On each raster position a number of chopper sweeps were performed. PHT was collecting data also during the raster slews.

6. After the raster had been completed the integration was halted by a pulse command (see PHT03 raster description). This pulse command also switched off the electronics. The detector was activated again and in case of a heated detector, a stabilisation heating time was included.

7. The map was concluded by a repetition of an FCS1 calibration measurement in the filter used for the preceding map at the last raster position.

8. From the last raster pointing the spacecraft moved back to the first raster pointing, in case the filter was not the last one in the selected sequence.

9. After the sequence in the last filter, the heater was switched off, detector assemblies were set to standby and the instrument was reconfigured to the default configuration.

Note: For AOT PHT32 the chopper was indirectly commanded depending on the detector (C100 or C200) chosen. In the case of C100 the chopper was commanded to perform in sawtooth mode 13 chopper steps with 15″ separation symmetrically with respect to the centre field of view. When C200 had been chosen, the chopper was commanded to perform in sawtooth mode 7 chopper steps with 30″ separation.

3.10.2.4 PHT37/38/39

The PHT37 AOT was the first AOT in the concatenated sequence PHT37, [PHT38], PHT39 which formed the PHT-C sparse map. It initiated the following

operations:

1. Pointing on requested position.
2. For C100 switch on heating and wait for heating stabilisation. Activate detector.

   Repeat points 3 - 4 for each filter using the activated detector:

3. Rotate the filter wheel to the commanded configuration, optimised according to instrument requirements. To minimize memory effects of the detectors the measurements were sorted by increasing power on the detector.
4. Integrate on source for the specified (or calculated) integration time. Measurement was performed in staring mode.
5. Perform calibration in staring mode on FCS1 with the last filter of the selected detector. After the calibration, FCS1 was switched off.
6. When moving to the next pointing of the sparse map, the detector remained switched on.

PHT38 initiated the following operations:

PHT38 modules were optional for a sparse map execution. Up to 28 PHT38 modules could be inserted into a sparse map sequence.

1. Pointing on requested position.

   Repeat points 2–3 for each filter using the activated detector:

2. Rotate the filter wheel to the commanded configuration, optimised according to instrument requirements. To minimize memory effects of the detectors the measurements were sorted by increasing power on the detector.
3. Integrate on the source for the specified (or calculated) integration time.
4. The detector was not switched off in this module.

PHT39 was the last AOT in the concatenated sequence PHT37, [PHT38], PHT39 which formed the sparse map. It initiated the following operations:

1. Pointing on requested position:

   Repeat points 2–3 for each filter using the activated detector:

2. Rotate the filter wheel to the commanded configuration, optimised according to instrument requirements. To minimize memory effects of the detectors the measurements were sorted by increasing power on the detector.

3. Integrate on source for the specified (or calculated) integration time. Measurement was performed in the staring mode, thus the observer had to provide an appropriate reference field measurement for background subtraction, which was usually one or more positions in the sequence.

4. Perform calibration measurement in staring mode on FCS1.

5. Switch off heaters, switch detector assemblies to standby and reset instrument to default configuration.

The minimum number of sparse map modules was two: one PHT37 followed by one PHT39.

3.10.3 PHT-S: PHT40

PHT40 initiated the following operations:
PHT40 in single pointing mode:

1. Pointing procedure, pointing:

   - on source in case of single pointing observations except when rectangular chopped mode was requested;
   - in between the source position and the chopper off-position in case of rectangular chopper mode;
   - on the first raster point in case of raster mapping.

2. Activate detectors.

3. Rotate wheels to configure DARK configuration for PHT-S (see Table 3.1).

4. Integrate in dark position for the specified dark current measurement time of 32 s. Measurement was performed in staring mode.

5. Rotate wheels to configure beam path to PHT-S.

6. Integrate on the source for the specified (or calculated) integration time. Measurement was performed in staring mode or one of the three following chopped modes:

```
  (i) RECTANGULAR
 (ii) SAWTOOTH
(iii) TRIANGULAR
```

7. After the integration the detector assemblies were set to standby and the instrument was reconfigured to the default mechanical set up.

PHT40 in raster mode:

Start with points 2– 6 at first raster position. Set the integration time such that it was longer than the time to perform the requested raster map. Perform point 6 in staring mode. After the raster had been completed the integration was halted by a pulse command (see PHT03 raster description). The instrument was measuring during micro-slews. Proceed with point 7.

3.10.4 Polarisation observations: PHT50, PHT51

3.10.4.1 PHT50

For PHT50 only the 25 μm filter could be used in combination with the 79″ aperture. The logic rounded the requested integration time per polariser to the nearest higher multiple of 128 s with a minimum of 256 s. A description of the CHW1 (change wheel I) positions is given in Section A.1.4. PHT50 initiated the following operations:

1. Pointing on target.
2. Switch on heating, wait for heating stabilisation, and activate P2.
3. Rotate the filter wheel to P_25 and aperture wheel to 79″.
   Repeat steps 4–6 to accumulate the requested integration time per polariser:
4. Rotate CHW1 to PHT-P polariser 1 (0°) and perform measurement of 128 s.
5. Rotate CHW1 to PHT-P polariser 2 (120°) and perform measurement of 128 s.
6. Rotate CHW1 to PHT-P polariser 3 (240°) and perform measurement of 128 s.
7. Rotate CHW1 to PHT-P polariser 1 (0°) and perform measurement of 128 s. This closed the polariser sequence with the start configuration allowing to assess long term detector drifts.
8. Rotate CHW1 to PHT-P 'no polariser' position and perform a sky measurement of 128 s.
9. Perform the calibration measurement in staring mode on the heated FCS1 with a measurement time of 128 s. After the calibration the FCS1 was switched off.
10. The heater was switched off, the P2 assembly was set to standby and the instrument was reconfigured to default mechanical set-up.

3.10.4.2 PHT51

For PHT51 only the C200 detector array in the 170 μm filter set-up could be used. The logic rounded the requested integration time per polariser to the nearest higher multiple of 128 s with a minimum of 256 s. A description of the first filter wheel (CHW1) positions is given in Section A.1.4. PHT51 initiated the following operations:

1. Pointing on target.
2. Activate the C200 detector.
3. Rotate the filterwheel 2 to C_160.
   repeat steps 4–6 to accumulate the requested integration time per polariser:
4. Rotate CHW1 to PHT-C polariser 1 (0°) and perform measurement of 128 s.
5. Rotate CHW1 to PHT-C polariser 2 (120°) and perform measurement of 128 s.
6. Rotate CHW1 to PHT-C polariser 3 (240°) and perform measurement of 128 s.
7. Rotate CHW1 to PHT-C 'no polariser' position and perform a sky measurement of 128 s.
8. Perform the calibration measurement in staring mode on the heated FCS1 with a measurement time of 128 s. After the calibration the FCS1 was switched off.

9. The C200 assembly was set to standby and the instrument was reconfigured to default mechanical set-up.

In many cases the full sequence was repeated in a 2×2 raster map with 1 pixel displacement and the source centred on each pixel. This yielded a 4-fold redundancy for the central position of the resulting 3×3 raster map. This method gave the highest source-to-background contrast and provided a consistency check from the results of the 4 individual pixels.

Chapter 4

Instrumental Characteristics

4.1 Overview

The ISOPHOT data processing contains several corrections due to the properties of the detector, due to instrumental effects by electronics and optics, and due to external effects such as cosmic ray bombardments. In this chapter the effects are described that could lead to a better understanding of the data and of the photometric calibration. The descriptions start with the detectors and their properties in Section 4.2, the features generated by the instrument electronics in Section 4.3, and ionising radiation effects in Section 4.4, which have a dramatic impact on the detector output. Subsequently the optical (Section 4.5), spectral (Section 4.6), and straylight performance (Section 4.7) are discussed. Finally, we mention the instrumental polarisation (Section 4.8) and the influence of the background on the photometric data (Section 4.9).

4.2 Detector Properties

4.2.1 Detector responsivity

All ISOPHOT detectors are photoconductors. Therefore, the crucial calibration measure is the photocurrent generated by the incident infrared photons. A detector is characterised by the *detector responsivity* R_{det} which is the ratio of the photocurrent I and the in-band power P_{src}:

$$R_{det} = \frac{I}{P_{src}} \qquad [\mathrm{A/W}]. \tag{4.1}$$

In the first stage of data collection the output voltage of an integrating amplifier is measured. From these data the *signal* or voltage increase per unit time is obtained, see Section 2.4.2. The in-band power can be derived from signal and responsivity, if the capacitance of the integration capacitor, C_{int}, is known:

$$P_{src} = \frac{C_{int} s_{src}}{R_{det}} \qquad [\mathrm{W}], \tag{4.2}$$

where s_{src} is the source signal in V/s. The value for C_{int} depends on the detector used and is assumed to be constant throughout the mission. R_{det}, however, is not a constant and can depend on external parameters such as the strength of the ionising radiation and flux history.

In principle, fine calibration source (FCS) measurements scheduled in all PHT-P and PHT-C AOTs should ensure that P_{src} can directly be obtained from the comparison between the sky and the FCS signal without knowledge of the exact value of R_{det}.

FCS measurements are obtained in all ISOPHOT AOTs, except PHT40. However, for some observations the FCS measurements can be of insufficient quality, or, completely absent due to technical problems (e.g. telemetry failure). In such cases a default responsivity should be adopted.

The default detector responsivities were derived during the in-orbit calibration. The values of the default responsivities are provided in Cal-G files, see Section 14.13. The relationships between FCS heating power and the corresponding in-band power measured by the different detectors are also given in Cal-G files.

The above description of the detector responsivity is still idealised and is only valid for responsivity values averaged over time scales longer than the measurement time. On shorter time scales the responsivity can still vary. The stability of the responsivity depends on the radiation history including the history of ionisation radiation. Detailed descriptions of the most important phenomena are presented in the next sections.

In case of a PHT-S observation with AOT PHT40 no FCS measurement is performed (see Section 2.7). The PHT-S signals are directly converted to flux densities. The Cal-G files containing the conversion factors for each PHT-S pixel are described in Section 14.19. The conversion factors for each pixel have been derived from the signals of several calibration stars.

4.2.2 Signal non-linearities

A detector is linear, if the photocurrent and hence the resulting output signal is proportional to the incident flux, i.e. the corresponding in-band power. Deviations from linearity introduce a bias when deriving the responsivity from the FCS measurement or when using a single (default) value for R_{det}. To avoid this bias the FCS signal is tuned close to the source signal by the AOT logic. This strategy may fail in the following cases:

- multi-aperture photometry,
- multi-filter photometry with the same detector on sources with a strong spectral gradient or a mixture of narrow and wide bands,
- maps and scans for which the source-to-background contrast is high.

In these cases a wide range of signals is produced during the sky measurements, whereas the calibration is performed by one or more FCS measurements yielding a single signal level at the maximum or mean of the range.

In-orbit calibration observations showed that the detector responsivity depends on the infrared flux falling on the detector. The responsivity R_{det} is a function of the photocurrent or signal $s = s_{src} + s_{bck}$ which consists of a source (s_{src}) and background (s_{bck}) component. Following Equation 4.2, the responsivity of the detector when it is pointed at the position of the source can be written:

$$R(s_{src} + s_{bck}) = \frac{(s_{src} + s_{bck})C_{int}}{P_{src} + \frac{s_{bck}C_{int}}{R(s_{bck})}} \qquad [\mathrm{W/A}] \tag{4.3}$$

In practice, $R(s_{src}+s_{bck})$ and $R(s_{bck})$ are not necessarily equal and the ratio between the signals measured on- and off-source is different from the respective in-band powers. The discrepancy is larger if very different source and background signals are compared, like for the cases listed above.

For the ISOPHOT photometric calibration a linear system is obtained by linearising the detector signals, s, according to:

$$s' = H(s) \qquad [\mathrm{V/s}]. \tag{4.4}$$

The condition for H is that s' inserted in $R(s') = s'C_{int}/P$ yields a constant responsivity, see also Section 5.2.2 for more details on the correction.

4.2.3 Transient behaviour after flux change

After an illumination change, the output signal of a PHT detector shows a systematic drift in time. Such a drift effect is also referred to as a detector *transient*. A common feature to all transient curves is the asymptotic approximation to a stable level. This typical slow response is due to the presence of low ohmic contact material necessary to connect the detector substrate with the metallic wires.

Typical drift curves are presented in Figure 4.1. In case of a flux drop, a signal decay and in case of increasing flux steps a signal rise (Figure 4.1) is observed. The doped silicon detectors (SS, SL, P1, and P2) exhibit a *hook response* during the first 40 seconds after large positive flux steps (Figure 4.1b). The signal shows a behaviour similar to a strongly damped oscillation around the asymptotic level. For even higher flux steps the signal behaviour can be restricted to an overshoot followed by a slow decay.

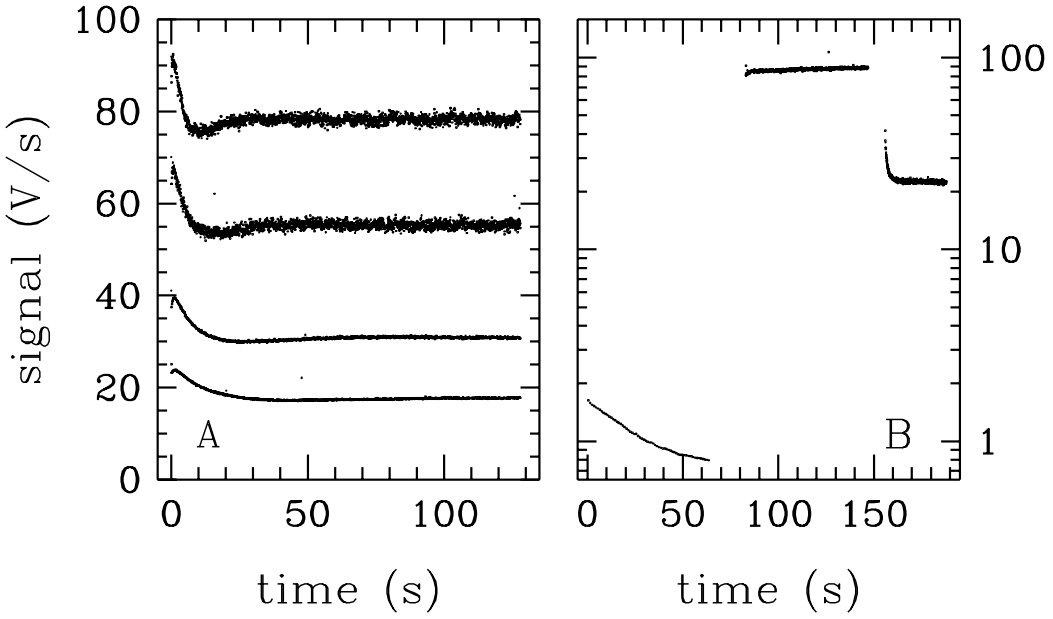

Figure 4.1: *Examples of P1 detector transients. Left panel (A): 4 transient curves after a flux step overplotted in the same graph for comparison, the highest curve corresponds to the largest positive flux step. In all cases the signal prior to each step was the same and had a strength of about 35 V/s. For these flux steps a signal overshoot is detected followed by a strongly damped oscillation. Right panel (B): multi-filter observation of the star HR6705, filter sequence P_16 (64 s integration), P_3.6 (64 s) followed by the P_3.6 (32 s) FCS measurement. Both the P_16 as well as the P_3.6 FCS measurement show a downward drift, with a longer stabilisation time for the fainter P_16 signal.*

The characteristic stabilisation time scales depend on (1) the detector material, (2) the flux change, (3) the illumination level, and (4) the temperature of the detector. They vary from a few seconds up to several minutes.

Typical time scales for stabilisation after a given flux step for the PHT-SS/SL detectors are presented in Table 4.1. These time scales can be taken as approximate values for detector P2 and lower limits for P1. The stabilisation time is defined as the time after a flux step to reach 90% of the signal at $t = \infty$ (S_∞).

Note that a signal of 0.5 mV/s is very close to the dark signal and - in practice - cannot be determined accurately. The relative stabilisation time is faster for positive flux steps - see Table 4.1 values below the diagonal versus those above the diagonal. Flux steps at low flux levels will take more time to stabilise. However, in such cases the S/N and the detector stability (see next section) might be more important.

The doped germanium detectors P3 and C100 tend to stabilise faster than the doped silicon detectors. C200 shows the shortest transient time scales. Typical time scales are 100 s for P3 and C100 and 40 s for C200, respectively.

Table 4.1: *Stabilisation times for a given flux step in seconds. The first row lists the initial signal, the first column the final signal in V/s.*

	$5\ 10^{-4}$	0.001	0.01	0.1	1	10
$5\ 10^{-4}$	...	6800	11500	11880	11900	11900
0.001	4070	...	5570	5900	5960	5960
0.01	1500	1220	...	560	592	595
0.1	240	210	122	...	55	59
1	32	30	21	12	...	5
10	4	4	3	2	1	...

For chopped measurements the same drift behaviour description applies. Due to the chopper modulation, the signal evolution on each chopper plateau can be regarded as a drift curve after a flux step. Consequently, the difference signal between the on- and off-target chopper plateaux is not only a function of flux step, but also a function of chopper frequency. Without applying drift corrections use of the difference signal seriously underestimates the actual flux of the target. It has been observed that the signal differences between neighbouring chopper plateaux remain stable, even in case of a measurement containing a general drift (see Section 4.2.4), provided that the flux difference between the chopper plateaux is less than 50% of the total signal. An example of a chopped measurement with P2 is presented in Figure 4.2.

PHT32 uses the chopper in the sawtooth mode to obtain oversampled maps. Detector transients of bright sources can introduce ghost images in neighbouring areas. This happens when a bright source was observed at the end of a sawtooth sweep. When the chopper mirror was directed back to the starting point of the sweep, the transient caused an increased signal which was recorded at the beginning of the next chopper sweep. The signal decays with the relevant time scale thereby mimicing a point source detection. Consequently, the ghost is always displaced from the bright source by $180''$ (=amplitude of the chopper sweep) in Y-direction.

The study of transients led to the development of a PHT AOT logic which should minimise disturbing effects by detector transients:

1. in multi-filter observations the measurements for a given detector were sorted according to increasing power on the detector (see Section 3.10).

2. in multi-aperture photometry PHT04 the measurements were arranged according to increasing aperture size.

3. the absolute photometry AOTs PHT05 and PHT25 comprised relatively long (64 to 128 s) staring measurements in order to ensure a stable signal at the end of each measurement.

4. each PHT-S observation (PHT40) started with a dark signal measurement to assess the presence of possible transients still present from a previous observation of a bright target.

5. telescope nodding was made available to achieve repeated quasi-staring observations between target and one or more background positions. Nodding was suitable for photometry of relatively bright targets for which the high frequency of the chopper would have caused serious transient effects. The nodding mode was in essence PHT03/PHT22/PHT40 raster mode for which the step in spacecraft Z-direction was set to $0''$.

Not every measurement lasted long enough to provide a stabilised signal. Laboratory and in-flight measurements showed that the transient curves were reproducible under the same flux conditions. Methods to correct for these transient drifts based on physical models as well as on empirical results have been developed.

A description of detector transients tested against the doped silicon detectors of PHT-S can be found in Schubert et al. 1995, [49]. C200 detector transients have been studied by Wilke 1995, [56]. A study of in-orbit transients and descriptions of correction methods and practical recipes are presented in Acosta-Pulido, Gabriel & Castañeda 2000, [3].

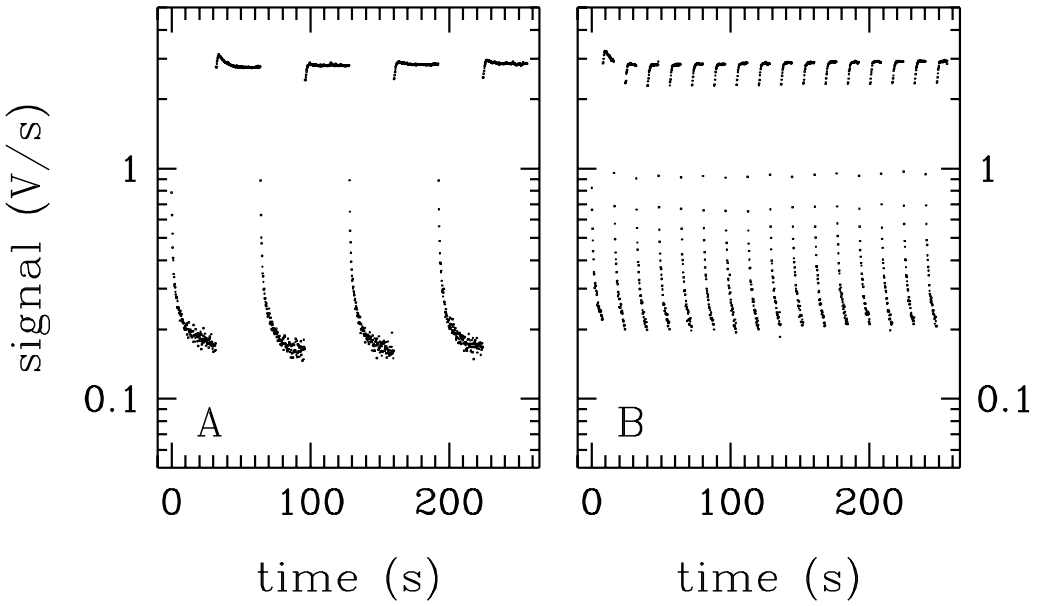

Figure 4.2: *Examples of P2 detector transients induced by the chopper modulation on a very high source-background contrast. Left panel (A): slow (32 s per chopper plateau) chopped measurement on a high source-background contrast. Right panel (B) same source-background contrast as under (A) but with a a higher chopper frequency (8 s per plateau). Note the strong overshoot in the first higher plateau; a straight signal average per chopper plateau would underestimate the background subtracted source signal in both cases.*

In OLP no sophisticated treatment of transients is applied. Instead, an algorithm is used which determines per chopper plateau whether a significant signal drift is present. In case such a drift is found, the last stable part of a chopper plateau is used (see also Section 7.3.5).

An alternative correction method is to perform the calibration measurement in the same way as the astronomical measurement of the unknown source and on a celestial standard of similar brightness. Then, the transients which show the same time scale and amplitude for both measurements cancel out in the calibration process. This method is succesfully applied for both chopped and staring PHT-S measurements.

4.2.4 Drift behaviour of responsivity

Besides the transient behaviour, the responsivity of a detector can vary or *drift* on time scales ranging from less than one hour up to the entire science window of 16 hours (see 'ISO Handbook, Vol. I: ISO – Mission & Satellite Overview', [20]). Responsivity drifts are mainly observed for the doped germanium

detectors (P3, C100 and C200) and are a result of both the illumination history of the detector as well as the rate of ionising radiation falling on the detector, see also Section 4.4.

Ionising radiation causes the detector responsivity to *increase* with time. This increase can be as high as 80%, 100% and 30% for P3, C100, and C200, respectively. The responsivity drift for these detectors is steeper at the end of the science window where the amount of ionising radiation rapidly increased. Long integrations with the same detector can be affected by this effect. Examples are multi-filter photometry with PHT22 and multi-aperture photometry with P3 in PHT04. For large (raster) maps available in AOTs PHT03, PHT22, PHT32, and in the sparse map modes PHT17/18/19 and PHT37/38/39, the responsivity drift can be assessed from the two FCS measurements collected at the beginning and end of each map. For polarisation observations the polarisers are cycled with a cycle time of 128 s per polariser to assess the long term stability of the detector during the observation.

On the other hand, very high flux levels in excess of 5 V/s for P3 and C100, and 10 V/s for C200 can cause a curing of the detector during the measurement (see also Section 4.2.5). The resulting effect is a *decrease* of the detector responsivity during the measurement. This decrease can amount to several percent up to a factor 1.5 of the initial responsivity. Such drifts are very difficult to correct for.

The observed responsivity drifts for the doped silicon detectors P1, P2 and PHT-SS/SL are less than 20% over the entire science window.

4.2.5 Curing procedures

Due to the high ionising radiation doses during perigee passage of ISO the responsivities and noise levels of the ISOPHOT detectors were strongly increased before the beginning of the new science window. Therefore, appropriate *curing procedures* were designed for the different detectors to restore the nominal responsivities. The procedures were applied after the switch-on of the instrument, before the beginning of the science window.

For the doped germanium detectors (P3, C100 and C200) a combination of bias boost (absolute increase of the bias voltage) and two to three infrared flashes using one of the FCSs were applied. For the doped silicon detectors (SS, SL, P1, and P2) curing was achieved by exposing the detector to a higher temperature at a reduced bias voltage for a defined period of time. In addition, P1 underwent an infrared flash curing.

The doped germanium detectors were much more susceptible to drifts caused by accumulating effects of the high energy radiation impacts (Section 4.4). In order to keep their responsivities within the nominal range a second curing procedure was applied around apogee passage in the handover window, when the satellite control was switched from VILSPA (Madrid) to Goldstone (California) (see 'ISO Handbook, Vol. I: ISO – Mission & Satellite Overview', [20]). More about the effects of ionising radiation inside the science window is described in Section 4.4.

Trend analysis of responsivity measurements performed immediately after the curing procedures indicates that the nominal responsivities are re-established with ±2% accuracy for all detectors, if the space environment conditions are stable.

The doped silicon detectors are not very sensitive to geomagnetic storms. The responsivity variations for PHT-SS, SL, P1, and P2 are presented in Figure 4.3. It shows that the responsivity could be restored to better than 2% of the mean value. A long term variation can be noticed which is possibly correlated with the position of the ISO orbit with respect to the asymmetric magnetic field of the Earth.

The doped germanium detectors are more sensitive to the space environment with variations in responsivity between 20-50% during geomagnetic storms. A striking illustration is given in Figure 4.3 where the P3, C100 and C200 responsivity variations over most of the ISO mission are shown. The detector responsivity peaks can last for several revolutions. They are correlated in time with the geomagnetic storm activity induced by solar flares.

An overview of the correlations between ISOPHOT detector responsivities and space weather parameters is presented in Castañeda and Klaas 2000, [5].

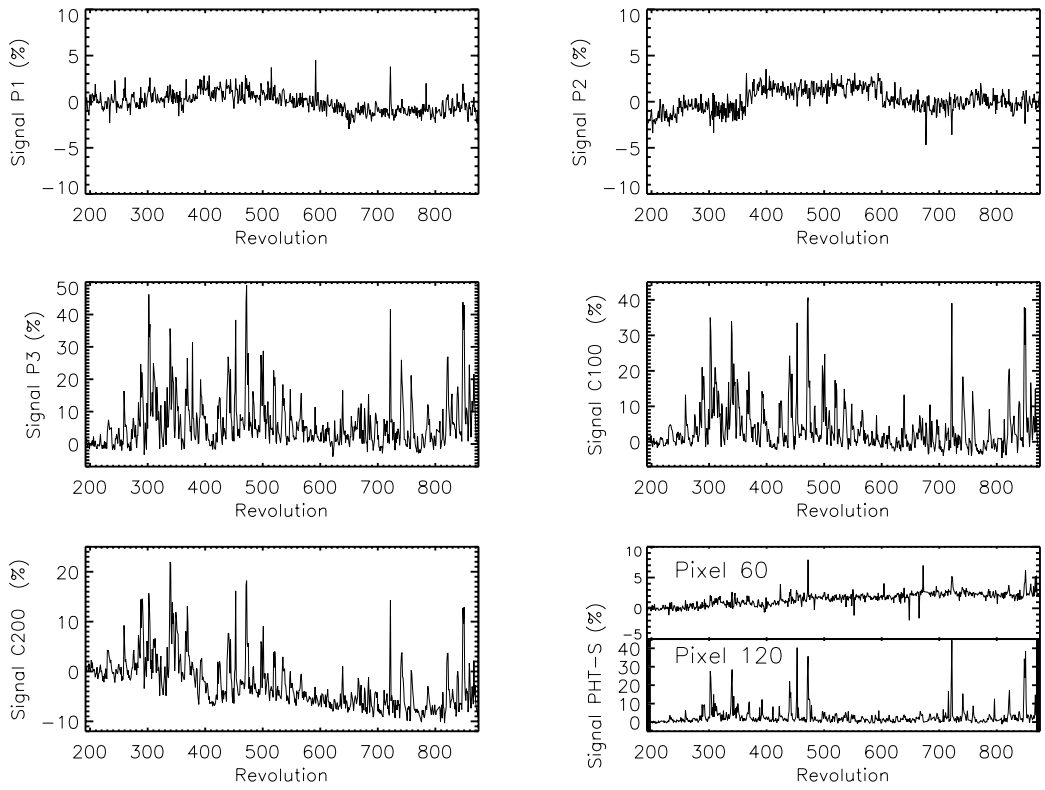

Figure 4.3: *The results of the responsivity checks during instrument activation (AOT PHT83). From top to bottom, left to right, are the detectors: P1, P2, P3, C100 (average of 9 pixels), and C200 (average of 4 pixels), PHT-S pixel 120 (SL) and pixel 60 (SS, dashed). All the data are represented as relative change from an adopted mean; for the P1 and P2 detectors the mean is the average signal during the mission; for P3, C100, and C200, and PHT-S the reference is the mean signal for revolutions 192–212, a period of stable space weather (taken from [5]).*

4.2.6 Dark signal and noise

Dark current in the detector assembly adds a spurious *dark signal* to the source signal. Dark signals for the different detectors have been measured by means of dedicated observations in the dark instrument configuration (c.f. Table 3.1). These observations have been collected frequently throughout the mission and distributed over the science window. The in-orbit dark signals were found to be several factors higher than expected from pre-flight data. For all detectors except P3, the dark signals increased by a factor 2-3. For P3 the dark signal is up by a factor $\leq$50. The increase is attributed to the effects of ionising radiation on the detectors.

The typical equivalent fluxes to dark signals for a number of detector/filter combinations are listed in Table 4.2. A flat spectrum (νF_ν = Constant) is assumed in the derivation of the dark flux values. In case one would like to know the typical dark flux for a different filter of the same detector one should multiply the values in the table with the factor C1(table_filter)/C1(new_filter) where C1 is the transmission parameter described in Section 5.2.5. The values in Table 4.2 were derived by assuming default responsivities for the detectors (given in Section 14.13). Note that pixel 6 of the C100 array shows a factor 3-7 higher dark signal than the other pixels in the C100 array.

The pixels of the PHT-S arrays have dark signals that show systematic variations with wavelength

Table 4.2: *Dark signal equivalent fluxes.*

Detector ID	Filter ID	Dark Flux [mJy]
P1	P_11p5	41
P2	P_25	410
P3	P_60	48
C100(1)	C_100	55
C100(2)	C_100	116
C100(3)	C_100	81
C100(4)	C_100	50
C100(5)	C_100	100
C100(6)	C_100	395
C100(7)	C_100	48
C100(8)	C_100	56
C100(9)	C_100	95
C200(1)	C_160	34
C200(2)	C_160	36
C200(3)	C_160	27
C200(4)	C_160	35

(see Figure 4.4). Improper dark signal subtraction could cause the presence of spurious features in the spectrum. The dark signals for a number of PHT-SS detectors can be negative, this is not due to a negative dark current but due to a CRE effect, see also Figure 4.4. The equivalent flux to the dark signal in PHT-SL is typically 50 mJy for pixel 65 up to 250 mJy for pixel 128. For more details about the PHT-S characteristics, see Klaas et al. 1997, [23].

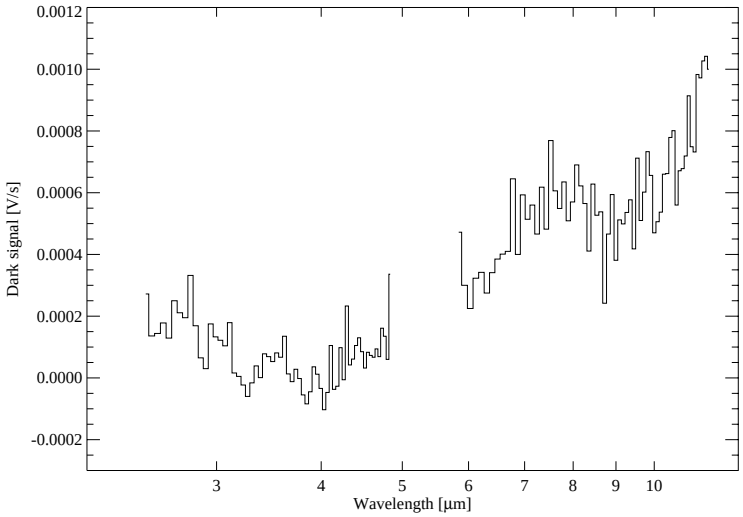

Figure 4.4: *Dark signals for both the PHT-SS and SL channels.*

Trend analysis of dark calibration observations shows for all detectors a systematic variation as a function of orbital position. The dark signal for P2, C100 and C200 gradually rises by a few percent per hour, accumulating to nearly a factor of two towards the end of the revolution. Around 18 hours after perigee, in the last few hours of the science window, the dark signal steeply increases for all detectors except for P2. This effect was caused by the rapidly increasing amount of ionising radiation at the end of the science window. The germanium doped detectors (P3, C100 and C200) exhibit the largest increase of up to a factor 2–3. The dark signals for PHT–SL long wavelength pixels show a relatively high level at the beginning of the science window which is decreasing within the first few hours. This results from a memory of the bright illumination of SL during the responsivity check after curing in order to verify the proper performance of both S–arrays. Dark signal corrections depending on orbital position are available since OLP Version 7.

The dark signals can be higher for all detectors during a geomagnetic storm. If there are suspicions about the impact of *space weather* on the quality of an observation, it is advised to check the planetary 'K-index'. This parameter is strongly correlated with the space weather conditions. If 48 hours before a given measurement or on the same day the K-index is larger than or equal to 4, it is possible that the measurement has been affected by the space weather. Tables of the K-index during the ISO mission are made available in the ISO Data Archive, see also Castañeda & Klaas 2000, [5].

For differential observations the dark signal cancels out, if the observations were taken close in time (< 1 hour). Possible uncertainties in the target signal caused by the dark signal are in such cases automatically removed. For absolute photometry measurements, in which the total sky flux must be determined, the dark signal contribution can be important. These observing modes (PHT05 and PHT25) offered the possibility to include a dedicated dark signal measurement.

All standard observations with PHT-S (AOT PHT40) are preceded by a 32 s measurement in dark instrument configuration. This 'pseudo dark' measurement cannot be used to subtract PHT-S dark signals, but offers the possibility to assess remaining detector transients from an earlier PHT-S observation, see Section 5.6.7.

Average dark signal values per orbital phase, obtained from many calibration observations are stored in a Cal-G file (see Section 14.7). These values are used to remove the dark signal from each measurement during SPD level processing.

4.2.7 Detector flat-fields

The pixels of the C100 and C200 arrays can be regarded as a number of individual detectors with their own responsivities. The detector *flat-field* gives the relative variation of the responsivites among the pixels with respect to the average responsivity over the array. The flat-fields measured in-orbit were found to be wavelength dependent. Therefore, for each C-detector/filter combination a separate flat-field is necessary.

For those observations where the associated FCS measurement is done with the same filter, the flat-field correction is included in the responsivity values derived from the FCS measurements after correction for illumination variations (see Section 4.5.4). However, observations with different filters compared to the FCS measurement need additional correction for the wavelength dependence of the flat-field. See also Section 7.10.4.

4.2.8 Detector saturation

This effect must not be confused with saturation of the readout electronics due to a wrong flux-estimate. The ISOPHOT detectors were specified for a certain flux range and laboratory measurements with replicas of the flight detectors demonstrated that up to 5×10^{-10} W could be imposed onto the detectors. Nevertheless, a few celestial sources like IRC+10216, 07 Car, VY CMa and Jupiter could have imposed higher powers onto the detectors in some bandpasses or pixel ranges of P1 and PHT-S. As there was

the potential danger that flooding these detectors with such a high photon rate could have led to a detector breakthrough with the detector becoming low ohmic, these targets were blocked for scheduling observations with P1 and PHT-S. Low ohmic detectors with a high bias voltage would have produced high currents onto the entrance of the sensitive readout electronics-multiplexer chain and would have irreversibly damaged them.

4.3 Features due to Electronics

4.3.1 Anomalous first readouts on a ramp

The CRE output voltage of the first few readouts on a ramp does not follow a linear increase in time but can remain constant or even show a decrease in voltage. The effect becomes more pronounced in case only a small fraction of the CRE dynamic range is used. This can happen in observations where the source + background flux was severely overestimated by the observer or in the low brightness regions of maps with high dynamic range.

To exclude this non-linear part of a ramp, the first fraction of the total number of non-destructive readouts is discarded in the SPD processing. The value of the fraction is stored in a dedicated calibration file (see Section 14.4)

4.3.2 CRE (ramp) linearity

Integration ramps are not exactly linear but exhibit higher order variations or in some cases 'knees' which are caused by the CRE. The deviations from linearity only depend on the absolute value of the CRE output voltage and not on e.g. the slope of the ramp (see Schulz 1993, [50]). Non-linearities can cause systematic errors up to 50% when comparing signals from the same source using ramps with different dynamic range in CRE voltage. This effect introduces an error in the flux calibration in case the FCS readouts span a different dynamic range than the source readouts. Improper correction for ramp non-linearities can also cause serious systematic brightness errors in maps with high dynamic range between background level and target. In addition, ramp non-linearities introduce a larger formal uncertainty in the signal when deriving a signal value by fitting a straight line through the ramps.

The deviations from linearity for all detectors except for PHT-SS and SL have been determined with respect to a standard linear ramp which was constructed from a stack of several thousand individual ramps. An example of the resulting deviations is presented in Figure 4.5.

In the SPD processing the CRE output voltage for each readout is corrected before deriving the signals. Calibration tables for the P, C100, and C200 detectors have been created containing CRE output voltages and the corresponding voltage corrections. These calibration tables are stored in Cal-G files (see Section 14.5).

Non-linearities in the CRE output of PHT-SS/SL data are not corrected for. Due to the selected calibration scheme for this detector where a standard source is chosen as close as possible to the output signal, the uncertainty imposed by this effect should be negligible.

4.3.3 Signal dependence on reset interval

Measurements of a given target obtained with the same detector/filter/aperture combination but with different readout timing (ROT) parameters showed that the signal depends on the commanded reset interval (see Section 2.4.4). For a constant detector illumination the signal level varies systematically from one reset interval to the other. The systematic variations are probably caused by the detector CRE (Section 2.4.2) while switching between different reset interval times.

For C100 and C200 these variations are of the order of 10–20% between measurements which differ in reset interval by a factor of 2. For reset intervals a factor of 8 apart the signal difference can be as large

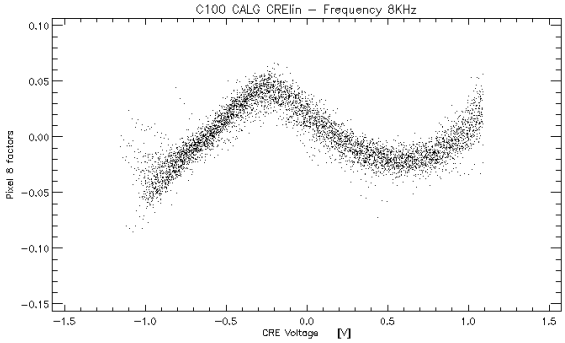

Figure 4.5: *Example of non-linear CRE output voltages for detector C100 pixel 8. Plotted are the deviations from a standard linear ramp as a function of CRE output voltage for a large number of in-orbit measured ramps that span the full CRE output voltage range. The mean relationship has been used in the corresponding Cal-G table.*

as 40%. P1, P2 and P3 show less variations. For the detectors of PHT-S the situation has not been investigated.

As long as the FCS calibration measurement is obtained with the same reset interval as the target measurement no error is introduced and therefore no corrections are necessary. But for the majority of the PHT observations with PHT-P and PHT-C, different measurements of the same AOT using the same detector were obtained with different reset intervals.

An empirical correction has been derived based on calibration observations where the same flux was observed with different reset interval parameters. It is found that signals measured with 2 different reset intervals show a linear dependence:

$$s(t_1) = A_0(t_1, t_2) + A_1(t_1, t_2) * s(t_2) \quad [\mathrm{V/s}] \tag{4.5}$$

where, $s(t_1)$ and $s(t_2)$ (in V/s) are the signals obtained with reset intervals t_1 and t_2 and $A_0(t_1, t_2)$ (in V/s) is the offset and the dimensionless $A_1(t_1, t_2)$ is the slope of the regression.

Once the relative signal variations between different reset intervals of the same detector are known, a signal (in V/s) can be corrected with respect to a reference reset interval according to the following relation:

$$s(t_1 = \frac{1}{4}\ s) \ = \ A_0(t_2) + A_1(t_2) * s(t_2) \qquad [\mathrm{V/s}], \tag{4.6}$$

where the reference reset interval was chosen to be $RI = \frac{1}{4}\ s$, and the constants A_0 and A_1 refer to the reference reset interval $t_1 = \frac{1}{4}$ s. The correction assumes a data reduction of 1 (see Section 2.4.4) for the corrected signal. The correction parameters together with their uncertainties are stored in Cal-G files - see Section 14.6

The transformation of all signals to an equivalent signal obtained with the reference reset interval has the consequence that the standard dark signals must also be transformed. Due to this correction, the dark signals for $t = \frac{1}{4}$ s of a given detector can have a negative value (see Section 14.7.1 for a description of the calibration file). This has no physical meaning, but reflects the zero point in the ISOPHOT signal calibration.

The accuracy of the correction is strongly coupled to uncertainties in the ramp linearisation correction (Section 4.3.2). In addition, the uncertainty increases for readout settings far outside nominal working

range of the integration ramps. The calibration observations for the reset interval corrections have been optimised for signals with ramps in the range of 20 % to 200 % of the maximum unsaturated CRE voltage. For signals outside this range, the uncertainties in the corrections can be as high as 20–30 %. It was found for the C100 detector that the consistency of the correction among the detector pixels quickly drops for ramps that are close or higher than the ramp saturation limits due to improper ramp non-linearity corrections.

The C200 detector exhibits a breakdown of Equation 4.5 for measurement times longer than 1800 s due to instabilities in the CRE performance. If these instabilities occur, they affect usually long mapping observations with C200 where the flux level during the measurement is nearly constant.

For the P1 detector, the reset interval correction was found to depend on the operating temperature of the detector and CRE. During operations after revolution 78 the P1 operating temperature was nearly constant at 2.9 K, but before that revolution (during Performance Verification phase) the operating temperature was 2.4 K. It is therefore recommended to be cautious applying the reset interval correction to P1 observations collected before revolution 78; the temperature as well as the reset interval difference between the FCS and sky measurement should be verified first.

4.3.4 Detector bias: de-biasing effects

Detectors PHT-SS, PHT-SL, and PHT-P1 are high bias, PHT-P2 medium and the PHT-P3, -C100, -C200 low bias detectors (see Table 4.3). For the low bias detectors *de-biasing* occurs when the full integrator voltage range is used. Infrared photons induce charged carriers in the detector which are accumulated on the feedback capacitor of the readout electronics (C_{int}, see Figure 2.5) during the integration. An electrical field is built up which reduces the actual bias. The stronger the illumination, the stronger the field and herewith the bias reduction[1]. For the C200 detector the effect is strongest: the bias can drop by a factor of about 2 from 80 down to 40 mV. This effect causes the ramps to become non-linear with a downward curvature (Wolf, Grözinger & Lemke 1995, [58]).

Table 4.3: *Detector bias voltages.*

Detector ID	Default Bias [V]
SS	–37
SL	–37
P1	–90
P2	–10
P3	–0.25
C100	–0.2
C200	–0.08

In contrast to the CRE ramp non-linearity (Section 4.3.2), the non-linearities caused by de-biasing depend on *i)* the CRE reset level (see Section 2.4) which can float and *ii)* the strength of the photo-current. This complicates possible solutions for correction. Presently no distinction is made between de-biasing and CRE non-linearity when correcting the ramps. For a given detector, there is one correction table taking care of both effects. Section 7.2.8 describes the correction that has been applied by the SPD processing software.

Consequently, signals are more underestimated the stronger the signals are. Signals derived from partially saturated ramps (Section 4.3.5) suffer most noticeably from this effect. Observers who collected maps

[1]The CRE amplifier gain in the AC coupled version as shown in Figure 2.5 is limited by the ratio $G = C_C/C_F = 56$. Consequently, the reference voltage for the detector bias, U_{in} at the CRE input, varied as $\Delta U_{in} = \Delta U_{out}/G$. For a maximum integrator voltage amplitude of $\Delta U_{out} = 2V$, the variation of the CRE input voltage $\Delta U_{in} \approx 40mV$

with high dynamic range in bright regions using P3, C100, or especially C200 should be aware of this effect before interpreting their results.

In addition, for high signals on low bias detectors charges on the feed-back capacitor can cause an increased glitch rate (Section 4.4) of the detector.

4.3.5 Readout saturation

If the astronomical source is brighter than anticipated, it may happen that parts of the integration ramps are *saturated*, i.e. the maximum CRE voltage level is reached before the next destructive readout. For most detectors the subsequent readouts after saturation remain at the maximum CRE voltage level until the next destructive readout. However, for some detectors the voltage of the saturated readouts can drop back below the threshold voltage.

The same can occur in case the actual detector responsivity exceeds the nominal responsivity by a large factor. A nominal responsivity was used to a-priori set the ROT parameters before execution of the observations.

The readouts taken during CRE saturation cannot be used and should be discarded. During SPD processing, all readouts in a ramp that are subsequent to a saturated readout are removed (Section 7.2.7). The threshold CRE voltages for saturation are presented in Table 4.4.

Table 4.4: *CRE saturation thresholds.*

Detector	Threshold [V]
P1	1.091
P2	1.091
P3	1.097
C100(1,2,3)	1.063, 1.088, 1.095
C100(4,5,6)	1.097, 1.098, 1.099
C100(7,8,9)	1.098, 1.098, 1.097
C200(1,2)	1.091, 1.090
C200(3,4)	1.091, 1.088
PHT-SS(1..64)	1.040, 1.093, 62×1.095
PHT-SL(1..64)	1.007, 1.099, 62×1.102

The signal per ramp can still be determined from the reduced number of readouts that remain below the CRE threshold voltage.

4.3.6 Disturbances by chopper commanding

The destructive readouts are synchronized with the chopper transitions. The synchronisation pulse triggering the chopper transition disturbed the subsequent integration. As a consequence, the first ramp of each chopper plateau stacks clearly out of the sequence of ramps. In case of a staring measurement, a chopper transition with zero deflection (a so–called virtual chopper transition) occured each 128 s.

For the disturbed ramps the CRE reset level (see Section 2.4.2) is high and also the ramp signal can be different from the average signal derived from the other ramps of the corresponding chopper plateau.

For staring mode observations, for which the signals are derived per ramp, the SPD processing discards the first ramp per chopper plateau and does not take it into account when computing the average signal. For chopped mode observations, for which signals are derived from read–out pairs in order to have a better statistics due to the limited number of ramps per chopper plateau, also the data from the first

ramp of each chopper plateau are considered in the biweight mean computation. In case this ramp produces significant signal outliers they are discarded in the biweight mean computational process.

4.3.7 CRE latch-up

The CREs for the ISOPHOT detectors were fabricated in CMOS technology. A known phenomenon of CMOS devices is the occurence of high supply currents after switch-on, which is called *latch-up*. The effect is due to the presence of a parasitic transistor in the CRE. A small amount of charge left in the basis region of this transistor can cause it to conduct thereby creating the high supply current. Latch-ups could be recognised by an increased voltage on one of the CRE supply lines. This supply voltage was monitored by the instrument controllers.

During the instrument activation sequence at the beginning of each revolution a latch-up recovery was performed which reset the CREs into their nominal status. The recovery procedure consisted of pseudo measurements of 1 s length which selected and subsequently deselected the individual CREs.

Besides the switch-on effect some CREs tended to show latch-up effects during the science window. Two types of latch-ups could be distinguished: 1) A spontaneous latch-up which was associated with the C100 and C200 devices towards the end of the mission. This latch-up was not correlated with any selection of the device but was cured whenever the device was selected for a measurement and thus was harmless. 2) An induced latch-up which was associated with the P2 device after selecting it when powering up the heater. This latch-up persisted during the measurement and caused noisy integration ramps.

In the beginning of the mission only P2 latch-ups happened. When a latch-up event occured, the measurement was aborted in real time by the instrument controllers. Subsequently they had to initiate a latch-up recovery procedure. Due to the duration of this procedure also the following AOT could be skipped. All affected AOTs were flagged as failed and the observations entered the queue for rescheduling.

As a first counter measure to prevent P2 latch-ups, the latch-up recovery sequence was included in the switch-on sequence of the P2 detector. This way of operation did not work properly either. The final fix was to select the P2 CRE only after a sufficient stabilisation time of the P2 heating which caused some additional overhead in the AOT execution time. P2 was operated in the original latch-up susceptible mode up to revolution 270. From revolution 270 to revolution 690, the mode with the pseudo measurements was applied. Afterwards P2 was operated in the final and stable mode. It should be noted that AOT PHT03 which combined measurements of P1 and P2 never failed (those had by design the switch-on of the P2 heater and the long stabilisation time from the beginning).

The pseudo measurement is present in the telemetry data (of revolutions 270–690) but is removed in Derive_ERD and should be transparent to the observer who starts processing from ERD.

The spontaneous latch-ups of C100 and C200 devices were at the end of the mission practically permanently present, as long as the device was not selected for measurement. As mentioned above, there was, however never any impact on any measurement.

4.4 Effects of Ionising Radiation

Ionising radiation had a strong disturbing effect on the performance of the detectors. The high flux of protons and electrons trapped in the Earth's radiation belts made operations impossible. At about 2^h30^m after perigee passage the temporary radiation damages of the detectors were cured by a combination of heating, flashing and bias increase (see Section 4.2.5). Outside the radiation belts, during the 16 hour science window, the ionising radiation remained a limiting factor to detector performance. Not only direct hits on the detector, but also secondary electrons released by satellite materials after a hit caused disturbances.

Primary, ionising radiation consisted of high energy protons and heavier nuclei. It caused several effects in the photoconducting detectors:

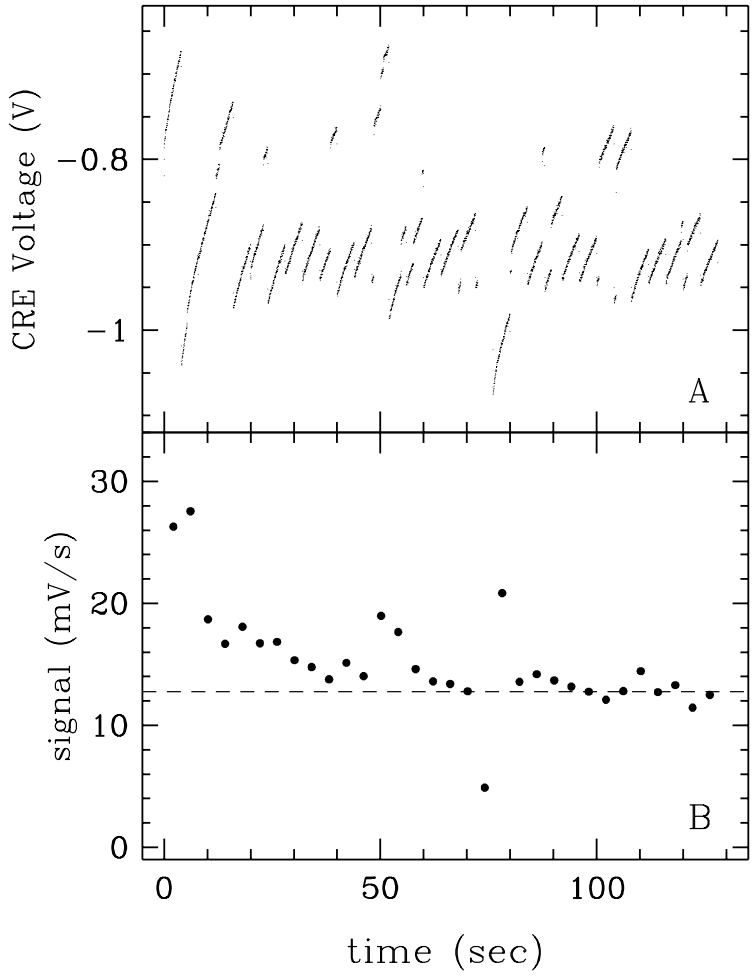

Figure 4.6: *Example of the effects of glitches during a measurement. The measurement is at a very low flux level (about 5 times the dark signal) so that even 'weak' glitches can clearly be distinguished. Upper panel (A): the 'raw' CRE voltage level as a function of time, each dot is a non-destructive readout. The measurement consists of 32 integration ramps of 4 s reset interval, each ramp contains 128 readouts. Most of the ramps show one or more significant voltage jumps between consecutive readouts caused by ionising radiation. Based on the average increase in voltage between the readouts in a ramp these glitches can be removed. Lower panel (B): the resulting signals after deglitching at CRE voltage level. Despite this deglitching the signals still show disturbances. The glitch which occured at around t=50 s caused a variation in detector responsivity lasting about 10–20 s. The dashed line is the final mean signal level after removing signal outliers and after applying a drift recognition algorithm. The corrections presented here are also used in Derive_SPD.*

- spiking, according to the hit rate,
- increase of the responsivity, caused by a lower recombination rate in sensors suffering from too many carriers produced by charged particles,
- increase in detector noise, faster than the responsivity gain, combined with an increased dark current.

A *glitch* can be recognised by a step on the integration ramp between two readouts. The influence of low level glitches to low signal data is illustrated in Figure 4.6.

Note that the energy of the particle passing through the detector is not directly correlated with the (measured) glitch energy. The glitch energy depends on the number of electrons freed by the high energy particle along its path through the detector. Higher energy glitches can cause ramps to saturate or can even cause a transient for several seconds. Low level glitches become more apparent in measurements with low in-band power. Examples are faint sources on a low background, PHT-S spectra of faint targets, observations with small apertures using detectors P1 or P2.

The glitch rate is a function of the detector size and the energy deposited. Calibration measurements were carried out to determine the particle hit rate as well as the signature of the glitches as a function of orbital position of the satellite with respect to perigee passage. On average, a clear glitch is detected every 10 s for standard science observations.

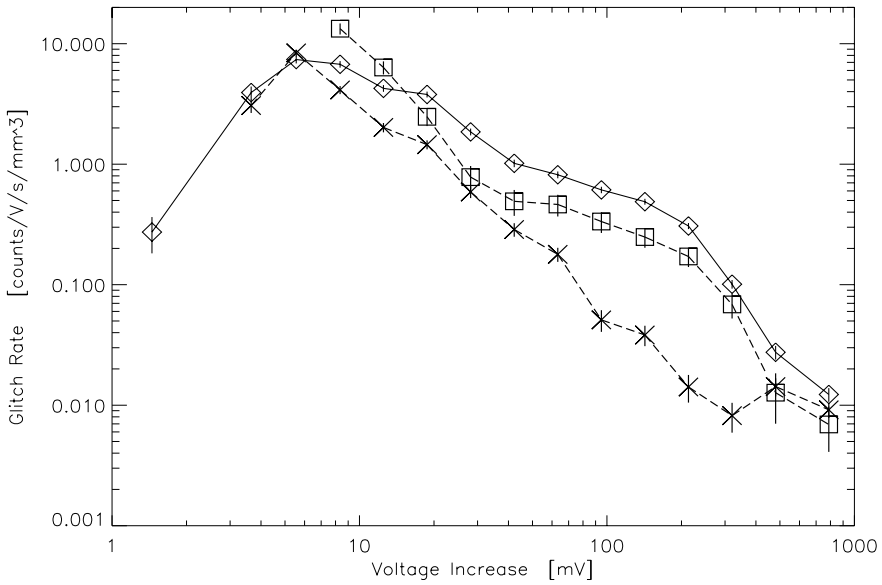

Figure 4.7: *The in-orbit glitch energy deposition spectra of detectors P3 (squares), C100 (diamonds), C200 (crosses). The spectra were obtained on the basis of dark signal calibration measurements collected throughout the mission, see Gabriel & Acosta-Pulido 2000, [8].*

Analyses of glitches have shown that they have a continuous energy distribution (Figure 4.7). Detectors P3 and C100 were more vulnerable to cosmic rays. These detectors exhibited a temporary responsivity variation for several seconds. Although special algorithms have been developed to remove these disturbances, they can determine the sensitivity limit of these channels.

The slow responsivity increase caused by cosmic rays in the 16 hour science window is about 20% for the silicon doped detectors P1, P2 and PHT-S. It can reach a factor 2 for the P3 and C200 detectors. These variations are calibrated out by FCS reference measurements which are equally affected as the celestial targets in the same observation sequence. Moreover, to minimize the disturbance, an extra curing procedure was introduced for the detectors P3, C100 and C200 to be carried out near apogee, when the satellite was handed over between the two ground stations.

The radiation effects described here became worse during periods of higher solar activity. Also measurements carried out near the end of the science window, when ISO was approaching the radiation belts, suffered from increased radiation effects.

The tuning of the parameters controlling the OLP deglitching algorithms has been performed empirically after evaluation of many datasets. Descriptions of the algorithms are presented in Section 7.3.4.

4.5 Optical Performance

4.5.1 Instrumental footprint on the sky

The image of a perfect point source obtained with a given detector or the *footprint* of a detector should be known in case one would like to perform:

- accurate flux determination of extended sources,
- accurate flux determination of point sources in the case of sources not centred in the aperture,
- image reconstruction, or
- determining relatively faint extensions around bright sources e.g. with multi-aperture measurements.
- a refined colour correction by including the wavelength dependence of the beam profiles.

As part of the PHT calibration programme, extensive mapping of astronomical point sources was carried out in order to determine the footprints of the PHT-SS/SL, C100 and C200 detectors and the PHT-P apertures.

4.5.1.1 PHT-C footprints

The footprints of the C100 detector array pixels were observed at 60 and 105 μm (filter bands C_60 and C_105) and of the C200 array at 120 and 200 μm. Footprint maps of the four C200 pixels at 120 μm are presented in Figure 4.8.

The measurements were compared with a theoretical model based on the telescope point spread function measured with ISOCAM. The model assumes a two mirror f/15 telescope with radii for the primary and secondary mirror of 30 and 10 cm, respectively. It includes the stray cones of the secondary's support tripod (Okumura 2000, [44]). The model footprint is calculated from the convolution of the point spread function with the pixel surface. Comparison between the predicted and the measured footprint shows good agreement. The inferred effective solid angles of the pixels are all larger by 20 - 60% than the values given in Table 9 of the 'ISOPHOT Observers Manual' 1994, [21]. This can be understood by the broadening of the point source profile due to infrared light scattered by the support legs.

The effective solid angle enters the extended source calibration in the conversion from Jy/pixel to MJy/sr, see Section 5.3.

4.5.1.2 PHT-P footprints

Scanning a point source over a number of the PHT-P apertures with stepsizes much smaller than the size of the apertures has revealed that the footprints of the apertures are not simple top-hat functions as suggested in Figure 2.2, but show strong irregular variations as a function of aperture radius. The variations are illustrated in Figure 4.9 where the scans over the largest aperture in the 7.3 and 12.0 μm filters are presented.

Figure 4.9 clearly shows that the energy of a uniform extended source in a given aperture is not necessarily proportional to the area of the aperture. Moreover, the flux density of an extended source with a size similar to the aperture depends on the position of the peak of its infrared brightness distribution in the aperture. E.g. in the case of the 12 μm filter combined with the 180″ aperture, the sensitivity at position ($Y = -70'', Z = 0''$) is some 5 times larger than at ($Y = +70'', Z = 0''$). Due to the large amount of possible filter/aperture combinations only a few cases have been investigated as detailed as presented in Figure 4.9 (Müller 2000a, [41]).

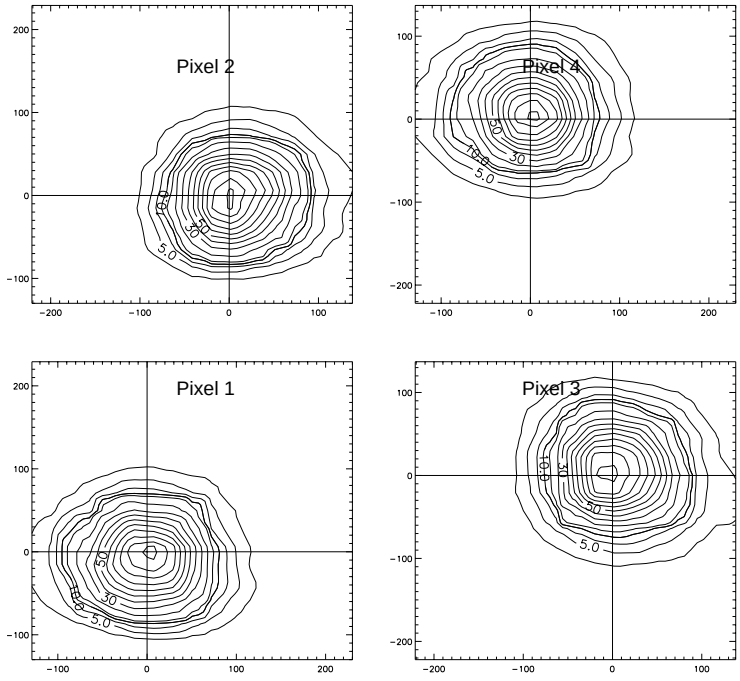

Figure 4.8: *The measured intensity distribution for each pixel in the C_120 filter by rastering the planetary nebula NGC 7027 which is assumed to be a point source for ISO. The footprints have been normalised to 1 at the peak position. Contour levels are 2.5, 5, 10, 12.5%, 20 to 90 with step of 10%, and 98% of peak.*

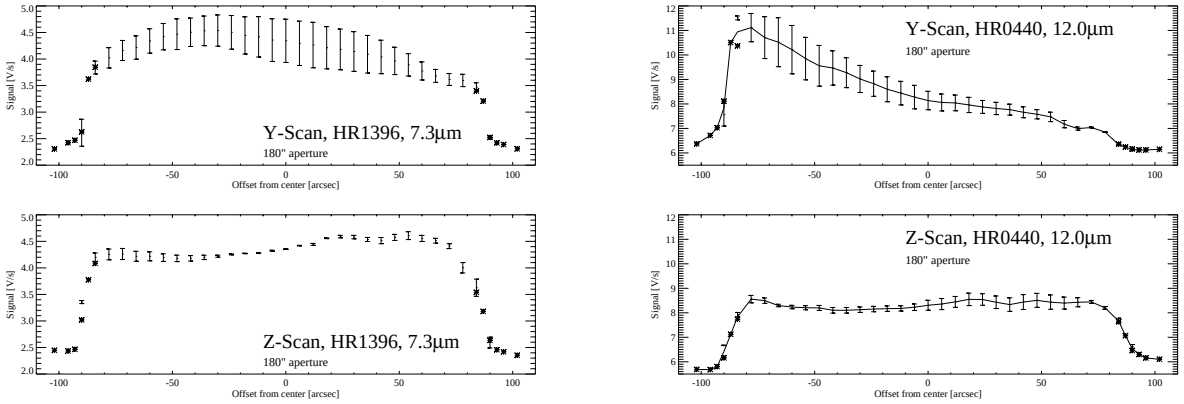

Figure 4.9: *Left panels: Aperture profile scans at 7.3 µm, 180″ aperture on the star HR 1396. Error bars indicate the signal reproducibility in the forward and backward scans. Note that the background signal level has not been subtracted in all panels. Right panels: Aperture profile scans at 12.0 µm, 180″ aperture on the star HR 0440.*

Not only the accuracy of the sky brightness measurements suffer from the irregular apertures, also the FCS calibration measurements require a separate calibration for the relation between power on the detector and aperture area for different levels of the FCS heating power. A complicating effect is that

the illumination of the aperture by the FCS can be inhomogeneous (see also Section 4.5.4) as is observed for the C100 and C200 detector arrays.

Due to the irregular properties of the PHT-P apertures, the point source calibration in non-standard apertures and the extended source calibration of PHT-P have not been scientifically validated. An investigation of PHT04 aperture sequences on point and extended sources can be found in Müller 2000a,b, [41], [42].

4.5.1.3 PHT-S footprints

The size of the PHT-S aperture ($24'' \times 24''$) has been designed to mask the part of the sky which is directly mapped onto the PHT-S pixel at a given wavelength. In-orbit observations have shown that the PHT-S response is very sensitive to pointing variations perpendicular to the dispersion direction which is along the spacecraft Y-direction (see Figure 4.10).

By scanning a point source over the PHT-S aperture in Y and Z-direction, and assuming axisymmetry, PHT-S footprints have been determined for each pixel of both the SS and SL arrays. The resulting profiles show that the general shape of the PHT-S footprints are sharply peaked in non-dispersion direction (spacecraft Y-direction). The profile in dispersion direction (spacecraft Z-direction) is flatter over the aperture. These in-orbit calibrations confirm the results of ground-based measurements of the beam profiles. An example of a footprint measured on ground is given in Figure 4.10.

Another feature of the PHT-S footprints is that not all peak at the centre of the aperture. For some pixels the centre of the array is on a steep flank of a footprint. As a result, the shape of the spectrum strongly depends on the exact pointing in Y-direction. For example, in case of pixel 60 (Figure 4.10) a pointing error of ± 3 arcsec in Y direction can cause a change in response of the order of 20%.

The PHT-S spectral response function used in the OLP is only valid for the centre position of the PHT-S aperture. Corrections for pointing offsets can be applied using the footprints of the individual pixels.

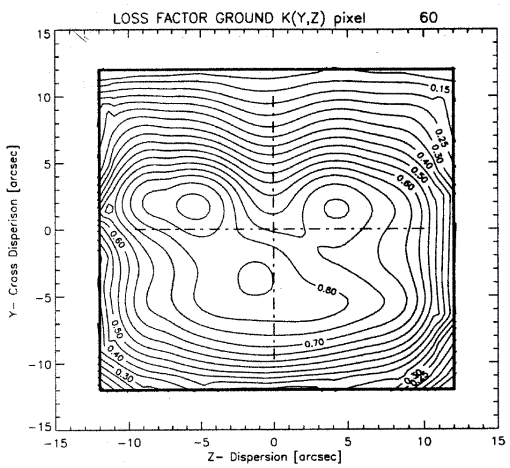

Figure 4.10: *Two dimensional beam profile of PHT-S pixel 60 as measured in the ISOPHOT ground calibration facility. This is an example where the intensity maxima are multiple and are off the major axes. In-orbit cross-scans along the major axes were performed which show qualitatively the same behaviour: a relatively flat and symmetrical shape in the dispersion direction and a slightly off-centre and steeply falling-off profile in cross-dispersion direction.*

Based on the footprints of all PHT-S pixels the correction factors for the transformation from point source flux to extended source surface brightness have been derived. A homogeneous illumination of the PHT-S aperture is assumed.

4.5.2 Point source intensity fractions

The intensity fractions, or f_{psf}, of a point source passing through a given filter/aperture combination of PHT-P or filter/pixel combination of PHT-C has been calculated using a simplified model of the point spread function. This model assumes a uniformly illuminated round mirror of 30 cm radius with a f/15 focal length and a central obscuration of 10 cm radius. The sizes of the apertures and detectors as determined on ground together with the central wavelength of the filters have been used to determine f_{psf}.

For C200 the fraction of light falling on the whole array is significantly different from the fraction calculated for the model described above in which the physical dimension of the detector arrays have been included. This is probably due to losses and diffraction at the inter-pixel gaps of order 100 μm when the point spread function is centred on the C200 array and not on one of the pixels. Empirical correction factors obtained from calibration observations have been determined to correct for this effect (Laureijs 1999, [32]).

The resulting values for f_{psf} are stored in a Cal-G file, see Section 14.18.

4.5.3 Chopper vignetting/offset

Although the guaranteed unvignetted field of view for the ISO instruments is 3 arcmin, PHT can have chop throws up to $\pm 90''$ for the largest aperture of $180''$ and $\pm 165''$ for the smallest aperture w.r.t. the CFOV. It is therefore expected that for larger chopper throws corrections should be made for possible *vignetting* of the chopper beams. As the chopped beam has a different ray path through the telescope-instrument system additional *chopper offsets* can occur which have been observed, too.

The combined effect of chopper vignetting and chopper offset can cause a relative signal difference between the on- and off- chopper beams for an otherwise flat sky. As a consequence, chopped observations of faint sources which are only a few percent brighter than the sky background can only be analyzed after correction for these effects.

Calibration observations indicate that chopper offsets for the PHT-P detectors are small: less than 1% flux difference between the chopper positions for a flat sky. For the PHT-C detectors, the offsets depend on the chopper throw and can become substantial for the largest amplitudes (as high as 6%). Note that maps obtained with PHT32 need to be corrected for this effect.

See Section 7.7.2 for the implementation of the correction.

4.5.4 Inhomogeneous FCS illumination

The detectors are not homogeneously illuminated by the FCS. For the PHT-P detectors the measured flux does not scale proportionally with the aperture area, while for the PHT-C detectors the different pixels are not receiving the same in-band power. *Illumination matrices* or factors for correcting the inhomogeneous illumination over the 180 arcsec field of view have been determined for each filter/detector/aperture by in-flight measurements.

The FCS illumination matrix is filter dependent. As a consequence, when using an FCS measurement made e.g. in the C_90 band to calibrate a measurement made in the C_60 band, the filter dependent flat-fields have to be accounted for, see Section 4.2.7.

For the PHT-P detectors strong deviations from a linear scale have been measured when changing the FCS aperture while maintaining the same FCS heating power. The calibration of the FCS against astronomical standards has been performed only with a few selected apertures, see Section 5.4.

Studies with a limited set of calibration data have indicated that the deviations from a linear scale can be as high as 20% for detectors P2 and P3. For P1 the effect can even be stronger, upto a factor 2. This means that a systematic error in the photometric calibration is made when using apertures for the FCS measurements that are different from the standard ones listed in Section 5.4.

The corrections using illumination matrices for C100 and C200 are included in the SPD processing, see Section 14.14 for a description of the related Cal-G file.

4.6 Spectral Performance

4.6.1 PHT-S instrumental line profile

The PHT-S instrumental line profiles have been measured in laboratory. The profiles exhibit a Gaussian shape to good approximation. For the PHT-SS pixels the FWHM is 42±4 nm, for SL 97±6 nm. The physical distance between adjacent pixels is 350 μm which corresponds to 38.3 nm and 91.8 nm in wavelength for SS and SL respectively, assuming a linear scale. The physical size of a pixel in dispersion direction is 310 μm which corresponds to a width in wavelength of 33.9 and 81.3 nm for SS and SL. In Table 4.5 we have summarized the laboratory data. Also listed are the fraction of the incident power measured by the detector pixel in the case the line is centred on a pixel and in case the line falls exactly in between two pixels of the PHT-S arrays. For these values it is assumed that the detectors have an ideal flat-topped responsivity profile in dispersion direction. Since this is not the case (see Section 4.5.1.3) the ratio between the centre and adjacent pixel in case the line is centred on the pixel is somewhat higher. For the values in Table 4.5 an accurate approximation for the wavelength scale is used. For the exact scale see Section 4.6.2. Under the given assumptions, a 10% variation in the FWHM changes the fraction in the centre pixel by less than 7%.

Table 4.5: *Instrumental line profile parameters.*

parameter	SS	SL	unit	description
Δx	350	350	μm	physical distance between pixels
$\Delta\lambda$	38.3	91.8	nm	wavelength difference corresponding to pixel distance
Δl	310	310	μm	physical pixel size in Z-direction
$\Delta\lambda_{pix}$	33.9	81.3	nm	pixel width in wavelength
FWHM	42	97	nm	mean full width at half power of profile
σ_{FWHM}	4	6	nm	uncertainty in FWHM
P_C/P_{total}	0.73	0.74	–	power fraction measured on pixel if line is centred
P_C^1/P_{total}	0.09	0.08	–	power fraction measured on adjacent pixel if line is centred
P_M/P_{total}	0.43	0.43	–	power fraction on pixel if line is centred between two pixels

4.6.2 PHT-S wavelength calibration

The PHT-S wavelength scale, i.e. the relation between pixel number and wavelength, is approximately linear. In orbit calibration confirms the presence of a small second order term. The wavelength scale has been calibrated to an accuracy of less than 1/10 of a pixel (see also Table 4.5) from the analysis of several targets with well defined emission lines. A polynomial fit to the wavelength scale for PHT-SS and PHT-SL gives:

$$\lambda(pix) = a_1 + a_2 * (pix - 1) - a_3 * (pix - 1)^2 \qquad [\mu\text{m}] \tag{4.7}$$

where *pix* is the integer pixel number in the SS or SL array, counting from 1 to 64 for both SS and SL. The coefficients a_1, a_2, and a_3 are presented in Table 4.6.

Table 4.6: *Coefficients for the conversion of PHT-S pixel to wavelength.*

Coefficient	SS	SL
a_1	2.4687	5.8396
a_2	4.0765 10^{-2}	9.4263 10^{-2}
a_3	4.1563 10^{-5}	3.9702 10^{-5}

4.7 Straylight

4.7.1 Straylight during FCS calibrations

The FCS signal is obtained by deflecting the focal plane chopper outside the sky field of view to one of the FCS positions (see Section 2.7). In-orbit tests have shown that FCS measurements do not only contain signals from the FCS proper and dark signal of the detectors but also a straylight component from the sky entering the instrument. The FCS straylight component was determined by performing an FCS measurement for which the FCS heating power was switched off. The FCS straylight component arises probably from the absence of a mechanical shutter to block the external beam. Both the dark signal as well as this straylight signal should be removed from the total FCS signal before calibrating the target signal.

In the derivation of the FCS calibration tables, the straylight contribution in the signal has been eliminated by subtracting the sky straylight signal obtained while pointing at the calibration target (see Section 5.2.4). For C200 the straylight contribution to the FCS signal can be as high as 10% of the background signal in case of observations near the galactic plane. The other detectors show a lower straylight contribution.

In the absolute photometry AOTs PHT05 and PHT25 it is possible to separate the straylight and dark signal components to increase the observational accuracy. The observer had the option to include an FCS measurement with no FCS heating power applied to it as well as a measurement for which a special configuration of the change wheel blocks the sky light (see Table 3.1).

4.7.2 Instrumental straylight

In order to fulfil the scientific objectives of ISO, stringent straylight requirements were imposed to the optical system. First, the parasitic light level in the focal plane should not exceed 10% of the minimum diffuse astronomical background for the wavelength range from 2.5 to 240 μm. Second, the thermal self-emission from the optical system should also be less than 10% of the minimum diffuse background. Main straylight sources are the Sun, Earth, Moon, and Jupiter.

Due to the many instrumental configurations available with PHT, in-orbit straylight verification measurements were mainly performed at 25 μm where the straylight contribution from the Earth and Moon are largest and at 170 μm which is the most sensitive band to detect straylight due to thermal self-emission.

The verification measurements have shown that straylight is a negligible contribution to most measurements, but it can be a small correction factor under rare observing conditions near the detection limit. An overview of the in-orbit results can be found in Klaas et al. 1998, [24] and Lemke et al. 2001, [38].

The observer is recommended to check the position of the brightest celestial sources with respect to the target position, particularly for absolute photometric observations.

4.7.2.1 Near-field straylight

The *near-field straylight* is the off-axis rejection within about 1 degree radius from the field of view of ISOPHOT. This was measured by performing cross-scans on Saturn using C200 in band C_160, *o* Ceti (Mira) with P2 in P_25, and γ Dra (HR 6705) with PHT-S. The target fluxes in the given filter bands are 32 kJy, 1.8 kJy, and between 3 kJy (at 3 μm) and 140 Jy (at 10 μm) for C200, P2 and PHT-S, respectively.

Comparison between the measured profiles and the beam profiles shows small or negligible straylight contributions, even from very bright sources, out to off-axis angles where the natural sky brightness dominates. An in-depth study for C_160 carried out before the mission predicted straylight levels now being confirmed by the in-orbit measurements of Saturn. This proves that the design assumptions were correct.

The computed straylight levels in the 160–200 μm range for a point source are listed in Table 4.7. Major straylight contributors are:

- the diffraction from the struts of the secondary mirror tripod contributing near the edge of the field of view,
- the edge of the secondary mirror contributing between 3 arcmin and 1 degree, and
- the secondary mirror contributing further away.

Because the 3 channels selected for the in-orbit verification of the straylight rejection are representative for the major subsystems of the instrument, it is concluded that straylight corrections can be made for all channels.

Table 4.7: *Near-field off-axis rejection at 160–200 μm predicted by an APART study of Breault Research, Tucson.*

Angle [arcmin]	Level
0	1
3	$3.6\ 10^{-3}$
10	$2.9\ 10^{-4}$
30	$6.2\ 10^{-6}$
60	$1.0\ 10^{-6}$
120	$1.6\ 10^{-7}$
300	$1.3\ 10^{-8}$

4.7.2.2 Far-field straylight of Sun, Earth and Moon

Straylight measurements of Sun and Moon were performed in autumn 1997 during eclipses of ISO by the Earth. The Sun straylight contribution could be measured directly by observing a reference target

before, after, and during the eclipse. A Moon straylight test could be performed without interference from the Sun while measuring during the eclipse a low background reference field at certain angles from the Moon.

The straylight component from the Earth was investigated by measuring the level of a low background reference field while the Earth was shining into the inner side of ISO's sunshade. This measurement was possible when the Earth-ISO-Sun angle was around 170 degrees and while the x-axis of ISO was pointing with a minimum inclination angle of 87 degrees w.r.t. Earth limb.

No detectable straylight levels from Sun, Earth, and Moon were measured. In Table 4.8 the measured 1 σ upper flux limits are listed (Kranz 1998, [29]. The upper limit at 170 μm is higher than the straylight requirement of 10% of the minimum astronomical background. The minimum brightness at 170 μm is estimated to be approximately 2 MJy sr^{-1} which implies a required upper limit of about 0.2 MJy sr^{-1}. It should be noted that the upper limits presented in Table 4.8 apply to the most unfavourable straylight configuration.

Table 4.8: *Upper limits (1 σ) for far-field straylight of Sun, Moon, and Earth at 25 and 170 μm, from Kranz 1998, [29].*

Source	λ_{ref} [μm]	Surface Brightness [kJy sr^{-1}]	Flux Density [mJy]	% of sky background in measurement
Sun	25	16	9.2	0.05
Moon	25	179	100	0.34
Earth	25	188	105	0.51
Sun	170	10	2.4	0.10
Moon	170	46	11	0.53
Earth	170	280	69	5.9

4.7.3 Spectral straylight

There is no indication of any spectral impurity and of the presence of ghosts in the PHT-S spectra.

4.8 Instrumental Polarisation

The ISOPHOT instrumental polarisation without the contribution of the ISO optical elements (primary, secondary and pyramidal mirrors) was investigated in laboratory, see Schlötelburg 1992, [48]. The laboratory measurements indicated a degree of linear polarisation of less than 10% for the P detectors. The polarisation degree of the arrays varies from pixel to pixel, some pixels showed polarisations as high as 10%.

For PHT-S the instrumental polarisation degree is measured to be considerably higher: starting at 10% at 2.5 μm rising approximately linearly to 45% at 5 μm with a polarisation angle of -6 ± 3 degrees, and for PHT-SL starting at 12% at 6 μm rising approximately linearly to 40% at 12 μm with a polarisation angle of -2 ± 2 degrees. The main cause of PHT-S instrumental polarisation is the grating.

PHT was equipped with a filterwheel in which linear polarisers are mounted for both the PHT-P and PHT-C subsystems (Klaas et al. 1999, [25]). The polarisers were used to measure polarisation of the sky at 25 μm using the P2 detector and filter P_25 and at 170 μm using the C200 detector array and filter C_160, see Section 3.10.4 for a detailed description of the observing modes. The instrumental polarisation in these filter bands was determined in-flight by measurements of unpolarised sources like stars or a large

sample of background fields. The instrumental polarisation degrees and angles measured in-orbit are listed in Table 4.9, the values have been taken from Klaas et al. 1999, [25] for the 25 μm band and Laureijs & Klaas 1999, [33] for the 170 μm band.

Table 4.9: *Polarisation degrees and angles at 25 and 170 μm measured in-orbit, from Klaas et al. 1999, [25] and Laureijs & Klaas 1999, [33].*

λ_{ref} [μm]	pixel	P [%]	Θ [°]
25	–	3.0±0.2	–19±2
170	1	3.6±0.6	–62±5
170	2	7.8±0.7	83±2
170	3	4.0±0.6	–37±4
170	4	4.6±0.7	71±5

4.9 Backgrounds

ISOPHOT was designed to measure the absolute sky brightness. As a consequence, all routine observations included emission from the astronomical background in the 2.5–240 μm wavelength range. Most ISOPHOT observations involved discrete astronomical sources for which the background emission had to be subtracted. The presence of background emission contribute to

- the photon noise in a measurement,
- uncertainties in the spatial zero level of the source due to the presence of structure in the background, or,
- uncertainties in the spectral energy distribution or spectrum of the source due to uncertainties in the intrinsic spectral energy distribution of the background which can vary with line of sight.

The PHT Instrument Dedicated Team together with the PHT Consortium have undertaken programmes to investigate the astronomical backgrounds. In the following sections the most important background emission components, the zodiacal and diffuse galactic emission, are discussed. In addition, confusion due to discrete galaxies is mentioned. Other components like the scattered light from zodiacal dust and the cosmic far-infrared background (Lagache & Puget 2000, [30]) are expected to give a minor contribution in most cases. More information can be found in the ISO Handbook Volume I, [20].

4.9.1 Confusion due to diffuse galactic emission

Confusion due to diffuse galactic emission or 'cirrus confusion' became apparent from the far-infrared maps produced by IRAS. The diffuse galactic emission component peaks around 170 μm and can be approximated by a λ^{-2} modified blackbody of 17 K. Analysis of the cirrus structure in IRAS maps (Gautier et al. 1992, [10]), Helou & Beichman 1990, [17]) showed that the cirrus confusion noise N_{cc} can be expressed:

$$N_{cc} \approx 1.08\ (\frac{\lambda}{100})^{2.5} \langle B_\nu(\lambda) \rangle^{1.5} \quad [\mathrm{mJy}], \tag{4.8}$$

where λ is wavelength in μm and $\langle B_\nu(\lambda) \rangle$ is the mean surface brightness in MJy sr^{-1}. For example, for a field at 200 μm and with a mean diffuse galactic emission of 5 MJy sr^{-1}, the cirrus confusion noise is

$N_{cc} \approx$70 mJy. Thus, two adjacent (point-)source free sky positions which are 1 beam apart (about 100″ at 200 μm) can differ 70 mJy per beam (1 σ) due to cirrus structure.

This result has been confirmed with ISOPHOT (Herbstmeier et al. 1998, [18] and references therein, Lagache & Puget 2000, [30]) at ISOPHOT wavelengths longward of 100 μm.

4.9.2 Confusion by galaxies

Photometry of a target in the presence of discrete background galaxies can be hampered by faint background galaxies which may lie in the beam but are not detected individually, or by the presence of a identifiable bright source close to the target.

Faint source confusion can affect photometric studies of individual sources and dominates as long as the cumulative galaxy source counts $N(F_\nu, \nu)$ rises more steeply than F_ν^{-1} with decreasing F_ν. Cosmological source count models predict the turnover at F_ν <0.1 mJy. Below this flux density, the bright ource confusion limits should be included. Assuming the in-orbit point source flux limits (after 128 s integration time and S/N = 10) in the most sensitive PHT filters at long wavelengths, the prediced level of galaxy confusion noise is given in Table 4.10.

Table 4.10: *Galaxy confusion noise N_{gc} for the tabulated point source flux limits with 128 s integration time and S/N = 10.*

Det.	λ_{ref} [μm]	Aperture [″]	F_ν [mJy]	N_{gc} [mJy]
P3	60	180	270	220
P3	100	180	240	280
C100	90	-	90	40
C200	170	-	200	120
C200	200	-	940	200

For on-target integration times longer than 128 s the noise level decreases but then galaxy confusion noise starts to become the main source of uncertainty: in the worst case 280 mJy (for the P3 detector, filter, 180″ aperture). The galaxy confusion is on most regions in the sky below the cirrus confusion noise. For ISOPHOT, galaxy confusion becomes only important if the mean background level due to diffuse galactic emission is $\langle B_\nu(\lambda)\rangle < 5\,\mathrm{MJy\,sr^{-1}}$

Bright source confusion determines the maximum amount of extragalactic sources which can be counted in deep surveys of the darkest regions on the sky at high galactic latitudes. Assuming an Euclidian universe the confusion limit in sources per solid angle n_q can be derived from Oliver 2001, [45]:

$$\Omega_{eff} = 0.18\pi(1.2\frac{\lambda}{D})^2 \qquad [\mathrm{sr}], \tag{4.9}$$

$$n_q = \frac{1}{3q^2\Omega_{eff}} \qquad [\mathrm{sr}^{-1}], \tag{4.10}$$

where $D = 0.6$ m is the diameter of the telescope and q is the detection level above the noise in multiples of σ. For q=5 and λ=170 μm, $n_5 = 2.04\times10^{-5}$ sr^{-1} = 62 point sources per square degree.

Analysis of the infrared emission observed by COBE showed the presence of a new background component, the cosmic far-infrared background (CFIRB) which originates from far-infrared galaxies. Using deep ISOPHOT observations at 170 μm in a region with low cirrus emission Lagache & Puget 2000, ([30])

isolated spatial fluctuations in the CFIRB. The CFIRB fluctuations are best described by a white noise power spectrum $P_{CFIRB} = 7400$ Jy^2 sr^{-1} corresponding to rms fluctuations around 0.07 MJy sr^{-1} at 170 μm.

4.9.3 Zodiacal light

For many types of ISOPHOT observations knowledge of the emission contribution from the zodiacal dust cloud is necessary. Data from COBE can be used but have to be adapted to the higher angular resolution observations of ISOPHOT. Absolute photometric observations in a number of ISOPHOT bands at several ecliptic longitudes/latitudes were obtained to establish the zodiacal emission distribution as seen by ISO.

COBE did not cover wavelengths between 5 and 12 μm, in the range where the brightness of the zodiacal light rises very steeply. The measurements obtained with PHT-S, PHT-P and ISOCAM suggest that the zodiacal emission spectrum can be well approximated by blackbodies of 260–290 K, depending on the Solar elongation and the ecliptic latitude. A method for subtracting the zodiacal emission in PHT-S spectra using the COBE data is presented in Ábrahám et al. 1997, [1]). ISOCAM CVF and ISOPHOT-S measurements have demonstrated that the spectrum is featureless between 5 and 16 μm down to about 5% of the total brightness (Ábrahám et al. 1998, [2], Blommaert, Boulanger & Okumura 2001, [4]).

Ábrahám et al. 1997, [1] have searched for arcminute structure in the zodiacal emission at low, intermediate and high ecliptic latitudes. No structures or fluctuations were found at a level higher than 0.2% of the total brightness. At low ecliptic latitudes ($\beta < 15°$) the zodiacal emission includes the dust bands and cometary tails (Ábrahám et al. 1998, [2]).

4.10 Global Instrument Data

See Appendix A for the following tables:

1. global filter specifications (Sections A.1.1, A.1.3),
2. aperture specifications (Section A.1.2),
3. other filterwheel components (Section A.1.4), and
4. filter/detector transmission curves (Section A.2).

Chapter 5

Photometric Calibration

5.1 Overview

The photometric calibration of ISOPHOT observations is described in this chapter. The calibration strategy for PHT-P and PHT-C using the FCS and the strategy for PHT-S, all measuring point sources, are given in Section 5.2. In the subsequent sections the extended source photometry, aperture calibration, and the PHT-S wavelength calibration are described. Section 5.6 summarizes the specific calibration procedures per AOT.

A general description of the kind of calibration files used in OLP is given in Section 5.7. Note that the uncertainties in the calibration are addressed in Chapter 9 and in the related documents 'ISOPHOT Error Budgets' by Laureijs & Klaas 1999, [31] and 'ISOPHOT Calibration Accuracies' by Klaas et al. 2002, [26].

5.2 Calibration Strategy

5.2.1 Calibration involving the FCS

An observation with PHT-P or PHT-C always includes a photometric reference measurement using one or both internal fine calibration sources (FCSs, see also Section 2.7) which are assumed to be stable throughout the mission. The stability assumption is confirmed by monitoring measurements against celestial standards throughout the ISO mission. The emission from an FCS can be changed by adjusting the FCS heating power. The FCS reference measurement assesses the actual detector responsivity at the time of the measurement.

The crucial photometric calibration as contained in the Cal-G files (see Section 5.7.1) is the relationship between heating power applied to the FCS as commanded by the AOT logic, and the resulting in-band power received by the detector. This is the basis of the derivation of the detector responsivity which fixes the relation between signal and flux for the detector at a given time. The detector responsivity enables *transfer of calibration* between filters of the same detector and/or between apertures.

Transfer of calibration is in practice necessary in case of multi-filter photometry (PHT03, PHT17/18/19, PHT22, PHT37/38/39) or multi-aperture photometry (PHT04) where a single FCS measurement is used to calibrate combinations of several filters and apertures.

The FCS calibration itself is obtained empirically by comparing the signal of a designated celestial calibration target and signals of several FCS measurements. Based on the known spectral energy distribution (SED) of the calibration target, the known spectral instrument transmissions and the relative spectral response of the detector, the in-band power is calculated for each FCS measurement. These in-band powers are then related to the FCS heating powers via a comparison of the detector signals.

Three types of astronomical targets - all being point sources - have been used as *prime calibrators* for the FCSs:

- Stars
  Stellar calibrators are most suitable for the 2.5 to 35 μm wavelength range. The brighter ones can still be extrapolated reliably out to 300 μm. A dedicated ground-based preparatory programme for ISO calibration standards was carried out to provide the ISO mission with the most consistent and most accurate set of calibration stars, see Jourdain de Muizon & Habing 1992, [19], van der Bliek et al. 1992, [54], and Hammersley et al. 1998, [14]. Another set of calibrated stellar spectral energy distributions was provided by M. Cohen from an independent calibration programme (Cohen et al. 1995, [7]). The $1\,\sigma$ confidence in the absolute calibration of the calibration stars is about 3% in the 2.5 to 35 μm wavelength range and better than 5–6% at longer wavelengths up to 300 μm. The model spectral energy distribution for Vega (α Lyr) has been used to define the zero point for both programmes.

- Asteroids
  Asteroids are used to cover the 45 to 200 μm wavelength range at intermediate flux levels between bright stars and planets. An extensive ground and airborne based calibration programme was carried out to quantify the fluxes and to monitor the light curves of the prime asteroids 1 Ceres, 2 Pallas, 4 Vesta, and 10 Hygiea, and other asteroids that have been observed with ISO. For the current calibration the absolute fluxes of the asteroids were derived using a thermophysical model (Müller & Lagerros 1998, [40]). The accuracy of the predicted asteroid fluxes is in general $\pm$10% in the wavelength range longward of 24 μm (Müller & Lagerros 2002, [43])

- Planets
  The outer planets Neptune and Uranus were used for calibration at the longer wavelengths in the high flux density range up to 1000 Jy. The model SED's of Uranus at a given time in the mission were derived from the model by Griffin & Orton 1993, [11] modified to match the Voyager IRIS data (see 'The ISO Handbook: Vol. III, LWS - The Long Wavelength Spectrometer', [12]). Comparison with independent model predictions for Uranus showed a consistency of better than 10% in the wavelength range between 30 and 240 μm.

The stability of both FCSs was monitored against the bright secondary standard NGC6543 as well as against a set of fainter stars.

The ISOPHOT calibration strategy is presented in detail by Klaas et al. 2001, [28]. A full description of the ISOPHOT calibration involving the FCS can be found in Schulz et al. 2002, [53].

5.2.2 Non-linear detector responsivity

Ignoring transient effects (see Section 4.2.3), the detector responsivity, which is the proportionality between in-band power and signal, can only be considered as constant under the following conditions:

- the time between the responsivity measurement and the sky measurement is short. Over longer time periods the responsivity is a function of orbital phase and shows a steady increase for detectors P3, C100, and C200 as a function of time after curing.

- the signal of the FCS measurement is close to the signal of the sky measurement. From calibration observations of standard stars it was found that the detector responsivity depends on the in-band power P falling onto the detector $R(P) \propto S(P)/P$, where the photo-current or signal $S(P)$ has a non-linear dependence on power.

Investigation of the validity of the second condition has shown that the *signal non-linearity* can be corrected under the assumption that the shape of the signal non-linearity function is independent of

time. Since the responsivity is proportional to signal, the responsivity can be linearised by introducing a linearisation correction $H(S)$ such that:

$$S' = H(S(P)) \qquad [\mathrm{V/s}] \tag{5.1}$$
$$S'/P = constant \qquad \text{for all } S \tag{5.2}$$

where S' is the linearised signal. Time dependencies, such as the responsivity dependency on orbital phase, are treated as random scatter. The correction function $H(S)$ has been determined empirically from observations of calibration standards. It is found that $H(S)$ is not only a function of detector, but also of filter. The determination of $H(S)$ is not straightforward due to the fact that all measurements of calibration standards include a background power which is not well known. In addition, time dependent variations of the responsivity introduces a substantial scatter in the data. A detailed description is provided by Schulz 1999, [51].

In the photometric calibration of PHT-P and PHT-C, the signal linearisation is applied to the mean signal per chopper plateau immediately after subtraction of the dark signal. In the remainder of this chapter we assume that the signals S have been linearised unless explicitly stated.

5.2.3 Signal correction for chopped observations with PHT-P and -C

The photometric accuracy of chopped observations is completely determined by losses in the difference signal between the 'source+background' ('on') and 'background' ('off') signals. This is caused by detector transients with time constants greater or equal than the chopper modulation time (see Section 4.2.3).

Due to these transients the determination of the difference signal is not trivial. A method was developed which includes the determination of a *generic pattern* for chopped measurements (see Section 7.5). The signal difference is determined from the generic pattern depending on the transient behaviour of a given detector - for example, in case of detector P3 the signal difference is determined from the maximum of the on-signals and the minimum of the off-signals of the pattern, and in case of P1 and P2 the median signals of the on- and off-plateaux are used.

This analysis of chopped measurements applied to a sample of calibration standards yielded an empirical signal correction function ζ which corrects a given (linearised) difference signal S_{src}:

$$S'_{src} = \zeta(S_{src},\, det,\, t_{plat}) \qquad [\mathrm{V/s}], \tag{5.3}$$

where S'_{src} is the signal corrected for losses due to the chopper modulation, *det* is the detector used, and t_{plat} is the chopper plateau time (in s). The dependency on *det* and t_{plat} is required to relate the chopper modulation frequency with the detector specific transient time scales.

The AOT PHT32 incorporated the chopper sawtooth mode to obtain oversampled maps with the PHT-C detector arrays (Sections 3.5 and 3.10.2). The movement of the chopper in PHT32 also caused signal transients. These cannot be corrected with ζ because there is no fixed on-source and background position as in the pointed chopped observations. Therefore no corrections are made in OLP for signal losses due to detector transients in PHT32.

The function ζ implicitly includes the correction for 'chopper vignetting/offset' (Section 4.5.3) with PHT-C because the choice of available chopper throws with PHT-C was limited. For PHT-P the chopper offsets are small. In the case of PHT32 the signals per chopper plateau are explicitly corrected for chopper offsets:

$$S' = c_{chop}(f, i, \theta) \times S \qquad [\mathrm{V/s}], \tag{5.4}$$

where f is the filter, i is the detector pixel and θ the chopper deflection with respect to the central field of view. The input signal S is the total sky signal.

5.2.4 Absolute calibration of FCS

The FCS calibration against celestial standards has been determined for all 25 PHT-P and PHT-C filter bands over the full range of possible astronomical flux densities.

Fluxes were measured of prime calibrators in each available filter band spanning 3–5 decades of flux range per filter band. For a given calibration target, the following measurements were obtained in a given filter:

- measurement of the FCS for which zero heating power is applied (also referred to as 'cold FCS measurement' or 'FCS straylight measurement'),
- measurement of one or more background positions,
- measurement of the calibration target, and
- measurement of one to several FCS illumination levels.

The cold FCS measurement provided the zero FCS signal level. All measurements of the celestial calibrators included an uncalibrated amount of background emission which had to be subtracted. The background level was determined by performing one or more separate background pointings in the same aperture. For the PHT-C arrays, small raster maps were often used to obtain the background level during the same measurement. In the case of multiple FCS measurements, the FCS illumination levels were tuned such that their in-band powers span a range of about one decade around the power expected from the calibration target plus background emission. It is assumed that the responsivity does not depend on signal in the measured power range (system linearity).

Using the total optical transmission of the instrument and detector chain (to determine $C1$ and k) and the source SED, the in-band power from the calibration source on the detector was computed from Equation 5.10. By relating the in-band power of the calibration target to its corresponding signal, the FCS signals were converted to in-band powers. These are derived for a measurement in a given aperture in case of PHT-P or for a pixel in case of PHT-C, according to:

$$P^f_{fcs}(h) = P^f_{cal}.\frac{(S^f_{fcs} - S^f_{str})}{S^f_{cal}} \qquad \text{[W]}, \tag{5.5}$$

where

- $P^f_{fcs}(h)$: the in-band power in W for filter f and FCS heating power h in mW;
- P^f_{cal}: in-band power in W of the celestial calibrator;
- S^f_{cal}: measured signal in V/s of the prime calibrator after subtraction of the background signal;
- S^f_{fcs}: measured FCS signal in V/s;
- S^f_{str}: measured dark FCS signal (straylight) in V/s.

The FCS power calibration tables give the in-band power as a function of the commanded FCS heating power. It is assumed that the difference signal between calibration source and background scales linearly with the difference signal from the FCS measurements. Consequently, the accuracy of the absolute calibration of the background level depends on the linearity of the detector from zero to the background level and on the suppression of parasitic flux, such as straylight. Uncertainties become higher for flux levels close to the astronomical background because of the absence of reliable celestial calibrators that are faint.

For PHT-P the tables are normalised to the aperture area, and for PHT-C the tables refer to the average array. The power falling onto an individual pixel is derived by for inhomogeneous FCS illumination (see Section 5.2.5).

The FCS calibration makes the observation independent of long term responsivity drifts. However, on measurement time scales of order of 32-2048 s, detector transients (Section 4.2.3) due to flux changes occur and have to be corrected for. For the determination of the overall FCS calibration drift corrections have been applied to estimate the signal level of the asymptotic limit.

5.2.5 Photometry with PHT-P and PHT-C

The FCS measurement together with the FCS power calibration tables (see Section 14.12) are used to determine the detector responsivity. In the following derivations a separation will be made between single detector, multi-aperture, and multi-filter subsystems PHT-P and the multi-filter detector arrays PHT-C.

For a given PHT-P FCS measurement taken with detector *det*, filter f', and aperture a', the responsivity R_{det} is derived from:

$$R_{det} = \frac{S_{fcs}^{f'}(a')C_{int}^{det}}{P_{fcs}^{f'}(h)A(a')\alpha^{f'}(a')\chi^{f'}} \quad [\mathrm{A/W}], \tag{5.6}$$

For a given PHT-C FCS measurement taken with detector *det* and filter f', and for pixel i, the responsivity R_{det} is derived from:

$$R_{det}(i) = \frac{S_{fcs}^{f'}(i)C_{int}^{det}}{P_{fcs}^{f'}(h)\Gamma^{f'}(i)\chi^{f'}(i)} \quad [\mathrm{A/W}], \tag{5.7}$$

where the prime ($'$) indicates the FCS measurement configuration and

- $S_{fcs}^{f'}$: the signal in V/s from the FCS measurement in filter f' after subtraction of dark signal or FCS straylight (the latter one is only possible with PHT05 and PHT25);
- C_{int}^{det}: the integration capacity in A/(V/s) (=farad) associated with detector *det* (see Figure 2.5 and Table 14.5);
- $P_{fcs}^{f'}(h)$: the in-band power in W for filter f' and FCS heating power h in mW as obtained from the FCS power table, for PHT-P the power is per mm^2, for PHT-C per pixel;
- $A(a')$: the area of aperture a' in mm^2;
- $\alpha^{f'}(a')$: dimensionless correction for inhomogeneous illumination of PHT-P aperture a by the FCS in filter band f';
- $\Gamma^{f'}(i)$: dimensionless correction for PHT-C pixel i due to inhomogeneous illumination of the array by the FCS;
- $\chi^{f'}(i)$: dimensionless correction for non-uniform filter-to-filter responsivity of pixel i of PHT-C or PHT-P where i is dropped (single pixel).

A few observations have no accompanying FCS measurement which can be used for the photometric calibration due to e.g. a failure during the observation or signal saturation. In those cases a *default responsivity* is applied which is a fixed value of $R_{det}(i)$ corrected for a predictable variation with orbital phase at the time of the observation.

Once the detector responsivity is known, measurements of a celestial source with filters of the same detector in a multi-filter photometry observation can be calibrated. For a given PHT-P measurement, the in-band power $P^f_{src}(a)$ for filter f and aperture a is:

$$P^f_{src}(a) = \frac{S_{src}(a)C^{det}_{int}}{R_{det}\chi^f} \qquad \text{[W]}, \tag{5.8}$$

For a given PHT-C measurement, the in-band power $P^f_{src}(i)$ for filter f and for pixel i is:

$$P^f_{src}(i) = \frac{S_{src}(i)C^{det}_{int}}{R_{det}\chi^f(i)} \qquad \text{[W]}, \tag{5.9}$$

where S_{src} is the linearised source signal in V/s after dark signal subtraction. Note that the correction χ^f cancels out for a source measurement taken in the same filter band as for the FCS measurement, i.e. when $f' = f$. To convert from in band power to point source flux density on the sky, the following relation is used for PHT-P:

$$\frac{F^f_\nu}{k_f} = \frac{P^f_{src}(a)}{C1^f f^f_{PSF}(a)} \qquad \text{[Jy]}, \tag{5.10}$$

and for PHT-C[1]:

$$\frac{F^f_\nu}{k_f} = \frac{\sum_i P^f_{src}(i)}{C1^f f^f_{PSF}} \qquad \text{[Jy]}, \tag{5.11}$$

where the summation is over all detector pixels i and where:

- F^f_ν: the source flux density in Jy for an assumed spectral energy distribution νf_ν = constant;
- k_f: the colour correction, for the spectrum of the observed celestial source;
- $C1^f$: constant in m^{2}Hz describing[2] the transmission of the whole optical path for a given filter and assuming a νF_ν = constant reference source spectrum. The effective size of the primary mirror, reflection losses, filter transmission, spectral response of the detector, etc. are included;
- f^f_{PSF}: (dimensionless) fraction of the ISO point spread function entering the field aperture in case of PHT-P or falling onto the entire array in case of PHT-C for filter f (details can be found in Salama et al. 2001, [47]).

F^f_ν is also referred to as the flux density at the reference wavelength of the filter band and is the value of the flux density computed by OLP. It is required that the constant $C1^f$ is identical to the one used in the determination of the FCS power tables.

5.2.6 Spectro-photometry with PHT-S

At the shortest wavelengths below 10 μm very high FCS heating powers are required to obtain a detectable in-band power. Due to the wavelength coverage of PHT-S no single FCS power can properly illuminate both SS and SL arrays without causing saturation in the SL array (a 300 K blackbody spans 5 orders of magnitude over the wavelength range 2.5–12 μm). Therefore and due to the fact that the PHT-S

[1] for C100 chopped observations only the centre pixel of the array is used for the point source flux determination. The f_{PSF} refers to the psf correction of that pixel, see also Section 10.12.

[2] $C1$ is the same parameter as the $C1$ factor given on page 58 of the 'ISOPHOT Observers Manual' 1994, [21]. Note that the values of $C1$ have changed.

detectors turned out to be very stable, the PHT-S measurements (PHT40) are not accompanied by any FCS measurement. Without any FCS measurement, the photometric calibration must be different from that of PHT-P or PHT-C.

Monitoring of the PHT-S responsivity at the beginning and end of each revolution showed that the daily responsivity variation is on average at most 10% depending on the space weather conditions, see Section 4.2.5. Shorter time scale responsivity variations are mainly due to transient behaviour of the detector responsivity following an illumination change. The PHT-S transient behaviour is corrected by applying the calibration method outlined in the remainder of this section.

The PHT-S measurement sequence as provided by the PHT40 AOT has always the same structure: an initial dark signal measurement of 32 s followed by a sky measurement of 2^n s ($5 < n < 12$) either in staring or chopped mode. This measurement sequence causes the detector to be in a well defined (dark) state before the illumination by the sky starts.

Due to the long term responsivity stability, the photometric accuracy of the PHT-S observations is mainly determined by the uncertainties caused by the responsivity transients (Schulz 1999, [52]). The photometric calibration of PHT-S is therefore based on the following assumptions:

- the transient response of an individual pixel depends on the illumination level.
- the transient response for a given illumination level is reproducible as long as the flux history is similar.

These assumptions are to a large extent fulfilled by the long term responsivity stability and the AOT PHT40 design. The only disturbing parameter is the operational temperature of the detector which affects the shape of the transient curves. It is, however, found that the temperature of the detector was quite stable (2.7–3.1 K) throughout the routine phase, i.e. revolution 78 and later. During the *Performance Verification Phase* the PHT-S detector temperature was lower (2.4 K) and the calibration methods outlined below are less accurate for observations obtained in that period.

5.2.6.1 PHT-S staring observations

By observing a large number of calibration stars covering a sufficient range in flux densities and integration time for each PHT-S pixel, one can construct an empirical transformation which directly relates the signal transient $S(i,t)$ of a given pixel i at time t to a flux density F_ν^t:

$$F_\nu^t(i) = \varphi(i,\, S(i,t),\, t) \qquad \text{[Jy]}, \tag{5.12}$$

$$w(i,t) = g(i,\, S(i,t),\, t), \tag{5.13}$$

where φ is the transformation and g a function which gives the weight of the correction. We give the flux density a *superscript* t to indicate that the flux itself is supposed to be constant and has no time dependence. The time resolution is determined by the reset interval length, i.e. the time between two consecutive signals. This calibration method is also called 'dynamic calibration', because the spectral response function is adapted to the total brightness and transient behaviour of each pixel.

The weighting function has been introduced to account for the fact that the transient correction is usually large on short time scales and close to unity for very long integration times. It is assumed that the transient signal reaches the long term detector response asymptotically in time. The final flux $F_\nu(i)$ is the weighted average of the transformed signals $F_\nu^t(i)$ along a given measurement.

5.2.6.2 PHT-S chopped observations

PHT-S observations in chopped mode have the property that the background emission (off position) is usually the zodiacal light which is faint at the PHT-SS wavelengths, and less than 1 Jy at the longest SL wavelengths. In addition, the available range in chopper frequencies at low flux densities is small.

From the analysis of a large range of chopped PHT-S observations of calibration stars it is found that an accurate photometry can be accomplished by assuming two calibration components. One component is the average spectral response function which is the zero order approximation for the conversion from signal in V/s to flux density in Jy for each pixel i. The second component involves the correction for flux dependent chopped signal losses due to signal transients and depends on the difference signal between the on-source signal and the background off signal:

$$C^{c,p}(i) = C^{c,p}_{ave}(i)(A_0(i) + A_1(i)\log_{10}(S_{on}(i) - S_{off})) \qquad [\mathrm{V\,s^{-1}Jy^{-1}}], \tag{5.14}$$

where

- $C^{c,p}(i)$ in (V/s)/Jy is the spectral response of pixel i for a point source p corrected for chopped c signal loss;
- $C^{c,p}_{ave}(i)$ in (V/s)/Jy is the PHT-S *average* spectral response function for a point source;
- $A_0(i)$ and $A_1(i)$ are first order corrections on spectral response function for chopped measurements depending on the signal difference;
- $S_{on}(i)$ and $S_{off}(i)$ (in V/s) are the on- and off-source signals.

The mean spectral response function was obtained by taking the average of the spectral response functions derived from a number of faint calibration stars.

5.2.6.3 PHT-S maps

PHT-S maps are obtained by observing a regular grid (raster) by moving the spacecraft from one grid point to the other. Although the measurement sequence in PHT40 mapping mode is the same as in staring or chopped mode (a dark measurement followed by the sky) the assumption of a flux history similar to that as for the calibration stars is not met for all raster points in a map except the first one. The photometric calibration is poorer than for staring or chopped mode observations because only a 'static' response function not correcting for responsivity transients can be applied. The photometric calibration on each raster point k is performed by direct conversion of the signal $S(i,k)$ to a flux $F_\nu(i,k)$:

$$F_\nu(i,k) = \frac{S(i,k)}{C^{s,p}_{ave}(i)} \qquad [\mathrm{V\,s^{-1}Jy^{-1}}], \tag{5.15}$$

where $C^{s,p}_{ave}(i)$ the average spectral response function for PHT-S staring observations derived from 40 observations of 4 different standard stars with different brightness.

5.3 Point Sources Versus Extended Sources

All targets used for flux calibration are point sources in the ISOPHOT wavelength range. For an extended source which is much larger than the aperture or pixel, the surface brightness is derived by involving the effective solid angle of the aperture or pixel.

For the P subsystems, the effective solid angle for each aperture corresponds to the area of the aperture in the focal plane projected on the sky. The areas were determined from the measured physical dimensions of the apertures.

The conversion from point source flux F^f_ν in Jy to a surface brightness can be written for PHT-P as follows:

$$I_\nu^f = \frac{F_\nu^f f_{PSF}^f}{(1-\epsilon^2)\Omega_{eff}^f} \quad [\mathrm{MJy\,sr^{-1}}], \tag{5.16}$$

where ϵ is the obscuration factor for the ISO secondary mirror, Ω_{eff}^f in sr is the effective solid angle of the aperture, for a given filter f. The PHT-C surface brightness is derived from the in-band powers of each pixel. The computation for PHT-C is as follows (with the same notation):

$$I_\nu^f = \frac{k^f P^f(i)}{C1^f(1-\epsilon^2)\Omega_{eff}^f} \quad [\mathrm{MJy\,sr^{-1}}], \tag{5.17}$$

A model of detector *footprints* (or beam profile) is used to determine the effective solid angles of the C100 and C200 detector pixels Ω_{eff} for each filter band. The model takes into account the ISO primary mirror, secondary mirror, the tripod supporting the secondary, and the linear sizes of the detectors as measured pre-flight.

For PHT-S the values of Ω_{eff} for each pixel were determined by combining in-flight calibration observations of the detector footprints inside the aperture and model calculations for the shape of the footprint outside the aperture. These values are included in the conversion from signal to extended source flux density.

5.4 Aperture Calibration

For a given filter of the PHT-P subsystems, the FCS calibration was obtained from observations always taken with the same *standard apertures* or *default apertures*:

- $23''$ aperture for P1 filters with a reference wavelength less or equal than 7.7 μm,
- $52''$ aperture for P1 filters with reference wavelengths longer or equal than 10 μm,
- $79''$ aperture for P2 filters, and
- $180''$ aperture for the P3 filters.

The applicability of the calibration to any given aperture is based on the following assumptions:

1. the apertures are perfectly circular or rectangular,
2. the effective solid angle of an aperture is proportional to its area,
3. the solid angle of an aperture is independent of filter,
4. the FCS in-band power is proportional to the area of an aperture.

The physical dimensions of the apertures were measured on ground and are given in Section A.1.2. From available calibration measurements deviations from these simple assumptions are clearly indicated:

- Aperture sequences on the FCS indicated that assumption 4 is not valid. Deviations up to 100%, 15%, and 40% were measured for P1, P2, and P3 respectively; the deviations also show a dependency on FCS heating power.
- Observations of flat sky areas have indicated a disproportional increase of signal for the largest apertures (size $> 120''$) arguing against assumption 2.

- Scans of point sources for a given aperture give profiles that show large deviations from the expected profiles based on assumption 1.

For a subset of PHT04 observations the PHT off-line processing provides an analysis based on an empirical calibration scheme (Müller 2000a, [41]; Müller 2000b, [42]). In the analysis the normalised source signals of an aperture sequence are compared with the normalised signals of a calibration (point) source. Subsequently, the algorithm determines whether the source is point-like or extended, see Section 7.9.

5.5 PHT-S Wavelength Calibration

The in-orbit PHT-S wavelength calibration was performed by measuring emission line objects with PHT-S: see Section 4.6.2. The accuracy in the central wavelength for each pixel is somewhat better than one tenth of a pixel except for a small part of SL where the uncertainty is marginally larger. The accuracy of the wavelength calibration is discussed in the 'ISOPHOT Calibration Accuracies' by Klaas et al. 2002, [26] document.

5.6 Photometric Calibration in AOTs

5.6.1 General signal derivation

All PHT raw data undergo the same processing steps to obtain the mean signal per chopper plateau or mean signal per raster point. These steps are described in detail in Chapter 7.

5.6.2 Multi-filter photometry: PHT03 and PHT22

Single pointing photometry AOTs include one FCS measurement for each detector used. The FCS measurement was taken after completion of the filter sequence for a given detector (see Section 3.10).

Assuming that the derived responsivity applies to all filters of the same detector, the signal from each filter is converted to an in-band power. The powers are converted to a flux density in Jy or MJy/sr using equations in Sections 5.2.5 and 5.3.

5.6.3 Mapping: PHT03, PHT22, PHT32

For AOTs in mapping mode each raster measurement is bracketed by two FCS measurements with identical FCS heating power. For the calibration it is assumed that the responsivity does not vary with time. The average responsivity of the two FCS measurements is used for each raster point. Since the map plus FCS measurements are obtained for one filter at a time, no systematic uncertainties due to $\chi^f(i)$ are involved.

5.6.4 Sparse maps: PHT17/18/19 and PHT37/38/39

During a sparse map concatenated chain (PHT17/18/19 for PHT-P or PHT37/38/39 for PHT-C) two FCS measurements were obtained, the first measurement after the first sky measurement in PHT17/PHT37 and the second one after the last sky measurement in PHT19/PHT39. The FCS in-band powers are adapted to the flux levels as specified in the start and end AOTs and can therefore be different FCS heating power settings. The average responsivity of the two FCS measurements is used for the responsivity of all measurements in the chain.

The multi-filter option can be used in the sparse map AOTs. In such case the two FCS measurements can be of different filter band and a transfer of the calibration is required to the filters for which no FCS calibrations were obtained.

5.6.5 Multi-aperture photometry: PHT04

In this mode one FCS measurement was collected for the last (largest) aperture in the sequence. An important source of systematic photometric uncertainty is the accuracy in the aperture scaling (see Section 5.4). Uncertainties in the beam profile can be minimized by comparison with a similar observation on a point source.

5.6.6 Absolute photometry: PHT05 and PHT25

For PHT05 and PHT25 only one filter band could be selected and the FCS measurement has the same integration time as the source measurement. The observer could therefore minimize statistical and transient uncertainties. Uncertainties due to dark signal and FCS zero signal level could be minimized by including dedicated dark and cold FCS measurements in the observation. Since the absolute photometry AOTs were single filter observations, the systematic photometric accuracy only depends on the uncertainties in the FCS power calibration tables and either in the illumination matrix for PHT-C or the aperture scaling for PHT-P (both for FCS and sky).

5.6.7 PHT-S: PHT40

The instrument set-up of a PHT40 observation is always the same. After dark signal subtraction, the signal of each pixel is directly converted to a flux density in units of Jy. The PHT-S spectral response function was determined from observations of calibration stars (Section 5.2.6). In-orbit beam profile measurements were used to determine the conversion from a point source flux to an extended source flux.

Each target measurement with PHT40 is preceded by a 'pseudo' measurement of 32 seconds in dark instrument configuration. This measurement offers a qualitative assessment whether the responsivity of the PHT-S detectors is affected by a transient introduced by a preceding PHT40 observation.

For example, in case the preceding PHT40 observation involved a source with bright spectral features, the pixels that detected the features could still be in a transient while the pseudo dark was taken. It is also found that different pixels in the PHT-S array show different transient behaviour. This can cause artifacts in the spectrum, especially after observing a strong continuum source.

Possible features in the dark spectrum at a certain wavelength should caution the observer that features in the same pixels of the actual source spectrum could have an instrumental cause. The dark measurement in PHT40 is *not* intended for subtraction from the source spectrum. Instead, an orbit dependent dark signal from dedicated calibration measurements is subtracted.

5.7 Calibration Files

5.7.1 Calibration-G files

The instrument characteristics required for the processing of the ISOPHOT raw data into calibrated products are stored in calibration files which are referred to as *general calibration products*: 'Calibration-G' or 'Cal-G' files. All Cal-G files are in FITS format. The Cal-G files are updated depending on the outcome of the dedicated calibration observations.

In Table 5.1 the types of Cal-G information mentioned in this chapter are listed together with references to the full descriptions elsewhere in this manual. A complete description of all Cal-G files can be found in Chapter 14.

Table 5.1: *Cal-G files related to the parameters described in this chapter.*

parameter	Description	full description
$H(S)$	Correction for signal non-linearities	Section 14.8
$\zeta(S_{src}, det, t_{dwell})$	Correction for chopped signal losses	Section 14.10
$c_{chop}(f, i, \theta)$	Correction for chopper vignetting/offset	Section 14.11
$P^f_{fcs}(h)$	FCS power calibration tables	Section 14.12
S^{det}_{dark}	Orbit dependent dark signals	Section 14.7
R_{det}	Default detector responsivities	Section 14.13
$A(a)$	Area of the aperture in mm^2 (hardcoded)	Section A.1.2
f^f_{PSF}	Point Spread Function factors	Section 14.18
$\alpha^f(a)$	Inhomogeneous FCS illumination of PHT-P	Section 14.15
$\Gamma^f(i)$	Array Illumination by FCS	Section 14.14
$\chi^f(i)$	Wavelength dependent detector flat-fields	Section 14.17
$\varphi(i, S, t)$	Conversion from staring PHT-S signal to flux density	Section 14.9
$g(i, S, t)$	Weight factors related to correction $\varphi(i, S, t)$	Section 14.9
Ω^f_{eff}	Effective solid angles of apertures and pixels	Section 14.21
$\lambda(i)$, $C^{c,p}_{ave}(i)$, $C^{s,p}_{ave}(i)$	PHT-S wavelength and average spectral response functions	Section 14.19
$A_0(i)$, $A_1(i)$	First order signal corrections for PHT-S chopped	Section 14.19
k_f	Colour corrections	Section 14.22

5.7.2 Calibration-A files

In contrast to the general calibration files applicable per instrument mode, there are calibration products per observation. These are related to the FCS measurements which are part of all PHT AOTs except PHT40. The resulting products are called 'Calibration-A' or 'Cal-A' files. Cal-A files are generated at the SPD processing level. Among other data items the Cal-A products contain the signal per chopper plateau of the FCS measurement. The FCS heating power as well as the expected in-band power is provided so that the responsivity of the detector close to the time of the target measurement can be obtained. The derived responsivity together with its uncertainty for each detector pixel has been included in the FITS header of the related SPD product.

See also Sections 13.3.7 and 13.3.8.

Chapter 6

Data Processing Level: Derive_ERD

The *Telemetry Distribution Files* (TDFs) from an entire revolution have been scanned in order to obtain a number of histories which are used to control the succeeding processing phases. These histories are: (i) the *Continuous Compact Status History* (CCSH) and (ii) the *Executed Observation History* (EOH). The CCSH and EOH contain all necessary information to extract the telemetry data covering a *Target Dedicated Time* (TDT). This first global step is called TDF_FIRST_SCAN.

The telemetry is accessed again to generate the first level of data products, called *Edited Raw Data* (ERD), being the format in which raw ISO telemetry is distributed to observers. ERD is basically reformatted TDF data from which invalid sections are removed. No scientific nor instrument-specific processing is performed. ERD products are in the form of binary FITS tables.

ERD generation is performed in units of an observation. The start and end times which are recorded in the EOH determine the interval of telemetry for a given observation[1].

The ERD processing also cuts the CCSH into *Compact Status History* (CSH) products. A CSH product contains all compact status information belonging to a given TDT for a given instrument.

As the telemetry data are in 'raw' engineering units, conversion algorithms should be applied to convert these engineering units to 'physical' units. In Appendix B descriptions of the main conversions are provided.

In order to facilitate the processing steps in the succeeding Derive_SPD level, the orbital phase of the spacecraft for 3 reference times (start, middle, and end) of a TDT are included in the ERD data. The corresponding ERD header keywords are TREFCORn and TREFPHAn (with n=1, 2, 3) for the UTC of reference time and corresponding orbital phase, respectively. The information is necessary for the application of calibration data which depend on the position of the spacecraft in the orbit. The orbital phase data are derived from the orbit file. Since this is processed with the APH (aperture pointing history) data, the orbital phase information is already available on ERD processing level.

The ISOPHOT ERD products have been defined on the basis of the data format of the different subsystems. There are 5 types of ERD:

1. with prefix PPER for single detector subsystems PHT-P1, P2, and P3 (see Section 13.2.2),
2. with prefix P1ER for PHT-C100 (see Section 13.2.3),
3. with prefix P2ER for PHT-C200 (see Section 13.2.4),
4. with prefix PSER for PHT-S (both PHT-SS and SL together in one file, see Section 13.2.6), and
5. with prefix P2ES for PHT-C200 Serendipity Mode scans (see Section 13.2.5).

The CSH data format is the same for all detector subsystems.

[1]These times correspond to the *Start_TDT* and *End_TDT* times in the *Pointed Observation File* (POF)

Chapter 7

Data Processing Level: Derive_SPD

7.1 Overview

Conceptually, for a given AOT the derivation of *Standard Processed Data* (SPD) can be divided into three main stages:

- *ramp processing*: Readouts of an integration ramp in V are reduced to a signal in V/s.
- *signal processing*: Signals are corrected for instrumental effects and averaged over a given period in time.
- *in-band power calibration*:
  - For PHT-P and PHT-C, one or more FCS measurements that were collected according to the AOT logic are processed to determine photometric calibration factors. These factors are used to convert the signals from the sky measurements to an in-band power (in W) on the detector for the selected filter band. In case FCS measurements cannot be applied, the conversion is based on a default detector responsivity.
  - In the case of PHT-S the signals per pixel are converted to Jy/pixel by comparison with similar signals obtained from standard stars.

SPD processing derives a record for each consecutive period in the sky measurement for which the power on the detector is expected to be constant:

- a staring measurement yields one SPD record;
- a raster yields one SPD record per raster position;
- a chopped measurement yields two SPD records: one $on-source$ and one mean *background* record;
- a PHT32 sky measurement contains one SPD record for each chopper plateau.

Apart from the mean in-band power, each record contains additional information such as the power uncertainty, median value, etc. (see Section 13.3).

The above description of SPD records applies to all AOTs except AOT PHT40 (PHT-S spectro-photometry). SPD for PHT40 contains flux densities (in Jy) instead of in-band powers (in W). In the processing level following SPD (see Chapter 8) the PHT-S flux densities are converted into flux densities per wavelength interval (in $\mathrm{Wm^{-2}}\mu\mathrm{m^{-1}}$) and surface brightness units (in $\mathrm{MJy\,sr^{-1}}$).

Besides the SPD products that yield the processed data for the sky measurements, a number of other products are derived based on non-sky internal measurements. The products refer to the following type of measurements (see Section 2.5):

- FCS measurement: The resulting product is also referred to as a *Calibration-A* ('Cal-A') file.
- Dark instrument configuration measurement: This measurement type is obtained with AOTs PHT05, PHT25, and PHT40 and is used to subtract dark signals (in case of PHT05 and PHT25) or to identify possible detector memory artifacts from a preceding measurement of a bright source in case of PHT40.
- Cold FCS measurement: This type of measurement occurs in the absolute photometry AOTs PHT05 and PHT25 to correct for straylight affecting the heated FCS measurement.

7.2 Ramp Processing

7.2.1 Discarding destructive readouts

Detailed description: Section 2.4.2

The destructive readout is the last readout of a ramp in parallel to the reset of the readout electronics and is in general disturbed by the pulse pattern of the electronics. Destructive readouts usually do not follow the highly linear relationship between time and readout voltage as is the case for the non-destructive readouts.

In Derive_SPD the destructive readout is assumed to be unreliable and is generally discarded. The only exception is for PHT32 processing, see Section 7.7

Ancillary data required:

None

7.2.2 Discarding disturbed non-destructive readouts

Detailed description: Section 4.3.1

At the beginning of an integration ramp immediately after a reset, the first non-destructive readout is unreliable. In case of a large number of non-destructive readouts per ramp, more than one readout can be disturbed.

In Derive_SPD a consecutive number of readouts at the beginning of an integration ramp is discarded. The value depends on the detector and the length of a ramp in terms of non-destructive readouts.

Ancillary data required:

The number of readouts to be discarded as a function of (1) detector and (2) the length of a ramp are stored in Cal-G file PSELNDR, see Section 14.4.

7.2.3 Discarding data with OTF or OPF 'off'

Detailed description: none

During a sky measurement the source can drift out of its nominal pointing due to telescope pointing instabilities. When this happens the *On-Target Flag* (OTF) is automatically set to 'off'.

Similarly, if the chopper is not correctly positioned, a chopper *On-Position Flag* (OPF) is also set to 'off'.

Initially, until revolution 524, the OTF is set to 'off' when the actual pointing drifts out of a cone with radius of 10″ around the intended pointing. Due to the good pointing performance of ISO the OTF cone has been reduced to 2″ for ISOPHOT as of revolution 524.

The OTF and OPF flags are contained in the readout records of the ERD products. If either of these flags is set to 'off' then the current integration ramp is abandoned and excluded from further processing. A record is kept per pixel per measurement of the number of integration ramps that are rejected for this reason.

For raster scans, it is assumed that the spacecraft moves off-target to the next raster point, when one of the two raster point identifiers changes. To avoid the inclusion of off-target data while the spacecraft is slewing and repositioning all data are rejected for a fixed (1 s) period after the change in the raster point identifier. After this period the OTF is checked: if the OTF is 'off' then data are rejected until the OTF is 'on' again.

Ancillary data required:

None

7.2.4 Data identification and separation

Detailed description: none

The different measurements that were performed as part of an AOT (like sky, FCS, and dark measurements) need to be identified and separated before they can be processed. For a given TDT all output data records of the same detector and measurement type will be stored inside the same SPD product.

Different measurements are sorted out by performing a cross-correlation between the ERD record and the corresponding CSH record with the same time key. The following flags are then inserted at the beginning of each data record in Derive_SPD to identify the type of measurement:

- Raster point ID
- Aperture ID
- Chopper position
- Filter ID
- Polariser ID

Note that the filter ID also determines the detector.

Ancillary data required:

None

7.2.5 Determine chopper position and step number

Detailed description: Sections 2.4.4, 2.8 and Appendix B.3

The telemetry contains the actual chopper position which is recorded every 2 s. The data are provided as voltages and must be converted to a deflection angle. The conversion algorithm can be found in Appendix B.3.

The chopper dwell time is directly related to the instrument readout timing parameters (see Section 2.4.4) and is therefore a reliable parameter in the instrument commanding. Using the chopper dwell time corrected for the chopper movement (Section 2.8), the moment (in ITK units) is determined when the chopper should have changed its position.

From the inferred chopper transitions and the ITK of the readouts the relative position of the chopper is obtained. In principle the same can be done from direct analysis of the chopper position in the telemetry data. The reasons why time is used rather than the chopper position are:

- the chopper position associated with the first integration ramp after a chopper transition is unreliable (on-board software feature), and
- the algorithm allows recovery of the correct position in the chopper cycle, if there is a gap in the data due to telemetry dropouts.

To remove possible contamination by unreliable chopper positions in the data products, a median filter is applied to the positions associated with each integration for a fixed chopper position.

Before the chopper position can be calculated it is necessary to determine the *step flag* I_{step} within a cycle. The total number of chopper plateaux in a chopper cycle depends on the chopper mode as follows:

Staring	1
Rectangular	2
Sawtooth	$2 \times steps + 1$
Triangular	$4 \times steps$

Where *steps* indicate the number of chopper offset positions at one side of the central field of view (CFOV). The ITK is used to calculate the position in the cycle. In general, for rectangular, sawtooth and triangular chopping, the first chopper position is an 'off-source' position, the second position is an 'on-source' position (Section 2.8). This is then digitised to the step flag I_{step} as follows:

Staring: $I_{step} = 1$, unless pointing at the FCS, in which case it is defined to be -1.

Rectangular: $I_{step} = -1$ on-source, 1 for background.

Sawtooth: For all chopped AOTs exept PHT32: $I_{step} = -1$ on-source, 1 for background. For PHT32: I_{step} varies from $-steps$ at maximum negative angle to $+steps$ at maximum positive angle. Step flag 0 represents the CFOV.

Triangular: $I_{step} = -1$ on-source, 1 for background.

Ancillary data required:

None

7.2.6 Conversion of digitised numbers to CRE output voltages

Detailed description: Section 2.4.3

The *Detector Interface Electronics* (DIE) in the PHT external electronics unit subtracts a commandable offset from the CRE voltage and amplifies the difference with a commandable gain factor before the analogue to digital conversion. The CRE output voltage must be reconstructed from the *Digitised Numbers* (DN).

There are two DIE chains. Each detector subsystem has a default connection to one of them (see Section 2.4.3). A change in default connection is indicated by the 'cross status' flag in the CSH (actually never

used during the mission). The CSH also contains the value of the selected gain of the differential amplifier in the DIE electronics. The CRE output voltage U_{CRE} and DNs are related by the following formula for a given DIE electronics chain and selected gain:

$$U_{CRE} = (D_o - DN - G_{signal} \times (DI - 2048)) \times \frac{20.0}{4096 \times G_{off}} + U_{off} \qquad [\mathrm{V}] \tag{7.1}$$

where,

D_o = fixed offset

G_{off} = offset gain

DI = selected OFFSET data word (0...4095)

G_{signal} = signal gain

U_{off} = G_{signal} dependent offset

Ancillary data required:

1. The selected OFFSET from the measurement record in the CSH.
2. The DIE transfer function tables are stored in Cal-G files PDIE1TRANS and PDIE2TRANS, see Section 14.3.

7.2.7 Discarding saturated readouts

Detailed description: Section 4.3.5

If the source is significantly brighter than anticipated, integration ramps can saturate, i.e. the CRE output voltage has reached its maximum value prior to reset. The readouts taken during times of detector saturation are useless and must be discarded. Saturation also occurs in case the responsivity of the detector exceeds the nominal value by a large factor. In practice this frequently happened towards the end of the science window where both FCS and sky measurement got saturated due to high responsivity. For detectors P3, C100 and C200 many FCS measurements taken during revolutions 94–191 were saturated due to over-illumination by changed FCS behaviour.

Threshold voltages for each detector are listed in Section 4.3.5. As soon as the threshold voltage has been crossed, all following readouts up to the end of the ramp are discarded.

Ancillary data required:

It is assumed for all detectors that saturation is reached for CRE output voltages greater than 1.0 V, this is with some safety margin below the actual thresholds given in Table 4.4.

7.2.8 Correction for non-linearities of the integration ramps

Detailed description: Sections 4.3.2 and 4.3.4

Integration ramps are not perfectly straight but show deviations from linearity. The non-linearity is caused by two independent effects:

- non-linearities due to the CRE (Section 4.3.2)

- downward curving due to de-biasing. Only low-bias germanium detectors P3, C100 and in particular C200 show this effect (Section 4.3.4).

The integration ramps are corrected for non-linearities before signals are derived.

In Derive_SPD it is assumed that the corrections are a function of only the absolute value of the CRE output voltage. It is assumed that non-linearities due to both CRE and de-biasing (as is the case for the germanium detectors P3, C100 and C200) can be corrected using one function which only depends on the CRE output voltage.

The ramps are linearized using tables which contain for a given CRE output voltage the correction voltage to be subtracted. In the tables the sampling of the CRE voltages is sufficiently fine to allow searching for the table value closest to the measured CRE voltage and using its corresponding correction.

Ancillary data required:

The CRE Transfer Function Table per detector pixel and clock frequency are stored in Cal-G files PC1CRELIN, PC2CRELIN,, and PPCRELIN, (Section 14.5). There is no ramp linearisation for PHT-S measurements.

7.2.9 Ramp deglitching

Detailed description: Section 4.4

A radiation hit or glitch shows up as a voltage increase between two subsequent readouts which is larger than the increase expected from the steady photo-current produced by the celestial or internal source illumination. In case the hit is very energetic, the voltage increase can be so high that it saturates a ramp or even causes a responsivity transient. In SPD two different deglitching algorithms are applied: the first algorithm is described in this section and is based on an analysis of the readouts per ramp; the second one checks for any outliers in the signals of a given chopper plateau and is described in Section 7.3.4.

For ramp deglitching, an iterative algorithm was implemented which identifies and removes excessive increases in CRE output voltage. The algorithm has the following settings:

N_{it}	=	4	number of iterations
κ_1	=	4	minimum number of standard deviations for glitch detection (first threshold)
κ_2	=	1	minimum number of standard deviations for second threshold
N_{min}	=	25	minimum number of readouts per ramp for application of algorithm
N'_{min}	=	32	minimum number of readouts per ramp for application of second threshold

For integration ramps with less than N_{min} readouts no ramp deglitching is applied and the deglitching can only take place at signal level (Section 7.3.4). For an integration ramp consisting of $N > N_{min}$ readouts with voltages V(1), V(2),...V(N), taken at times t(1), t(2),...t(N), the slope between each consecutive readout is calculated:

$$s(k) = \frac{V(k+1) - V(k)}{t(k+1) - t(k)} \qquad [V/s]. \tag{7.2}$$

Outliers in $V(i)$ are always positive because of the extra photocurrent due to ionising radiation. The maximum $s_{max}(k)$ is removed from the $N-1$ differences prior to calculating the mean S and standard deviation σ of the voltage differences. The exclusion of the most extreme element makes the computation of the mean and sigma of the distribution more robust and efficient.

In case

$$s(k) > S + \kappa_1 * \sigma \qquad [\mathrm{V/s}], \tag{7.3}$$

then a glitch is detected in readout k, which will be flagged. If the ramp contains more or equal than N'_{min} readouts, then this detection triggers the algorithm to change the threshold κ_1 into κ_2 for $l > k$ until

$$s(l) < S + \kappa_2 * \sigma, \qquad l > k \qquad \text{[V/s]}. \tag{7.4}$$

As soon as Equation 7.4 is satisfied, the threshold is reset to κ_1. All readouts which do not satisfy Equation 7.4 are flagged. This two-threshold deglitching is very efficient in removing the 'tail' of a glitch. This tail is due to transient behaviour of the detector signal.

If readout k is flagged then the voltages $k+1$ to N are corrected by subtracting the excess voltage due to the glitch:

$$V_{corrected}(k+1) = (V(k+1) - V(k)) - (V(j+1) - V(j)) + \Delta V \quad \text{[V]}, \quad k = j, ..., N-1 \tag{7.5}$$

where $\Delta V = S * \Delta t$ is the mean voltage difference for all readouts of a given ramp.

The procedure is repeated N_{it} times to remove successively smaller glitches.

A check is made on the parameter which defines the minimum number of readouts that can be processed. If this parameter is less than 7, then an error message is logged (PRDE) and the deglitching algorithm is not executed. This avoids the possibility of an execution error occurring if the minimum number of readouts parameter is set too low in the Cal-G file PCONTROL.

Ancillary data required:

None, the thresholds and other deglitching parameters are hardcoded.

7.2.10 Extraction of the signals and their uncertainties

Detailed description: Section 2.4.2

Of each ramp j, the slope $s(j)$ (or *signal* in V/s) is proportional to the photo-current which is a measure of the number of photons falling on the detector per unit time. In the SPD processing all valid readouts between two reset intervals are used to fit a first order polynomial.

The uncertainty $\Delta s(j)$ is the rms of the fit residuals.

Ancillary data required:

None

7.3 Signal Processing: Staring PHT-P and PHT-C

7.3.1 Reset interval correction

Detailed description: Section 4.3.3

The detector CRE's give systematically different signals for different reset intervals under constant illumination conditions. Analysis of a photometric measurement requires signal information of other measurements such as internal calibration, background, external calibration, target, etc. If these measurements have not the same readout set-up systematic errors are introduced into the photometric calibration.

It is found that a signal $s(RI,\ DAT\_RED)$ obtained with a given reset interval RI and data reduction DAT_RED can be converted to a signal $s(RI_x,\ DAT\_RED_x)$ of a different CRE setting according to:

$$s(RI_x,\ DAT\_RED_x) = A_0^x(RI_x, DAT\_RED_x, RI, DAT\_RED) + A_1^x(RI_x, DAT\_RED_x, RI, DAT\_RED)\cdot s(RI,\ DAT\_RED) \qquad [V/s], \tag{7.6}$$

where A_0^x is the offset value and A_1^x is the slope in the relationship. Both parameters differ for different detectors. The reset interval dependence is corrected for by transforming all signal values $s(RI, DAT\_RED)$ to the corresponding values $s(RI = \frac{1}{4}\,s, DAT\_RED = 1)$ of a *reference reset interval*:

$$s(RI = \frac{1}{4}\ s,\ DAT\_RED = 1) = A_0(RI,\ DAT\_RED) + A_1(RI,\ DAT\_RED)\cdot s(RI,\ DAT\_RED) \qquad [\mathrm{V/s}], \tag{7.7}$$

where the superscripts and subscripts x have been dropped to indicate that the constants A_0 and A_1 only refer to the reference reset interval with DAT_RED=1.

Ancillary data required:

For each detector the correction factors A_0 and A_1 are stored in Cal-G files PP1RESETI, PP2RESETI, and PP3RESETI for the P detectors and PC1RESETI and PC2RESETI for the C detectors (Section 14.6). There is no reset interval correction for PHT-S measurements.

7.3.2 Dark signal subtraction

Detailed description: Section 4.2.6

The dark signal is subtracted from the signal as follows:

$$s'(\phi(t)) = s(\phi(t)) - s_{dark}(\phi(t)) \tag{7.8}$$

Where $s'(\phi(t))$, $s(\phi(t))$, and $s_{dark}(\phi(t))$, are the corrected, initial, and dark signal, respectively. The orbital phase $\phi(t)$ ranges between 0 and 1 where 0 is the moment of perigee passage and 1 is a full revolution later. The ERD contains the keyword TREFPHA2, which is the orbital phase at the start of the measurement. The value for $\phi(t)$ in Equation 7.8 corresponds to the time at mid-point of a chopper plateau.

For chopped measurements with PHT-P and PHT-C the dark signal is subtracted from the generic pattern according to Equation 7.8 (Section 7.5). Dark signal subtraction is necessary because the subsequent signal analysis can involve not only the difference signal but also the absolute signal level. In the case of chopped measurements with PHT-S, the dark signal subtraction is not necessary (Section 7.6.4).

Ancillary data required:

Dark signal tables for each detector-pixel combination have been derived from dedicated in-flight observations. The tables contain a value for the dark signal plus uncertainty (in V/s) for each detector pixel as a function of orbital phase. The data are stored in Cal-G files PPDARK (for detectors P1, P2, P3), PC1DARK (for all 9 pixels of C100), PC2DARK (for all 4 pixels of C200), see Section 14.7.

7.3.3 Correction for non-linear detector response of PHT-P and PHT-C

Detailed description: Section 5.2.2

Analysis of measurements of celestial standards showed that the derived values of the detector responsivities (photo-current per incident flux) are not constant. This can be due to gradual responsivity changes of a detector during a revolution independent of incident flux, we call this the *time dependent part* of the responsivity variation. Variations can also be due to the fact that the detector responsivity is a function of incident flux. This processing step corrects for the latter effect, the *signal dependent detector responsivity*.

The non-linear behaviour is found to be different for the different filters. The PHT-P and PHT-C photometric calibration scheme uses the internal reference source (FCS) measurements for the derivation of the actual detector responsivity at a given flux level. The inaccuracy due to non-linear detector response is minimized when the in-band powers for the sky and FCS measurement are similar. Large inaccuracies are introduced in case of multi-filter, multi-aperture, and mapping measurements where a large dynamic range in signals has to be calibrated with one FCS signal level. For a detailed description of the signal linearisation see Schulz 1999, [51].

To correct for responsivity non-linearities, a signal correction H is applied such that in measurements of known sources the detector responsivity $R(s)$ becomes constant independent of flux or signal s_{new} (see Section 5.2.5):

$$s_{new} = H^{f,i}(|s_{old}|), \tag{7.9}$$

where H is not only a function of signal but also of filter f and detector pixel i. For the determination of H the time dependent responsivity component was assumed to add only statistical noise to the measurements. In principle H is defined only for positive signals. To make H useful in practice, it is assumed that the correction function goes through the origin (zero) and is point-mirrored in the origin to cope with negative signals.

Ignoring the time dependent component in $R(s)$, the signal linearisation causes the responsivity of a detector to become one value independent of the signal level: $R(s_{new}) = R'$. In principle, for the flux calibration, the precise value of R' is arbitrary as long as an FCS measurement is performed close in time, which relates the corrected signal s_{new} to the power on the detector. The signal linearisation tables are derived per filter and are normalised to yield the median of all measured responsivities.

Ancillary data required:

The corrections are stored in Cal-G files P*SLINR.FITS, where (*) stands for P1, P2, P3, C1, and C2, see Section 14.8. These are in essence lookup tables giving the corrected signal for a given input signal per filter and detector pixel. To determine signal values intermediate between the table values, a linear interpolation is applied.

7.3.4 Signal deglitching

Detailed description: Section 4.4

The charges released by a cosmic particle hit cause an effective increase in signal level. Low energetic hits affect only one signal, but high energetic hits can cause several consecutive signals to be higher. A high hit rate can cause the mean signal level in a measurement to increase.

Assuming that the signal distribution is normal on a local scale, a *local distribution* method is used to filter out signal outliers. The method consists of a 'box' sliding along the time axis, defining local distributions as it goes. The maximum and minimum values of the signals are excluded from the calculation of the

standard deviation. The exclusion of the extremes in the local distribution makes the deglitching more robust and efficient.

Signals are flagged that are outside a given number of standard deviations from the median for a given local distribution. A signal is eventually discarded in case it is flagged a pre-set number of times. This process is iterated several times.

If the number of available signals is insufficient then a signal is discarded whenever its uncertainty $\Delta s(i)$ (Section 7.2.10) is greater than a given threshold. The controlling parameters of the algorithm are given in Table 7.1.

Table 7.1: *Parameters for signal deglitching.*

Parameter	Value	Description
min_deglitch	5	minimum points to apply
max_error	1 [V/s]	maximum error allowed if number of points is less than min_deglitch
n_iter	2	number of iterations of deglitch filter
n_local	20	number of points in local distribution
n_step	1	the number of points to move the 'box' for the local distribution each time
n_sigma	3	rejection factor: number of standard deviations from local median.
n_bad	2	number of times a point has to be flagged as 'bad' before it is rejected.

The accuracy of this method depends on the glitch frequency and the values of the tuning parameters (Guest 1993, [13]). The number of signals affected by glitches is stored in the header of the SPD product (keyword RAMPDEGL, see Section 13.3.1.3)

Ancillary data required:

None

7.3.5 Transient correction

Detailed description: Section 4.2.3

A routine has been implemented which detects the presence of a significant signal transient on a chopper plateau. When a transient is detected, a range of unreliable signals will be flagged. The algorithm is iterative and is applied until either

- no significant systematic variation can be detected in the remaining signals or,
- a minimum number of signals is left.

It is assumed that a detector transient shows up as a trend which causes either a systematic increase or decrease of the signal level. The signal level will eventually become stable in time when the signal reaches its asymptotic limit. The presence of such a trend is detected by applying the non-parametric Mann statistical test to the signals (e.g. Hartung 1991, [15]). This involves computing a statistic C:

$$C = \sum_{k=1}^{N-1} \sum_{j=k+1}^{N} sign(s(j) - s(k)) \tag{7.10}$$

where,

$$\begin{array}{rcll} \text{sign(s(j) – s(k))} & = & +1 & \text{if s(j)} > \text{s(k)} \\ & = & 0 & \text{if s(j)} = \text{s(k)} \\ & = & -1 & \text{if s(j)} < \text{s(k)} \end{array}$$

for all signals s(k), where $k = 1$,...,N and N is the number of signals on the chopper plateau. The presence of a transient can be detected by comparing C against the corresponding Kendall k-statistic for a given confidence level.

Alternatively, as the number of signals is generally large, it is more convenient to compute the statistic C(*) which can be compared with the quantile of a normal distribution:

$$C(*) = \frac{C}{\sqrt{N(N-1)(2N+5)/18}} \; . \tag{7.11}$$

The algorithm requires the following parameters:

- N(min) = 7 - the minimum number of signals for application of the Mann test,
- $\alpha = 0.05$ - the probability that the null hypothesis (=no drift) is rejected.

The result, $C(*)$, is tested against the null hypothesis which assumes absence of drift. This corresponds to a critical value of $C(*) < 1.645$ for $\alpha = 0.05$. A test is made on whether the drift is up ($C(*) < 1.645$) or down ($C(*) > -1.645$).

The algorithm initially performs the test on all available signals on a chopper plateau. If the null hypothesis is rejected, then the test is performed on the second half of the data and the first half is rejected. If the null hypothesis is again rejected, then the second half of the second half is tested etc. The iteration stops either when the null hypothesis is accepted or when there are too few signals (N≤N(min)) to apply the test. Information on the outcome of the procedure is stored per chopper plateau by setting the pixel status flags 2 ('drift fit applied successfully') or 4 ('drift fit may not be accurate') in the SPD records (see Sections 7.12 and 13.3.14).

Since the absolute signal of the FCS measurement determines the responsivity and hence the absolute level of the flux calibration any unstabilised FCS signal has direct impact on the calibration accuracy. For a given observation, the SPD header keyword FCSDRIFT is set to TRUE if the pixel status flag has value 4 in the first FCS measurement of a given detector. The flag is set as soon as a pixel is encountered with pixel status=4.

Ancillary data required:

None

7.3.6 Averaging signals of same instrument set-up

Detailed description: Section 4.2.6

To increase the signal-to-noise ratio, all valid signals on a single chopper plateau are averaged. The following formula is applied:

$$\langle s \rangle = \frac{\sum_1^N w_j \times s'_j}{\sum_1^N w_j} \qquad [V/s], \tag{7.12}$$

where N is the total number of valid signals on the plateau and $w_j = (\Delta s(j))^{-2}$ is the statistical weight of each signal obtained from its associated statistical uncertainty propagated from the previous signal processing steps. The value of N is stored in the PxxSNSIG field of the SPD record.

The plateau average is either (1) the average of the signals which are not flagged as drifting according to the test described in Section 7.3.5 or (2), if the test fails, the average of the last 7 signals of the plateau or the last 8 s of data, whichever is longer in time.

If it is not possible to calculate a weight for *any* of the signals on a plateau, then all signals will have a weight $\mathrm{w_j} = 1$ assigned. This can happen when the ramps consist of only 2 useful readouts. If no weight can be calculated for *a subset* of the signals on the plateau, then these will be ignored by setting $\mathrm{w_j} = 0$.

The uncertainty of the average signal is derived from the rms of the individual signals:

$$\Delta\langle s \rangle = \sqrt{\frac{\sum_1^N w_j \times (s'_j - \langle s \rangle)^2}{(N-1)\sum_1^N w_j}} \qquad [V/s]. \tag{7.13}$$

Ancillary data required:

None

7.3.7 Obtaining the median of all photo-currents

Detailed description: none

The signal distribution can be non-Gaussian due to signal transients or due to the presence of many positive signal outliers caused by glitches which have not been filtered out completely. In such case, the median signal is a better estimate for the signal per chopper plateau than the average. The median and the quartiles in conjunction with the weighted average should retain information on a non-Gaussian signal distribution. For a gaussian distribution the median is close to the average, and the quartiles fall within the uncertainty interval.

Therefore the median ($\langle \mathrm{s(j)} \rangle^M$) and first and third quartile of all available signals are calculated. In contradistinction to the computation of the weighted average, the determination of the median, first, and third quartile values does not exclude signals that are flagged as unreliable by the signal deglitching or transient correction.

For very small signals and ramps with few readouts the quantization by the A/D converter becomes important. The signals in a measurement will have only a discrete number of values. In these cases the median and quartiles are not good estimates.

Ancillary data required:

None

7.3.8 Ramp statistics in SPD and Cal-A headers

Detailed description: none

Useful statistics about readout and signal discarding collected along the signal processing chain is made available to the observer. The statistical information is stored in the SPD product headers.

- **PLATDROP:** number of plateaux missed due to gaps in the data
- **PLATNORP:** number of times during an observation that all ramps of a plateau have been rejected. In most cases this is due to the spacecraft being off-target.
- **RAMPDEGL:** number of ramps rejected from processing due to detected glitches in signal.
- **RAMPINVD:** number of times a bad ramp is flagged, that is ramps affected by being off target, etc.
- **RAMPSAT:** number of times that only one readout in an integration ramp is available for processing. This can happen at the end of a chopper cycle or due to partial saturation of ramps.
- **RAMPZSG:** number of signal values less than or equal to zero, it is only written to the header when the count is more than zero.
- **READAUTO:** number of readouts with automatic data reduction flag set.
- **READCOP:** number of readouts with chopper off position flag set
- **READOFFT:** number of times that the OTF indicated that the spacecraft was off-target during an observation, which can happen during raster observing modes.
- **READSUSP:** number of ERD records that have been flagged as 'suspicious' due to the presence of a corrupted science floating block in the telemetry.

Ancillary data required:

None

7.4 Signal Processing: Staring PHT-S

The signal processing of PHT-S staring mode data starts at the level where one signal in V/s has been derived for each integration ramp. In the following processing steps, the signal records of ramps that are completely saturated are skipped.

7.4.1 Dark signal subtraction

Detailed description: Section 4.2.6

This step is similar to the step described in Section 7.3.2.

Ancillary data required:

The dark signal data are stored in Cal-G file PSDARK (128 pixels of PHT-S), see Sections 14.7 in particular 14.7.1.

7.4.2 Transient correction and calibration of signals

Detailed description: Section 5.2.6

For each pixel i the signals $s(i,t)$ are directly converted to flux densities $F_\nu^t(i)$ using a transfer function:

$$F_\nu^t(i) = \varphi(i, s(i,t), t) \quad [Jy], \tag{7.14}$$

$$\Delta F_\nu^t(i) = \frac{\Delta s(i,t)}{s(i,t)} F_\nu^t(i) \quad [Jy], \tag{7.15}$$

The function $\varphi(i, s(i,t), t)$ has been implemented as a table with logarithmic signal and time spacings. The value is obtained from linear interpolaton. We give the flux a superscript t to indicate that the flux itself is supposed to be constant and has no time dependence. Time t along a measurement is computed from

$$t = t_{mid} - t_0 \quad [s], \tag{7.16}$$

where t_{mid} is the time at the midpoint of a given ramp and t_0 the time of the first readout of a given measurement. Signals with $t < 1\,\mathrm{s}$ are not processed.

This transformation yields transient corrected flux densities $F_\nu^t(i)$ along the measurement. Due to the transient behaviour of the PHT-S detectors, the transient correction is larger at the beginning of a measurement where the signal is less stabilised than after a long period of integration. The stabilisation time depends on the absolute brightness of the source.

To include this information, a weight is given to each $F_\nu^t(i)$ based on the degree of transient correction:

$$w'(i,t) = g(i, s(i,t), t). \tag{7.17}$$

Signals obtained for times $t < 1$ s get $w'(i,t) = 0$.

Ancillary data required:

The transfer function $\varphi(i,s,t)$ and corresponding weight table $g(i,s,t)$ are stored in Cal-G files PSDYNAMIC and PSDYNWT, see Section 14.9 for detailed descriptions.

7.4.3 Computation of the weighted mean flux

Detailed description: none

The weighted mean of the array of flux densities $F_\nu^t(i)$ is computed using weights obtained from the combination of the weighting factor $w(i,t)$ and the statistical uncertainty $\Delta F_\nu^t(i)$:

$$w(i,t) = \frac{w'(i,t)}{\Delta^2 F_\nu^t(i)}, \tag{7.18}$$

and hence,

$$\langle F_\nu(i) \rangle = \frac{\sum_{t>1s} F_\nu^t(i) w(i,t)}{\sum_t w(i,t)} \quad [\mathrm{Jy}], \tag{7.19}$$

$$\Delta\langle F_\nu(i) \rangle = \sqrt{\frac{\sum_1^N w(i,t) \times (\langle F_\nu(i) \rangle - F_\nu^t(i))^2}{(N-1)\sum_1^N w(i,t)}} \quad [\mathrm{Jy}]. \tag{7.20}$$

The calibration for PHT-S is most valid for detector temperatures of $2.7 < T_{det} < 3.1$ K. Since there were occasions during operations where PHT-S operated outside this temperature interval, a warning will be written to the SPD header in case the temperatures as given by the ERD keywords PSERTEM1 and PSERTEM2 are outside the interval.

If $F_\nu(i)$ for pixel i is outside the flux density range then a warning message will be written to the SPD header that the flux for pixel i is out of the calibration range.

Ancillary data required:

The flux limits for which the calibration is reliable are stored in the header of the Cal-G file PSDYNAMIC (Section 14.9) under keywords FLXiL and FLXiU (lower and upper bound, resp.). where i is the pixel number.

7.5 Signal Processing: Chopped PHT-P and PHT-C

7.5.1 Processing overview for chopped observations

Detailed description: see also Section 5.2.3

Analysis of many chopped observations performed with PHT-P and PHT-C (involving AOTs PHT03, PHT04, and PHT22) has shown that the 'conventional' processing method had to be changed drastically. The main driver for this is that chopped measurements do not give stabilised signals which cause significant losses on the true difference signal. Most of the processing steps which were commonly shared between the staring and chopped observations became obsolete for the chopped observations. Instead, a separate SPD level processing was used.

The present signal derivation relies on the analysis of signals from pairs of consecutive readouts rather than signals per ramp. This gives better statistics of the signals per chopper plateau, since in many chopped measurements each chopper plateau covers only a few (typically 4) ramps.

To increase further the robustness in determining the difference signal, the repeated pattern of off-source and on-source chopper plateaux is converted into a 'generic pattern'. The generic pattern consists of only 1 off- and 1 on-source plateau and is generated using an outlier resistant averaging of all plateaux. The shape of the generic pattern determines the correction factors with regard to stabilised staring measurements.

The FCS measurement is used to determine the responsivity of a given observation. The chopped FCS measurements are treated in the same way as the chopped sky measurements, namely for both types of measurement a generic pattern is constructed.

Using a symmetry assumption, the corrected signal level of FCS1 is determined from the measured signal levels of FCS1 and FCS2 and applying the same signal loss correction as for the sky measurements. Following the creation of a generic pattern, the DERIVE_SPD processing proceeds as for staring mode observations from reset interval correction to flux calibration, which uses the corrected FCS1 signal of the chopped FCS measurement.

After reading the ERD the following processing steps are performed for Derive_SPD:

1. ramp linearisation,
2. generic pattern creation,
3. reset interval correction,
4. dark signal subtraction,
5. signal linearisation,

6. determination of the difference signal $s_{s+b} - s_b$ from pattern,
7. determination of the difference signal corrected for chopped signal losses,
8. flux calibration.

Steps 2, 6, and 7 are explained in more detail in the following sections.

Ancillary data required:

None

7.5.2 Setting up data for generic pattern construction

Detailed description: none

A *chopper unit* comprises two consecutive chopper plateaux, in particular either plateaux on the background and source or on FCS2 and FCS1. The number of chopper units N_u and *chopper dwell time* t_{dwell} of a measurement in a given chopper mode is determined according to:

$$N_u = \frac{t_m}{2N_r t_r} \quad \text{rectangular and triangular mode} \tag{7.21}$$

$$N_u = \frac{2t_m}{3N_r t_r} \quad \text{sawtooth mode} \tag{7.22}$$

and

$$t_{dwell} = N_r t_r = 2^{(n_d - 1)}, \tag{7.23}$$

where:

- t_m in s is the measurement time,
- N_r is the number of ramps per chopper plateau,
- t_r in s is the reset interval time,
- n_d is the index representing the dwell time in the calibration files.

In rectangular mode one full chopper cycle corresponds to one chopper unit:

$$unit = background + source, \tag{7.24}$$

in triangular mode one chopper cycle corresponds to two consecutive chopper units:

$$1^{st}\ unit = background\ 1 + source, \tag{7.25}$$

$$2^{nd}\ unit = background\ 2 + source, \tag{7.26}$$

and in sawtooth mode, one chopper cycle ($background\ 1 \Rightarrow source \Rightarrow background\ 2$) also corresponds to two consecutive chopper units, but the last plateau of the second unit is regarded as missing and filled up with zeros:

$$1^{st}unit = background1 + source, \quad (7.27)$$
$$2^{nd}unit = background2. \quad (7.28)$$

The time interval of a *logical ramp* is defined as 1/8 of the duration of a chopper unit and can be derived from:

$$N_{read} = \frac{(NDR+1)N'_r}{4} \quad (7.29)$$

where:

- N_{read} is the total number of readouts, which includes both destructive and non-destructive readouts;
- NDR is the number of non-destructive readouts;
- N'_r is the actual number of ramps per chopper plateau in the telemetry and is derived from $N'_r = N_r/DAT\_RED$ where N_r is the commanded number of ramps per chopper plateau and DAT_RED is the applied data reduction factor.

Before the signal derivation, readouts which can cause systematic deviations are 'cleaned' or flagged 'bad':

- destructive readouts, see Section 7.2.1;
- a fixed fraction of readouts at the beginning of a ramp, the same fraction is used as for staring measurements, see Section 7.2.2;
- saturated readouts, determined in the same way as described in Section 7.2.7;
- If for a given measurement $N_u > 4$ in case of rectangular mode or $N_u > 8$ in case of triangular or sawtooth modes, then the first 25% of the whole measurement is discarded;
- In case of a gap in the data stream due to e.g. a telemetry drop, the entire chopper unit in which the gap occurs is discarded. The start of the next unit is determined from the start time (in ITK) of the last chopper unit before the gap.

For all available pairs of consecutive readouts the *difference signal* s_{diff} is computed:

$$s_{diff} = \frac{V_{i+1} - V_i}{t_{i+1} - t_i} \quad (7.30)$$

where V_i and V_{i+1} in V are the voltages and t_i and t_{i+1} are the times of consecutive readouts. Note that the time difference ($\Delta t = t_{i+1} - t_i$) is always the same for a given measurement. After calculation, each s_{diff} is stored in an array in which each element represents a logical ramp in the measurement. In total there are $8 \times N_u$ elements in this array. In case of sawtooth chopper mode, the array elements belonging to the logical ramps of the second plateau of the even chopper units (2, 4, 6, ...) are set to zero.

Ancillary data required:

None

7.5.3 Generic pattern construction

Detailed description: Section 5.2.3 for an overview

The generic pattern is constructed by stacking the chopper units onto one single unit. However, long term transients or detector drifts which usually last longer than several consecutive chopper units introduce an unwanted noise in the generic pattern. Therefore, before stacking the chopper units, the measurement is corrected for a drift by normalising the chopper units u (u=1, 2, 3,...,N_u):

Rectangular chop mode:
◇ compute the median of s_{diff} per chopper unit u: $m(u)$
◇ compute $s'_{diff} = s_{diff}(u)/m(u)$
◇ store $m(u)$ in an array with N_u elements
◇ determine a scaling factor $\overline{m(u)}$ from the average over elements $N_u/2$ to N_u.

Triangular chop mode:
◇ compute the median of s_{diff} in two consecutive chopper units $u, u+1$: $m(u,\, u+1)$, (u is odd)
◇ compute $s'_{diff} = s_{diff}(u,\, u+1)/m(u,\, u+1)$
◇ store $m(u,\, u+1)$ in an array with $N_u/2$ elements
◇ determine a scaling factor $\overline{m(u)}$ from the average over elements $N_u/4$ to $N_u/2$.

Sawtooth chop mode:
◇ compute the median of s_{diff} of the first of every two consecutive units $u, u+1$: $m(u)$, (u is odd)
◇ compute $s'_{diff} = s_{diff}(u,\, u+1)/m(u)$
◇ store $m(u)$ in an array with $N_u/2$ elements
◇ determine a scaling factor $\overline{m(u)}$ from the average over elements $N_u/4$ to $N_u/2$.

Before the generic pattern is created two intermediate patterns are obtained by stacking of the n =odd (pattern 1) and n =even (pattern 2) chopper units. The 8 average signals plus their associated uncertainties which correspond to the 8 logical ramps in each pattern are obtained by computing an outlier resistant mean of the values of s'_{diff} for each logical ramp. For triangular mode the two patterns correspond to the different background positions. For the sawtooth mode, s'_{diff} of the logical ramps 5 to 8 of the even chopper units (pattern 2) is always zero.

The *generic pattern* for rectangular and triangular chop mode is determined from:

$$s(i) = \overline{m(u)}\frac{(s_1(i) + s_2(i))}{2}, \tag{7.31}$$

$$\Delta 1 = \overline{m(u)}(s_1(i) - s_2(i)), \tag{7.32}$$

$$\Delta 2 = \overline{m(u)}\sqrt{\Delta^2 s_1(i) + \Delta^2 s_2(i)}, \tag{7.33}$$

$$\Delta s(i) = max(\Delta 1, \Delta 2), \tag{7.34}$$

similarly, for sawtooth mode:

$$s(i) = s_1(i)\overline{m(u)}, \tag{7.35}$$

$$\Delta s(i) = \Delta s_1(i)\overline{m(u)}, \tag{7.36}$$

where:

- i=1,. . .,8 is the logical ramp index,
- $s_1(i)$, $s_2(i)$ (in V/s) are the outlier resistant means of pattern 1 and pattern 2,

- $\Delta s_1(i)$, $\Delta s_2(i)$ (in V/s) are the associated uncertainties,
- $\Delta 1$ and $\Delta 2$ (in V/s) are intermediate uncertainties,
- $\Delta s(i)$ (in V/s) is the final signal uncertainty for each logical ramp in the generic pattern.

The 8 signals in the generic pattern are subsequently subject to reset interval correction (Section 7.3.1), dark current subtraction (Section 7.3.2), and signal linearisation (Section 7.3.4).

Ancillary data required:

None

7.5.4 Determination of source signal

Detailed description: none

Based on the generic pattern, the signal of the source s_{src} is determined. The calibration analysis has shown that the appearance of the pattern depends on several parameters such as the detector used, the signal difference, the mean signal level, as well as the chopper dwell time. The determination of the signal s_{src} depends on the detector used:

$$\text{P1}: \quad s_{src} = med(s(i),\, i = 5,8\,) - med(s(i),\, i = 1,4\,) \tag{7.37}$$

$$\text{P2}: \quad s_{src} = med(s(i),\, i = 5,8\,) - med(s(i),\, i = 1,4\,) \tag{7.38}$$

$$\text{P3}: \quad s_{src} = max(s(i),\, i = 5,8\,) - min(s(i),\, i = 1,4\,) \tag{7.39}$$

$$\text{C100}: \quad s_{src} = ave(s(i),\, i = 5,8\,) - ave(s(i),\, i = 1,4\,) \tag{7.40}$$

$$\text{C200}: \quad s_{src} = \frac{(s(7)+s(8))}{2} - \frac{(s(3)+s(4))}{2} \tag{7.41}$$

To determine the median, the middle two values of the 4 elements are averaged. Depending on the operation, the signal uncertainties are determined via:
I. In case of average value:

$$\text{on source}: \quad \Delta 1 = \sum_{i=5}^{8} \frac{\Delta s(i)}{4}, \tag{7.42}$$

$$\text{off source}: \quad \Delta 2 = \sum_{i=1}^{4} \frac{\Delta s(i)}{4}. \tag{7.43}$$

II. For the median value, where j_1 and j_2 are the indices of the two values averaged to obtain the median:

$$\text{on source}: \quad \Delta 1 = \frac{\Delta s(j_1) + \Delta s(j_2)}{2}, \tag{7.44}$$

$$\text{off source}: \quad \Delta 2 = \frac{\Delta s(j_1) + \Delta s(j_2)}{2}. \tag{7.45}$$

III. In case of minimum-maximum value, where j_1 and j_2 are the indices of the maximum and minimum, respectively:

$$\text{on source}: \quad \Delta 1 = \Delta s(j_1), \tag{7.46}$$

$$\text{off source}: \quad \Delta 2 = \Delta s(j_2). \tag{7.47}$$

Finally, the source signal uncertainty is derived from

$$\Delta s_{src} = \sqrt{\Delta 1^2 + \Delta 2^2}. \tag{7.48}$$

Ancillary data required:

None

7.5.5 Correction for chopped signal loss: Sky measurement

Detailed description: Section 5.2.3

The source signal s_{src} is corrected for signal loss by the chopper modulation by means of a transformation:

$$s^c_{src} = \zeta(s_{src}, det, t_{dwell}), \tag{7.49}$$

where s^c_{src} in V/s is the corrected value. The correction function ζ depends besides s_{src} also on the detector pixel *det* and chopper dwell time t_{dwell}. The function is implemented via look-up tables. Each table gives the correction values for a given detector. Within each table the correction values are ordered by dwell time and detector pixel.

The zero point of ζ takes care of the vignetting or chopper offset correction (see Section 4.5.3). As a consequence, separate vignetting correction tables are not required.

Assuming that the signal loss is symmetric, i.e. the loss from the on-source signal is gained from the off-source signal, it is possible to correct the on- and off-source signals:

$$s_{on} + s_{off} = s^c_{on} + s^c_{off}, \tag{7.50}$$

$$s^c_{diff} = s^c_{on} - s^c_{off} \tag{7.51}$$

then the corrected signals can be determined from:

$$s^c_{on} = \frac{s_{on} + s_{off}}{2} + \frac{s^c_{diff}}{2}, \tag{7.52}$$

$$s^c_{off} = \frac{s_{on} + s_{off}}{2} - \frac{s^c_{diff}}{2}. \tag{7.53}$$

In practice, the signal loss is asymmetric for detectors P3, C100, and C200. For these detectors the loss on the on-source signal is not equivalent to the gain from the off-source signal. Based on the previous results, the asymmetry is included by using an empirical asymmetry factor A_{chop}:

$$x = 2\left|\frac{s_{diff}}{s^c_{on} + s^c_{off}}\right|, \tag{7.54}$$

$$A_{chop} = A_0 e^{-\frac{1}{2}\left(\frac{x-A_1}{A_2}\right)^2} + A_3 + A_4 x + A_5 x^2 \tag{7.55}$$

where $A_0 \ldots A_5$ are empirical constants with $A_0 = 0.3558$, $A_1 = -8.129{\cdot}10^{-7}$, $A_2 = 2.579$, $A_3 = 0.6472$, $A_4 = -1.463{\cdot}10^{-8}$, $A_5 = 1.285{\cdot}10^{-4}$. Finally, the on- and off-signals corrected for the signal asymmetry are computed for $A_{chop} \neq 0$ and:

If $s^c_{diff} > 0$:

$$s^{c*}_{on} = \frac{s^c_{on}}{A_{chop}}, \tag{7.56}$$

$$s^{c*}_{off} = s^{c*}_{on} - s^c_{diff}. \tag{7.57}$$

If $s^c_{diff} \leq 0$:

$$s^{c*}_{off} = \frac{s^c_{off}}{A_{chop}}, \tag{7.58}$$

$$s^{c*}_{on} = s^{c*}_{off} + s^c_{diff}. \tag{7.59}$$

In case $A_{chop} = 0$ and for detectors P1 and P2, $s^{c*}_{off} = s^c_{off}$ and $s^{c*}_{on} = s^c_{on}$.

Ancillary data required:

Cal-G files PP1CHOPSIG, PP2CHOPSIG, PP3CHOPSIG, PC1CHOPSIG, and PC2CHOPSIG contain the look-up tables for $\zeta(s_{src}, det, t_{dwell})$. The description of these files is given in Section 14.10.

7.5.6 Correction for chopped signal loss: FCS measurement

Detailed description: none

For the FCS measurements only rectangular chop mode is used. The generic pattern is constructed in the same way as for the chopped sky measurements for which on-source corresponds to beam deflection to FCS1 and off-source corresponds to FCS2. Adopting the same notation as before but with 'on'=FCS1, 'off'=FCS2, the same signal loss corrections as presented in Section 7.5.5 apply.

Ancillary data required:

Cal-G files PP1CHOPSIG, PP2CHOPSIG, PP3CHOPSIG, PC1CHOPSIG, and PC2CHOPSIG contain the look-up tables for $\zeta(s_{src}, det, t_{dwell})$. The description of these files is given in Section 14.10.

7.6 Signal Processing: Chopped PHT-S

In this section we first describe the extraction of the source signal from [source+background] and background signal. Subsequently the flux calibration for PHT-S is presented.

7.6.1 Obtaining the average signal per chopper plateau

Detailed description: none

The average signal per chopper plateau is obtained by applying processing steps 7.3.4 (deglitching), 7.3.5 (drift recognition), and 7.3.6 (mean signal per plateau).

Ancillary data required:

None

7.6.2 Separation of source and background signal

Detailed description: none

The background subtraction for a given chopper cycle and chopper mode is performed in this step.

For a given chopper cycle the background signal is subtracted from the [source+background] signal to obtain the source signal. This operation is repeated until the end of a measurement is encountered.

Weighting factors are derived from the uncertainties which are used for the averaging of all chopper cycles at the end of a measurement.

In the following we describe the background subtraction method for the different chopper modes. Note that each cycle in triangular chopping mode consists of 4 plateaux referring to 2 [source+background] and 2 different background positions. In sawtooth mode there are 3 plateaux: 1 [source+background] and two different background positions. The following symbols are used for chopper cycle k:

- $s_k(x+b)_1,\ w_k(x+b)_1$: signal and weight of first [source+background] plateau;
- $s_k(x+b)_2,\ w_k(x+b)_2$: signal and weight of second [source+background] plateau (triangular mode only);
- $s_k(b1),\ w_k(b1)$: signal and weight of the background at the first reference positiont;
- $s_k(b2),\ w_k(b2)$: signal and weight of the background at the second reference position;
- $s_k(x+b),\ w_k(x+b)$: average signal and weight from source plus background plateaux;
- $s_k(x),\ w_k(x)$: source signal and weight;
- $s_k(b),\ w_k(b)$: background signal and weight.

All signals are given in V/s, the weights are dimensionless.

7.6.2.1 Rectangular mode

Each cycle contains only 1 [source+background] plateau and 1 reference background position. For chopper cycle k:

$$\begin{aligned} s_k(b) &= s_k(b1) \\ s_k(x) &= s_k(x+b)_1 - s_k(b1) \end{aligned}$$

The weighting factor is determined from the signal uncertainties:

$$\begin{aligned} w_k(u) &= \tfrac{1}{\sigma_k^2(u)} \quad \text{for } u = (x+b),\, b \\ w_k(x) &= \tfrac{1}{[\sigma_k^2(x+b)+\sigma_k^2(b)]} \end{aligned}$$

where $\sigma_k(x+b)$ is the uncertainty in signal for the measurement on [source+background], etc.

7.6.2.2 Sawtooth mode

Each chopper cycle contains 1 [source+background] chopper plateau and 2 reference positions. For chopper cycle i:

$$\begin{aligned} s_k(b) &= \frac{s_k(b1)+s_k(b2)}{2} \\ s_k(x) &= s_k(x+b) - s_k(b). \end{aligned}$$

With weighting factors:

$$\begin{aligned} w_k(u) &= \frac{1}{\sigma_k^2(u)} \quad \text{for } u = (x+b),\ b1,\ b2 \\ w_k(b) &= \frac{4}{[\sigma_k^2(b1)+\sigma_k^2(b2)]} \\ w_k(x) &= \frac{1}{[\sigma_k^2(x+b)+(\sigma_k^2(b1)+\sigma_k^2(b2))/4]} \end{aligned}$$

where $\sigma_i(x+b)$ is the uncertainty in the signal for the measurement on [source+background], etc.

7.6.2.3 Triangular mode

Each chopper cycle contains 2 [source+background] chopper plateaux and 2 reference positions. For chopper cycle k:

$$\begin{aligned} s_k(x+b) &= \frac{s_k(x+b)_1+s_k(x+b)_2}{2} \\ s_k(b) &= \frac{s_k(b1)+s_k(b2)}{2} \\ s_k(x) &= s_k(x+b) - s_k(b) \end{aligned}$$

A weighting factor is also determined from the power uncertainties:

$$\begin{aligned} w_k(u) &= \frac{1}{\sigma_k^2(u)} \quad \text{for } u = (x+b)_1,\ (x+b)_2,\ b1,\ b2 \\ w_k(x+b) &= \frac{4}{[\sigma_k^2(x+b)_1+\sigma_k^2(x+b)_2]} \\ w_k(b) &= \frac{4}{[\sigma_k^2(b1)+\sigma_k^2(b2)]} \\ w_k(x) &= \frac{4}{[\sigma_k^2(x+b)_1+\sigma_k^2(x+b)_2+\sigma_k^2(b1)+\sigma_k^2(b2)]}. \end{aligned}$$

7.6.3 Determine the signals averaged over a measurement

Detailed description: none

The average source and background signals of all chopper cycles in a measurement is determined.

For all chopper cycles in a measurement, the weighted average is computed from the parameters per chopper cycle. For a given set of signals $s_k(X)$ with weights w_k obtained over a measurement, the weighted mean $s(X)$ and its associated uncertainty $\sigma(s(X))$ is computed according to Equation 7.20. The mean can be either the signal of the source or background.

7.6.3.1 Rectangular mode

In rectangular mode the following mean signals are derived for each pixel:

- $s(x) \pm \sigma(s(x))$, $s(b) \pm \sigma(s(b))$, and $s(x+b) \pm \sigma(s(x+b))$

7.6.3.2 Sawtooth and Triangular mode

In sawtooth and triangular mode the following mean signals are derived for each pixel:

- $s(x) \pm \sigma(s(x))$, $s(b) \pm \sigma(s(b))$, $s(x+b) \pm \sigma(s(x+b))$, $s(b1) \pm \sigma(s(b1))$, and $s(b2) \pm \sigma(s(b2))$

7.6.4 Spectral response function corrected for chopped signal losses

Detailed description: Section 5.2.6

Analysis of chopped PHT-S data obtained from standard stars have shown that the PHT-S spectral response function is not unique but depends on the brightness of the source due to chopped signal losses. It is found that the amount of signal loss in a given detector pixel strongly depends on the source brightness in that pixel.
An accurate spectral response function $C^c(i)$ for pixel i is obtained by assuming an average spectral response function which is corrected per pixel for a source dependent signal loss:

$$C^{c,p}(i) = \phi(i) C^{c,p}_{ave}(i) \qquad [(\mathrm{V/s})/\mathrm{Jy}] \tag{7.60}$$

with

$$\phi(i) = A^0(i) + A^1(i)^{10}\log(|s(x,i)|) \ , \tag{7.61}$$

where the superscripts c refer to a chopped observation, and p to a point source, and

- $C^{c,p}(i)$ in (V/s)/Jy is the spectral response corrected for chopped signal loss for a given pixel i;
- $C^{c,p}_{ave}(i)$ in (V/s)/Jy is the PHT-S *average* chopped spectral response function for a point source;
- $\phi(i)$ is the signal dependent correction for the average spectral response function;
- $A^0(i)$ and $A^1(i)$ (in $({}^{10}\log(V/s))^{-1}$) are the coefficients for the signal dependent correction.

Ancillary data required:

The Cal-G file PSPECAL contains the average spectral response functions for both staring and chopped mode observations of point and extended sources, see Section 14.19.1. The file includes also the first order correction factors $(A^0(i), A^1(i))$.

7.6.5 Determination of source and background spectrum

Detailed description: none

The chopped PHT-S spectral energy distribution for the source and [source+background] is computed using the spectral response function corrected for chopper losses:

$$F_\nu(x,i) = \quad s(x,i)/C^{c,p}(i) \quad [\mathrm{Jy}], \tag{7.62}$$
$$F_\nu(x+b,i) = \quad s(x+b,i)/C^{c,p}(i) \quad [\mathrm{Jy}], \tag{7.63}$$

with

$$\Delta F_\nu(x,i) = \quad \sigma(s(x,i))/C^{c,p}(i) \quad [\mathrm{Jy}] \tag{7.64}$$
$$\Delta F_\nu(x+b,i) = \quad \sigma(s(x+b,i))/C^{c,p}(i) \quad [\mathrm{Jy}]. \tag{7.65}$$

The background spectrum is derived from the difference:

$$F_\nu(b,i) = \quad F_\nu(x+b,i) - F_\nu(x,i) \quad [\mathrm{Jy}] \tag{7.66}$$
$$\Delta F_\nu(b,i) = \quad \sqrt{\Delta F^2_\nu(x,i) + \Delta F^2_\nu(x+b,i)} \quad [\mathrm{Jy}]. \tag{7.67}$$

The resulting spectra are stored in the SPD products.

Ancillary data required:

none

7.7 Signal Processing: PHT32 Raster Maps

Detailed description: see also Sections 3.5, 3.10.2

PHT32 applied the fast chopper scanning mode in combination with a spacecraft raster grid to obtain oversampled linear scans or maps. In general, the chopper dwell time is short with respect to the reset interval. The number of ramps collected per chopper plateau is in most cases 4. In addition, the number of readouts per ramp can also be as low as 4. If the first readouts per ramp and destructive readouts were to be removed as described in Sections 7.2.1 and 7.2.2, only a few usable readouts would be left on a chopper plateau. This would make the signal processing very sensitive to glitches.

An alternative method for determining the average signal per chopper plateau is applied in OLP. This method uses the same readout processing methods as used for the chopped photometric observations. Since the PHT32 signal processing already include special processing on readout level, the ramp processing steps have been modified.

Ancillary data required:

none

7.7.1 Obtaining the average signal per chopper plateau

Detailed description: none

The average signal per chopper plateau is obtained by first applying ramp processing steps 7.2.3 until 7.2.8. The discarding of destructive readouts (7.2.1) and discarding of disturbed non-destructive readouts (7.2.2) are not carried out. For each detector pixel i a difference signal is computed from readout k and $k-1$ ($k \geq 2$) of a given ramp:

$$s_i(k) = \frac{V_i(k) - V_i(k-1)}{t(k) - t(k-1)} \qquad [\mathrm{V/s}], \tag{7.68}$$

where $V_i(k)$ is a valid readout, and $t(k)$ is the corresponding time. After all difference signals on a chopper plateau have been determined, an outlier resistent mean, a median, lower and upper quartile values are obtained.

The subsequent processing steps are common to the signal processing steps for staring PHT-P and PHT-C: reset interval correction (7.3.1), dark current subtraction (7.3.2) and correcttion for non-linear detector responsivity (7.3.3).

Ancillary data required:

none

7.7.2 Correction for chopper vignetting

Detailed description: section 4.5.3

The throughput of the ISO and ISOPHOT optics depends on the chopper deflection. The level of variation is of order of a few percent for the maximum chopper deflection in case of the C100 and C200 subsystems. Especially for weak sources on a strong background this phenomenon can cause spurious detections or negative signals for some pixels on the arrays.

For each average and median signal $\langle s \rangle$ the correction c_{chop} is applied:

$$\langle s_c \rangle = c_{chop}(f, i, \theta_{chop}) \times \langle s \rangle \qquad [\mathrm{V/s}], \tag{7.69}$$

where i is the detector pixel, f is the filter, and θ_{chop} is the chopper deflection. In case of an absence of chopper vignetting $c_{chop} = 1$.

Ancillary data required:

The correction for C100 and C200 are stored in the Cal-G files PC1VIGN and PC2VIGN, see section 14.11.

7.8 Signal Processing: PHT-S Raster Maps

The calibration which has been developed for single pointing PHT-S observations cannot be applied to PHT-S raster maps. This is because single pointing staring PHT-S measurements are always preceded by a 32 s dark measurement which stabilises the initial jump behaviour of the following sky measurement. For PHT-S raster maps, however, there is only one dark measurement at the very beginning and the initial illumination conditions from raster point to raster point change depending on the brightness distribution of the sky w.r.t. the raster pointings.

For OLP it has been decided to perform a direct calibration from signal per raster point to flux density using the average spectral response function for staring observations.

7.8.1 Obtaining the average signal per raster point

Detailed description: none

The average signal per raster point is obtained by applying processing steps 7.3.4 (deglitching), 7.3.5 (drift recognition), and 7.3.6 (mean signal per plateau). The PHT-S orbit dependent dark signal (step 7.4.1) is subsequently subtracted from the average signal.

Ancillary data required:

see respective processing steps.

7.8.2 Determination of the spectrum per raster point

Detailed description: Section 5.2.6 for calibration overview

The flux density $F_\nu^j(i)$ for raster point j and PHT-S pixel i is obtained by simply dividing the signal of that raster point by the average point source spectral response function for staring observations $C_{ave}^{s,p}(i)$:

$$F_\nu^j(i) = s^j(i)/C_{ave}^{s,p}(i) \qquad [\mathrm{Jy}], \text{ and} \tag{7.70}$$

$$\Delta F_\nu^j(i) = \frac{\Delta s^j(i)}{s^j(i)} F_\nu^j(i) \qquad [\mathrm{Jy}]. \tag{7.71}$$

Ancillary data required:

The average spectral response function $C^{s,p}_{ave}(i)$ is listed in Cal-G file PSPECAL, see Section 14.19.1.

7.9 Signal Processing: PHT04 Staring Multi-Aperture Photometry

In this section processing steps are described which apply to a specific subset of multi-aperture photometry (PHT04) observations. We refer to Müller 2000a, [41] and Müller 2000b, [42] for details. Different from all other ISOPHOT observations, the outcome of these processing steps is not a dedicated photometry product but an indication whether the source is extended or not. Since the analysis depends only on the signal variation between different apertures and not on the absolute photometric calibration, it was decided to include the processing steps in Derive_SPD.

The processing steps start at average signal per measurement level and applies only to PHT04 observations with suitable settings. Subsequently, the background subtracted relative source signals are derived whereby the background signal is determined from the largest aperture measurements. Finally, the resulting curve of growth is compared to the expected curve based on calibration observations on point sources.

The outcome of the analysis is given in SPD header of the photometry product.

7.9.1 Sorting out eligible PHT04 observations

Detailed description: None

The analysis of background subtracted relative source signals can only take place for PHT04 observations which satisfy the following criteria:

- source type 'P', extended component $\geq 0\%$, number of apertures ≥ 4, and $120''$ and $180''$ apertures included;
- source type 'E', number of apertures ≥ 4, and $120''$ and $180''$ apertures included;

If one of these two criteria are satisfied the SPD header keyword BACKSRSS, the background subtracted relative source signal processing flag, is set to 'TRUE' otherwise 'FALSE'. In case of the latter the analysis is not applied. Instead a clear warning is given in the SPD header.

Ancillary data required:

none

7.9.2 Analysis of the background subtracted source signal

Detailed description: Section 4.5.1

The analysis assumes that the processing steps for staring measurements with PHT-P have already been performed up to the average signal per measurement, i.e. all processing steps of Section 7.3.

To subtract the background signal level, the background signal per aperture area S_{back} and its uncertainty ΔS_{back} are determined from the $180''$ and $120''$ apertures:

$$S_{back} = \frac{s(180)f_{PSF}(120) - s(120)f_{PSF}(180)}{A(180)f_{PSF}(120) - A(120)f_{PSF}(180)} \quad [\mathrm{V/s}], \tag{7.72}$$

and uncertainty

$$\Delta S_{back} = S_{back}\sqrt{(\frac{\Delta s(180)}{s(180)})^2 + (\frac{\Delta s(120)}{s(120)})^2} \quad [\mathrm{V/s}], \tag{7.73}$$

where

- $s(180), s(120)$ in V/s are the signals in the $180''$ and $120''$ apertures;
- $\Delta s(180), \Delta s(120)$ in V/s are the corresponding uncertainties;
- $A(180), A(120)$ in mm^2 are the areas of the apertures, see Appendix A.1.2;
- $f_{PSF}(180), f_{PSF}(180)$ are the point spread function factors of the apertures, see Section 2.6.1.

Once the background level S_{back} has been determined, the background contribution to the total signal of a measurement with a given aperture can be derived:

$$s_{back}(i) = S_{back}A(i)A^*_{corr}(i) \quad [\mathrm{V/s}], \tag{7.74}$$

and

$$\Delta s_{back}(i) = \Delta S_{back}A(i)A^*_{corr}(i) \quad [\mathrm{V/s}], \tag{7.75}$$

where $s_{back}(i)$ and $\Delta s_{back}(i)$ are the background signal for aperture i and its corresponding uncertainty, and $A^*_{corr}(i)$ is a correction factor such that $A(i)A^*_{corr}(i)$ gives the empirical aperture area for aperture i assuming that the theoretical area of the $180''$ aperture is correct. In Table 7.2 we have listed the values of A_{corr} for a given aperture diameter.

Table 7.2: *Aperture correction factors A^*_{corr}, the value 1.0 indicates that the correction factor could not be determined empirically.*

filter	$5''$	$7.6''$	$10''$	$13.8''$	$18''$	$23''$	$52''$	$79''$	$99''$	$120''$	$180''$
P1_3.29	1.0	1.0	1.0	1.0	1.0	1.0	1.0	1.0	1.0	1.0	1.0
P1_3.60	1.0	1.0	1.0	1.0	1.0	1.0	1.0	1.0	1.0	1.0	1.0
P1_4.85	1.0	1.0	1.0	1.0	1.0	1.0	1.0	1.0	1.0	1.0	1.0
P1_7.30	0.50	0.50	0.50	0.50	0.50	0.50	0.50	0.50	0.65	0.80	1.00
P1_7.70	1.0	1.0	1.0	1.0	1.0	1.0	1.0	1.0	1.0	1.0	1.0
P1_10.0	0.40	0.40	0.40	0.40	0.40	0.40	0.40	0.40	0.50	0.65	1.00
P1_11.3	1.0	1.0	1.0	1.0	1.0	1.0	1.0	1.0	1.0	1.0	1.0
P1_11.5	1.0	1.0	1.0	1.0	1.0	1.0	1.0	1.0	1.0	1.0	1.0
P1_12.8	0.35	0.35	0.35	0.35	0.35	0.35	0.35	0.57	0.63	0.72	1.00
P1_16.0	0.90	0.90	0.90	0.75	0.75	0.80	0.62	0.68	0.70	0.78	1.00
P2_20	0.40	0.40	0.40	0.40	0.40	0.65	1.00	1.08	1.01	1.00	1.00
P2_25	0.45	0.45	0.45	0.45	0.45	0.45	0.48	0.82	0.91	0.97	1.00
P3_60	0.30	0.30	0.30	0.30	0.40	0.40	2.30	1.75	1.17	1.08	1.00
P3_100	1.0	1.0	1.0	1.0	1.0	1.0	1.0	1.0	1.0	1.0	1.0

Several entries in Table 7.2 could not be determined from in-orbit observations, these have been set to '1.0'. If one of these entries have to be used, a warning will be issued in the SPD product header and the header keyword 'FILTCORF' is set to FALSE.

For each measurement a background subtracted source signal $s_{src}(i)$ plus uncertainty is computed:

$$s_{src}(i) = s(i) - s_{back}(i) \quad [\mathrm{V/s}] \tag{7.76}$$
$$\Delta s_{src}(i) = \sqrt{\Delta s(i)^2 + \Delta s_{back}(i)^2} \tag{7.77}$$

If the source signal is is non-zero, then the background subtracted source signal normalised to the 180″ aperture $R(i)$ is computed:

$$R(i) = s_{src}(i)/s_{src}(180'') \tag{7.78}$$
$$\Delta R(i) = R(i)\sqrt{(\frac{\Delta s(i)}{s(i)})^2 + (\frac{\Delta s_{src}(180'')}{s_{src}(180'')})^2}, \tag{7.79}$$

otherwise $R(i)$ and $\Delta R(i)$ are set to zero, the header keyword NORMCALC is set to FALSE, and a warning message is issued in the SPD product header.

The calculations are repeated for each aperture i and the results are stored in the SPD header.

Ancillary data required:

none

7.9.3 Summary of SPD warning messages for PHT04

Detailed description: Chapter 5, Section 4.5.4

The results of the analysis of the PHT04 aperture photometry are completely stored in the SPD product header. We refer to Section 13.3.2 for a full description of the header keywords. The processing of PHT04 measurements is more constrained than other SPD processing steps. Consequently, several warning messages are issued in case the measurements fall outside the given processing constraints.

- if the observation does not satisfy the criteria given in Section 7.9.1:
  The processing of a background subtracted source signal normalised to the signal in the 180″ aperture has not been applied to this observation due to insufficient measurement configurations.

- if the filter does not have empirical values of A^*_{corr} (Table 7.2):
  The filter used in this observation does not have a measured signal aperture correction factor - value set to 1.

- if the background subtracted source signal is zero:
  The ratio of source signal to signal in 180" aperture can not be derived due to insufficient S/N for 180" aperture signal.

These messages are transferred to the Auto-Analysis Result product header if they occur in the SPD header.

Ancillary data required:

none

7.10 In-band Power Calibration

Detailed description: Chapter 5, Section 4.5.4

The steps described in this section are applied to all measurements both in staring and chopped mode except those collected with PHT-S.

The detector responsivity varies from revolution to revolution, and along a revolution, in particular the long wavelength detectors P3, C100, and C200 show significant variations. To ensure proper photometric calibration, all PHT AOTs except PHT 40 contain at least one FCS measurement per detector used during an AOT. The FCS measurement determines the responsivity of the detector at approximately the same time as the sky is observed.

The derivation of the target's in-band power using the FCS calibration requires important instrumental corrections to ensure the best photometric calibration. The related processing steps are described in the following sections.

Ancillary data required:

None

7.10.1 Default responsivities

Detailed description: Section 4.2

The in-orbit calibration observations of the FCS on celestial standards were also used to analyse the properties of the detector responsivity, see also Section 4.2. The FCS calibration observations were frequently performed throughout the mission enabling a statistical assessment of the responsivities as a function of orbital phase. This analysis showed that the responsivities scatter around a mean value which is a function of orbital phase due to ionising radiation. The time dependent mean responsivity provides a first order estimate of the detector responsivity and is used as *default responsivity* $R_{default}(i,t)$ in W/A, where i indicates the detector pixel and t the orbital dependence.

The default responsivity for the P and C detectors is applied in case:

- FCS measurements are missing or are of insufficient quality for the derivation of reliable detector responsivities. Such an event occurs e.g. in case all ramps/signals during the FCS measurement were rejected due to saturation or glitches.
- Chopped observations with detector P2 were obtained. The responsivity of P2 was extremely constant throughout the mission, and using the default responsivity provides more accurate photometry than the responsivity determined from the chopped FCS measurement.
- The FCS heating power is outside the calibrated range. The FCS heating powers were calibrated using a range of astronomical standards covering a finite flux range. Some FCS measurements were commanded with heating powers yielding fluxes outside this range.

For each measurement the orbital phase is read from ERD keyword TREFCOR2 which gives the orbital phase corresponding to the mid point of an AOT. The default responsivity is determined by linear interpolation in the Cal-G file which contains the default responsivity versus orbital position for a given detector.

Derive_SPD also computes the FCS1 responsivity from the FCS measurement and the results are stored in the designated Cal-A file. To give the observer some information on the discrepancies, the ratio:

$$r(i) = \frac{R_{FCS}(i)}{R_{default}(i,t)}, \tag{7.80}$$

is stored for each pixel i in the SPD header with keyword RESPRi.

Ancillary data required:

Orbit dependent default detector responsivities are stored in Cal-G files PPRESP, PC1RESP, and PC2RESP for the P, C100 and C200 subsystems, respectively, see Section 14.13.

7.10.2 Determination of in-band power from FCS measurement

Detailed description: Chapter 5

The electrical heating power h applied to the FCS directly corresponds to an FCS power on the detector P_{FCS}. The conversion is obtained from dedicated in-orbit FCS calibration observations where the signal of a celestial calibration source is directly compared with the signal of the FCS for a given heating power h. However, the calibration observations could only cover a limited range in h due to limited availability of suitable calibration targets. FCS measurements with values for h outside the range, which can be calibrated, will get less reliable P_{FCS} based on extrapolations.

In Derive_SPD the value for h is checked. In case the value of h is outside the valid range, the default responsivity (Section 7.10.1) is used.

Ancillary data required:

The valid heating power ranges are included in the FCS power calibration Cal-G files PPxFCSPOW (x=1,2,3) for the P detectors, and PCxFCSPOW (x=1,2) for the C100 and C200 detectors, see Section 14.12.

7.10.3 Signal to in-band power conversion for P detectors

Detailed description: Section 5.2.5

From the electrical power (in mW) applied to the FCS, an in-band power on the detector P_{fcs} normalised to the aperture area (in $\mathrm{W\,mm^{-2}}$) is obtained using FCS calibration tables, see Chapter 5. The FCS measurement taken with detector *det* provides the detector responsivity:

$$R_{det} = \frac{\langle s_{fcs} \rangle \cdot C_{int}^{det}}{P_{fcs}(f,h) \cdot A(a) \alpha(f,a) \chi_{det}(f)} \qquad \text{[A/W]}, \tag{7.81}$$

where

- f is the filter and a the aperture selected for the measurement,
- $\langle s_{fcs} \rangle$ in V/s is the weighted mean signal of the FCS measurement,
- C_{int}^{det} in F is the integration capacitance associated with detector P1, P2, or P3,
- $P_{fcs}(f,h)$ in $\mathrm{W\,mm^{-2}}$ is the in-band power on the detector from the FCS due to heating power h in mW,
- $A(a)$ in [$\mathrm{mm^2}$] is the area of aperture a,
- $\alpha(f,a)$ is a dimensionless correction for inhomogeneous illumination in aperture a by the FCS,
- $\chi_{det}(f)$ the relative filter-to-filter correction for a given detector *det* (P1, P2, or P3) to obtain the same responsivity independent of filter.

Although filter transmissions were measured in laboratory, and instrumental geometry was well known, correction factors to adjust the photometry were necessary. The resulting detector responsivities were found to vary from filter to filter. The calibration factors to achieve a filter independent responsivity are stored in $\chi_{det}(f)$.

The in-band power P_{target} from the source is obtained from:

$$P_{target}(f') = \frac{\langle s_{target} \rangle C_{int}^{det}}{R_{det} \cdot \chi_{det}(f')} \qquad [\mathrm{W}], \tag{7.82}$$

and

$$\Delta P_{target}(f') = \frac{\Delta \langle s_{target} \rangle}{\langle s_{target} \rangle} P_{target}(f') \qquad [\mathrm{W}], \tag{7.83}$$

where f' indicates a filter available for the same detector as for which the responsivity R_{det} has been derived.

Caveat: In principle, inhomogeneous illumination by the FCS (see Section 7.10.4) affects the calibration involving apertures. The FCS power on the detector is not proportional to the aperture area for a given electrical power applied to the FCS. Although a provision for correction has been implemented, the present version of the Cal-G files provides no correction i.e. $\alpha(f, a) = 1$.

Ancillary data required:

- The PHT-P FCS calibration tables $P_{fcs}(f, h)$ in units of $\mathrm{W\,mm^{-2}}$ are stored in Cal-G files PP1FCSPOW, PP2FCSPOW, and PP3FCSPOW for the three P detectors, see Section 14.12.
- The values of the FCS aperture area $A_{fcs}(a)$ in $\mathrm{mm^2}$ from the aperture ID are hardcoded in the software. The values used are listed in Section A.1.2. These areas were obtained from on-ground measurements of the instrumentation.
- The filter-to-filter correction factors $\chi_{det}(f)$ for a given detector *det* are stored in the Cal-G file PPFTOF (see Section 14.16).
- The correction method for inhomogeneous FCS illumination of the apertures $\alpha(f, a)$ assume the following Cal-G files (see Section 14.15): PP1FCSAP, PP2FCSAP, and PP3FCSAP.

7.10.4 Signal to in-band power conversion for C detectors

Detailed description: Section 5.2.5

First, the FCS measurement is used to determine the responsivity of each pixel $R(i)$ for the filter in which the FCS measurement is taken:

$$R(i) = \frac{\langle s_{fcs}(i, f) \rangle \cdot C_{int}^{det}}{P_{fcs}(f, h) \cdot \Gamma(i, f) \cdot \chi(i, f)} \quad [\mathrm{A/W}], \tag{7.84}$$

where

- f indicates the filter, i the pixel number,
- $\langle s_{fcs}(i, f) \rangle$ in V/s is the FCS signal per chopper plateau,
- C_{int}^{det} is the detector capacitance,

- $P_{fcs}(f,h)$ is the in-band power (in W/pixel) for a given FCS heating power h,
- $\Gamma(i,f)$ is the FCS *illumination matrix*, and
- $\chi(i,f)$ the relative filter-to-filter responsivity correction for a given detector pixel i (C100 or C200) to obtain the same responsivity independent of filter.

The values of $\chi(i,f)$ (see Section 7.10.3) are not the same for different pixels of the same detector array. These differences are suspected to be due to spatial filter inhomogeneities which are projected onto the array.

The illumination matrix $\Gamma(i,f)$ is needed to correct for the fact that the FCS illumination is not flat but varies from pixel to pixel in the C100 and C200 arrays. This correction is applied to each pixel in the array (Section 4.5.4).

Second, for a measurement of the sky, the power on each pixel for any filter f' of the same detector can be derived from the mean signal per chopper plateau $\langle s_{target}(i,f')\rangle$:

$$P_{target}(i,f') = \frac{\langle s_{target}(i,f')\rangle \cdot C_{int}^{det}}{R(i)\cdot\chi(i,f')} \quad [\mathrm{W}], \tag{7.85}$$

and

$$\Delta P_{target}(i,f') = \frac{\Delta\langle s_{target}(i,f')\rangle}{\langle s_{target}(i,f')\rangle} P_{target}(i,f') \quad [\mathrm{W}]. \tag{7.86}$$

Ancillary data required:

- The PHT-C FCS calibration tables $P_{fcs}(f,h)$ in units of W/pixel are stored in Cal-G files PC1-FCSPOW and PC2FCSPOW. The tables give the mean in-band power from the FCS averaged over all pixels, see Section 14.12.
- The illumination matrices $\Gamma(i,f)$ which give the FCS illumination for each pixel normalised to the mean pixel illumination are stored in Cal-G files PC1ILLUM and PC2ILLUM, see Section 14.14.
- The filter-to-filter responsivity correction $\chi(i,f)$ for C100 and C200 are stored in Cal-G files PC1FLAT and PC2FLAT, see Section 14.17. For each filter the correction is normalised with respect to the filter yielding the largest responsivity for the C100 or C200 detectors.

7.10.5 In-band power for PHT-P and PHT-C chopped observations

Detailed description: none

The SPD product for chopped observations contains the in-band powers of the on-source position (i.e. source plus background power) and the off-source position (i.e. background power) plus the associated uncertainties. These are computed from the corrected signals s_{on}^{c} and s_{off}^{c} (derived in Section 7.5.5) using the expressions given in Section 7.10.3 for PHT-P and Section 7.10.4 for PHT-C.

The signal values of the generic pattern, the difference between the two intermediate patterns, as well as the derived uncertainties are stored in the header of the SPD product under keywords PFfPiLl, PDfPiLl, and PUfPiLl, where $f = 1\ldots$no. of filters, $i = 1\ldots$no. of pixels and $l = 1\ldots8$.

Ancillary data required:

None

7.10.6 In-band power for raster and sparse maps

Detailed description: None

In case of a raster or sparse map, two FCS measurements are collected (see Sections 3.10.1 and 3.10.2). For a raster map one FCS measurement is taken immediately before and one immediately after the map measurement. For a sparse map the FCS measurements are taken after the last measurement in the first AOT and after the last measurement in the last AOT of the sparse map chain.

In both cases the detector responsivity is obtained from the average responsivity $\overline{R(i)}$ of the two FCS measurements $R_1(i)$ and $R_2(i)$:

$$\overline{R(i)} = \frac{R_1(i) + R_2(i)}{2} \quad \mathrm{A\,W^{-1}}, \tag{7.87}$$

with uncertainty[1]:

$$\Delta\overline{R(i)} = \frac{\sqrt{\Delta^2 R_1(i) + \Delta^2 R_2(i)}}{2}. \quad \mathrm{A\,W^{-1}} \tag{7.88}$$

The values of $\overline{R(i)}$ and $\Delta\overline{R(i)}$ are written to the SPD header. The index i refers to the detector pixel in case of the C100 or C200 array. There are a number of exceptions for which the above computation cannot be performed:

1. if only one valid FCS measurement is available, then the responsivity from this FCS measurement is used;
2. if for raster mode observations the FCS heating power is out of the calibrated range for both FCS measurements, then the default responsivity (Section 7.10.1) is used;
3. if for sparse maps the heating power is out of the calibrated range for one of the FCS measurements, then the responsivity from the other valid FCS measurement is used;
4. if for sparse maps the heating power is out of the calibrated range for both FCS measurements, then the default responsivity (Section 7.10.1) is used;

If instances (2) and (4) occur, a warning message will be written in the SPD product header.

Ancillary data required:

None

7.10.7 Dependencies on mission dates

Detailed description: None

During the mission two main events took place which seriously impacted the ISOPHOT calibration:

- the change in FCS1/TRS2 emission properties (see Section 2.7) between revolution 93 and 94. This event caused the FCS emission for the long wavelength detectors (P3, C100 and C200) to become about a factor 2 higher than before for the same electrical power. Consequently, new uplink and FCS power tables had to be constructed after extensive in-orbit measurements of the FCS1/TRS2 properties.

[1] the uncertainty given here is different from OLP where the factor 2 in the denominator has been omitted

- an extra curing procedure was introduced approximately halfway in the ISO science window for detectors P3, C100 and C200 as of revolution 150 onwards. The extra curing was performed during the handover period between the VILSPA and Goldstone ground stations. The procedure restored the nominal detector performance whereas, without the procedure, both detector noise and responsivity continue increasing.

As a consequence, the following calibration files have different entries depending on the revolution date:

- FCS power Cal-G files (PP3FCSPOW, PC1FCSPOW, and PC2FCSPOW see Section 7.10.2) are different before and after revolution 94.
- the Cal-G files giving the matrices of the PHT-C illumination by the FCS (PC1ILLUM, and PC2ILLUM, see Section 14.14) are different before and after revolution 94.
- orbit dependent default responsivities Cal-G files (PPRESP, PC1RESP, and PC2RESP see Section 7.10.1) are different before and after revolution 150.

Ancillary data required:

Information on the time dependence of ISOPHOT Cal-G files is stored in Cal-G file PTIMEDEP, a detailed description is given in Section 14.2.

7.11 Ancillary SPD Data

7.11.1 FCS measurements

Detailed description: Section 2.5 and Chapter 3

For PHT-P and PHT-C observations in staring or raster mode, the FCS measurement is processed similar to the sky measurement to obtain a weighted mean signal for each detector per measurement. The signal records (which also include the uncertainty, median, and first and third quartiles) are stored in a Cal-A product. In the case of raster mode observations there are two FCS measurements. The signal records of both of these FCS measurements are stored in the same product.

Ancillary data required:

None

7.11.2 PHT-S dark measurement

Detailed description: Section 2.5 and Section 3.7

Each PHT-S sky measurement is preceded by a 32 s dark measurement. This measurement can be used to assess whether the detectors are still affected by a transient from a preceding sky observation.

The weighted average of the signals of the dark measurement are determined without prior subtraction of the dark signal. The signals are stored without further processing in the dedicated SPD dark signal files PSSD and PSLD, see Sections 13.3.9 and 13.3.10.

Ancillary data required:

None

7.11.3 Dark signal measurement

Detailed description: Section 2.5 and Section 3.4

The signals of the optional dark measurement of PHT 05 or PHT 25 are processed in the same way as the PHT-S dark measurement. The average signal per measurement per detector is obtained without subtraction of the standard dark signal. The signals are stored in the dedicated SPD dark signal files PP1D, PP2D, PP3D, PC1D, and PC2D, see Sections 13.3.11 13.3.12 and 13.3.13.

Ancillary data required:

None

7.11.4 FCS straylight measurement

Detailed description: Section 2.5 and Section 3.4

The signals of the optional FCS straylight measurement of PHT 05 or PHT 25 are processed in the same way as a normal FCS measurement. The signal record is included in the Cal-A product of the FCS measurement of the same observation.

Ancillary data required:

None

7.12 Quality Flags for SPD Records

The quality of the processed data in each SPD record is given in the SPD quality flag field 'PxxSFLAG' where 'xx' identifies the detectors as follows C1, C2, P1, P2, P3 SS, and SL. Table 7.3 gives the coding of each bit in the (8 bit) flag.

Table 7.3: *Quality flags for SPD records.*

Bit	Description
0	nominal
1	calibration measurement saturated
2	part of plateau data affected by drift
3	all ramps on plateau rejected
4	plateau data affected by residual drift
5	zero standard deviation
6	empty
7	zero signal for plateau

Chapter 8

Data Processing Level: Derive_AAR

8.1 Overview

In *Derive Auto-Analysis Results (Derive_AAR)*, the calibrated data from Derive_SPD are further processed to more advanced astronomical products such as point source flux per filter, flux sequences in multi-aperture mode, maps, or spectra. PHT SPD products provide in essence the average power on the detector in units of W per record and are independent of the observing mode. Each SPD record corresponds to a chopper plateau or raster position. Differences among PHT SPD products emerge mainly from the detector subsystem (PHT-P, -C or -S) used.

In contrast to SPD, the auto-analysis results (AAR) products are defined by the observing mode selected. As a consequence, the processing sequence and resulting AAR products are to a large extent determined by the observing template (AOT) applied and the specific instrument settings used in the AOT.

Nevertheless, different ISOPHOT AOT's may require identical Derive_AAR processing steps. To avoid repetition in the descriptions, we first describe the common routines. The following generic observing modes can be identified, for which a more global description can be given:

- Photometry (Section 8.4)
- Mapping (Section 8.5)
- Spectroscopy (Section 8.6)

In the remainder of this Chapter we first give an overview of the processing steps for each AOT (Section 8.2). In the subsequent sections the processing steps shared by all PHT AOTs (Section 8.3) and the processing details related to the different observation modes are described.

8.2 PHT Auto Analysis Processing Per AOT

No description is given of the polarisation AOTs PHT50 and PHT51 because these AOTs are not included in the pipeline SPD and AAR levels.

8.2.1 PHT03

This AOT performs photometry in user-selected wavebands using the PHT-P subinstrument, with either the staring or chopping mode. If the staring mode is selected, a raster scan may be performed by the satellite.

The description of the processing required for rasters is incorporated, since the same steps are required to process measurements at each raster position.

Processing steps:

1. Read SPD Header
   Common step 8.3.1.
2. Read SPD record
   Common step 8.3.2.
3. If single pointing:
   (a) Average source power and off-source background(s) power
   Staring mode No action required.
   Chopped mode Determine source power, step 8.4.1
   (b) If point source was indicated by observer:
   i. Convert power to flux density
   Photometry step 8.4.6.
   ii. Write PHT-P point source photometry product
   Photometry step 8.4.8.
   (c) If extended source was indicated by observer:
   i. Convert power to flux density
   Photometry step 8.4.6.
   ii. Convert flux density to surface brightness
   Photometry step 8.4.7;
   iii. Write PHT-P extended source photometry product
   Photometry step 8.4.9.
4. If raster mapping performed:
   (a) Determine celestial coordinates of detector origin and centre;
   loop over all measurements in AOT
   Common step 8.3.3;
   (b) For each record, convert power to surface brightness
   Photometry step 8.4.7;
   (c) Produce photometric image
   Mapping steps 8.5.2 to 8.5.5;
   (d) Write raster map products 8.5.6;
   (e) Write PHT-P raster scan photometry product
   Mapping step 8.5.7.

8.2.2 PHT04

This AOT performs multi-aperture photometry with a single user-selected filter at one sky position using the PHT-P subinstrument. The focal plane chopper may be operated in either staring or chopping mode. Raster scans may *not* be selected.

Processing steps:

1. Read SPD Header
   Common step 8.3.1.

2. Read SPD record
   Common step 8.3.2.

3. Average source power and off-source background(s) power

   Staring mode No action required.

   Chopped mode Determine source power, step 8.4.1

4. If point source indicated by observer:

   (a) Convert power to flux density
   Photometry step 8.4.6.

   (b) Write PHT-P point source photometry product
   Photometry step 8.4.8.

5. If extended source indicated by observer:

   (a) Convert power to flux density
   Photometry step 8.4.6;

   (b) Convert flux density to surface brightness
   Photometry step 8.4.7;

   (c) Write PHT-P extended source photometry product
   Photometry step 8.4.9.

8.2.3 PHT05

This AOT performs absolute photometry of the sky brightness with a single filter/aperture combination at one sky position using the PHT-P subinstrument. Raster scans cannot be selected.

Processing steps:

1. Read SPD Header
   Common step 8.3.1.

2. Read SPD record
   Common step 8.3.2.

3. If point source was indicated by observer:

   (a) Convert power to flux density
   Photometry step 8.4.6.

   (b) Write PHT-P point source photometry product
   Photometry step 8.4.8.

4. If extended source was indicated by observer:

   (a) Convert power to flux density
   Photometry step 8.4.6.

   (b) Convert flux density to surface brightness
   Photometry step 8.4.7;

   (c) Write PHT-P extended source photometry product
   Photometry step 8.4.9.

8.2.4 PHT17/18/19

These AOTs perform photometry in user-selected wavebands with a single user-selected aperture as part of a sparse map using the PHT-P subinstrument. Only staring mode can be used. The following processing steps are performed:

Processing steps:

1. Loop over all PHT17, PHT18. . ., PHT19 of the same TDT
   (a) Read SPD Header
   Common step 8.3.1.
   (b) Read SPD record
   Common step 8.3.2.
2. If last product was found then loop over all measurements read:
   (a) If point source was indicated by observer:
      i. Convert power to flux density
      Photometry step 8.4.6.
      ii. Write PHT-P point source photometry product
      Photometry step 8.4.8.
   (b) If extended source was indicated by observer:
      i. Convert power to flux density
      Photometry step 8.4.6.
      ii. Convert flux density to surface brightness
      Photometry step 8.4.7;
      iii. Write PHT-P extended source photometry product
      Photometry step 8.4.9.

8.2.5 PHT22

This AOT performs photometry in user-selected wavebands using the PHT-C subinstrument, with either the staring or chopping mode. If the staring mode is selected a raster scan may be performed.

Processing steps:

1. Read SPD Header
   Common step 8.3.1.
2. Read SPD record
   Common step 8.3.2.
3. If single pointing:
   (a) Average source power and off-source background(s) power
   This step is applied to *each* pixel.
   Staring mode No action required.
   Chopped mode Determine source power, step 8.4.1
   (b) Summation of powers in array, step 8.4.2
   (c) If point source was indicated by observer:
      i. Determine Gaussian parameters

Interpolation: Interpolate missing pixels
Photometry step 8.4.4;

Fitting: Determine source peak and position
Photometry step 8.4.5;

ii. Convert power to flux density
Photometry step 8.4.6;

iii. Write PHT-C point source photometry product
Photometry step 8.4.10.

(d) If extended source was indicated by observer:

i. Convert power to flux density
Photometry step 8.4.6;

ii. Convert flux density to surface brightness
Photometry step 8.4.7;

iii. Write PHT-C extended source photometry product
Photometry step 8.4.11.

4. If raster mapping performed:

(a) Determine celestial coordinates of each detector pixel for each record;
loop over all measurements
Common step 8.3.3;

(b) For each record and pixel, convert power to flux density
Photometry step 8.4.6;

(c) For each record and pixel, convert flux density to surface brightness
Photometry step 8.4.7;

(d) Produce photometric image
Mapping steps 8.5.1 to 8.5.5;

(e) Write raster map products
Mapping step 8.5.6.

(f) Write PHT-C raster scan photometry product
Mapping step 8.5.8.

8.2.6 PHT25

This AOT performs absolute photometry of the sky brightness with a single filter on one sky position using the PHT-C subinstrument. Raster scans cannot be selected, only staring mode is available.

Processing steps:

1. Read SPD Header
Common step 8.3.1.

2. Read SPD record
Common step 8.3.2.

3. If point source was indicated by observer:

(a) Summation of powers in array, step 8.4.2

(b) Determine Gaussian parameters

Interpolation: Interpolate missing pixels
Photometry step 8.4.4;

Fitting: Determine source peak and position
Photometry step 8.4.5;

(c) Convert power to flux density
Photometry step 8.4.6.

(d) Write PHT-C point source photometry product
Photometry step 8.4.10.

4. If extended source was indicated by observer

(a) Convert power to flux density
Photometry step 8.4.6.

(b) Convert flux density to surface brightness
Photometry step 8.4.7;

(c) Write extended source photometry product
Photometry step 8.4.11.

8.2.7 PHT32

This AOT performs multi-filter mapping using either the C100 or C200 arrays. The map may take the form of a linear scan. A raster scan is performed; the focal plane chopper being used to sample at intermediate positions from the raster pointings in sawtooth mode.

Processing steps:

1. Read SPD Header
Common step 8.3.1.

2. Read SPD record
Common step 8.3.2.

3. Determine celestial coordinates of each detector pixel for each record;
loop over all measurements
Common step 8.3.3;

4. For each record and pixel, convert power to flux density
Photometry step 8.4.6;

5. For each record and pixel, convert flux density to surface brightness
Photometry step 8.4.7;

6. Produce photometric image
Mapping steps 8.5.1 to 8.5.5;

7. Write raster map products
Mapping step 8.5.6.

8. Write PHT-C raster scan photometry product
Mapping step 8.5.8.

8.2.8 PHT37/38/39

These AOTs perform photometry in user-selected wavebands as part of a sparse map using the PHT-C subinstrument. Only staring mode observations are performed.

Processing steps:

1. Loop over all PHT37, PHT38. . ., PHT39 of the same TDT
   (a) Read SPD Header
   Common step 8.3.1.
   (b) Read SPD record
   Common step 8.3.2.
2. If last product was found then loop over all measurements read:
   (a) If point source was indicated by observer:
      i. Convert power to flux density
      Photometry step 8.4.6.
      ii. Write PHT-C point source photometry product
      Photometry step 8.4.10.
   (b) If extended source was indicated by observer:
      i. Convert power to flux density
      Photometry step 8.4.6.
      ii. Convert flux density to surface brightness
      Photometry step 8.4.7;
      iii. Write PHT-C extended source photometry product
      Photometry step 8.4.11.

8.2.9 PHT40

Spectrophotometry with the PHT-S subsystem. Staring, chopped, and mapping modes are available. Point or extended sources can be observed. The short (SS) and the long (SL) wavelength detectors are processed separately.

Processing steps:

1. Read SPD Header
   Common step 8.3.1.
2. Read SPD record
   Common step 8.3.2.
3. If single pointing:
   (a) If point source was indicated by observer:
      i. Determine point source spectrum $F_\lambda(i)$: step 8.6.1
      ii. Write point source spectroscopy product
      Spectroscopy step 8.6.3.
   (b) If extended source was indicated by observer:
      i. Determine surface brightness spectrum $F_\lambda(i)$: step 8.6.2
      ii. Write extended source spectroscopy product
      Spectroscopy step 8.6.3.
4. If raster mapping performed:
   (a) Determine celestial coordinates of each raster point:
   loop over all raster points in AOT
   Common step 8.3.3.

(b) For each raster point j, determine surface brightness spectrum $F_\lambda(i,j)$:
step 8.6.2.

(c) Write raster map product:
Spectroscopy step 8.6.3.

For raster observations no images are produced. For each raster pointing a record containing a spectrum plus the associated coordinates area are written to the product.

8.3 Common Processing Steps

8.3.1 Read SPD header

Operation: Extract all relevant data from the SPD header.

The keywords from the SPD FITS header are read and stored internally for processing. The information is eventually passed to the AAR product headers. The following items are extracted from the SPD, the symbols in parenthesis will be used in the remainder of this chapter:

- **General SPD header keywords:**

  EOHAAOTN, AOT name (e.g. P03)
  ATTYPE, type of attitude operation (P, T, or R for single pointing, tracking or raster observation, respectively)
  DETECTOR, detector used
  NMEAS, number of measurements
  PTOREXT, point or extended source expected
  FPCMODE, chopper mode used
  FPCAMP, chopper amplitude [arcsec]
  CALSEQU, calibration sequence

- **Spacecraft attitude data:**

  CINSTRA, corrected reference instrument J2000 right ascension in degrees (α_c)
  CINSTDEC, corrected reference instrument J2000 declination in degrees (δ_c)
  CINSTROLL, corrected reference instrument J2000 roll angle in degrees (ϕ)
  in case a raster mode was executed:
  ATTRNPTS, number of raster points (M)
  ATTRNLNS, number of raster lines (N)
  ATTRDPTS, increment between points (dM)
  ATTRDLNS, increment between lines (dN)
  ATTRROTA, raster rotation angle ϕ_{raster}

- **Chopper mode information if FPCMODE is not staring:**

  FPCNSTEP, number of chopper steps
  FPCINCR, increment between steps

- **Spectrophotometric mode information if PHT40 used; for each pixel:**

  LAMBDA, LUNC, the central wavelengths and uncertainty
  if point source: RESPP, RPUNC, point source responsivity and uncertainty - ($C_{phts,pixel}$, $\Delta C_{phts,pixel}$)
  if extended source: RESPE, REUNC, extended source responsivity and uncertainty - ($C^E_{phts,pixel}$, $\Delta C^E_{phts,pixel}$)

CALDATE, date of production of spectral response function

- **Results of SPD aperture photometry analysis, if PHT04 used:**

  BACKSRSS, (logical) *true* if SPD aperture photometry analysis could be applied
  NORMCALC, (logical) *true* if sufficient S/N
  FILTCORF, (logical) *true* if empirical aperture correction factor was available
  NRMSIGi, relative background subtracted source flux ratio for aperture i
  NRMSIGUi, uncertainty in ratio for aperture i

- **Information for remaining AOTs; for each filter:**

  FILTER, filter identification
  EXFLUX, expected flux density
  UNCFLX, uncertainty in expected flux density
  MXBACK, maximum expected background

- **Detector responsivity related flags from SPD:**

  RESPDEF, (logical) *true* if default responsivity was used.
  FCSDRIFT, (logical) *true* if signal of FCS measurement contained a residual drift.

Ancillary data required:

SPD product

8.3.2 Read SPD record

Operation: Extract necessary information from an SPD record.

The following data are taken from each SPD record:

Instrument time key (ITK)
Raster point identifiers
Filter identifier
Aperture identifier
Polariser identifier
Number of destructive readouts
Chopper plateau length (chopper dwell time) [1/128 s]
Chopper step number
Chopper position
Measurement time [s]
Measured powers plus uncertainties in [W] if PHT-P, PHT-C
Measured flux densities plus uncertainties in [Jy] if PHT-S
Plateau length [1/128 s]
Data quality flags

For PHT-C and PHT-S, power, uncertainty, plateau length, and quality flags refer to each pixel separately. The chopper step number is used to check that an on-source and off-source pair are available for each chopped measurement in the AA processing.

Ancillary data required:

SPD product

8.3.3 Determine celestial coordinates of each pixel in record

Operation: For all SPD records, derive:
(1) the sky position (in RA and Dec) of the detector origin, and
(2) the RA and Dec offsets (in arcsec) for each detector pixel with respect to the raster centre.

8.3.3.1 Overview

For a given SPD record, the position of a pixel on the sky is determined by:

- the pixel's position in the detector array;
- a deflection of the focal plane chopper, by design the deflection is only in the spacecraft Y direction;
- application of the raster mode, the raster mode can be defined either in spacecraft reference coordinates (i.e. raster increments only in Y and Z directions) or equatorial coordinates (raster increments in RA and Dec directions).

All three instances can occur during the same measurement in case of AOT PHT32 where the chopper is performing a saw-tooth scan using one of the C-arrays while the spacecraft is rastering in spacecraft reference coordinates.

For single pointing photometry the pointing keywords in the SPD product header (Section 8.3.1) are used.

For raster maps the PHT OLP software will determine for each SPD record the equatorial coordinates of the PHT centre field of view thereby considering the raster position as well as a possible chopper deflection. Subsequently, the RA and Dec offsets in arcseconds with respect to the centre of the map or *image coordinates* are computed. The map centre has been provided by the observer. Finally, the image coordinates for each pixel are derived taking into account the individual pixel offsets and the spacecraft roll angle.

8.3.3.2 Extracting pointing data from IRPH

The instrument reference pointing history (IRPH) contains pointing information expressed in quaternions (see 'ISO Handbook, Vol. I: ISO – Mission & Satellite Overview', [20]). The quaternion Q_{raster} that defines the position of the PHT central field of view for a given raster point in the J2000 inertial frame can be computed from:

$$Q_{raster} = Q_{str} \cdot Q_r \cdot Q_{str/qss} \cdot Q_{qss/pht} \cdot Q_{cor}, \tag{8.1}$$

where quaternions

- Q_{str} defines the J2000 pointing of the ISO star tracker,
- Q_r defines the raster point relative to the raster centre of the scan,
- $Q_{str/qss}$ describes the misalignment between the star tracker and the quadrant star sensor (QSS),
- $Q_{qss/pht}$ describes the QSS to instrument aperture alignment; there is one value for $Q_{qss/pht}$ per PHT subsystem and is listed in the focal plane geometry Cal-G file IFPG.FITS (see 'ISO Handbook, Vol. I: ISO – Mission & Satellite Overview', [20]),
- Q_{cor} gives a fine pointing correction to the star tracker calibration; since this correction depends on the position of the guide star in the star tracker field of view, a different correction is given for each raster position.

The following records are read from the IRPH:

ATTMISQ(1:4), = $Q_{str/qss}$, star tracker to QSS misalignment quaternion

ATTINSQ(1:4), = $Q_{qss/pht}$, QSS to instrument aperture misalignment quaternion

A more detailed description on the contents of the IRPH is given in 'ISO Handbook, Vol. I: ISO – Mission & Satellite Overview', [20]. Note: due to different conventions adopted for the misalignment, Q(str/qss) as given in the IRPH should be converted to the PHT OLP convention:

$Q^{PHT}_{str/qss}(2) = -Q^{IRPH}_{str/qss}(2)$

$Q^{PHT}_{str/qss}(3) = -Q^{IRPH}_{str/qss}(3)$

For each raster record in the IRPH, the following parameters are extracted:

- raster point ID (RPID)
- Q_r, raster point quaternion (RPQ)
- Q_{str}, star tracker quaternion (STRQ)
- Q_{cor}, raster point correction quaternion (CORQ)

With this information the quaternion Q_{raster} in Equation 8.1 can be derived.

8.3.3.3 Inclusion of chopper information

We define the *detector origin* to be the centre of the aperture in case of a P detector, the centre of the central pixel 5 in case of C100, and the centre of the array in case of C200.
Assuming a perfect alignment between chopper and spacecraft y-axis, the quaternions representing the rotations of the detector origin with respect to a given raster point are:

$$\begin{aligned} Q_1 = &\quad (0, 0, sin(y_{det}/2), cos(y_{det}/2)) \\ Q_2 = &\quad (0, sin(-z_{det}/2), 0, cos(-z_{det}/2)), \end{aligned}$$

where y_{det} is the chopper deflection and $z_{det} = 0$ is the spacecraft z-offset.
The quaternion of the detector origin for a given chopper position in a raster can now be computed via:

$$Q_{chop} = Q_{raster} \cdot (Q_1 \cdot Q_2), \tag{8.2}$$

where Q_{raster} is the raster point quaternion as derived in Equation 8.1. Q_{chop} can be converted to RA (α), Dec (δ), and Roll-angle (ϕ) according to standard quaternion transformation:

$$\begin{aligned} sin(\delta) &= 2Q(1)Q(3) - Q(2)Q(4) \\ sin(\alpha)cos(\delta) &= 2Q(1)Q(2) - Q(3)Q(4) \\ sin(\phi)cos(\delta) &= 2Q(1)Q(4) - Q(2)Q(3). \end{aligned}$$

8.3.4 Determination of the equatorial offsets of the detector centre

We define the *detector centre* to be the centre of the aperture in case of PHT-P or the centre of a detector pixel in case of PHT-C. Note that for PHT-P the detector origin and centre are identical.

Based on the position of the *detector origin* the detector centre is obtained. For a given record the sky position in RA and Dec of the detector origin is converted into offsets ($\Delta\alpha$ and $\Delta\delta$) with respect to the centre of the raster (α_c, δ_c). The offsets are aligned with the RA and Dec axes in the equatorial coordinate system.

For each pixel the RA and Dec offsets with respect to the detector origin are computed from the detector roll angle and the relative pixel positions. It is assumed that the pixels are positioned in an idealized configuration:

- the pixels in the C100 array are arranged in a regular 3×3 grid with $46''$ spacings in spacecraft Y and Z direction and with the centre of pixel 5 in the origin at $(0'', 0'')$;
- the pixels in the C200 array are arranged in a regular 2×2 grid with $92''$ spacings in Y and Z direction. The origin is at the centre of the array;
- in case of PHT-P the detector centre is the detector origin.

Adding the offsets of the detector origin this will give the map offsets in arcsec for any raster position, detector pixel, and chopper plateau combination.

Ancillary data required:

1. SPD product
2. IRPH product

8.4 Photometry

The conversion from power on the detector in units of W to flux density in Jy or surface brightness in $\mathrm{MJy\,sr^{-1}}$ is presented. The processing of measurements of PHT-P and PHT-C on one hand and PHT-S on the other hand have been separated due to the distinct photometric calibration schemes. Finally, the writing of the resulting data to product files is briefly described.

8.4.1 Determine source in-band power for chopped observations

Operation: Extract the source power from the powers of the different chopper positions.

The in-band powers of on-source $P(s+b)$ with uncertainty $\sigma P(s+b)$ and off-source $P(b)$ with uncertainty $\sigma P(b)$ are read from the SPD product. For each measurement the source power is computed:

$$P(s) = P(s+b) - P(b), \quad [\mathrm{W}] \tag{8.3}$$

$$\sigma P(s) = \sqrt{\sigma^2 P(s+b) + \sigma^2 P(b)} \quad [\mathrm{W}]. \tag{8.4}$$

8.4.2 Summation of the in-band powers over all PHT-C detector pixels

Operation: Derive the sum of the in-band powers of all pixels for a given PHT-C array.

In case the observer requested the measurement of a point source flux with the PHT-C detector arrays, the total [source+background] power as well as the background power on the array is determined by summing the respective powers over all pixels i.

$$P(s) = \sum_i P_i(s) \qquad \text{[W]}, \tag{8.5}$$

and for the [source+background] and background power:

$$P(s+b) = \sum_i P_i(s+b) \qquad \text{[W]}, \tag{8.6}$$

$$P(b) = \sum_i P_i(b) \qquad \text{[W]}. \tag{8.7}$$

The uncertainties are computed according to:

$$\sigma(P(s)) = \sqrt{\sum_i \sigma^2(P_i(s))} \qquad \text{[W]}. \tag{8.8}$$

The relations for $\sigma(P(s+b))$ and $\sigma(P(b))$ are similar.

8.4.3 Fit two-dimensional Gaussian to point sources in the C-arrays

Operation: In case the observer has requested a point source measurement, a 2 dimensional Gaussian function is fitted to the intensity pattern on the array. This processing is done in addition to the sum of all pixel in-band powers (Section 8.4.2).

Caveat: This method of providing point source photometry is not scientifically validated. In particular in the case of faint sources and noisy data, the derived fluxes and uncertainties are not reliable.

To secure a converging fit, an interpolation is performed whenever there are undefined in-band powers for some pixels. The fitting of the 2 dimensional Gaussian itself is performed using standard iterative fitting routines provided by the NAG mathematical routines library (routines E04FDF and E04YCF).

The following parameters are obtained:

- $P_{gauss}(s), \sigma(P_{gauss}(s))$: peak power value and associated error (indicated with d in Section 8.4.5);
- $P_{gauss}(b), \sigma(P_{gauss}(b))$: background power value and error (indicated with c in Section 8.4.5);
- $\alpha, \sigma(\alpha)$: x offset of peak in arcsec and error;
- $\beta, \sigma(\beta)$: y offset of peak in arcsec and error;
- g_{fit}: goodness of fit
- fit status, if status=0, fit is successful.

Details of the procedure are given in the next sections (Sections 8.4.4 and 8.4.5).

8.4.4 Interpolate missing pixels

The fitting routine described in Section 8.4.5 requires only valid pixel intensities on the detector array. Interpolation is necessary in case there are 'bad' data pixels.

A check is performed to determine whether there is a sufficient number of good pixels for interpolation. For C200 one pixel is allowed to be missing. For C100 the criteria are (1) the presence of the centre pixel (pixel 5) where the source is expected to be and (2) there must be at least 2 good pixels on any side of the array. Criterion (2) is imposed to avoid interpolation using an already interpolated value.

The rules for interpolation are

```
C200:  a b    :   a = b + c - d
       c d

C100:  a b c  :   b = (a + c)/2
       d e f
       g h i      a = b + d - (c + g)/2
```

where the individual pixels are designated by letters. Note that there is a rotational symmetry about each side; only one orientation is given. The accuracy of the method depends on

- the location of the source in the array,
- the presence of any extended features, and
- the uniformity of the pixel response.

8.4.5 Determination of Gaussian parameters

The height of the source peak, its position, and the background level is obtained by fitting a Gaussian function to the data. The accuracy of this method depends on the correctness of the assumption of a Gaussian on top of a constant background. The in-band power distribution is considered as a 2 dimensional array:

$$g(x, y) = c + d\, e^{\frac{-z^2}{2}}$$

where

$$z^2 = (x - \alpha)^2 + (y - \beta)^2$$

and

- c is a constant background.
- d is the (background subtracted) height of the source peak.
- α is the x offset of the peak from the array centre.
- β is the y offset of the peak from the array centre.

The x and y axes are the first (along spacecraft z-axis) and second (along spacecraft y-axis) dimension of the pixel array, respectively, with origin at the centre of the array. A chi-squared 'goodness of fit' function is defined as

$$\chi^2 = \sum_{x,y} (P_{x,y}(s + b) - g(x, y))^2$$

The best fit can be found by determining the minimum of χ^2.

For C100, estimates of the uncertainties on the parameters can be derived from the Jacobian of the function at the solution. Detailed discussion of the method is beyond the scope of this document; the NAG algorithm E04YCF is used. The nominal uncertainty of the fit is

$$s = \sqrt{\frac{\chi^2}{\delta}},$$

where δ is the number of degrees of freedom which is determined by the number of pixels n, the number of parameters (4), and the number of interpolations ι performed on C100 (Section 8.4.4):

$$\delta = n - 4 - \iota$$

Since the position of the peak (α, β) is not related to its size or the level of the background on which it is located, (α, β) and (c, d) are largely independent of each other. Thus adding 2 to the degrees of freedom is justified. This argument implies that the uncertainties for C100 may be overestimated. For C200 it is assumed that:

$$\delta = 2$$

The variances are calculated from:

$$\sigma_\alpha^2 = \frac{\chi^2}{(\delta + 2) \cdot m_{pix}^2}$$

$$\sigma_\beta^2 = \frac{\chi^2}{(\delta + 2) \cdot m_{pix}^2}$$

$$\sigma_c^2 = \frac{\chi^2}{(\delta + 2)}$$

$$\sigma_d^2 = \frac{\chi^2}{(\delta + 2)}$$

where m_{pix} is the mean pixel value used to scale into the correct units:

$$m_{pix} = \frac{\sum_{pixels} P_{pix}}{N_{pix} \cdot (P^{max} - P^{min})}$$

The uncertainty of the fit is estimated as

$$s' = \sqrt{\frac{\chi^2}{\delta + 2}}$$

Ancillary data needed

None. See Chapter E04 of the NAG manual.

8.4.6 Photometry with PHT-P and PHT-C

Operation: Convert the mean in-band power on a PHT-P or PHT-C detector (pixel) to a monochromatic flux density (Jy) assuming a ν^{-1} or - equivalently - constant νF_ν spectral energy distribution.

The monochromatic flux density F_ν in Jy for PHT-P or PHT-C is derived as follows (see Equation 5.10):

$$F_\nu(\lambda_c) = 10^{26}\frac{P}{C1{\cdot}f_{PSF}(\lambda_c, aperture)} \qquad \text{[Jy]} \tag{8.9}$$

with uncertainty

$$\Delta F_\nu(\lambda_c) = 10^{26}\frac{\sigma(P)}{C1{\cdot}f_{PSF}(\lambda_c, aperture)} \qquad \text{[Jy]} \tag{8.10}$$

where,

- $F_\nu(\lambda_c)$ in Jy is the flux density at the reference wavelength of the filter, and
- $\Delta F_\nu(\lambda_c)$ in Jy the corresponding uncertainty;
- P in W is the in-band power on the detector in the selected filter band, and
- $\sigma(P)$ in W the corresponding uncertainty;
- $C1$ in m^2Hz is a constant related to each filter band and describes the total transmission of the bandpass along the optical path onto the detector; this includes the size of the mirror, reflections, filter transmission, spectral response of the detector;
- $f_{PSF}(\lambda_c, aperture)$ is the fraction of the telescope point-spread function falling into a given aperture for PHT-P or onto the full array for PHT-C.

For chopped measurements, the powers $P(s)$, $P(s+b)$, and $P(b)$ are converted to flux densities in Jy. For chopped measurements with C100 only pixel 5 is used for the determination of the source flux. This is different in case of staring mode where the sum over the 9 C100 pixels is employed.

Ancillary data needed

- power calibration factors C1 for all filters read from Cal-G file PFLUXCONV, see Sections 5.2.5 and 14.20.1.
- reference wavelengths λ_c for all PHT-P and C bands also stored in PFLUXCONV, see Section 14.20.1.
- point spread function factors are stored in Cal-G file PPPSF for PHT-P and PCPSF f or PHT-C, see Section 14.18. Note: the PCPSF file contains correction factors for the entire array (for staring mode) and for a single pixel (for chopped mode).

8.4.7 Surface brightness determination for PHT-P and PHT-C

Operation: Convert flux density F_ν in Jy to surface brightness I_ν in $\mathrm{MJy\,sr^{-1}}$.

The surface brightness calculation assumes that the point source flux density has been derived. Based on the point source flux density the surface brightness is determined from:

$$I_\nu(\lambda_c) = \frac{F_\nu(\lambda_c){\cdot}f_{PSF}}{(1-\epsilon^2){\cdot}\Omega_\lambda} \qquad \text{[MJy sr}^{-1}\text{]} \tag{8.11}$$

with the uncertainty computed according to

$$\Delta I_\nu(\lambda_c) = \frac{\Delta F_\nu(\lambda_c){\cdot}f_{PSF}}{(1-\epsilon^2){\cdot}\Omega_\lambda} \qquad \text{[MJy sr}^{-1}\text{]} \tag{8.12}$$

where with the same definitions as in the previous sections,

- $I_\nu(\lambda_c)$ in MJy sr^{-1} is the surface brightness at the reference wavelength of the filter, and
- $\Delta I_\nu(\lambda_c)$ in MJy sr^{-1} the corresponding uncertainty;
- Ω in sr is the effective solid angle on the sky of the detector pixel or selected aperture;
- (1-ϵ^2)=0.91 (ϵ=0.30) is the correction for the obscuration by the secondary mirror.

The values of Ω_λ were computed by using a model which takes into account the ISO telescope mirrors as well as the physical sizes of the apertures in case of PHT-P or detectors in case of PHT-C. The model provided the 2-dimensional beam profile (or 'footprint') of each possible aperture/filter (PHT-P) or pixel/filter (PHT-C) combination. The value of Ω_λ was eventually obtained from the integral of the footprint.

Ancillary data needed

- Effective solid angles Ω_λ for each filter/aperture and filter/pixel combination. The values are read from Cal-G files PPOMEGA in case of PHT-P, PC1OMEGA in case of PHT-C100 and PC2OMEGA in case of PHT-C200. See also Appendix A.1.2, and Section 14.21.

8.4.8 Write PHT-P point source photometry product

Operation: Write a complete PHT-P point source photometry product.

Write the product FITS header followed by the processed data in a binary table with each record containing the data for a single filter or aperture.
Detailed product descriptions can be found in Sections 13.4 and 13.4.2 (product PPAP).

8.4.9 Write PHT-P extended source photometry product

Operation: Write a complete PHT-P extended source photometry product.

Write the product FITS header followed by the processed data in a binary table with each record containing the data for a single filter or aperture.
Detailed product descriptions can be found in Sections 13.4 and 13.4.3 (PPAE) for a single pointing product.

8.4.10 Write PHT-C point source photometry product

Operation: Write a complete PHT-C point source photometry product.

Write the product FITS header followed by the processed data in a binary table with each record containing the data for a single filter.
Detailed product descriptions can be found in Sections 13.4 and 13.4.4 (PCAP).

8.4.11 Write PHT-C extended source photometry product

Operation: Write a complete PHT-C extended source photometry product.

Write the product FITS header followed by the processed data in a binary table with each record containing the data for a single filter.
Detailed product descriptions can be found in Section 13.4 and 13.4.5 (PCAE) for a single pointing product.

8.5 Mapping

Two dimensional raster and spatially oversampled mapping observations are processed to images in the equatorial (RA and Dec) coordinate system. For the construction of the images it is assumed that a detector footprint (or beam profile) can be represented by a simple 'top-hat' function: the emission is 1 inside the detector area and zero outside. In addition, the circular apertures have perfectly circular footprints and the square PHT-P apertures and PHT-C detector pixels are considered to be perfectly square. The positions of each detector pixel per raster point have already been determined in the processing steps described in Section 8.3.3. This section describes the co-addition steps to obtain an image.

Note that in the remainder of this section a clear distinction should be made between *detector pixel* and *image pixel*, the former being one of the 9 (for C100) or 4 (for C200) elements in the detector array and the latter being a 'picture element' of an image.

The mapping software yields three products:

- surface brightness map in units of MJy/sr, this is the average surface brightness of all detector pixel exposures for each image pixel;
- uncertainty map in units of MJy/sr, mean brightness uncertainty per image pixel;
- exposure map in s, giving for each image pixel the total time that it has been covered by any detector pixel.

8.5.1 Statistical flat-field correction for C100 and C200

Operation: Correct for possible flat-field patterns

Assessment of PHT22 or PHT32 maps have shown that there are systematic flat-field patterns of the C100 and the C200 arrays due to inconsistent surface brightness calibration of the individual detector pixels. The patterns are most prominent in maps with a poor overlap among the individual pixels.

To correct for these patterns a statistical flat-field was applied according to the following steps:

- determine for each pixel i the 10-percentile of the surface brightness of all raster positions: $I^*(i)$
- compute the flat-field correction $\mathrm{ff}(i)$ for each pixel, by normalising the 10-percentiles to the average:

$$\mathrm{ff}(i) = \frac{I^*(i)}{\frac{1}{N}\sum_i I^*(i)}, \qquad [\,] \tag{8.13}$$

  where N is the number of detector pixels in the array.

- apply the flat-field correction to all brightness values $I(i,j)$:

$$I'(i,j) = \frac{I(i,j)}{\mathrm{ff}(i)}, \qquad [\,] \tag{8.14}$$

  where j is the raster step or chopper plateau.

This correction is only applied if the raster map contains 20 or more raster steps for PHT22 raster maps or $\geq$20 chopper plateaux for PHT32 maps. The corrections $\mathrm{ff}(i)$ are written in the PGAI product header with keyword FFPiFk, where i is pixel number and k filter number in AOT.

Table 8.1: *Image pixel sizes used in OLP. For reference the size of the Airy disc at the shortest detector wavelength is given.*

Detector used	Shortest wavelength [μm]	Airy disc diameter [arcsec]	Pixel size [arcsec]
P1	3.2	2.8	8.0
P2	20	17.7	8.0
P3	60	50.3	8.0
C100	70 (C_50)	41.9	15.0
C200	120	101.0	15.0

8.5.2 Establish image pixel size

Operation: Define the size of the image pixel

The angular dimensions of an image pixel in OLP depend only on the detector subsystem used and is independent on the filter/aperture combination. The values are listed in Table 8.1.

Based on the image pixel size, the *fine-grid* is defined to compute the fractional pixel coverage. The optimum fine-grid size in terms of realistic processing times has been decided to be:

$$S_{fine\ grid} = S_{pixel}/5 \qquad \text{[arcsec]} \tag{8.15}$$

Ancillary data needed

- None, parameters are hardcoded

8.5.3 Establish maximum image size

Operation: Calculate the angular dimensions of the image required to contain the full raster scan in equatorial coordinates.

The maximum size of the image is calculated using the following parameters:

- M: the number of raster steps along a raster leg;
- N: the number of raster legs;
- dM: step size in arcsec along raster leg;
- dN: step size in arcsec in between raster legs;
- α_c, δ_c: the J2000 RA and Dec position in decimal degrees of the raster centre;
- $\alpha_{m,n}$, $\delta_{m,n}$: the J2000 RA and Dec position in decimal degrees of raster point (m,n), with m= 1...M, and n= 1...N;
- D_A: the diameter in arcsec of the aperture used, in case of a C-array: the sidelength of the array in arcsec;
- θ_{chop}: the maximum chopper deflection while mapping (only for PHT32 maps).

The centre of the raster scan is defined as the image centre. The dimensions of the frame in equatorial coordinates are derived as follows. For all raster points (m,n) determine:

$$\begin{aligned} \alpha_{max} = &\quad max(\Delta\alpha(m,n)) \\ \alpha_{min} = &\quad min(\Delta\alpha(m,n)) \\ \delta_{max} = &\quad max(\Delta\delta(m,n)) \\ \delta_{min} = &\quad min(\Delta\delta(m,n)) \end{aligned}$$

where:

- $\Delta\alpha(m,n)$: RA component of the difference vector between $(\alpha_{m,n}, \delta_{m,n})$ and (α_c, δ_c)
- $\Delta\delta(m,n)$: Dec component of the difference vector between $(\alpha_{m,n}, \delta_{m,n})$ and (α_c, δ_c)

The components $\Delta\alpha(m,n)$ and $\Delta\delta(m,n)$ are computed using spherical trigonometry. The margins around the raster grid is determined by D_A and the maximum chopper deflection $\theta_{chop,max}$, in raster orientation:

$$\begin{aligned} x_m = &\quad D_A/2 + \theta_{chop,max} \\ x_n = &\quad D_A/2 \end{aligned}$$

Then the map dimensions L_α and L_δ are computed from:

$$\begin{aligned} L_\alpha = &\quad \alpha^*_{max} - \alpha^*_{min} \\ L_\delta = &\quad \delta^*_{max} - \delta^*_{min} \end{aligned}$$

with

$$\begin{aligned} \alpha^*_{max} = &\quad \alpha_{max} + (|x_m cos(\phi)| + |x_n sin(\phi)|) \\ \alpha^*_{min} = &\quad \alpha_{min} - (|x_m cos(\phi)| + |x_n sin(\phi)|) \\ \delta^*_{max} = &\quad \alpha_{max} + (|x_m sin(\phi)| + |x_n cos(\phi)|) \\ \delta^*_{min} = &\quad \delta_{min} - (|x_m sin(\phi)| + |x_n cos(\phi)|) \end{aligned}$$

where ϕ is the spacecraft roll angle.

The rectangular image frame is therefore chosen so large that the entire area covered by the detectors in the raster fits inside. Depending on the rotation angle of the raster as well as the sampling step sizes with respect to the size and rotation of the detector, undefined frame areas may be present.

The minimum number of image pixels required to map the whole of the raster area is calculated from the dimensions of the raster and the image pixel size S_{pixel}, as follows:

$$\begin{aligned} n_\alpha &= 2(\|\frac{L_\alpha}{2S_{pixel}}\| + 1) + 1 \\ n_\delta &= 2(\|\frac{L_\delta}{2S_{pixel}}\| + 1) + 1, \end{aligned}$$

in which $\|$ denotes 'the integer value of' - i.e. the initial value is rounded down to the nearest integer.
Also calculated at this stage are the angular coordinates of the image pixel origin which is defined as the bottom left hand corner (blhc) of image pixel $(1, 1)$.

$$\begin{aligned} x_0 &= -\frac{n_\alpha S_{pixel}}{2} \\ y_0 &= -\frac{n_\delta S_{pixel}}{2} \end{aligned}$$

These are used subsequently to translate between the coordinate origin at the centre of the image and the origin of the pixel coordinates.
Finally, the angular coordinates of an image pixel (i, j) are:

$$\begin{aligned} x(i,j) &= (i - 1 - \frac{n_\alpha}{2})S_{pixel} \\ &= (i-1)S_{pixel} + x_0 \\ y(i,j) &= (j - 1 - \frac{n_\delta}{2})S_{pixel} \\ &= (j-1)S_{pixel} + y_0 \end{aligned}$$

8.5.4 Determination of the coverage by a sky sample in the image

Operation: Map data from a given detector pixel, raster position, and chopper offset combination onto the image.

We define a *sky sample* to be a sky observation for a given detector pixel, at raster position (m,n), and chopper deflection θ_{chop}. A sky sample has a raster dwell time or chopper dwell time (in case of PHT32 maps).
The fine grid (Section 8.5.2) is used to determine the fractional coverage of the image pixel by the detector footprint. The fine-grid size is chosen such that it is a simple factor of the image pixel size: there is an integral number of grid points per image pixel.
Therefore for each sky sample the following steps are performed:

- determine the image pixel range $([x_{min}, x_{max}], [y_{min}, y_{max}])$ in which the detector pixel footprint can completely be contained;
- for each image pixel contained in this range determine the number of fine-grid positions N_{fg} which fall within the detector footprint.
- for each image pixel in the range determine the coverage factor $f_{cov} = N_{fg}/N_{total}$, where N_{total} is the total number of fine-grid positions on a pixel.

8.5.5 Binning sky samples onto image pixels

Operation: Accumulate the sky samples and derive the average surface brightness, uncertainty and exposure.

The contribution from the n$^{\text{th}}$ sky sample to the mean brightness, brightness uncertainty, and exposure time at image pixel i, j are denoted $b_n(i, j)$, $u_n(i, j)$ and $e_n(i, j)$ respectively. The accumulated sums of the contributions from the first n pointings are denoted by $B_n(i, j)$, $U_n(i, j)$ and $E_n(i, j)$.

The effective exposure time of sky sample n at image pixel i, j is the fraction of the image pixel covered by the aperture for a given sample multiplied by the plateau length (Section 8.3.2) converted to seconds, t_n:

$$e_n(i,j) = f_{cov}(i,j)\, t_n \qquad [\mathrm{s}] \tag{8.16}$$

To calculate the total exposure on the image pixel, the contributions from all sky samples are summed. The surface brightness values and the corresponding uncertainties are summed thereby using the exposure times as weights.

$$\begin{aligned}
E_{n+1}(i,j) = &\quad E_n(i,j) + e_{n+1}(i,j) && [\mathrm{s}] \\
B_{n+1}(i,j) = &\quad B_n(i,j) + e_{n+1}(i,j) b_{n+1}(i,j) && [\mathrm{MJy\,sr^{-1}}] \\
U_{n+1}(i,j) = &\quad U_n(i,j) + e_{n+1}(i,j) u^2_{n+1}(i,j) && [\mathrm{MJy\,sr^{-1}}].
\end{aligned}$$

The accumulated sums for all sky samples are used to derive images of total exposure time E_{total}, mean brightness $\overline{B}$ and brightness uncertainty U_{rms}.

$$\begin{aligned}
E_{total}(i,j) &= E_N(i,j) \\
&= \sum_{n=1}^{N} e_n(i,j) \qquad [\mathrm{s}]
\end{aligned}$$

$$\begin{aligned}
\overline{B}(i,j) &= B_N(i,j)/E_N(i,j) \\
&= \frac{1}{E_N} \sum_{n=1}^{N} e_n(i,j) b_n \qquad [\mathrm{MJy\,sr^{-1}}]
\end{aligned}$$

$$\begin{aligned}
U_{rms}(i,j) &= \left(\frac{1}{E_N} U_N(i,j) \right)^{\frac{1}{2}} \\
&= \left(\frac{1}{E_N} \sum_{n=1}^{N} e_n(i,j) u^2_n(i,j) \right)^{\frac{1}{2}} \qquad [\mathrm{MJy\,sr^{-1}}]
\end{aligned}$$

8.5.6 Write image products

Operation: Write a set of complete photometric image products.

First write the product FITS header followed by the processed data in a primary array. The derived surface brightness (in MJy/sr), brightness uncertainty (in MJy/sr) and exposure time (in s) images are stored in separate products.

Detailed product descriptions can be found in Sections 13.4, 13.4.6 (product PGAI), 13.4.7 (product PGAU), and 13.4.8 (product PGAT) for the brightness, uncertainty and exposure time images.

8.5.7 Write PHT-P raster scan photometry products

Operation: Write a complete PHT-P raster photometry product.

Write the product FITS header followed by the processed data in a binary table with each record containing the data for a single filter and sky position.

Detailed product descriptions can be found in Sections 13.4 and 13.4.9 (product PPAS).

8.5.8 Write PHT-C raster scan photometry products

Operation: Write a complete PHT-C raster photometry product.

Write the product FITS header followed by the processed data in a binary table with each record containing the data for a single filter and sky position.

Detailed product descriptions can be found in Sections 13.4 and 13.4.10 (product PCAS).

8.6 Spectroscopy with PHT40

The processing of PHT-S data during Derive_SPD created PHT-S spectra where for each pixel the flux density is given in Jy. In Derive_AAR the PHT-SS and PHT-SL detector arrays are processed separately in line with the separate treatment in SPD. Due to the relatively few PHT-S raster maps collected during the mission, no raster images with PHT-S are produced.

8.6.1 PHT-S spectrum in wavelength units for point sources

Operation: Derive a PHT-S spectrum in F_λ

The PHT-S flux density $F_\nu(i)$ in frequency units of Jy of detector array element i with uncertainty $\Delta F_\nu(i)$ is converted to wavelength units according to:

$$F_\lambda(i) = \frac{10^{-32}c}{\lambda^2(i)} F_\nu(i) \qquad [\mathrm{W\,m^{-2}\mu m^{-1}}] \tag{8.17}$$

$$\Delta F_\lambda(i) = \frac{10^{-32}c}{\lambda^2(i)} \Delta F_\nu(i) \tag{8.18}$$

where,

- $F_\lambda(i)$ in $\mathrm{W\,m^{-2}\mu m^{-1}}$ is the flux density in wavelength units, and
- $\Delta F_\lambda(i)$ the corresponding uncertainty;
- $\lambda(i)$ in μm is the centre wavelength of a pixel;
- $c = 299792500$ m/s is the speed of light used in OLP.

This conversion is applied to

- PHT40 point source observations in staring mode, and
- the chopped source and the chopped (source+background) spectrum of PHT40 point source observations in chopped mode.

Ancillary data needed

The values for $\lambda(i)$ are stored in Cal-G file PSPECAL, see Section 14.19.1.

8.6.2 PHT-S spectrum for extended sources

Operation: Derive a PHT-S spectrum for extended sources.

The PHT-S flux density $F_\nu(i)$ in frequency units of Jy of detector array element i with uncertainty $\Delta F_\nu(i)$ is converted to surface brightness:

$$I_\lambda(i) = \frac{10^{-26}c}{\lambda(i)^2} F_\nu(i) \frac{C^p_{ave}(i)}{C^e_{ave}(i)} \qquad [\mathrm{W\,m^{-2}\mu m^{-1}sr^{-1}}] \tag{8.19}$$

$$\Delta I_\lambda(i) = \frac{10^{-26}c}{\lambda(i)^2} \Delta F_\nu(i) \frac{C^p_{ave}(i)}{C^e_{ave}(i)} \tag{8.20}$$

where

- $I_\lambda(i)$ in $\mathrm{W\,m^{-2}\mu m^{-1}sr^{-1}}$ is the surface brightness for a given detector array element i, and
- $\Delta I_\lambda(i)$ is the corresponding uncertainty;
- $\lambda(i)$ in μm is the central wavelength of a PHT-S detector pixel;
- $C^p_{ave}(i)$ in $\mathrm{V\,s^{-1}/Jy}$ is the average spectral response function for the conversion from signal in $\mathrm{V\,s^{-1}}$ to point source flux density in Jy;
- $C^e_{ave}(i)$ in $(\mathrm{V\,s^{-1}})/(\mathrm{MJy\,sr^{-1}})$ is the average spectral response function for the conversion from signal in $\mathrm{V\,s^{-1}}$ to surface brightness in $\mathrm{MJy\,sr^{-1}}$;
- c = 299792500 $\mathrm{m\,s^{-1}}$ is the speed of light.

This conversion is applied to

- extended source PHT40 observations in staring mode,
- each raster pointing in PHT40 raster mode.

Ancillary data needed

The values for $\lambda(i)$, $C^p_{ave}(i)$, and $C^e_{ave}(i)$ are stored in Cal-G file PSPECAL, see Section 14.19.1.

8.6.3 Write spectroscopy products

Operation: Write spectroscopy products.

To maintain the separation between the short wavelength and long wavelength PHT-S detector arrays SS and SL, the different array data are stored in separate products.

Detailed product descriptions can be found in Sections 13.4, 13.4.11 (product PSAP), 13.4.12 (product PLAP), 13.4.13 (product PSAE), 13.4.14 (product PLAE), 13.4.15 (product PSAS), 13.4.16 (product PLAS), for the PHT-SS and SL point source, extended source and raster products, respectively.

Chapter 9

Photometric Calibration Accuracies

9.1 Overview

In this chapter we show the status of the scientific validity of products of the ISOPHOT AOTs as of OLP v10. The scientific validity of an observing mode is decided after thorough evaluation of the corresponding Auto Analysis (AAR) products (see Chapter 8) of observations of known test targets. Only when the results are according to the expectations a mode is declared 'scientifically valid'. A detailed description of the validation of ISOPHOT observing modes can be found in Klaas & Richards 2002,[27]

The reliability of the OLP products is best described by the photometric accuracies that can be achieved per observing mode. The photometric accuracies for those modes that are scientifically validated as of OLP v10 are presented in detail in the document 'ISOPHOT Calibration Accuracies' by Klaas et al. 2002, [26]. A full discussion of the error budgets and resulting uncertainties is given in the document 'ISOPHOT Error Budgets' by [31]. The tables presented in the following sections were taken from Klaas et al. (2001) [28].

9.2 Calibration Accuracies per Detector

The calibration accuracy consists of the following items:
Absolute accuracy: is a measure of the uncertainty of the flux with respect to an independently and absolutely calibrated flux standard.
Relative (multi-filter) accuracy: is a measure of the uncertainty of a spectral energy distribution derived from an ISOPHOT multi-filter observation. For PHT-S this is a measure of the uncertainty of the spectral shape between different wavelength ranges of groups of about 20 consecutive pixels.
Relative flux reproducibility: is a measure of the flux consistency between repeated observations of a non-variable source.

An overview of the calibration accuracies per detector in the light of the accuracy definitions given above is presented in Table 9.1.

9.3 Status of Scientific Validation of PHT AOTs

An overview of the scientific validation of the ISOPHOT modes is given in Table 9.2. The 11 AOTs have been divided into 28 submodes and the respective number of executed astronomical observations is given. An observation in multi-filter and multi-aperture mode can comprise several measurements. The sparse map modules have been counted individually. OLP Versions 5 and 6 were released during the ISO

Table 9.1: *ISOPHOT photometric calibration accuracy overview.*

detector	source type point / extended	source brightness	typical on-source integration [s]	absolute accuracy [%]	reproducibility $1\,\sigma$ of 20 samples [%]	multi-filter accuracy [%]
P1	p, star	50 – 6000 Jy	32	<10	5	<20
P1	p, star	0.1 – 50 Jy	≤256	40	10	–
P1	p, chop	0.06 – 10 Jy	128	<25	<16	<25
P2	p, star	10 – 200 Jy	32	<10	2	5
P2	p, star	0.5 – 10 Jy	≤256	<15	12	–
P2	p, chop	0.2 – 20 Jy	128	<30	<10	–
P3	p, star	0.5 – 25 Jy	32	10	7	<10
P3	p, star	<0.5 Jy	≤256	20	7	–
P3	p, chop	≥0.8 Jy**	128	<25	<15	<25
C100	p, star	0.5 – 25 Jy	32	15	≥3	<25
C100	p, star	0.05 – 0.5 Jy	≤256	<25*	20	–
C100	e, star	5 – 15 MJy sr^{-1}	32	25	10	20
C100	p, chop	≥0.2 Jy**	128	<30	<15	<20
C200	p, star	1 – 900 Jy	128	10	10	20
C200	p, star	0.2 – 1 Jy	≤256	<20*	10	–
C200	e, star	4 – 10 MJy sr^{-1}	64	20	10	20
C200	p, chop	≥1.5 Jy**	128	<40	–	–
SS	p, star	1 – 6000 Jy	256	<10	–	<15
SS	p, chop	0.5 – 500 Jy	1024	<10	–	<10
SS	e, star	30 – 3000 MJy sr^{-1}	256	<10	–	<15
SL	p, star	0.3 – 1500 Jy	256	<10	–	<15
SL	p, chop	0.2 – 200 Jy	1024	<10	–	<10
SL	e, star	5 – 10000 MJy sr^{-1}	256	<10	–	<15

Notes
* for mini-map photometry using PCAS products
** for fainter fluxes careful estimate of cirrus confusion necessary

mission, OLP Version 7 is the end-of-mission pipeline, OLP Versions 8, 9 and 10 were released during the post-operational phase.

Table 9.2: *Scientific validation of ISOPHOT OLP AOT processing. 'No' means that the submode is not validated.*

AOT	observation type	submode	# of AOs	scientific validation with	comments
PHT03 (P)	multi-filter photometry	staring point source	961	V6	for standard apertures
		staring ext. source	270	no	
		nodding	230	V6	for standard apertures
		chopped	1134	V10	
		raster map	431	no	
PHT04 (P)	multi-aperture photometry	staring point source	219	V10	relative curve of growth
		staring ext. source	36	V10	for extent < 2 arcmin
		chopped	17	no	sequ: ≥ 4 aper. (120,180)
PHT05 (P)	absolute photometry	staring point source	57	V6	for standard apertures
		staring ext. source	162	no	
PHT17 (P) 18 , 19	sparse map photometry	staring point source	682	V6	for standard apertures
		staring ext. source	524	no	
PHT22 (C)	multi-filter photometry	staring point source	373	V7	
		staring ext. source	123	V7	
		nodding	29	V7	
		chopped	1887	V10	limited by sky confusion
		raster map	2884	V8.4	ff quality for > 20 RP
PHT25 (C)	absolute photometry	staring point source	54	V7	
		staring ext. source	149	V7	
PHT32 (C)	oversampled mapping	chopped mapping	1565	V10	partially validated w.r.t. SB, ff quality
PHT37 (C) 38 , 39	sparse map photometry	staring point source	2109	V7	
		staring ext. source	710	V7	
PHT40 (S)	spectroscopy	staring point source	835	V5	
		staring ext. source	102	V6	
		chopped	412	V6	
		raster map	135	V6	
PHT50 (P)	aperture polarimetry	staring point & ext. source	15	V7	interactive processing & special FORTRAN routine
PHT51 (C)	array polarimetry	staring point & ext. source	110	V7	interactive processing & special FORTRAN routine
		raster map		V7	beam effects for ext. sources

Notes

ext.:	extended
ff:	detector flat-field
RP:	raster points

Chapter 10

Caveats

10.1 Overview

The quality and reliability of both data products and documentation depend on several aspects. In this chapter we summarize the pending issues related to documentation, to product reliability, and, closely connected to the products, to the OLP software.

In Section 10.2 the shortcomings of the present version of the documentation are given.

In the remaining sections of this chapter we list the limitations of, and caveats on the ISOPHOT data and software. Issues concerning incomplete instrumental calibrations are discussed in detail. The list was compiled during the scientific validation process of the pipeline with OLP 10 using the PHT calibration files Version 7.0. For more details concerning the validation process, see Klaas & Richards 2002, [27].

10.2 Caveat on this Document

This handbook describes the OLP 10 ISOPHOT data products, the related calibration and the processing steps. Ongoing research of ISOPHOT data can lead to improved calibration corrections, calibration tables, and processing steps. It is advised to visit regularly the related ISO web pages to check whether better data products can be obtained.

10.3 Error Calculation and Propagation

Whenever possible, uncertainties are included in the OLP products. However, the formal propagation of these uncertainties does not yield a reasonable error estimate in the photometry. This is due to the presence of different types of errors: statistical uncertainties, systematic uncertainties, and photometric bias. The relative contribution of these components in the processing chain depends on the details of the measurement mode.

For an estimate of the total uncertainty associated with a specific measurement the observer is referred to the previous Chapter 9 and the documents 'ISOPHOT Error Budgets' by Laureijs & Klaas 1999, [31] and 'ISOPHOT Calibration Accuracies' by Klaas et al. 2002, [26].

Caveat: The PHT OLP software does only provide an uncertainty based on the statistical evaluation of the signals. No estimates are given of the systematic uncertainties introduced by calibration steps. Therefore, OLP 10 uncertainties are 'minimal' errors. It is essential to refer to special documentation which provides an overview of the uncertainties introduced step by step. These depend on the exact observing conditions and evaluation steps which may even not be completed inside OLP, e.g. background subtraction in maps or from independent staring measurements.

10.4 Validity Ranges of FCS Calibration Files

For measurements with FCS heating power outside the validity range, the default responsivity is used, see Section 7.10. The validity ranges are given in the header of the P*FCSPOW*.FITS Cal G files, see Section 14.12. Sparse maps may have different FCS settings. The FCS with a setting inside the validity range is used in case the setting of the other falls outside. The selected responsivity calibration (single, both, first, second, default) is indicated in the SPD product file header. For P1 and P2 detectors there is no severe impact on calibration quality by using default responsivities.

Caveat: A poorer calibration accuracy can be expected for observations with detectors P3, C100 or C200 for which the headers of the PHT SPD data products indicate that the FCS power settings were outside the validity range and default responsivities were used. Due to the dependence of the FIR detector responsivities on space weather conditions calibration offsets by 30–50 % are possible.

Caveat: The FCS calibration for P3, C100 and C200 before revolution 94 is less well sampled with standard calibration observations than after revolution 94. Therefore, the photometric calibration of observations taken before revolution 94 can be poorer than that of later observations. This caveat also applies to the FCS flat-field calibration for the C100 and C200 detectors.

10.5 Inhomogeneous FCS Illumination of PHT-P Apertures

Caveat: In case the FCS calibration of an observation is performed in a non-standard aperture (see Section 5.4) strong deviations up to a factor $\simeq 2$ of the correct responsivity and thus the derived fluxes can occur. The strongest deviations are expected for the largest apertures of the P1 filters.

10.6 Non-Geometric Aperture Beam Size Scaling

Caveat: If observations are performed in non-standard apertures (see Section 5.4), deviations from the correct flux calibration can occur. Especially extended source observations with P1 and P2 using the largest apertures are expected to exhibit the largest deviations (see Section 4.5.1). This caveat often applies to background observations which are required to determine the source flux.

10.7 Detector Signal Transients

Caveat: Detector transients are very often the limiting factor for the achieved accuracy. The PHT-P and PHT-C transient correction (Section 7.3.5) only works satisfactorily for measurements which are long compared to the detector transient time at a given illumination. Measurements flagged by the OLP software as 'plateau data affected by residual drift' (Table 13.3) can be unreliable due to a residual drift greater than 5%. Raster measurements with PHT-S generally suffer from transient effects, since a static spectral response function is applied.

10.8 Long Term Detector Drifts

For single pointing measurements with one FCS measurement per detector no attempt is made to correct for long term responsivity drifts. It is assumed that the detector responsivity is stable during the execution time of an AOT.

For raster pointing observations and sparse maps, the average of the two bracketing responsivity values is used, provided both have neither a real time problem nor are outside the validity range of the FCS heating power (see Section 10.4).

However, investigations of long measurements have shown that the responsivity is not stable but exhibits a non-linear drift. An exponential behaviour is observed due to switch-on effects. Detailed models of the detector behaviour or baseline fits would be required for optimum correction.

Caveat: PHT OLP does not correct for PHT-P and PHT-C long term detector drifts within an AOT. In case of maps with bracketing FCS measurements only the average responsivity value is used.

10.9 Limitations in Use of PHT Colour Correction Factors

Caveat: Colour correction factors above 2 should be considered as less accurate and factors above 4 only as an indication of the order of the correction, as they clearly depend on the integration and interpolation method used. In these cases it is recommended to establish the colour correction factor independently by using the bandpass transmission (Section 14.24) and a model for the spectral energy distribution of the source.

10.10 Non-Linearity of Detector Responsivity with Flux

The linearity calibration (Section 5.2.2) is only valid for certain signal ranges. Table 10.1 lists the lower and upper signal limits as given in the headers of the calibration files PxySLINR, see Section 14.8. The polynomial approximations to the non-linearity curves are not extrapolated beyond the calibrated signal ranges but are kept at the level of the boundary. In different filters different relative signal ranges may be covered. As a consequence, in some multi-filter observations unsteadiness in calibration accuracy may be introduced at the boundaries of the calibrated signal ranges.

10.11 Incomplete Looking Raster Maps

This caveat comes from the investigation of PHT-P raster maps:

Caveat: If the flux on the detector is small, close to zero or even negative signals can occur at the end of the DERIVE_SPD processing stage. The signals are flagged 'zero signal for plateau' (see Table 13.3). OLP 10 does not continue to process these flagged data in DERIVE_AAR, see Section 13.3 for SPD product types. This leads to PGAI map products which look apparently incomplete. The most likely observations that are affected involve the short wavelength filters of PHT-P1 (where the sky background is low) in combination with small aperture sizes.

10.12 Point Spread Function Fraction Factors in the Data Products

Caveat: The point spread function correction factors are applied to all point source photometry products, like PPAP and PCAP, regardless of whether a background subtraction was performed or not (see Section 5.2.5). For staring mode observations without background subtraction this has to be accounted for when subtracting the separate background measurement.

The background measurement can be either a point source product of type PPAP or PCAP (in Jy):

$$\begin{aligned} F_{\mathrm{src+back}} &= F_{\mathrm{on}}/f_{\mathrm{PSF}} \\ F_{\mathrm{back}} &= F_{\mathrm{off}}/f_{\mathrm{PSF}} \\ \rightarrow F_{\mathrm{src}} &= F_{\mathrm{src+back}} - F_{\mathrm{back}} \end{aligned}$$

Table 10.1: *Calibrated signal ranges of non-linearity correction tables.*

Detector	Filter	Lower Limit [V/s]	Upper Limit [V/s]
P1	3.3	0.0000	55.39
P1	3.6	0.0000	166.19
P1	4.8	0.0000	126.77
P1	7.3	0.0000	95.52
P1	7.7	0.0000	27.14
P1	10.0	0.0000	23.47
P1	11.3	0.0000	2.86
P1	12.0	0.0237	35.69
P1	12.8	0.0310	11.26
P1	15.0	0.0197	3.66
P2	20.0	0.0745	9.46
P2	25.0	0.0994	10.93
P3	60.0	0.2470	56.93
P3	100.0	0.2658	68.08
C100	60.0	0.0000	55.41
C100	65.0	0.0000	44.95
C100	80.0	0.2022	32.24
C100	90.0	0.0000	44.78
C100	100.0	0.0000	36.53
C100	105.0	0.0000	34.61
C200	120.0	0.0000	25.23
C200	150.0	0.0000	33.33
C200	170.0	0.0000	23.94
C200	180.0	0.0000	21.10
C200	200.0	0.0000	7.30

$$= \frac{F_{\rm on} - F_{\rm off}}{f_{\rm PSF}},$$

or an extended source product of type PPAE or PCAE (in $\mathrm{MJy\,sr^{-1}}$). For the conversion of in-band power to surface brightness, see Section 8.4.7:

$$\begin{aligned} F_{\rm src+back} &= F_{\rm on}/f_{\rm PSF} \\ B_{\rm back} &= \frac{F_{\rm off\_pix}}{(1-\varepsilon^2)\cdot\Omega} \\ \rightarrow F_{\rm src} &= F_{\rm src+back} - F_{\rm back} \\ &= \frac{F_{\rm on} - n_{\rm pix}\cdot(B_{\rm back}\cdot(1-\varepsilon^2)\cdot\Omega)}{f_{\rm PSF}} \end{aligned}$$

$F_{\rm on}$, $F_{\rm off}$, $F_{\rm off\_pix}$ are fluxes in the aperture uncorrected for point source function effects (the latter one for one single pixel of the array). $B_{\rm back}$ is the surface brightness of the background.
Please note the following definitions with regard to application of $f_{\rm PSF}$-factors to header keywords:

1) For PPAP and PPAE:
   $f_{\rm PSF} = f_{\rm PSF}^{\rm aperture}$
   $n_{\rm pix} = 1$

2) For PCAP and PCAE staring modes:
total flux of the array is used!
$f_{\rm PSF} = f_{\rm PSF}^{\rm array}$
converted flux from surface brightness has to be multiplied with number of pixels, because the solid angle Ω is defined per pixel!
$\rm n_{pix} = 9$ for C100, $n_{\rm pix} = 4$ for C200

3) For C100 PCAP and PCAE chopped mode (PHT22):
$f_{\rm PSF} = f_{\rm PSF}^{\rm pixel}$
because only the central pixel is used!
$n_{\rm pix} = 1$
Note that $f_{\rm PSF}^{\rm array}$ is applied to the data fields PCAPSRCE for consistency with the staring mode!

4) For C200 PCAP and PCAE chopped mode (PHT22):
$f_{\rm PSF} = f_{\rm PSF}^{\rm array}$
$n_{\rm pix} = 4$

10.13 Residual Flat-Field Structures in PHT22 Raster Maps

A statistical flat-field method is applied to remove flat-field residuals in PHT22 maps with more than 20 raster points, see Section 8.5.1. Smaller raster maps are usually obtained for photometry of individual sources centred in the map, the so-called mini-map photometry. Dedicated analysis methods have been developed for mini-maps. The following caveat applies to mapping measurements executed with AOT P22 in raster mode:

Caveat: Temporal variations of the flat-field in case of C100 maps limit the ability of faint source detections and photometry on low sky background levels.

10.14 Point Source Photometry from Mini-Maps

Mini-maps are staring raster maps with restricted grid size typical, 3×3 for C100 or 2×2 for C200 executed with AOT PHT22 in raster mode.

Caveat: Aperture photometry on PGAI map products gives reliable fluxes only for a rather limited flux range. These products should mainly be used as a check on what can be seen in the maps. To obtain reliable photometry the PCAS products should be used where the flux is given per detector per raster position.

10.15 Filters with Less Reliable Photometry

Caveat: Several filters display systematic flux offsets in multi-filter SEDs. The filters and the flux levels for which these artifacts were found are listed below.

- P1 12.8 μm filter: positive flux offset from +10 % at flux level 50 Jy to factor of 2 at background level.
- C100 65 and 80 μm filters: +15 to +30 % at background level.
- Background measurements in the shortest wavelength PHT-P filters (3.3, 3.6, 4.8 μm) in apertures considerably smaller than the 180 arcsec aperture (including the 23 arcsec default aperture for these filters) usually do not give any meaningful results, because the measurement is dominated by dark signal.

It is assumed that the background level is at or a few times above the lowest possible sky background.

10.16 PHT-S Dynamic Spectral Response Calibration

The nature of the PHT-S dynamic spectral response calibration (Section 5.2.6) implies the following restrictions for measurements executed with AOT P40 in staring mode:

Caveat: The transient behaviour of the PHT-S detectors is temperature dependent. The calibration was established for a certain temperature range of the detectors. Since PHT-S was not actively temperature controlled, the detector temperature can occur outside the calibrated range ($2.7\,\mathrm{K} < T < 3.1\,\mathrm{K}$). In this case, a different transient behaviour of the signals can be observed, leading to absolute and relative accuracies which are worse than quoted. A warning message is included in the PSSS and/or PSLS product headers.

Caveat: For certain wavelength ranges, fluxes of some targets can be outside the range covered by standard stars. For these targets a worsening is possible of the accuracy in the relative spectral shape. A warning message is included in the PSSS and/or PSLS product headers.

The scientific validation of the PHT-S observations led to the following two general caveats:

Caveat: The Zodiacal Light level (see Section 4.9.3) is below the sensitivity limit of PHT-SS where the Zodiacal Light intensity is less than $1\,\mathrm{MJy\,sr^{-1}}$ for 2.5 to 4.9 μm.

Caveat: Quoted absolute accuracies are only valid for the Zodiacal Light level in the PHT-SL range (Zodiacal Light intensity $\sim 5 - 20\,\mathrm{MJy\,sr^{-1}}$ for 5.8 to 11.6 μm), if the exposure time is ≥ 1024 seconds.

10.17 PHT-S Pointings Not Centred in the Aperture

PHT-S exhibits a steep beam profile in particular in the cross-dispersion (spacecraft y-axis) direction, see Section 4.5.1.3. As a consequence, a small pointing offset can cause both a significant absolute flux offset and a change of the relative spectral shape. The latter is also visible via flux jumps at the wavelength borders of the order sorting filters. These borders are situated at 3.7 μm for the PHT-SS array and 8.8 μm for the PHT-SL array.

Caveat: The accuracies for PHT-S point source spectrophotometry are only valid for sources within ± 3 arcsec of the centre of the aperture. Off-pointings can lead to significant flux losses and modifications of the spectral shape. Conspicuous artifacts are flux jumps at the wavelengths of the order sorting filter transitions at 3.7 μm for the SS array and 8.8 μm for the SL array.

It is therefore advisable to cross-check the PHT-S pointing with independent determinations of the source position.

Chapter 11

Getting Started with ISOPHOT Data

11.1 Obtaining ISOPHOT Data

We will illustrate the PHT data retrieval with an example. Suppose one would like to obtain ISOPHOT data from the bright star Altair. Then the following steps should be taken:

- assuming that an internet connection and web browser are available, one should go to the ISO Data Archive (IDA) at:

  `http://www.iso.vilspa.esa.es/` → `Access the Archive`

  and start the IDA applet. The *'Query Specification'* screen will be displayed. To be able to retrieve the data one should be a registered user, and one must login during an IDA session.

- select PHT data products by de-selecting the AOTs of the other instruments. Then type 'Altair' and click on *'Execute Query'*. A *'Latest Results'* screen will appear containing all ISOPHOT observations related to Altair. Each AOT is accompanied by a postcard created from the auto-analysis results. The postcard provides a first look at the data. The postcard can be enlarged by clicking on it. Multi-filter single pointing observations are displayed in the form of spectral energy discributions. Products of mapping (including nodding) observations have the image of only the **first** filter in the AOT displayed in the postcard.

- the data products can be retrieved by moving a selected AOT to the shopping basket. Click on *'Shopping Basket'* to look at what has been selected. In order to download all PHT OLP products of a given AOT including both Derive_SPD and Derive_AAR products, select *'All'* for *'Products Desired'* and click on *'Submit Request'*. An identification number is assigned to the request and the OLP Version 10 data products are transfered to an anonymous `ftp` area at `ftp.iso.vilspa.esa.es`[1]. When the transference of files is finished the system sends an e-mail message to the electronic address of the registered user telling where to get the data from. To leave this screen press *'Dismiss'*.

- if e.g. a PHT03 multi-filter staring observation was selected (in this case TDT 3001001) then the following files will be placed in the anonymous `ftp` area:

```
aocs13001001.fits          pcsh130.fits
apph130.fits               pcsv130.fits
```

[1] Archive products can also be downloaded directly from the *'Latest Results'* screen by clicking on the *'Retrieve'* button after IDA Version 5.2, released in July 2002

```
ccsh130.fits                pisr13001001.fits
eoha130.fits                polr13001001.fits
eohc130.fits                pp2a13001001.fits
eohi130.fits                pp2s13001001.fits
gehk13001001.fits           ppap13001001.fits
gshh130.fits                pper13001001.fits
iiph13001001.fits           psp13001001.fits
irph13001001.fits           psta13001001.fits
lcsh130.fits                scsh130.fits
```

For first look purposes, several files are not relevant. Look in Chapter 12 and the subsequent Chapters in this handbook to determine which products can be expected from PHT OLP and to determine the product contents. According to the Table given in Section 12.2 either PPAP or PPAE are the auto analysis products for this PHT03 observation depending whether the observer of the initial proposal has selected 'point source' (PPAP) or 'extended source' (PPAE).

11.2 First Look at the Products

The ISOPHOT auto-analysis products are *binary FITS tables* in case of single pointing photometry and spectro-photometry or *FITS images* in case of mapping mode. All products consist of an ASCII header in which are stored:

- general information about the observation,
- parameters and (error) messages generated by the OLP processing,
- descriptions of the contents of the tables or images, and
- some selected results, such as source and background fluxes.

Detailed descriptions of the headers as well as the FITS records of the products are given in Chapters 13 and 14. As the headers are in ASCII, the header information of the FITS files can be browsed with a 'TYPE' (in VMS) or 'more' (in unix) command.

For a quick look of the binary FITS table data, utilities are required to convert the binary contents of a FITS file into an ASCII file. For the single pointing photometry data, the tables are usually not very big, so that the ASCII file can immediately be downloaded in a general utility such as a spreadsheet.

Dedicated software to generate an ASCII file of the ISOPHOT auto analysis data is provided by IPAC by means of the 'First Look' (FL) tool *flpht*. For a description see:

`http://www.iso.vilspa.esa.es/` → `ISO Explanatory Library` → `PHT`

It should be noted that the first look tool cannot read the products PPAS, PSAE, PLAE, PSAS, and PLAS. As an illustration we run *flpht* on the AAR product of the observation retrieved from IDA (Section 11.1):

```
flpht -v -o out.txt ppap13001001.fits
```

where out.txt is the output ASCII file with the following contents:

```
"First Look" generated by IPAC "flpht", version 5.0 on  2 Apr 2002
ppap13001001.fits created on 2001-08-18 by version OLP_10   at ESA
--------------------------------------------------------------------------------
```

```
Observer HHABING   , Proposal HJHVEGA3  , Equinox 2000.0
AOT      Target name    RA           DEC          Obs Date  Start UT  End UT
P03      HD 187642      19h50m47.06s +8d52m04.5s  26 Mar 96 14:10:12 14:17:28


Name of the AAR file                          : 'ppap13001001.fits'

Primary FITS headers:
=====================

 AAR file Creation date                       : '2001-08-18'         (DATE    )
 Type of attitude operation (P/R/T)           : Pointed              (ATTTYPE )
 Chopper mode                                 : 'TR      '           (FPCMODE )
 file does conform to FITS standard           :                    T (SIMPLE  )
 number of bits per data pixel                :                    8 (BITPIX  )
 number of data axes                          :                    0 (NAXIS   )
 FITS dataset may contain extensions          :                    T (EXTEND  )
COMMENT   FITS (Flexible Image Transport System) format defined in Astronomy and
COMMENT   Astrophysics Supplement Series v44/p363, v44/p371, v73/p359, v73/p365.
COMMENT   Contact the NASA Science Office of Standards and Technology for the
COMMENT   FITS Definition document #100 and other FITS information.
Data Origin                                   : 'ESA     '           (ORIGIN  )
Telescope                                     : 'ISO     '           (TELESCOP)
 Instrument used                              : 'PHT     '           (INSTRUME)
COMMENT    PHT-P point source photometry
 File name                                    : 'PPAP13001001'       (FILENAME)
File version ID in ISO archive                : '2570    '           (FILEVERS)
 SOC OLP system version                       : 'OLP_10  '           (OLPVERS )
 SOC OLP CAL-G files version                  : 'CALG_70 '           (CALGVERS)
 Product not catalogued                       : 'PIPEPAR '           (USERNAME)
 Target ID as given by proposer               : 'HD 187642'          (OBJECT  )
 Proposer ID in ISO Mission DB                : 'HHABING '           (OBSERVER)
 Equinox                                      :               2000.0 (EQUINOX )
 Telemetry rate in Kbps (Kbits/sec)           :                   32 (TMRATE  )
 Approx. UTC of start of observation          : '96086141012'        (EOHAUTCS)
 Approx. UTC of end of observation            : '96086141728'        (EOHAUTCE)
 AOT name                                     : 'P03     '           (EOHAAOTN)
 Proposal ID                                  : 'HJHVEGA3'           (EOHAPLID)
 Observation sequence number                  : '01      '           (EOHAOSN )
 Pointing sequence number                     : '00      '           (EOHAPSN )
 Proposal category                            : '1       '           (EOHAPCAT)
 Calibration indicator                        : '        '           (EOHACIND)
 Target type                                  : '003     '           (EOHATTYP)
 AOT-to-OCT logic version                     : '03.01   '           (AOTVERS )
 UTC of start time of slew to intended target  : '96086140828'       (ATTUTCSL)
 UTC of time of first arrival at intended targe: '96086140947'       (ATTUTCS )
 On-target flag threshold (arc secs)          :                 10.0 (ATTOTFTH)
 Intended Right Ascension of instrument viewing:            297.69608 (ATTRA   )
 Intended DEClination (with ATTRA)            :              8.86792 (ATTDEC  )
 Guide star reference number                  :               111435 (ATTGUIDE)
 Solar aspect angle (degrees)                 :                 68.1 (ATTSAANG)
 CONTINGEncy flag(0=success; 1=target not acq'd:                    0 (ATTERROR)
 UTC (whole seconds since 01-01-1989)         :            228233412 (TREFUTC1)
 UTC (remaining fraction of second)           :              1413920 (TREFUTC2)
 ISO Uniform Time Key (UTK)                   :            303969888 (TREFUTK )
 ISO INSTRUMENT Time Key (ITK)                :                    0 (TREFITK )
 ITK unit length in seconds                   :    0.00006103515630 (TREFITKU)
Reference instrument J2000 right ascension (deg:            297.69608 (INSTRA  )
Reference instrument J2000 declination (deg)  :             +8.86791 (INSTDEC )
Reference instrument J2000 roll angle (deg)   :                90.90 (INSTROLL)
 RTA maximum severity level                   :                    0 (ISRRSEV )
 QLA maximum severity level                   :                    0 (ISRQSEV )
 RA-warning flag from IS user                 : 'ok      '           (ISRRWARN)
 No. of out-of-soft-limit errors              :                    0 (ISRNOOSL)
 No. of out-of-hard-limit errors              :                    0 (ISRNOOHL)
```

```
 No. of monitor warnings                     :                   1 (ISRNMW  )
 No. of command verification errors          :                   0 (ISRNCVW )
 No. of bad telemetry errors                 :                   0 (ISRNBTW )
 No. of memory verification errors           :                   0 (ISRNMVW )
 No. of severe QLA errors                    :                   0 (ISRNSQLA)
 Corrected instrument RA (deg)               :          297.696136 (CINSTRA )
 Corrected instrument Dec (deg)              :            8.867890 (CINSTDEC)
 Corrected instrument roll angle (deg)       :           90.900002 (CINSTROL)
 On-source RA(deg)                           :          297.696136 (CONSCRA )
 On-source Declination(deg)                  :            8.867890 (CONSCDEC)
 Version ID of each input file               : '2517/EOHA130'       (VERS1   )
 Version ID of each input file               : '2570/PP2S13001001'  (VERS2   )
 Version ID of each input file               : '2420/PPPSF'         (VERS3   )
 Version ID of each input file               : '2322/PCPSF'         (VERS4   )
 Version ID of each input file               : '2022/PFLUXCONV'     (VERS5   )


Extension Table Column Formats:
===============================

 Binary table FITS extension                 : 'BINTABLE'           (XTENSION)
 8 BITS character format                     :                    8 (BITPIX  )
 Tables are 2-d character array              :                    2 (NAXIS   )
 Characters in a row                         :                   80 (NAXIS1  )
 Number of rows in a table                   :                    1 (NAXIS2  )
 Parameter count always 0                    :                    0 (PCOUNT  )
 Group count always 1                        :                    1 (GCOUNT  )
 No of columns in table                      :                   20 (TFIELDS )
                                             : '1J      '           (TFORM1  )
 Filter ID (CHW3 position)                   : 'PPAPFILT'           (TTYPE1  )
                                             : '1J      '           (TFORM2  )
 Aperture ID (CHW2 position)                 : 'PPAPAPER'           (TTYPE2  )
                                             : '1J      '           (TFORM3  )
 Number of background reference positions    : 'PPAPNBCK'           (TTYPE3  )
                                             : '1E      '           (TFORM4  )
 Source flux                                 : 'PPAPSRCE'           (TTYPE4  )
                                             : 'Jy      '           (TUNIT4  )
                                             : '1E      '           (TFORM5  )
 Uncertainty in source flux                  : 'PPAPSRCU'           (TTYPE5  )
                                             : 'Jy      '           (TUNIT5  )
                                             : '1E      '           (TFORM6  )
 Source surface brightness                   : 'PPAPSRCB'           (TTYPE6  )
                                             : 'MJy/sr  '           (TUNIT6  )
                                             : '1E      '           (TFORM7  )
 Uncertainty in source surface brightness    : 'PPAPSCBU'           (TTYPE7  )
                                             : 'MJy/sr  '           (TUNIT7  )
                                             : '1E      '           (TFORM8  )
 Background for given aperture               : 'PPAPBACK'           (TTYPE8  )
                                             : 'Jy      '           (TUNIT8  )
                                             : '1E      '           (TFORM9  )
 Uncertainty in background                   : 'PPAPBCKU'           (TTYPE9  )
                                             : 'Jy      '           (TUNIT9  )
                                             : '1E      '           (TFORM10 )
 Source plus background                      : 'PPAPSPB '           (TTYPE10 )
                                             : 'Jy      '           (TUNIT10 )
                                             : '1E      '           (TFORM11 )
 Uncertainty in source plus background       : 'PPAPSPBU'           (TTYPE11 )
                                             : 'Jy      '           (TUNIT11 )
                                             : '1E      '           (TFORM12 )
 Source plus background (brightness)         : 'PPAPSBB '           (TTYPE12 )
                                             : 'MJy/sr  '           (TUNIT12 )
                                             : '1E      '           (TFORM13 )
 Uncertainty in source plus background (brightn: 'PPAPSBBU'         (TTYPE13 )
                                             : 'MJy/sr  '           (TUNIT13 )
                                             : '1E      '           (TFORM14 )
```

```
 Background at reference position 1           : 'PPAPBCK1'          (TTYPE14 )
                                              : 'Jy      '          (TUNIT14 )
                                              : '1E      '          (TFORM15 )
 Uncertainty in background 1                  : 'PPAPBK1U'          (TTYPE15 )
                                              : 'Jy      '          (TUNIT15 )
                                              : '1E      '          (TFORM16 )
 Background at reference position 2           : 'PPAPBCK2'          (TTYPE16 )
                                              : 'Jy      '          (TUNIT16 )
                                              : '1E      '          (TFORM17 )
 Uncertainty in background 2                  : 'PPAPBK2U'          (TTYPE17 )
                                              : 'Jy      '          (TUNIT17 )
                                              : '1E      '          (TFORM18 )
 Mean background intensity                    : 'PPAPBINT'          (TTYPE18 )
                                              : 'MJy/ster'          (TUNIT18 )
                                              : '1E      '          (TFORM19 )
 Uncertainty in background intensity          : 'PPAPBINU'          (TTYPE19 )
                                              : 'MJy/ster'          (TUNIT19 )
                                              : '1J      '          (TFORM20 )
 Number of accepted chopper cycles            : 'PPAPNCYC'          (TTYPE20 )
COMMENT *******************************************************
COMMENT !!!WARNING!!!
COMMENT The DEFAULT responsivity has been used in the processing.
COMMENT *******************************************************


User specified parameters per filter/aperture configuration:
------------------------------------------------------------


Filter/aperture configuration No.1:
===================================

 Filter                                       : 'P2_25_UM'          (FILTER1 )
 Central Wavelength of filter (m)             :          2.50000E-05 (LAMBDA1 )
 Expected source flux (Jy)                    :          5.80003E+00 (EXFLUX1 )
 Uncertainty in expected flux (Jy)            :          5.80003E+00 (UNCFLX1 )
 Max expected background (MJy/ster)           :          3.69999E+01 (MXBACK1 )
 Aperture                                     : '52" = 2.3mm'       (APER1   )
 Flux density (source) (Jy)                   :          6.70837E+00 (SOURCE1 )
 Uncertainty in flux (source)(Jy)             :          1.96585E+00 (SOURCU1 )
 Flux density (source + background) (Jy)      :          9.67763E+00 (SBACK1  )
 Uncertainty in flux (source + background)(Jy) :          1.86946E+00 (SBACKU1 )


Measurements per filter/aperture configuration:
-----------------------------------------------


Filter/aperture configuration No.1:
===================================

 Filter                                       : 'P2_25_UM'          (FILTER1 )
 Aperture                                     : '52" = 2.3mm'       (APER1   )


 Measured background (MJy/ster)               :          5.59831E+01 (BACK1   )
 Number of background reference positions     =        1             (PPAPNBCK)
 Source flux                                  =   6.7084             (PPAPSRCE)
 Uncertainty in source flux                   =   1.9658             (PPAPSRCU)
 Source surface brightness                    =   2.9693             (PPAPSRCB)
 Uncertainty in source surface brightness     =   0.6080             (PPAPSCBU)
 Background for given aperture                =   9.6776             (PPAPBACK)
 Uncertainty in background                    =   1.8695             (PPAPBCKU)
 Source plus background                       =   2.9693             (PPAPSPB )
 Uncertainty in source plus background        =   0.6080             (PPAPSPBU)
```

```
Source plus background (brightness)          =   0.0000            (PPAPSBB )
Uncertainty in source plus background (brightn=   0.0000            (PPAPSBBU)
Background at reference position 1           =  55.9831            (PPAPBCK1)
Uncertainty in background 1                  =  11.4634            (PPAPBK1U)
```

The meaning of the keywords in the FITS file is provided in Chapter 13. We see that the auto analysis product *ppap*13001001.*fits* contains information of a triangular chopped measurement in the 25 μm filter using the 52″ aperture. The flux of Altair as determined by OLP10 is $F_\nu = 6.7 \pm 2.0$ Jy, not colour corrected. The measurement time is not given, this information is stored in the PSTA product. Note that the measurement time can be found in the IDA, under source *'Details'* in either the *'Latest Results'* or *'Shopping Basket'* screen.

Another utility which can be used for such a purpose is the *ldump* routine in FTOOLS. For more information on FTOOLS see:

`http://heasarc.gsfc.nasa.gov/` → `Software` → `FTOOLS`

Any image processing or displaying system should be able to display the AA FITS image files (PGAI, PGAU, PGAT). A frequently used tool for such purposes is SAOimage, available at:

`http://tdc-www.harvard.edu/` → `SAOimage`

11.3 Further Processing

The ESA Astrophysics Division and the ISOPHOT consortium led by the Max Planck Institut für Astronomie in Heidelberg (MPIA) have developed in a joint effort the ISOPHOT Interactive Analysis (PIA) package. Although this package was initially developed for the processing of the calibration data, the package is available for the general astronomical community. PIA runs under IDL 5.0 and many routines are available for the processing and scientific analysis of ISOPHOT products. For more information we refer to:

`http://www.iso.vilspa.esa.es/`
→ `ISO Data Analysis Software` → `ISOPHOT Interactive Analysis (PIA)`

To perform all OLP processing as described in this handbook starting from ERD, PIA requires the products IRPH, PSTA, and P*ER where the (*) stands for S, P, 1, or 2 depending on the subsytem used, see e.g. next chapter. Contrary to what is provided by IDA, the input filenames for PIA must be in upper case to conform to the descriptions provided in this document.

Chapter 12

Guide to Data Products

This chapter may serve as a starting point for ISOPHOT data product queries.

12.1 Quick Reference: Synopsis of all ISOPHOT Products

In the next subsections the data products generated at the different processing levels are tabulated. For each product, 4 columns are given. The first defines the product. The next names the type of product. The third column indicates for which AOT's the product is generated. The final column refers to the section of this manual which contains a full description of the product.

12.1.1 ERD products

Product	Description	AOTs	Section
PSTA	Compact Status	All	13.2.7
PPER	P ERD	P03, 04, 05, 17/18/19, 50	13.2.2
P1ER	C100 ERD	P22, 25, 32, 37/38/39	13.2.3
P2ER	C200 ERD	P22, 25, 32, 37/38/39, 51	13.2.4
PSER	S ERD	P40	13.2.6
P2ES	Serendipity Mode	–	13.2.5

12.1.2 SPD products

Product	Description	AOTs	Section
PP1S	P1 SPD	P03, 04, 05, 17/18/19	13.3.2
PP2S	P2 SPD	P03, 04, 05, 17/18/19	13.3.2
PP3S	P3 SPD	P03, 04, 05, 17/18/19	13.3.2
PC1S	C100 SPD	P22, 25, 32, 37/38/39	13.3.3
PC2S	C200 SPD	P22, 25, 32, 37/38/39	13.3.4
PSSS	SS SPD	P40	13.3.5
PSLS	SL SPD	P40	13.3.6

Calibration-A files generated

See Section 5.7.2

Product	Description	AOTs	Section
PP1A	P1 Cal-A	P03, 04, 05, 17/18/19	13.3.7
PP2A	P2 Cal-A	P03, 04, 05, 17/18/19	13.3.7
PP3A	P3 Cal-A	P03, 04, 05, 17/18/19	13.3.7
PC1A	C100 Cal-A	P22, 25, 32, 37/38/39	13.3.8
PC2A	C200 Cal-A	P22, 25, 32, 37/38/39	13.3.8

Dark signal files generated by the absolute photometry AOTs and spectrophotometry AOT

see Sections 13.3.11, 13.3.12, and 13.3.13. Note that the cold FCS measurements of PHT05 and PHT25 are processed to Cal-A files.

Product	Description	AOTs	Section
PP1D	P1 Dark	P05	13.3.11
PP2D	P2 Dark	P05	13.3.11
PP3D	P3 Dark	P05	13.3.11
PC1D	C100 Dark	P25	13.3.12
PC2D	C200 Dark	P25	13.3.13
PSSD	PHT-SS Dark	P40	13.3.9
PSLD	PHT-SL Dark	P40	13.3.10

12.1.3 AAR products

Product	Description	AOTs	Section
PPAP	P point source photom.	P03, 04, 05, 17/18/19	13.4.2
PPAE	P extended source photom.	P03, 04, 05, 17/18/19	13.4.3
PPAS	P raster map photom.	P03	13.4.9
PCAP	C point source photom.	P22, 25, 37/38/39	13.4.4
PCAE	C extended source photom.	P22, 25, 37/38/39	13.4.5
PCAS	C raster map photom.	P22, 32	13.4.10
PGAI	surface brightness image	P03, 22, 32	13.4.6
PGAU	uncertainty image	P03, 22, 32	13.4.7
PGAT	exposure time image	P03, 22, 32	13.4.8
PSAP	SS point source spectros.	P40	13.4.11
PSAE	SS ext. source spectros.	P40	13.4.13
PSAS	SS scan spectros.	P40	13.4.15
PLAP	SL point source spectros.	P40	13.4.12
PLAE	SL ext. source spectros.	P40	13.4.14
PLAS	SL raster map spectros.	P40	13.4.16

12.1.4 Cal-G products: Derive_SPD

Product	Description	Section
PTIMEDEP	calibration file time dependency	14.2.1
PDIE1TRANS	DIE1 power calibration table	14.3.1
PDIE2TRANS	DIE2 power calibration table	14.3.2
PSELNDR	NDR (de-)selection	14.4.1
PPCRELIN	P CRE Linearisation	14.5.1
PC1CRELIN	C100 CRE Linearisation	14.5.2
PC2CRELIN	C200 CRE Linearisation	14.5.3
PP1RESETI	P1 reset interval correction	14.6.1
PP2RESETI	P2 reset interval correction	14.6.2
PP3RESETI	P3 reset interval correction	14.6.3
PC1RESETI	C100 reset interval correction	14.6.4
PC2RESETI	C200 reset interval correction	14.6.5
PSDARK	S Dark Current correction	14.7.1
PPDARK	P Dark Current correction	14.7.2
PC1DARK	C100 Dark Current correction	14.7.3
PC2DARK	C200 Dark Current correction	14.7.4
PP1SLINR	signal linearisation for PHT-P1	14.8.1
PP2SLINR	signal linearisation for PHT-P2	14.8.2
PP3SLINR	signal linearisation for PHT-P3	14.8.3
PC1SLINR	signal linearisation for PHT-C100	14.8.4
PC2SLINR	signal linearisation for PHT-C200	14.8.5
PSDYNAMIC	PHT-S dynamic calibration - flux correction	14.9.1
PSDYNWT	PHT-S dynamic calibration - weighting function	14.9.2
PP1CHOPSIG	PHT-P1 chopped signal correction	14.10.1
PP2CHOPSIG	PHT-P2 chopped signal correction	14.10.2
PP3CHOPSIG	PHT-P3 chopped signal correction	14.10.3
PC1CHOPSIG	PHT-C100 chopped signal correction	14.10.4
PC2CHOPSIG	PHT-C200 chopped signal correction	14.10.5
PP1VIGN	P1 vignetting correction	14.11.1
PP2VIGN	P2 vignetting correction	14.11.2
PP3VIGN	P3 vignetting correction	14.11.3
PC1VIGN	C100 vignetting correction	14.11.4
PC2VIGN	C200 vignetting correction	14.11.5
PP1FCSPOW	P1 FCS power calibration table	14.12.1
PP2FCSPOW	P2 FCS power calibration table	14.12.2
PP3FCSPOW	P3 FCS power calibration table	14.12.3
PC1FCSPOW	C100 FCS power calibration table	14.12.4
PC2FCSPOW	C200 FCS power calibration table	14.12.5
PPRESP	P default responsivities	14.13.1
PC1RESP	C100 default responsivities	14.13.2
PC2RESP	C200 default responsivities	14.13.3
PP1FCSAP	P1 FCS aperture correction	14.15.1
PP2FCSAP	P2 FCS aperture correction	14.15.1
PP3FCSAP	P3 FCS aperture correction	14.15.1
PC1ILLUM	C100 illumination correction	14.14.1
PC2ILLUM	C200 illumination correction	14.14.2
PPFTOF	PHT-P filter-to-filter correction	14.16.1
PC1FLAT	C100 filter-to-filter correction	14.17.1
PC2FLAT	C200 filter-to-filter correction	14.17.2

12.1.5 Cal-G products: Derive_AAR

Product	Description	Section
PPPSF	PHT-P point spread function corrections	14.18.1
PCPSF	PHT-C point spread function corrections	14.18.2
PSPECAL	S wavelength calib. and spectral response	14.19.1
PFLUXCONV	P/C power to flux density calib.	14.20.1
PPOMEGA	P apertures and Ω's	14.21.1
PC1OMEGA	C100 dimensions and Ω's	14.21.2
PC2OMEGA	C200 dimensions and Ω's	14.21.3

12.1.6 Cal-G products: auxillary

Product	Description	Section
PCCBB	colour correction: blackbody	14.22.1
PCCMBBONE	colour correction: $\nu^1 \cdot B_\nu(T)$	14.22.2
PCCMBBTWO	colour correction: $\nu^2 \cdot B_\nu(T)$	14.22.3
PCCPOWER	colour correction: ν^α	14.22.4
PP2FOOTP	PHT-P2 footprint matrices	14.23.1
PP3FOOTP	PHT-P3 footprint matrices	14.23.2
PC1FOOTP	PHT-C100 footprint matrices	14.23.3
PC2FOOTP	PHT-C200 footprint matrices	14.23.4
PPFILTRAN	PHT-P relative system response	14.24.1
PCFILTRAN	PHT-C relative system response	14.24.2

12.2 Product Types Sorted by AOT

Per AOT the observer receives a set of data products. Depending on the details of the AOT, different data sets are distributed. In this section all possible combinations of sets of ISOPHOT data products have been listed. Each horizontal line in the tables represents a possible set. The tables contain the following abbreviations:

sp:	single pointing
ps:	point source
es:	extended source
pola:	polarisation
raster:	raster mode

AOT	ERD	SPD	AAR	Comment
P03	PSTA,PPER	PP1S,PP1A	PPAP	P1, sp, ps
	PSTA,PPER	PP1S,PP1A	PPAE	P1, sp, es
	PSTA,PPER	PP1S,PP1A	PPAS,PGAI,PGAU,PGAT	P1, raster
	PSTA,PPER	PP2S,PP2A	PPAP	P2, sp, ps
	PSTA,PPER	PP2S,PP2A	PPAE	P2, sp, es
	PSTA,PPER	PP2S,PP2A	PPAS,PGAI,PGAU,PGAT	P2, raster
	PSTA,PPER	PP3S,PP3A	PPAP	P3, sp, ps
	PSTA,PPER	PP3S,PP3A	PPAE	P3, sp, es
	PSTA,PPER	PP3S,PP3A	PPAS,PGAI,PGAU,PGAT	P3, raster
P04	PSTA,PPER	PP1S,PP1A	PPAP	P1, sp, ps
	PSTA,PPER	PP1S,PP1A	PPAE	P1, sp, es
	PSTA,PPER	PP2S,PP2A	PPAP	P2, sp, ps
	PSTA,PPER	PP2S,PP2A	PPAE	P2, sp, es
	PSTA,PPER	PP3S,PP3A	PPAP	P3, sp, ps
	PSTA,PPER	PP3S,PP3A	PPAE	P3, sp, es
P05	PSTA,PPER	PP1S,PP1A,PP1D	PPAP	P1, sp, ps
	PSTA,PPER	PP1S,PP1A,PP1D	PPAE	P1, sp, es
	PSTA,PPER	PP2S,PP2A,PP2D	PPAP	P2, sp, ps
	PSTA,PPER	PP2S,PP2A,PP2D	PPAE	P2, sp, es
	PSTA,PPER	PP3S,PP3A,PP3D	PPAP	P3, sp, ps
	PSTA,PPER	PP3S,PP3A,PP3D	PPAE	P3, sp, es
P17	PSTA,PPER	PP1S,PP1A	PPAP	P1, sp, ps
	PSTA,PPER	PP1S,PP1A	PPAE	P1, sp, es
	PSTA,PPER	PP2S,PP2A	PPAP	P2, sp, ps
	PSTA,PPER	PP2S,PP2A	PPAE	P2, sp, es
	PSTA,PPER	PP3S,PP3A	PPAP	P3, sp, ps
	PSTA,PPER	PP3S,PP3A	PPAE	P3, sp, es
P18	PSTA,PPER	PP1S	PPAP	P1, sp, ps
	PSTA,PPER	PP1S	PPAE	P1, sp, es
	PSTA,PPER	PP2S	PPAP	P2, sp, ps
	PSTA,PPER	PP2S	PPAE	P2, sp, es
	PSTA,PPER	PP3S	PPAP	P3, sp, ps
	PSTA,PPER	PP3S	PPAE	P3, sp, es
P19	PSTA,PPER	PP1S,PP1A	PPAP	P1, sp, ps
	PSTA,PPER	PP1S,PP1A	PPAE	P1, sp, es
	PSTA,PPER	PP2S,PP2A	PPAP	P2, sp, ps
	PSTA,PPER	PP2S,PP2A	PPAE	P2, sp, es
	PSTA,PPER	PP3S,PP3A	PPAP	P3, sp, ps
	PSTA,PPER	PP3S,PP3A	PPAE	P3, sp, es

AOT	ERD	SPD	AAR	Comment
P22	PSTA,P1ER	PC1S,PC1A	PCAP	C100, sp, ps
	PSTA,P1ER	PC1S,PC1A	PCAE	C100, sp, es
	PSTA,P1ER	PC1S,PC1A	PCAS,PGAI,PGAU,PGAT	C100, raster
	PSTA,P2ER	PC2S,PC2A	PCAP	C200, sp, ps
	PSTA,P2ER	PC2S,PC2A	PCAE	C200, sp, es
	PSTA,P2ER	PC2S,PC2A	PCAS,PGAI,PGAU,PGAT	C200, raster
P25	PSTA,P1ER	PC1S,PC1A,PC1D	PCAP	C100, sp, ps
	PSTA,P1ER	PC1S,PC1A,PC1D	PCAE	C100, sp, es
	PSTA,P2ER	PC2S,PC2A,PC2D	PCAP	C200, sp, ps
	PSTA,P2ER	PC2S,PC2A,PC2D	PCAE	C200, sp, es
P32	PSTA,P1ER	PC1S,PC1A	PCAS,PGAI,PGAU,PGAT	C100
	PSTA,P2ER	PC2S,PC2A	PCAS,PGAI,PGAU,PGAT	C200
P37	PSTA,P1ER	PC1S,PC1A	PCAP	C100, sp, ps
	PSTA,P1ER	PC1S,PC1A	PCAE	C100, sp, es
	PSTA,P2ER	PC2S,PC2A	PCAP	C200, sp, ps
	PSTA,P2ER	PC2S,PC2A	PCAE	C200, sp, es
P38	PSTA,P1ER	PC1S	PCAP	C100, sp, ps
	PSTA,P1ER	PC1S	PCAE	C100, sp, es
	PSTA,P2ER	PC2S	PCAP	C200, sp, ps
	PSTA,P2ER	PC2S	PCAE	C200, sp, es
P39	PSTA,P1ER	PC1S,PC1A	PCAP	C100, sp, ps
	PSTA,P1ER	PC1S,PC1A	PCAE	C100, sp, es
	PSTA,P2ER	PC2S,PC2A	PCAP	C200, sp, ps
	PSTA,P2ER	PC2S,PC2A	PCAE	C200, sp, es
P40	PSTA,PSER	PSSS,PSLS,PSSD,PSLD	PSAP,PLAP	sp
	PSTA,PSER	PSSS,PSLS,PSSD,PSLD	PSAE,PLAE	es
	PSTA,PSER	PSSS,PSLS,PSSD,PSLD	PSAS,PLAS	raster
P50	PSTA,PPER	none	none	P2 pola
P51	PSTA,P2ER	none	none	C200 pola

Chapter 13

Products Description

13.1 Overview

This chapter contains detailed descriptions of all ISOPHOT OLP products except for the Cal-G files (see Chapter 14). The contents and structure of the FITS headers and records are presented. References to additional information given in this manual are provided.

The PHT instrument incorporates several subsystems including single detector photometers, detector arrays and a low-resolution grating spectrometer. Those can be operated with several filters, polarisers and apertures in single pointing and raster pointing mode, the latter with different sampling steps by the chopper. This means that a wide variety of products are produced for the various detectors and operating modes.

All products have header information which can be divided into the following categories.

- General FITS information which is part of the FITS standard. For more about the FITS standard see the 'ISO Handbook Volume I: ISO – Mission & Satellite Overview', [20].
- ISO (spacecraft) related information. This includes descriptions of ISO related fields - see also [20] for complete lists.
- General ISOPHOT header information which is used for several PHT products.
- Product specific header fields.

Table 13.1 gives a summary of ISO common fields in headers. More information is available in the 'ISO Handbook Vol. I: ISO – Mission & Satellite Overview', [20].

For the binary FITS records, the following abbreviations are used in the tables given in this chapter:

Off offset in bytes of field in record
N number of values
T type of field (I=integer, R=real, C=character, L=logical)

13.2 ERD Product Types

13.2.1 Rationale behind product design

As the ERD is reformatted telemetry data, the different ERD products reflect the data structures related to the different PHT sub-systems: single pixel data (P1, P2, and P3), 9 pixel data (PHT-C100), 4

Table 13.1: *List of ISO common fields in the product header.*

Field	Description
OLPVERS	Version of OLP used to generate this file
CALGVERS	Version of the calibration files used to generate this file
EOHA...	Executed Observation History per AOT
ATT...	Attitude information
TREF...	Information on Spacecraft motion
GPSC...	General prefix for main science ERD/SPD
GEPR...	General prefix for ERD files
ISR...	Information on events logged during the execution of the observation from the 'instrument station report' which was generated on-line by the real-time and quick-look analysis (RTA/QLA) software.
VERS..	Versions of files from previous steps used in OLP

pixel data (PHT-C200) and 128 pixel data (PHT-S). Each ERD product is accompanied by one compact status product with product name prefix 'PSTA'. A compact status record defines the instrument configuration for one measurement. The structure of the compact status product is the same for all PHT subinstruments.

13.2.2 Product PPER

PHT-P Edited Raw Data
Record length: 28 bytes

FIELD	**Off**	**N**	**T**	**Description**	**Comment**
GPSCTKEY	0	1	I*4	Instrument time key	see IDPD, unit= 2^{-14} s
GPSCRPID	4	2	I*1	Raster point ID	points and lines
GPSCFILL	6	1	I*2	Filler	empty
PPERPIXF	8	1	I*2	Bit flags accompanying pixels	Appendix B.4
PPERPCS1	10	1	I*2	Power of calibration source 1	Appendix B.2
PPERPCS2	12	1	I*2	Power of calibration source 2	Appendix B.2
PPERFIL1	14	1	I*2	Spare	
PPERTEMP	16	1	I*2	Measured temperature P1, P2, or P3	Appendix B.1
PPERFIL2	18	2	I*2	Spare	
PPERCPOS	22	1	I*2	Measured chopper position	Appendix B.3
PPERMBV	24	1	I*2	Measured bias voltage P1, P2, or P3	
PPERPIX	26	1	I*2	IR data (1 pixel)	12 bits used, see Appendix B.2

13.2.3 Product P1ER

PHT C100 Edited Raw Data
Record length: 48 bytes

FIELD	**Off**	**N**	**T**	**Description**	**Comment**
GPSCTKEY	0	1	I*4	Instrument time key	see IDPD, unit= 2^{-14} s
GPSCRPID	4	2	I*1	Raster point ID	points and lines
GPSCFILL	6	1	I*2	Filler	
P1ERPIXF	8	1	I*2	Bit flags accompanying pixels	Appendix B.4
P1ERPCS1	10	1	I*2	Power of calibration source 1	Appendix B.2
P1ERPCS2	12	1	I*2	Power of calibration source 2	Appendix B.2
P1ERCREV	14	1	I*2	Measured CRE checkout voltage	see note below
P1ERTEMP	16	1	I*2	Measured temperature C100	Appendix B.1

P1ERFILL	18	2	I*2	Spare	
P1ERCPOS	22	1	I*2	Measured chopper position	Appendix B.3
P1ERMBV	24	1	I*2	Measured bias voltage C100	
P1ERPIXR	26	1	I*2	IR data (resistor)	see note below
P1ERPIXO	28	1	I*2	IR data (open)	
P1ERPIX	30	9	I*2	IR data: 9 pixels	for pixel ordering see Section 2.6.2 12 bits used, see Appendix B.2

Note: The CRE checkout voltage is of no importance for the analysis of the IR data. It was a diagnostic DC voltage which was applied to the CRE resistor pixel for PHT-C and PHT-S and produced a kind of load curve at the output of the resistor pixel. This worked like a connection to a normal CRE channel of a detector pixel. However, the resistance of this special channel was much smaller than that of a high-ohmic detector pixel.

13.2.4 Product P2ER

PHT C200 Edited Raw Data
Record length: 44 bytes

FIELD	Off	N	T	Description	Comment
GPSCTKEY	0	1	I*4	Instrument time key	see IDPD, unit= 2^{-14} s
GPSCRPID	4	2	I*1	Raster point ID	points and lines
GPSCFILL	6	1	I*2	Filler	
P2ERPIXF	8	1	I*2	Bit flags accompanying pixels	Appendix B.4
P2ERPCS1	10	1	I*2	Power of FCS 1	Appendix B.2
P2ERPCS2	12	1	I*2	Power of FCS 2	Appendix B.2
P2ERCREV	14	1	I*2	Measured CRE checkout voltage	see Note 13.2.3
P2ERTEMP	16	1	I*2	Measured temperature C200	Appendix B.1
P2ERFILL	18	2	I*2	Spare	
P2ERCPOS	22	1	I*2	Measured chopper position	Appendix B.3
P2ERMBV1	24	1	I*2	Measured bias voltage pixel 1	see Section 2.6.2–
P2ERMBV2	26	1	I*2	Measured bias voltage pixel 2	–for pixel position on sky
P2ERMBV3	28	1	I*2	Measured bias voltage pixel 3	
P2ERMBV4	30	1	I*2	Measured bias voltage pixel 4	
P2ERPIX1	32	1	I*2	IR data (pixel 1)	see Section 2.6.2 –
P2ERPIX2	34	1	I*2	IR data (pixel 2)	–for pixel position on sky
P2ERPIX3	36	1	I*2	IR data (not used)	
P2ERPIX4	38	1	I*2	IR data (pixel 3)	
P2ERPIX5	40	1	I*2	IR data (pixel 4)	see Appendix B.2 for bit usage
P2ERPIX6	42	1	I*2	IR data (resistor)	

13.2.5 Product P2ES

PHT C200 Edited Raw Data for PHT serendipity mode
Record length: 44 bytes
Identical record structure as for product P2ER (Section 13.2.4), the prefix P2ER should be replaced by P2ES.

13.2.6 Product PSER

PHT-S Edited Raw Data
Record length: 292 bytes

FIELD	Off	N	T	Description	Comment
GPSCTKEY	0	1	I*4	Instrument time key	see IDPD, unit= 2^{-14} s
GPSCRPID	4	2	I*1	Raster point ID	points and lines
GPSCFILL	6	1	I*2	Filler	

PSERPIXF	8	1	I*2	Bit flags accompanying pixels	Appendix B.4
PSERPCS1	10	1	I*2	Power of calibration source 1	no meaning, FCS always off in AOT
PSERPCS2	12	1	I*2	Power of calibration source 2	no meaning, FCS always off in AOT
PSERCREV	14	1	I*2	Measured CRE checkout voltage	see note Section 13.2.3
PSERTEM1	16	1	I*2	Measured temperature S1(SL)	Appendix B.1
PSERTEM2	18	1	I*2	Measured temperature S2(SS)	Appendix B.1
PSERFILL	20	1	I*2	Spare	
PSERCPOS	22	1	I*2	Measured chopper position	Appendix B.3
PSERMBV1	24	1	I*2	Measured bias voltage S1(=SL)	
PSERMBV2	26	1	I*2	Measured bias voltage S2(=SS)	
PSERPIX1	28	66	I*2	IR data for SL branch	includes 2 resistor pixels: no. 65 and 66 12 bits used, see Appendix B.2
PSERPIX2	160	66	I*2	IR data for SS branch	includes 2 resistor pixels: no. 65 and 66 12 bits used, see Appendix B.2

13.2.7 Product PSTA

PHT-ERD Compact Status
Record length 128 bytes

FIELD	**Off**	**N**	**T**	**Description**	**Comment**
CSGPUKST	0	1	I*4	UTK start time	Universal Time Keys–
CSGPUKEN	4	1	I*4	UTK end time	– see [20]
CSGPIKST	8	1	I*4	ITK start time	
CSGPIKEN	12	1	I*4	ITK end time	
CSGPUTST	16	2	I*4	UTC start time	Universal Time–
CSGPUTEN	24	2	I*4	UTC end time	– Coordinated
CSGPOSN	32	1	I*1	Observation Sequence Number	also ION, as in PGA
CSGPFILL	33	15	I*1	Spare	
PSTAERR	48	1	I*4	Housekeeping ExHK discrepancy err. code	flags discrepancies in the housekeeping
PSTASUBS	52	1	I*2	Subsystem	
PSTAOPFO	54	1	I*2	Chopper OPF Override	
PSTAF1TS	56	1	I*2	TRS(FCS1)	value: 1 or 2 see Section 2.7
PSTAF2TS	58	1	I*2	TRS(FCS2)	value: 1 or 2
PSTAF1PS	60	1	I*2	FCS1 power sel.	in mW
PSTAF2PS	62	1	I*2	FCS2 power sel.	in mW
PSTAC1PS	64	1	I*2	CHW1 position (selected)	value: 1 - 14, see Appendix A.1
PSTAC2PS	66	1	I*2	CHW2 position (selected)	idem
PSTAC3PS	68	1	I*2	CHW3 position (selected)	idem
PSTACMOD	70	1	I*2	Chopper mode	see Table 13.2
PSTACAMP	72	1	I*2	Chopper amplitude	as commanded in arcsec
PSTACSTE	74	1	I*2	Chopper step	as commanded
PSTACINC	76	1	I*2	Chopper increment	as commanded in arcsec
PSTACRES	78	1	I*2	CRE switch	
PSTADETA	80	1	I*2	Detector assy	detector assembly
PSTADRS	82	1	I*2	Data reduction size	integer, see Section 2.4.4
PSTAMUX1	84	1	I*2	MUX1 line	multiplexer line
PSTAMUX2	86	1	I*2	MUX2 line	multiplexer line
PSTAXSTA	88	1	I*2	Cross status	of multiplexer line
PSTAD1OF	90	1	I*2	DIE1 offset	see Section 7.2.6
PSTAD1GA	92	1	I*2	DIE1 gain	idem
PSTAD2OF	94	1	I*2	DIE2 offset	idem
PSTAD2GA	96	1	I*2	DIE2 gain	idem
PSTAFREQ	98	1	I*2	clock speed of CRE	value 1, 4, or 8 (kHz)
PSTANNDR	100	1	I*2	No. NDRs per ramp	$2^n - 1$ †
PSTANDR	102	1	I*2	No. DRs per chopper plateau	2^n †
PSTAINTT	104	1	I*2	Integration time	2^{7-n} sec †
PSTAMEAT	106	1	I*2	Measurement time	2^n sec †
PSTAMPC1	108	1	I*2	Measurement position CHW1	value: 1 - 14, see Appendic A.1
PSTAMPC2	110	1	I*2	Measurement position CHW2	idem
PSTAMPC3	112	1	I*2	Measurement position CHW3	idem
PSTAMET	114	1	I*2	Measured EEU temperature	see Appendix B.1
PSTASER	116	1	I*2	PHT serendipity mode flag	1 = serendipity; 0 = prime instrument

PSTAFILL 118 10 I*1 Filler

Table 13.2: *Coding of chopper mode.*

Mode	Description
0,1	sawtooth chopping
2, 3	triangular chopping
4, 5, 6, 7	rectangular chopping
8	chopping between FCS1 and FCS2
13	staring CFOV
14	staring FCS1
9, 10, 11, 12, 15	not used in AOTs

† The value given in the product is n. The formula in the last column above gives the actual value.

13.3 SPD Product Types

13.3.1 Rationale behind product design

PHT generates per detector an SPD record for each signal per chopper plateau or for each raster point. There are 7 separate SPD products:

1. - C100 SPD data
2. - C200 SPD data
3. - P1 SPD data
4. - P2 SPD data
5. - P3 SPD data
6. - PHT-SS SPD data
7. - PHT-SL SPD data

In order to retain the information on the actual observing conditions, each SPD record contains additional information to identify the operating conditions under which the data were collected. Within an SPD file, the type of record is determined by:

- spacecraft viewing direction (e.g. in case of raster maps)
- chopper viewing direction (CFOV, offset position, or FCS)
- aperture
- filter

Within one AOT, data of different types can be archived inside the same SPD file. Examples:

- For chopped measurements, one mean on-source and one mean background plateau are stored as separate records in the same SPD file
- Data from each raster position within a raster map are stored in separate records in chronological order in the same SPD file.
- Multi-filter AOT's produce one SPD file per detector. Data from different filters for a given detector are stored as a series of records ordered chronologically inside the same SPD file.
- In case of multi-aperture photometry with PHT04, one SPD file is created. The aperture measurements are stored as series of records ordered chronologically inside the same SPD file.
- In case of oversampled maps with PHT32, each map position can yield several SPD records corresponding to the number of chopper plateaux collected on that position.

13.3.1.1 General SPD header items I

The following header keywords are included in all PHT SPD products.

FIELD	T	Description	Comment
DETECTOR	C	Detector subsystem	
NPIXEL	I	Number of detector pixels	
NMEAS	I	Number of measurements	
CALSEQU	I	Calibration sequence	
PTOREXT	C	Point(P) or Extended(E)	
FPCMODE	C	Focal plane chopper mode	see Table 13.2
FPCAMP	I	Chopper amplitude	in arcsec
FPCNSTEP	I	Number of chopper steps	only if chop mode
FPCINCR	I	Increment between steps (arcsec)	only if chop mode
DARKPi	R	dark signal	in [V/s] for pixel i, both keywords –
DARKUPi	R	dark signal uncertainty	–repeated for each pixel

Notes:

- the dark signals (DARK..) are given in units of V/s.
- FPC modes: 'ST' = staring, 'RE' = rectangular, 'SW' = sawtooth, 'TR' = triangular,'CB' = chop between FCS1 and FCS2.

13.3.1.2 Filter dependent SPD header items

The following header keywords are repeatedly given for each filter of measurement m:

FIELD	T	Description	Comment
FILTERm	C	Filter	filter name of measurement m
EXFLUXm	R	Expected source flux (Jy or MJy/sr)	Jy if PTOREXT=P
UNCFLXm	R	Uncertainty (Jy or MJy/sr)	Jy if PTOREXT=P
MXBACKm	R	Maximum background (^{10}log MJy/sr)	
A0RIm	R	Reset interval corr. offset, A0	in V/s, see Section 4.3.3
A0RIUm	R	Uncertainty in A0	in V/s
A1RIm	R	Reset interval corr. slope, A1	
A1RIUm	R	Uncertainty in A1	
PFmPiLl	R	Mean of signal for logical ramp	for pixel i in V/s, chopped mode only $l = 1 \ldots 8$, see Section 7.5
PDmPiLl	R	Difference between patterns for logical ramp	for pixel i in V/s, chopped mode only
PUmPiLl	R	Uncertainty in mean signal for logical ramp	for pixel i in V/s, chopped mode only
CALPiFm	C	Cal. used to determine responsivity	'Average' for maps
CALFILT	I	Filter for calibration measurement	
CALAPm	I	Aperture used for cal (CHW position)	
TRS1Sm	I	Selected TRS for FCS1	1 or 2
POW1Sm	R	Selected power for FCS1	in mW
POW1Mm	R	Measured power for FCS1	in mW
CALPOW1	R	In-band power on detector for cal	in W
RESPDEF	L	TRUE if default responsivity is used	
CALPOLm	I	Polariser used for cal (CHW position)	see Section A.1
CALTYPm	I	Type of processing for cal. measurement	number of cal. measurements
RESPRi	R	ratio actual/default responsivity	for pixel i
RS1PiFm	R	Responsivity (A/W) for first cal.	for pixel i
RU1PiFm	R	Uncertainty in responsivity	in A/W, for pixel i
RQ1PiFm	R	Quality flag for cal. measurement	see Table 13.3.14
RS2PiFm	R	Responsivity for second cal.	in A/W, for pixel i
RU2PiFm	R	Uncertainty in responsivity	in A/W, for pixel i
RQ2PiFm	R	Quality flag for cal. measurement	see Table 13.3.14
RSPiFm	R	Responsivity for measurement	in A/W, for pixel i
RUPiFm	R	Uncertainty in responsivity	in A/W, for pixel i
FCSDRIFT	R	TRUE if residual drift in FCS measurement	only if RQ1PiFm=4, for any i and given m
DRS1Pi	R	Default responsivity	in A/W for pixel i
DRU1Pi	R	Uncertainty in default responsivity	in A/W for pixel i

Notes:

- CALP1F can have the following values: *single, first, second, both,* and *default*, depending on the calibration method in the AOT and the quality of the FCS measurements.
- EXFLUX, UNCFLX, and MXBACK were the initial estimates from the observer entered in PGA.
- for AOT PHT32 there is no one-to-one match between the keyword description and the AOT parameter as given by the observer in the ISO proposal generation aids (PGA): EXFLUX= maximum unsaturated surface brightness, UNCFLX= minimum surface brightness flux.
- the keywords DRS1Pi and DRU1Pi only appear if the default responsivity was applied, these keywords are accompanied with the warning message: *'The default processing has been used in the processing'*.

13.3.1.3 General PHT related SPD header items II

The following header keywords are appended after all filters have been listed:

FIELD	T	Description	Comment
SATLIMi	R	Saturation limit	in Volts for pixel i
FITDRi	L	Drift fit flag	always T (no fitting implemented)
MINDEG	I	Min points for deglitcher	see Section 7.3.4–
MAXERR	R	Max error if points < MINDEG	–for signal deglitching
NITERATE	I	No. of iterations of deglitcher	
NLOCAL	I	No. of local points used by deglitcher	
NSTEP	I	Deglitcher step size	
NSIGMA	R	Deglitcher: rms from local median	
NBAD	I	Deglitcher: badness count limit	
CALFCS	I	FCS used for cal calculations	FCS 1 or 2
RDITER	I	Ramp deglitch: no. iterations	see Section 7.2.9–
RDFSIG	R	Ramp deglitch: sigma for detection	–for ramp deglitching
RDMINP	I	Ramp deglitch: min. readouts in ramp	
DRALPHA	R	Drift removal: significance level	see Section 7.3.5 –
DRMINPTS	I	Drift removal: min. points	–for drift recognition
READAUTO	I	Readouts with automatic data reduction	
READSUSP	I	Readouts flagged as suspicious	
READOFFT	I	Readouts off-target	
READCOP	I	Readouts with chopper off position	
RAMPSAT	I	Ramps saturated	
RAMPDEGL	I	Ramps deglitched	
RAMPPCT	I	% ramps accepted	
RAMPUSET	I	% time for accepted ramps	
RAMPINVD	I	Bad cycles	
RAMPZSG	I	Zero signals on plateau	plateaux with no accepted signals
PLATNORP	I	Plateaux with no good ramps	
PLATDROP	I	Plateaux dropouts due to gaps	
USEDRS	L	Use destructive readouts?	always 'F' for OLP
DISCNDRS	I	Discard 1st NDRs of ramps	number of readouts per ramp removed see Section 7.2.2

13.3.1.4 Product specific SPD header items: PHT05 and PHT25

The following keywords are only present in SPD products from absolute photometry observations with PHT05:

FIELD	T	Description	Comment
MEASPW1	R	FCS1 heating power	in mW
POWFCS1	R	Power from FCS1	in W
RESPR	R	ratio Actual/Default responsivity	

CAL	R	Responsivity used	in A/W
CALUNC	R	uncertainty	in V/s
CALQUAL	R	FCS quality	
RESPP1	R	FCS responsivity	in A/W
RUNCP1	R	FCS responsivity uncertainty	in A/W
DRESP1	R	Default responsivity	in A/W
DRUNP1	R	Default responsivity uncertainty	in A/W
COLD	R	Cold FCS measurement	in V/s
COLDUNC	R	Cold FCS uncertainty	in V/s

In case of PHT25:

FIELD	**T**	**Description**	**Comment**
MEASPW1	R	FCS1 heating power	in mW
POWFCS1	R	Power from FCS1	in W
RESPPi	R	FCS responsivity	in A/W, for pixel i
RUNCPi	R	FCS responsivity uncertainty	in A/W, for pixel i
DRESPi	R	Default responsivity	in A/W, for pixel i
DRUNPi	R	Default responsivity uncertainty	in A/W, for pixel i
RESPRi	R	ratio Actual/Default responsivity	for pixel i
CALPi	R	Responsivity used	in A/W
CALUPi	R	uncertainty	in A/W, for pixel i
CALQPi	R	FCS quality	for pixel i
COLDPi	R	Cold FCS measurement signal in V/s	in V/s, for pixel i
COLDUPi	R	Uncertainty	in V/s, for pixel i

13.3.1.5 Product specific SPD header items: PHT04

The following keywords are only present in SPD product of aperture photometry observations PHT04. The keywords ending with m are repeated for each measurement (aperture) in the observation. Note: BSRSS stands for 'background subtracted relative source signal'.

FIELD	**T**	**Description**	**Comment**
BACKSRSS	L	TRUE if BSRSS processing performed	
FILTCORF	L	TRUE if aperture correction available	for given filter
APERm	C	Aperture m	m=1...N, N is the no. measurements)
APERCWm	I	Change wheel position for aperture m	
SRCSIGm	R	Source signal for aperture m	in V/s
SCSIGUm	R	Uncertainty in source signal	in V/s
BCKSIGm	R	Background signal for aperture m	in V/s
BKSIGUm	R	Uncertainty in background signal	in V/s
NORMCALC	L	TRUE if signal ratio calculated	
NRMSIGm	R	Ratio src(m)/src(180) for aperture m	
NMSIGUm	R	Uncertainty in ratio	

13.3.2 Product PPxS

PHT-P1/2/3 Standard Processed Data where x = 1,2, or 3; m is the aperture number in the measurement sequence.

HEADER
Product specific header entries:

FIELD	**T**	**Description**	**Comment**
CALAPm	I	Aperture used for FCS calibration	CHW2 position
CAL	R	Responsivity used	in A/W
CALUNC	R	uncertainty	in V/s
CALQUAL	R	FCS quality	
RESPP1	R	FCS responsivity	in A/W

RUNCP1	R	FCS responsivity uncertainty	in A/W
DRESP1	R	Default responsivity	in A/W
DRUNP1	R	Default responsivity uncertainty	in A/W
COLD	R	Cold FCS measurement signal	in V/s
COLDUNC	R	Uncertainty	in V/s

RECORD
record length: 68 bytes

FIELD	N	T	Description	Comment
GPSCTKEY	1	I*4	Instrument time key	
GPSCRPID	2	I*1	Raster point ID	points and lines
GPSCFILL	1	I*2	Filler	
PPxSKYID	1	I*2	Keyword identifier	
PPxSMNUM	1	I*2	Measurement number	
PPxSSPAR	1	I*2	Spare	
PPxSFILT	1	I*2	Filter ID (CHW3 position)	value: 1 - 14, see Appendix A.1
PPxSAPER	1	I*2	Aperture ID (CHW2 position)	idem
PPxSPOLZ	1	I*2	Polariser ID (CHW1 position)	idem
PPxSNDRS	1	I*2	Number of destructive readouts	per chopper plateau
PPxSCSTP	1	I*2	Chopper step number	see Section 7.2.5
PPxSDWEL	1	I*4	Chopper dwell time	in 2^{-7} s, commanded time
PPxSMEAS	1	I*4	Measurement time	in s
PPxSCPOS	1	I*4	Chopper position	in arcsec
PPxSMNPW	1	R*4	Mean or fitted power	in W
PPxSMNPU	1	R*4	Uncertainty	in W
PPxSMDPW	1	R*4	Median power	in W
PPxSQ1PW	1	R*4	1st quartile of power	in W
PPxSQ3PW	1	R*4	3rd quartile of power	in W
PPxSPLEN	1	I*4	Chopper plateau length	in 2^{-7} s effective time after discarding signals
PPxSNSIG	1	I*4	No. of valid signals on plateau	
PPxSFLAG	1	I*1	Status flag	see Section 13.3.14
PPxSFILL	3	I*1	Filler	

13.3.3 Product PC1S

PHT-C100 Standard Processed Data

HEADER
Product specific header entries:

FIELD	T	Description	Comment
CALPi	R	Responsivity used	in A/W
CALUPi	R	uncertainty	in A/W, for pixel i
CALQPi	R	FCS quality	for pixel i
COLDPi	R	Cold FCS measurement signal in V/s	in V/s, for pixel i
COLDUPi	R	Uncertainty	in V/s, for pixel i
STATPIX	I	Pixel used in statistics	

RECORD
Record length: 300 bytes

FIELD	N	T	Description	Comment
GPSCTKEY	1	I*4	Instrument time key	
GPSCRPID	2	I*1	Raster point ID	points and lines
GPSCFILL	1	I*2	Filler	
PC1SKYID	1	I*2	Keyword identifier	
PC1SMNUM	1	I*2	Measurement number	
PC1SSPAR	1	I*2	Spare	
PC1SFILT	1	I*2	Filter ID (CHW3 position)	value: 1 - 14, see Appendix A.1

PC1SAPER	1	I*2	Aperture ID (CHW2 position)	idem
PC1SPOLZ	1	I*2	Polariser ID (CHW1 position)	idem
PC1SNDRS	1	I*2	Number of destructive readouts	
PC1SCSTP	1	I*2	Chopper step number	see Section 7.2.5
PC1SDWEL	1	I*4	Chopper dwell time	in 2^{-7} s, commanded time
PC1SMEAS	1	I*4	Measurement time	in s
PC1SCPOS	1	I*4	Chopper position	in arcsec
PC1SMNPW	9	R*4	Mean or fitted power	in W
PC1SMNPU	9	R*4	Uncertainty	in W
PC1SMDPW	9	R*4	Median power	in W
PC1SQ1PW	9	R*4	1st quartile of power	in W
PC1SQ3PW	9	R*4	3rd quartile of power	in W
PC1SPLEN	9	I*4	Chopper plateau length	in 2^{-7} s effective time after discarding signals
PC1SNSIG	9	I*4	No. of valid signals on the plateau	
PC1SFLAG	9	I*1	Status flag	see Section 13.3.14
PC1SFILL	3	I*1	Filler	

13.3.4 Product PC2S

PHT-C200 Standard Processed Data

HEADER
Product specific header entries:

FIELD	**T**	**Description**	**Comment**
CALPi	R	Responsivity used	in A/W
CALUPi	R	uncertainty	in A/W, for pixel i
CALQPi	R	FCS quality	for pixel i
COLDPi	R	Cold FCS measurement signal in V/s	in V/s, for pixel i
COLDUPi	R	Uncertainty	in V/s, for pixel i
STATPIX	I	Pixel used in statistics	

RECORD
Record length: 152 bytes

FIELD	**N**	**T**	**Description**	**Comment**
GPSCTKEY	1	I*4	Instrument time key	
GPSCRPID	2	I*1	Raster point ID	points and lines
GPSCFILL	1	I*2	Filler	
PC2SKYID	1	I*2	Keyword identifier	
PC2SMNUM	1	I*2	Measurement number	
PC2SSPAR	1	I*2	Spare	
PC2SFILT	1	I*2	Filter ID (CHW3 position)	value: 1 - 14, see Appendix A.1
PC2SAPER	1	I*2	Aperture ID (CHW2 position)	idem
PC2SPOLZ	1	I*2	Polariser ID (CHW1 position)	idem
PC2SNDRS	1	I*2	Number of destructive readouts	
PC2SCSTP	1	I*2	Chopper step number	
PC2SDWEL	1	I*4	Chopper dwell time	in 2^{-7} s
PC2SMEAS	1	I*4	Measurement time	in s
PC2SCPOS	1	I*4	Chopper position	in arcsec
PC2SMNPW	4	R*4	Mean or fitted power	in W
PC2SMNPU	4	R*4	Uncertainty	in W
PC2SMDPW	4	R*4	Median power	in W
PC2SQ1PW	4	R*4	1st quartile of power	in W
PC2SQ3PW	4	R*4	3rd quartile of power	in W
PC2SPLEN	4	I*4	Chopper plateau length	in 2^{-7} s effective time after discarding signals
PC2SNSIG	4	I*4	No. of valid signals on the plateau	
PC2SFLAG	4	I*1	Status flags	see Section 13.3.14

13.3.5 Product PSSS

PHT-SS Standard Processed Data

HEADER
Product specific header entries:

FIELD	T	Description	Comment
CALDATE	C	Date cal defaults generated	
PTOREXT	C	Point(P) or Extended(E)	
LAMBDAd	C	Central wavelength of pixel	in m
LUNCd	C	Uncertainty	in m
STATPIX	C	Pixel used in statistics	

note:
d = 1,...,64

RECORD
Record length: 1560

FIELD	N	T	Description	Comment
GPSCTKEY	1	I*4	Instrument time key	
GPSCRPID	2	I*1	Raster point ID	points and lines
GPSCFILL	1	I*2	Filler	
PSSSPOLZ	1	I*2	Polariser ID (CHW1 position)	value: 1 - 14, see Appendix A.1
PSSSNDRS	1	I*2	Number of destructive readouts	
PSSSDWEL	1	I*4	Chopper dwell time	in 2^{-7} s, commanded time
PSSSMEAS	1	I*4	Measurement time	in s
PSSSCPOS	1	I*4	Chopper position	in arcsec
PSSSSPB	64	R*4	source+background flux density	in Jy
PSSSSPBU	64	R*4	uncertainty	in Jy
PSSSBCK	64	R*4	background flux density	in Jy
PSSSBCKU	64	R*4	uncertainty	in Jy
PSSSSRCE	64	R*4	source flux density	in Jy
PSSSSRCU	64	R*4	uncertainty	in Jy

13.3.6 Product PSLS

PHT-SL Standard Processed Data

HEADER
Product specific header entries are the same as for product PSSS.

RECORD
Record of PSLS is identical to that of PSSS.

13.3.7 Product PPxA

PPxA (where x=1,2,3) contains the SPD of the FCS measurements obtained with detector P1, P2 or P3. PPxA products are also referred to as Cal-A files (see Section 5.7.2). The product of a chopped measurement contains 1 record per chopper plateau. In case a cold FCS measurement is selected in the absolute photometry AOT PHT05, the first record contains the cold FCS measurement and the second record contains the results of the heated FCS measurement.

RECORD
Record length: 84

FIELD	N	T	Description	Comment
GPSCTKEY	1	I*4	Instrument time key	
GPSCRPID	2	I*1	Raster point ID	points and lines
GPSCFILL	1	I*2	Filler	
PPxAQFLG	1	I*2	Quality flag	
PPxAKYID	1	I*2	Keyword identifier	
PPxAMNUM	1	I*2	Measurement number	
PPxASPAR	1	I*2	Spare	
PPxAFILT	1	I*2	Filter ID (CHW3 position)	value: 1 - 14, see Appendix A.1
PPxAAPER	1	I*2	Aperture ID (CHW2 position)	idem
PPxAPOLZ	1	I*2	Polariser ID (CHW1 position)	idem
PPxASTAT	1	I*2	FPC state	0 = CFOV, 1 = FCS1, 2 = FCS2
PPxADWEL	1	I*4	Commmanded chopper dwell time	in 2^{-7} s
PPxACPOS	1	R*4	Chopper position	in arcsec
PPxAFCS1	1	R*4	Measured FCS1 power	in mW
PPxAFCS2	1	R*4	Measured FCS2 power	in mW
PPxATEMP	1	R*4	Detector temperature	in K
PPxAFILR	1	R*4	Filler	
PPxABIAS	1	R*4	Measured bias voltage	in V
PPxAMNSG	1	R*4	Mean or fitted signal	in V/s
PPxAMNSU	1	R*4	Uncertainty	in V/s
PPxAMDSG	1	R*4	Median signal	in V/s
PPxAQ1SG	1	R*4	1st quartile of signal	in V/s
PPxAQ3SG	1	R*4	3rd quartile of signal	in V/s
PPxAPLEN	1	I*4	Chopper plateau length	in 2^{-7} s effective time after discarding signals
PPxANSIG	1	I*4	No. of valid signals on the plateau	
PPxAFLAG	1	I*1	Status flag	
PPxAFILI	3	I*1	Filler	

Note: FPC state (PPxASTAT) cannot be zero for these measurements.

13.3.8 Product PCxA

PCxA (where x=1 or 2) is a Cal-A product which contains the SPD of the FCS measurements obtained with the C100 or C200 detector arrays. In case a cold FCS measurement is selected in the absolute photometry AOT PHT25, the first record contains the cold FCS measurement and the second record contains the results of the heated FCS measurement.

HEADER
Product specific header entries:

STATPIX	I	Pixel used in statistics

RECORD
Record length: 316 for x=1, 180 for x=2

FIELD	N	T	Description	Comment
GPSCTKEY	1	I*4	Instrument time key	
GPSCRPID	2	I*1	Raster point ID	points and lines
GPSCFILL	1	I*2	Filler	
PCxAQFLG	1	I*2	Quality flag	
PCxAKYID	1	I*2	Keyword identifier	
PCxAMNUM	1	I*2	Measurement number	
PCxASPAR	1	I*2	Spare	
PCxAFILT	1	I*2	Filter ID (CHW3 position)	value: 1 - 14, see Appendix A.1
PCxAAPER	1	I*2	Aperture ID (CHW2 position)	idem
PCxAPOLZ	1	I*2	Polariser ID (CHW1 position)	idem
PCxASTAT	1	I*2	FPC state	0 = CFOV, 1 = FCS1, 2 = FCS2
PCxADWEL	1	I*4	Chopper dwell time	in 2^{-7} s, commanded time

PCxACPOS	1	R*4	Chopper position	in arcsec
PCxAFCS1	1	R*4	Measured FCS1 power	mW
PCxAFCS2	1	R*4	Measured FCS2 power	mW
PCxATEMP	1	R*4	Detector temperature	K
PCxAFILL	1	R*4	Filler	
PCxABIAS	1	R*4	Measured bias voltage	in V
PCxAMNSG	j	R*4	Mean or fitted signal	in V/s
PCxAMNSU	j	R*4	Uncertainty	in V/s
PCxAMDSG	j	R*4	Median signal	in V/s
PCxAQ1SG	j	R*4	1st quartile of signal	in V/s
PCxAQ3SG	j	R*4	3rd quartile of signal	in V/s
PCxAPLEN	1	I*4	Chopper plateau length	in 2^{-7} s effective time after discarding signals
PCxANSIG	1	I*4	No. of valid signals on the plateau	
PCxAFLAG	j	I*1	Status flags	
PCxAFILL	k	I*1	Filler	

For product PC1A the parameters j and k are 9 and 3, respectively; for product PC2A both j is 4 and k is zero.

Note: FPC state (PCxASTAT) cannot be zero for these measurements.

13.3.9 Product PSSD

PPSD contains the SPD of the PHT-SS dark measurement. This measurement is only obtained with AOT PHT40.

RECORD
Record length: 840

FIELD	**N**	**T**	**Description**	**Comment**
GPSCTKEY	1	I*4	Instrument time key	
GPSCRPID	2	I*1	Raster point ID	points and lines
GPSCFILL	1	I*2	Filler	
PSSDDARK	64	R*4	Dark signal	in V/s
PSSDDUNC	64	R*4	Uncertainty	in V/s
PSSDNSIG	64	R*4	No. of valid signals on the plateau	
PSSDFLAG	64	I*1	Status Flag	

13.3.10 Product PSLD

PPSD contains the SPD of the PHT-SL dark measurement. This measurement is only obtained with AOT PHT40.

The record is identical to that of PHT-SS, see Section 13.3.9.

13.3.11 Product PPxD

PPxD (where x=1,2,3) contains the SPD of the dark measurements obtained with detector P1, P2 or P3. These measurements are only obtained with AOT PHT05.

RECORD
Record length: 24

FIELD	**N**	**T**	**Description**	**Comment**
GPSCTKEY	1	I*4	Instrument time key	
GPSCRPID	2	I*1	Raster point ID	points and lines
GPSCFILL	1	I*2	Filler	

PPxDDARK	1	R*4	Dark signal	in V/s
PPxDDUNC	1	R*4	Uncertainty	in V/s
PPxDNSIG	1	I*4	No. of valid signals on the plateau	
PPxDFLAG	1	I*1	Status Flag	
PPxDFILI	3	I*1	Filler	

13.3.12 Product PC1D

PC1D contains the SPD of the dark measurements obtained with detector C100. These measurements are only carried out for AOT PHT25.

RECORD
Record length: 128

FIELD	**N**	**T**	**Description**	**Comment**
GPSCTKEY	1	I*4	Instrument time key	
GPSCRPID	2	I*1	Raster point ID	points and lines
GPSCFILL	1	I*2	Filler	
PC1DDARK	9	R*4	Dark signal	in V/s
PC1DDUNC	9	R*4	Uncertainty	in V/s
PC1DNSIG	9	I*4	No. of valid signals on the plateau	
PC1DFLAG	9	I*1	Status Flag	
PC1DFILI	3	I*1	Filler	

13.3.13 Product PC2D

PC2D contains the SPD of the dark measurements obtained with detector C200. These measurements are only carried out for AOT PHT25.

RECORD
Record length: 60

FIELD	**N**	**T**	**Description**	**Comment**
GPSCTKEY	1	I*4	Instrument time key	
GPSCRPID	2	I*1	Raster point ID	points and lines
GPSCFILL	1	I*2	Filler	
PC2DDARK	4	R*4	Dark signal	in V/s
PC2DDUNC	4	R*4	Uncertainty	in V/s
PC2DNSIG	4	I*4	No. of valid signals on the plateau	
PC2DFLAG	4	I*1	Status Flag	

13.3.14 Pixel status flag

The pixel status flag in the SPD products gives an indication of the data processing quality for each detector pixel. The status flag is one byte of information, the coding of the decimal value of the byte is given in Table 13.3. All success and warning codes are even; all failure (do not process further) codes are odd.

Table 13.3: *Coding of the pixel status flag.*

Decimal Value	Description
0	normal (pixel ok)
1	calibration measurement saturated
2	plateau partly affected by drift
3	all ramps on plateau rejected
4	plateau data affected by residual drift
5	zero standard deviation
6	not used
7	zero signal for plateau

13.4 AAR Product Types

13.4.1 Rationale behind product design

The AAR products represent fully processed data, therefore each AAR product reflects not only the PHT subinstrument used but also the mode of operation. The definition of products necessarily involves a compromise between a number of conflicting desires. The naming convention for PHT Auto-Analysis products is to use the product type *PdAt*, where:

- *d* represents the detector, i.e.:
  - C is for PHT-C.
  - P is for PHT-P.
  - S is for PHT-SS.
  - L is for PHT-SL.
  - G is for generic (not detector-specific)
- *t* is a letter to identify the type of product. These are:
  - P is for point source photometry or spectroscopy in staring mode (single point or raster).
  - E is for extended source photometry.
  - I is for a photometric image.
  - U is for an uncertainty map.
  - T is for an exposure time map.
  - S is for raster photometry (including linear scans).

The following table summarises the products that are associated with each AOT:

PHT03	PPAP, PPAE, PPAS, PGAI, PGAU, PGAT
PHT04	PPAP, PPAE
PHT05	PPAP, PPAE
PHT17/18/19	PPAP, PPAE
PHT22	PCAP, PCAE, PCAS, PGAI, PGAU, PGAT
PHT25	PCAP, PCAE
PHT32	PCAS, PGAI, PGAU, PGAT
PHT37/38/39	PCAP, PCAE
PHT40	PSAP, PSAE, PLAP, PLAE, PSAS, PLAS

In case of rectangular chopped observations, the spacecraft pointing is exactly in between the two chopper positions (see Sections 2.8 and 3.10). For these PHT specific observations, the general auto-analysis header contains the pointing keywords CONSCRA and CONSCDEC. These keywords give the actual source position of the on-source chopper beam.

13.4.2 Product PPAP

PPAP is the standard product for PHT-P photometry AOTs when observing a point source. It contains the flux densities for each of the filters and/or apertures used.

```
Origin:         PHT03, PHT04, PHT05, PHT17, PHT18, PHT19
Units:          Jy
Format:         FITS binary table file
Limitations:    No colour correction performed.
                Photometry with non-standard apertures is not scientifically
                validated.
```

HEADER
The following product specific header keywords are present:

FIELD	T	Description	Comment
FILTERn	C	Filter	n=1 to number of filters used
APERn	C	Aperture	n=1 to number of apertures used
EXFLUXn	R	Expected source flux	in Jy, AOT input parameter
UNCFLXn	R	Uncertainty	in Jy, AOT input parameter
MXBACKn	R	Expected Maximum background	in MJy/sr, AOT input parameter
SBACKn	R	Flux density of source plus background	in Jy
SBACKUn	R	Uncertainty	in Jy
BACKn	R	Measured background intensity	in MJy/sr, 0 if staring measurement
LAMBDAn	R	Central wavelength	n is the record number
SOURCEn	R	Flux density of source	in Jy, only in case of chopper mode
SOURCUn	R	Uncertainty	in Jy, only in case of chopper mode
NORMCALC	L	TRUE if signal ratio calculated	only in case of PHT04
NRMFLXn	R	relative background subtracted flux ratio	only in case PHT04
NMFLXUn	R	Uncertainty	only in case of PHT04

RECORD
Record length: 80

FIELD	Off	N	T	Description	Comment
PPAPFILT	0	1	I*4	Filter ID (CHW3 position)	
PPAPAPER	4	1	I*4	Aperture ID (CHW2 position)	
PPAPNBCK	8	1	I*4	Number of background reference positions	
PPAPSRCE	12	1	R*4	Source flux	in Jy
PPAPSRCU	16	1	R*4	Uncertainty	in Jy
PPAPSRCB	20	1	R*4	Source surface brightness	in MJy/sr
PPAPSCBU	24	1	R*4	Uncertainty	in MJy/sr
PPAPBACK	28	1	R*4	Background for given aperture	in Jy
PPAPBCKU	32	1	R*4	Uncertainty	in Jy
PPAPSPB	36	1	R*4	Source plus background	in Jy
PPAPSPBU	40	1	R*4	Uncertainty	in Jy
PPAPSBB	44	1	R*4	Source plus background surface brightness	in MJy/sr
PPAPSBBU	48	1	R*4	Uncertainty	in MJy/sr
PPAPBCK1	52	1	R*4	Background reference 1	in Jy
PPAPBK1U	56	1	R*4	Uncertainty	in Jy
PPAPBCK2	60	1	R*4	Background reference 2	in Jy
PPAPBK2U	64	1	R*4	Uncertainty	in Jy
PPAPBINT	68	1	R*4	Mean background intensity	in MJy/sr
PPAPBINU	72	1	R*4	Uncertainty	in MJy/sr
PPAPNCYC	78	1	I*4	Number of accepted chopper cycles	

13.4.3 Product PPAE

PPAE is the standard product for PHT-P photometry AOTs when observing an extended source. It contains the surface brightness for each of the filters and/or apertures used.

```
Origin:         PHT03, PHT04, PHT05, PHT17, PHT18, PHT19
Units:          MJy/sr
Format:         FITS binary table file
Limitations:    No colour correction performed.
                Photometry from chopped observations is not scientifically
                validated.
                Surface brightness obtained with non-standard apertures is
                not scientifically validated.
```

HEADER
The following product specific header keywords are present:

FIELD	T	Description	Comment
FILTERn	C	Filter	n is the record number
APERn	C	Aperture	
LAMBDAn	R	Central wavelength	n is the record number
EXFLUXn	R	Expected source brightness	in MJy/sr, AOT input parameter
UNCFLXn	R	Uncertainty	in MJy/sr, AOT input parameter
MXBACKn	R	Expected Maximum background	in MJy/sr, AOT input parameter
SBBRTn	R	Brightness of source+background	in MJy/sr
SBBRTUn	R	Uncertainty	in MJy/sr
BACKn	R	Measured background intensity	in MJy/sr, value=0, if staring measurement
SBRTn	R	Source brightness	in MJy/sr
SBRTUn	R	Uncertainty, only in case of chopper mode	in MJy/sr
NORMCALC	L	TRUE if signal ratio calculated	only in for PHT04
NRMFLXn	R	relative background subtracted flux ratio	only for PHT04
NMFLXUn	R	Uncertainty	only for PHT04

RECORD
Record length: 72

FIELD	Off	N	T	Description	Comment
PPAEFILT	0	1	I*4	Filter ID (CHW3 position)	
PPAEAPER	4	1	I*4	Aperture ID (CHW2 position)	
PPAENBCK	8	1	I*4	Number of background reference positions	
PPAESRCE	12	1	R*4	Source brightness	in MJy/sr
PPAESRCU	16	1	R*4	Uncertainty	in MJy/sr
PPAEFLUX	20	1	R*4	Source flux density	in Jy
PPAEFLXU	24	1	R*4	Uncertainty	in Jy
PPAEBACK	28	1	R*4	Background for given aperture	in MJy/sr
PPAEBCKU	32	1	R*4	Uncertainty	in MJy/sr
PPAESPB	36	1	R*4	Source plus background	in MJy/sr
PPAESPBU	40	1	R*4	Uncertainty	in MJy/sr
PPAESBFX	44	1	R*4	Source plus background flux density	in Jy
PPAESBFU	48	1	R*4	Uncertainty	in Jy
PPAEBCK1	52	1	R*4	Background reference 1	in MJy/sr
PPAEBK1U	56	1	R*4	Uncertainty	in MJy/sr
PPAEBCK2	60	1	R*4	Background reference 2	in MJy/sr
PPAEBK2U	64	1	R*4	Uncertainty	in MJy/sr
PPAENCYC	68	1	I*4	Number of accepted chopper cycles	

13.4.4 Product PCAP

PCAP is the standard product for PHT-C photometry AOTs when observing a point source. It contains the flux densities for each of the filters used.

```
Origin:         PHT22, PHT25, PHT37, PHT38, PHT39
Units:          Jy
Format:         FITS binary table file
Limitations:    No colour correction performed.
```

HEADER

The following product specific header keywords are present:

FIELD	T	Description	Comment
FILTERn	C	Filter (n is the record number).	
EXFLUXn	R	Expected source flux	in Jy, AOT input parameter
UNCFLXn	R	Uncertainty	in Jy, AOT input parameter
MXBACKn	R	Expected Maximum background	in MJy/sr, AOT input parameter
SBACKn	R	Flux density of source plus background	in Jy
SBACKUNn	R	Uncertainty	in Jy
BACKn	R	Measured background	in MJy/sr, value=0, if staring measurement
LAMBDAn	R	Central wavelength	n is the record number
SOURCEn	R	Flux density of source	in Jy, only in case of chopper mode
SOURCUn	R	Uncertainty	in Jy, only in case of chopper mode

RECORD

Record length: 560

FIELD	Off	N	T	Description	Comment
PCAPFILT	0	1	I*4	Filter ID (CHW2 position)	
PCAPNBCK	4	1	I*4	Number of background reference positions	
PCAPNPIX	8	1	I*4	Number of pixels defined	
PCAPSRCE	12	9	R*4	Source flux	in Jy
PCAPSRCU	48	9	R*4	Uncertainty	in Jy
PCAPSRCB	84	9	R*4	Source surface brightness	in MJy/sr
PCAPSCBU	120	9	R*4	Uncertainty	in MJy/sr
PCAPSPB	156	9	R*4	Source plus background	in Jy
PCAPSPBU	192	9	R*4	Uncertainty	in Jy
PCAPSBB	228	9	R*4	Source plus background surface brightness	in MJy/sr
PCAPSBBU	264	9	R*4	Uncertainty	in MJy/sr
PCAPB1	300	9	R*4	Background at off position 1	in MJy/sr
PCAPB1U	336	9	R*4	Uncertainty	in MJy/sr
PCAPB2	372	9	R*4	Background at off position 2	in MJy/sr
PCAPB2U	408	9	R*4	Uncertainty	in MJy/sr
PCAPPEAK	444	1	R*4	Fitted source peak	in Jy, from Gaussian fitting
PCAPPKU	448	1	R*4	Uncertainty	in Jy
PCAPBCKS	452	1	R*4	Background at source position	in Jy
PCAPBKSU	456	1	R*4	Uncertainty	in Jy
PCAPBCK1	460	1	R*4	Avg. Background at off position 1	in Jy
PCAPBK1U	464	1	R*4	Uncertainty	in Jy
PCAPBCK2	468	1	R*4	Avg. Background at off position 2	in Jy
PCAPBK2U	472	1	R*4	Uncertainty	in Jy
PCAPBINS	476	1	R*4	On-source background intensity	in MJy/sr
PCAPBISU	480	1	R*4	Uncertainty	in MJy/sr
PCAPBIN1	484	1	R*4	Off-source background intensity 1	in MJy/sr
PCAPBI1U	488	1	R*4	Uncertainty	in MJy/sr
PCAPBIN2	492	1	R*4	Off-source background intensity 2	in MJy/sr
PCAPBI2U	496	1	R*4	Uncertainty	in MJy/sr
PCAPOFF	500	2	R*4	(x,y) offset of source peak	in arcsec, see Section 8.4.5–
PCAPOFFU	508	2	R*4	(x,y) uncertainty in offset	in arcsec, for Gaussian fit
PCAPFITU	516	1	R*4	Uncertainty of Gaussian fit	in Jy
PCAPSTAT	520	1	I*4	Fit status	
PCAPNCYC	524	9	I*4	Number of accepted chopper cycles	

13.4.5 Product PCAE

PCAE is the standard product for PHT-C photometry AOTs when observing an extended source. It contains the surface brightness for each of the filters used.

```
Origin:          PHT22, PHT25, PHT37, PHT38, PHT39
Units:           MJy/sr
Format:          FITS binary table file
Limitations:     No colour correction performed.
```

HEADER
The following product specific header keywords are present:

FIELD	T	Description	Comment
FILTERn	C	Filter (n is the record number)	
EXFLUXn	R	Expected source brightness	in MJy/sr, AOT input parameter
UNCFLXn	R	Uncertainty	in MJy/sr, AOT input parameter
MXBACKn	R	Expected Maximum background	in MJy/sr, AOT input parameter
LAMBDAn	R	Central wavelength	n is the record number
SBBRTn	R	Brightness of source plus background	in MJy/sr
SBBRTUn	R	Uncertainty	in MJy/sr
BACKn	R	Measured background intensity	in MJy/sr
SBRTn	R	Source brightness	in MJy/sr
SBRTUn	R	Uncertainty, only in case of chopper mode	in MJy/sr

RECORD
Record length: 504

FIELD	Off	N	T	Description	Comment
PCAEFILT	0	1	I*4	Filter ID (CHW2 position)	
PCAENBCK	4	1	I*4	Number of background reference positions	
PCAENPIX	8	1	I*4	Number of pixels defined	
PCAESRCE	12	9	R*4	Source brightness	in MJy/sr
PCAESRCU	48	9	R*4	Uncertainty	in MJy/sr
PCAEFLUX	84	9	R*4	Source flux density	in Jy
PCAEFLXU	120	9	R*4	Uncertainty	in Jy
PCAESPB	156	9	R*4	Source plus background	in MJy/sr
PCAESPBU	192	9	R*4	Uncertainty	in MJy/sr
PCAESBFX	228	9	R*4	Source plus background flux density	in Jy
PCAESBFU	264	9	R*4	Uncertainty	in Jy
PCAEB1	300	9	R*4	Background reference 1	in MJy/sr
PCAEB1U	336	9	R*4	Uncertainty	in MJy/sr
PCAEB2	372	9	R*4	Background reference 2	in MJy/sr
PCAEB2U	408	9	R*4	Uncertainty	in MJy/sr
PCAEBACK	444	1	R*4	Average background	in MJy/sr
PCAEBCKU	448	1	R*4	Uncertainty	in MJy/sr
PCAEBCK1	452	1	R*4	Avg. background at off position 1	in MJy/sr
PCAEBK1U	456	1	R*4	Uncertainty	in MJy/sr
PCAEBCK2	460	1	R*4	Avg. background at off position 2	in MJy/sr
PCAEBK2U	464	1	R*4	Uncertainty	in MJy/sr
PCAENCYC	468	9	I*4	Number of accepted chopper cycles	

13.4.6 Product PGAI

PGAI is the standard product for a photometric image. It contains a map of surface brightness.

```
Origin:          PHT03, PHT22, PHT32
Units:           MJy/sr
```

```
Format:         FITS Image
Limitations:    Maps obtained with PHT03 (using PHT-P subsystems) and
                PHT32 are not scientifically validated.
```

HEADER
The following product specific header keywords are present:

FIELD	T	Description	Comment
NAXIS	3	number of axes	
NAXIS1	I	Number of pixels per row of image	
NAXIS2	I	Number of pixels per column of image	
NAXIS3	I	Number of measurements (wavelengths)	
BUNIT	C	Units in map	MJy/sr
CTYPE1	C	Right Ascension	in degrees
CTYPE2	C	Declination	in degrees
CTYPE3	C	wavelength	
BLANK	I	Blank value	value used: -987654322
CRPIX1	R	Pixel origin of RA-axis	image centre
CRPIX2	R	Pixel origin of DEC-axis	image centre
CRPIX3	R		n/a
CRVAL1	R	Right Ascension of raster centre	in degrees
CRVAL2	R	Declination of raster centre	in degrees
CRVAL3	R	Wavelength index	
CD1_1	R	Pixel size	in degrees
CD1_2	R		set to 0.0
CD1_3	R		set to 0.0
CD2_1	R		set to 0.0
CD2_2	R	Pixel size	in degrees
CD2_3	R		set to 0.0
CD3_1	R		set to 0.0
CD3_2	R		set to 0.0
CD3_3	R	index	set to 1.0
CUNIT1	R	RA units	
CUNIT2	R	Dec units	
CUNIT3	R	Wavelength index	unity
CDELT1	R	Pixel size	in degrees
CDELT2	R	Pixel size	in degrees
CDELT3	R	Index	
CROTA1	R	Position angle of first axis	(=0)
CROTA2	R	Position angle of second axis	(=0)
CROTA3	R		n/a
APERTURE	C	Aperture	(if PHT-P)
FILTERn	C	Filter	n=number of filters
LAMBDAn	R	Central Wavelength of filter	in m
EXBRGTn	R	Expected maximum brightness	in MJy/sr, AOT input parameter
DATAMIN	R	Minimum brightness	in MJy/sr, minimum for all filters
DATAMAX	R	Maximum brightness	in MJy/sr, maximum for all filter
SBRMAXn	R	Maximum brightness for filter n	in MJy/sr
SBRMINn	R	Minimum brightness for filter n	in MJy/sr
FFPiFn	R	Flat-field factor for pixel i of filter n	

Note: The header keywords CDn_i and CUNITi with n =1, 2, 3 and i =1, 2, 3 have been introduced to accomodate the FITS world coordinate system. To be compatible with other (older) systems the keywords CDELTi and CROTAi have also been included in the header. Similar headers are implemented for the PGAU and PGAT products.

IMAGE

AXIS no	LENGTH	Description	Comment
1	N1	Points per raster line	
2	N2	Number of lines	
3	N3	Filters	detector

13.4.7 Product PGAU

PGAU is an accompanying product for a photometric image. It contains a map of uncertainty in the surface brightness as found in product PGAI.

```
Origin:         PHT03, PHT22, PHT32
Units:          MJy/sr
Format:         primary FITS file containing a real array
Limitations:    Maps obtained with PHT03 (using PHT-P subsystems) and
                PHT32 are not scientifically validated.
```

The product specific header keywords and image axis are the same as for PGAI, except for:

FIELD	T	Description	Comment
DATAMIN	R	Minimum uncertainty	in MJy/sr, for all filters
DATAMAX	R	Maximum uncertainty	in MJy/sr, for all filters
SBUMAXn	R	Maximum brightness uncertainty	in MJy/sr, for filter n
SBUMINn	R	Minimum brightness uncertainty	in MJy/sr, for filter n

13.4.8 Product PGAT

This is an accompanying product for a photometric image. It contains a map of the exposure time as measured in product PGAI.

```
Origin:         PHT03, PHT22, PHT32.
Units:          Seconds
Format:         primary FITS file containing a real array
Limitations:    Maps obtained with PHT03 (using PHT-P subsystems) and
                PHT32 are not scientifically validated.
```

HEADER
The product specific header keywords and image axis are the same as for PGAI, except for:

FIELD	T	Description	Comment
EXPMINn	R	Minimum exposure	in s
EXPMAXn	R	Maximum exposure	in s
DATAMAX	R	Maximum exposure	in s, for all filters
DATAMIN	R	Maximum exposure	in s, for all filters
DATAAVGn	R	Average exposure	for filter n

13.4.9 Product PPAS

This is the photometric table product for PHT-P raster maps. The data serve as input for alternative image reconstruction algorithms. Each record contains the surface brightness and sky coordinates for each sampled position. The records are ordered in time according to the raster scan, records of a next filter are appended to the ones of the previous.

```
Origin:         PHT03
Units:          MJy/sr
Format:         FITS binary table file
Limitations:    Maps obtained with PHT03 (using PHT-P subsystems) are not
                scientifically validated.
```

HEADER
The following product specific header keywords are present:

FIELD	T	Description	Comment
FPCMODE	C	Chopper mode	
APERTRn	C	Aperture	n is the record
FILTERn	C	Filter identifier	
EXFLUXn	R	Expected source brightness	in Jy, AOT input parameter
UNCFLXn	R	Uncertainty	in Jy, AOT input parameter
MXBACKn	R	Max.expected background	in MJy/sr, AOT input parameter
MXBRGTn	R	Measured maximum brightness	in MJy/sr
UNBRGTn	R	Uncertainty	in MJy/sr
LAMBDAn	R	Central wavelength	

RECORD
Record length: 48 bytes

FIELD	Off	N	T	Description	Comment
PPASFILT	0	1	I*4	Filter ID (CHW3 position)	
PPASRA	4	1	R*4	Right Ascension	in degrees
PPASRAU	8	1	R*4	Uncertainty	in degrees
PPASDEC	12	1	R*4	Declination	in degrees
PPASDECU	16	1	R*4	Uncertainty	in degrees
PPASROLL	20	1	R*4	Roll angle	in degrees
PPASROLU	24	1	R*4	Uncertainty	in degrees
PPASBRGT	28	1	R*4	Surface brightness	in MJy/sr
PPASBRGU	32	1	R*4	Uncertainty	in MJy/sr
PPASFLUX	36	1	R*4	Flux density	in Jy
PPASFLXU	40	1	R*4	Uncertainty	in Jy
PPASSTAT	44	1	I*1	Status flag	from SPD
PPASFILL	45	3	I*1	Filler	

13.4.10 Product PCAS

This is the photometric table product for PHT-C raster maps. The data serve as input for alternative image reconstruction algorithms. Each record contains the surface brightness and sky coordinates for each sampled position. The records are ordered in time according to the raster scan, records of a next filter are appended to the ones of the previous. For PHT32 observations each record contains data of a chopper plateau.

```
Origin:         PHT22, PHT32
Units:          MJy/sr
Format:         FITS binary table file
Limitations:    Uncertainties in coordinates are not available.
                Maps obtained with PHT32 are not scientifically validated.
```

HEADER
The following product specific keywords are present:

FPCMODE	C	Chopper mode	(ST= staring, RE= rectangular, SW= sawtooth, TR= triangular
FILTERn	C	Filter identifier	see Section A.1
EXFLUXn	R	Expected source brightness	in MJy/sr, AOT input parameter
UNCFLXn	R	Uncertainty	in MJy/sr, AOT input parameter
MXBRGTn	R	Measured maximum brightness	in MJy/sr
UNBRGTn	R	Uncertainty	in MJy/sr
LAMBDAn	R	Central wavelength	n is the record number
MXBACKn	R	Max expected background	in MJy/sr

RECORD
Record length: 192 bytes

FIELD	Off	N	T	Description	Comment
PCASFILT	0	1	I*4	Filter ID (CHW2 position)	
PCASRA	4	1	R*4	Right Ascension	in degrees
PCASRAU	8	1	R*4	Uncertainty	in degrees
PCASDEC	12	1	R*4	Declination	in degrees
PCASDECU	16	1	R*4	Uncertainty	in degrees
PCASROLL	20	1	R*4	Roll angle	in degrees
PCASROLU	24	1	R*4	Uncertainty	in degrees
PCASAVGB	28	1	R*4	Average brightness over array	in MJy/sr
PCASNPIX	32	1	I*4	Number of pixels defined	
PCASBRGT	36	9	R*4	Surface brightness per pixel	in MJy/sr
PCASBRGU	72	9	R*4	Uncertainty	in MJy/sr
PCASFLUX	108	9	R*4	Flux density per pixel	in Jy
PCASFLXU	144	9	R*4	Uncertainty	in Jy
PCASSTAT	180	9	I*1	Status flags	from SPD
PCASFILL	189	3	I*1	Filler	

13.4.11 Product PSAP

This is the photometric table product for PHT-SS single pointing of a point source.

```
Origin:          PHT40
Units:           W/m^2/micron
Format:          FITS binary table file
Limitations:     -
```

HEADER
The following product specific keywords are present:

CALSEQ	I	Calibration Sequence	
CALDATE	C	Date Calibration defaults generated	
FPCMODE	C	Focal plane chopper mode	(ST, RE, SW or TR)
LAMBDAd	R	Central Wavelength of pixel (m)	d = 1,2,...,64

RECORD
Record length: 2568 bytes

FIELD	Off	N	T	Description	Comment
PSAPDFLG	0	1	I*4	Dark background flag	dark=1, otherwise=0
PSAPNBCK	4	1	I*4	Number of background reference positions	
PSAPSRCE	8	64	R*4	Source Flux	in $Wm^{-2}\mu m^{-1}$
PSAPSRCU	264	64	R*4	Uncertainty	in $Wm^{-2}\mu m^{-1}$
PSAPBCK	520	64	R*4	Mean Background	in $Wm^{-2}\mu m^{-1}$
PSAPBCKU	776	64	R*4	Uncertainty	in $Wm^{-2}\mu m^{-1}$
PSAPSPB	1032	64	R*4	Source + Background	in $Wm^{-2}\mu m^{-1}$
PSAPSPBU	1288	64	R*4	Uncertainty	in $Wm^{-2}\mu m^{-1}$
PSAPBCK1	1544	64	R*4	Background reference 1	in $Wm^{-2}\mu m^{-1}$
PSAPBK1U	1800	64	R*4	Uncertainty	in $Wm^{-2}\mu m^{-1}$
PSAPBCK2	2056	64	R*4	Background reference 2	in $Wm^{-2}\mu m^{-1}$
PSAPBK2U	2312	64	R*4	Uncertainty	in $Wm^{-2}\mu m^{-1}$

13.4.12 Product PLAP

This is the photometric table product for PHT-SL single pointing of a point source.

```
Origin:         PHT40
Units:          W/m^2/micron
Format:         FITS binary table file
Limitations:    -
```

HEADER
Similar to product PSAP

RECORD
Similar to product PSAP, only all record keywords start with 'PLAP'

13.4.13 Product PSAE

This is the photometric table product for PHT-SS single pointing of an extended source.

```
Origin:         PHT40
Units:          of W/m^2/micron/sr
Format:         FITS binary table file
Limitations:    -
```

HEADER
Similar to product PSAP

RECORD
Similar to product PSAP, only all record keywords start with 'PSAE' and all surface brightness values are in units of $\mathrm{Wm^{-2}\mu m^{-1}\,sr^{-1}}$.

13.4.14 Product PLAE

This is the photometric table product for PHT-SL single pointing of an extended source.

```
Origin:         PHT40
Units:          W/m^2/micron/sr
Format:         FITS binary table file
Limitations:    -
```

HEADER
Similar to product PSAP

RECORD
Similar to product PSAP, only all record keywords start with 'PLAE' and all surface brightness values are in units of $\mathrm{Wm^{-2}\mu m^{-1}\,sr^{-1}}$.

13.4.15 Product PSAS

This is the photometric table product for PHT-SS raster pointing. Each record contains the surface brightness and sky coordinates for each sampled position. The records are ordered in time according to the raster scan.

```
Origin:         PHT40
Units:          W/m^2/micron/sr
Format:         FITS binary table file
Limitations:    No image product available.
```

HEADER
The following product specific keywords are present:

CALSEQ	I	Calibration Sequence	
CALDATE	C	Date Calibration defaults generated	
LAMBDAd	R	Central Wavelength of pixel (m)	d=1,64

RECORD
Record length: 604 bytes

FIELD	Off	N	T	Description	Comment
PSASDFLG	0	1	I*4	Dark background flag	dark=1, otherwise=0
PSASRA	4	1	R*4	Right Ascension of raster point	in degrees
PSASRAU	8	1	R*4	Uncertainty in Right Ascension	in degrees
PSASDEC	12	1	R*4	Declination of raster point	in degrees
PSASDECU	16	1	R*4	Uncertainty in Declination	in degrees
PSASROLL	20	1	R*4	Roll angle	in degrees
PSASROLU	24	1	R*4	Uncertainty in roll angle	in degrees
PSASSPB	28	64	R*4	Source plus background brightness	in $Wm^{-2}\mu m^{-1}sr^{-1}$
PSASSPBU	284	64	R*4	Uncertainty	in $Wm^{-2}\mu m^{-1}sr^{-1}$
PSASSTAT	540	64	I*1	Status flags	

13.4.16 Product PLAS

This is the photometric table product for PHT-SL raster pointing.

```
Origin:         PHT40
Units:          W/m^2/micron/sr
Format:         FITS binary table file
Limitations:    No image product available.
```

HEADER
Similar to product PSAS

RECORD
Similar to product PSAS, only all record keywords start with 'PLAS'

Chapter 14

Calibration-G Products

14.1 Overview

General calibration files or 'Cal-G' files contain either correction factors or instrumental parameters necessary to

- steer the processing,
- to remove or to correct for instrumental effects in the data, and
- to carry out the flux calibration.

The contents of the Cal-G files reflect the best or most recent instrument calibration parameters. The files were only updated as part of an official upgrade of the OLP software. In this chapter detailed descriptions are given of the structure and contents of the Cal-G files.

Note:
• See Section 2.6.2 for the definition of C-arrays pixel identifiers throughout this chapter.

14.2 Observation Time Dependent Calibration

`Description Parameter:`	`Section 7.10.7`
`Processing Level:`	`SPD`
`Usage in processing:`	`Section 7.10.7`
`File Type:`	`Binary FITS table`
`File names:`	`PTIMEDEP`

During the mission two events took place that directly affected calibration parameters of the instrument:

- the change in the illumination properties of the TRS2 of FCS1 which took place in the activation window of revolution 94. The illumination power for the same electrical power applied to the FCS increased by approximately a factor two. The cause of the change is not clear. The change in FCS properties requires different calibration parameters for FCS related calibrations of P3, C100 and C200.

- the addition of an extra curing procedure for detectors P3, C100 and C200 during the otherwise idle telescope time in ground station handover between VILSPA and Goldstone sometime after the apogee passage of ISO. The extra curing was introduced on rev 150 and affects the orbit dependent responsivity of the three detectors.

Consequently, the OLP must use different sets of Cal-G files depending on the date and time of the observation. This calibration file lists the names of the Cal-G files that are affected together with the date and time when the change took place. Depending on the time of the observation the appropriate Cal-G files are selected.

14.2.1 Product PTIMEDEP: PHT calibration time dependency

Binary FITS table with record length 80. The record fields are:

Field	Offset	Number	Type	Description
CALGROOT	0	1	C*12	Root name: referred to when file is opened
CALGFILE	12	1	C*12	Corresponding filename
CALGTIME	24	1	C*11	Time from which this file applies in yydddhhmmss
CALGCOMM	35	1	C*45	Optional comment

14.3 DIE Power Calibration

```
Description Parameter:          Section 2.4.3
Processing Level:               SPD
Usage in processing:            Section 7.2.6
File Type:                      Binary FITS table
Number of Records:              3
File Names:                     PDIE1TRANS, PDIE2TRANS
```

There are 2 sets of Detector Interface Electronics (DIE) in the external electronics unit (see Section 2.4.3). The DIE subtracts a commandable offset from the cold readout electronics voltage and amplifies the difference with a commandable gain factor. There were 3 possible DIE settings available but in practice only one was used. To convert the digital numbers (DNs) to Voltages, a set of 'gain' parameters were used depending on which of the 3 possible settings were commanded. See also Section 7.2.6 for the conversion formula.

Table 14.1: *DIE used for detector.*

DIE number	detector
1	P1, P2, SL, C200
2	P3, SS, C100, C200

The possible settings of the 2 DIEs are stored in 2 Cal-G products. Both DIEs were used during operations depending on which detector was active, the relation between detector and DIE is given in Table 14.1. Each record in the Cal-G products refers to the settings for a given DIE gain that was commanded, see Table 14.2.

Table 14.2: *Conversion from record in Cal-G to gain value.*

Record number	Gain
1	1
2	8
3	40

14.3.1 Product PDIE1TRANS: PHT DIE1 power calibration table

Binary FITS table with record length 16. The record fields are:

Field	Offset	Number	Type	Description
PDIE1FIX	0	1	R*4	Fixed offset
PDIE1UOF	4	1	R*4	Offset dependent on signal gain in V
PDIE1GN1	8	1	R*4	Signal gain (=$GAIN_1$)
PDIE1GN1	12	1	R*4	Offset gain (=$GAIN_2$)

14.3.2 Product PDIE2TRANS: PHT DIE2 power calibration table

Similar to PDIE1TRANS, but DIE1 should be substituted by DIE2.

14.4 Selection of Readouts

```
Description Parameter:          Section 4.3.1
Processing Level:               SPD
Usage in processing:            Section 7.2.2
File Type:                      Binary Fits Table
Number of Records:              8
File Names:                     PSELNDR
```

It has been observed that the first few readouts of each integration ramp do not increase in a linear way but can stay flat for a while or can even decrease. The disturbance is due to the preceding reset and is a switch-on effect of the integrator which is independent of the reset voltage level. This effect is not related to the voltage dependent non-linearity for which the corrections are stored in the Cal-G linearisation files (Section 14.5). The best correction method so far is to discard these readouts. The number of readouts that should be removed is a function of the number of readouts per ramp. The optimum values have been determined in flight.

In total there are 8 records, each record gives the number of readouts to be discarded for a given NDR value. The record ordering is given in Table 14.3.

14.4.1 Product PSELNDR: PHT non-destructive readout selection

Binary FITS table with record length 32. The record fields are:

Table 14.3: *Relation between record number and NDR in PSELNDR.*

Record number	number of non-destructive readouts	Record number	number of non-destructive readouts
1	0	5	15
2	1	6	31
3	3	7	63
4	7	8	127

Field	Offset	Number	Type	Description
PP1SNDR	0	1	I*4	NDRs to discard for PHT-P1
PP2SNDR	4	1	I*4	NDRs to discard for PHT-P2
PP3SNDR	8	1	I*4	NDRs to discard for PHT-P3
PFILSNDR	12	1	I*4	Filler
PSSSNDR	16	1	I*4	NDRs to discard for PHT-SS
PSLSNDR	20	1	I*4	NDRs to discard for PHT-SL
PC1SNDR	24	1	I*4	NDRs to discard for PHT-C100
PC2SNDR	28	1	I*4	NDRs to discard for PHT-C200

14.5 CRE Linearisation Corrections

```
Description Parameter:          Section 4.3.2
Processing Level:               SPD
Usage in processing:            Section 7.2.8
File Type:                      FITS Image
Units:                          V
File Names:                     PPCRELIN, PC1CRELIN, PC2CRELIN
```

The linearisation of ramps is performed by adding a correction voltage to each readout voltage. The value of the correction depends on the the value of the readout voltage itself, the detector used, and the readout clock frequency. The correction tables are provided by FITS images for the P, C100, and C200 detectors, respectively.

The index is determined in axis 1 which corresponds to the CRE output voltage. For the given detector (or pixel) and readout clock frequency, the voltage correction and uncertainty are provided through axis 4.

All products have:
NAXIS = 4
TYPE = R*4

14.5.1 Product PPCRELIN: linearisations for P1, P2, and P3

AXIS	Length	Description
1	121	CRE Output Voltages. The voltages are binned in steps of 0.02 V in the voltage range −1.2 V to +1.2 V

2	3	PHT-P detectors: P1, P2, P3
3	3	readout clock frequency 1, 4, 8 kHz
4	2	Correction voltage and uncertainty in V

14.5.2 Product PC1CRELIN: linearisations for C100

Same as PPCRELIN, but for AXIS 2:
Length = 9, Description = C100 pixels

14.5.3 Product PC2CRELIN: linearisations for C200

Same as PPCRELIN, but for AXIS 2:
Length = 4, Description = C200 pixels.

14.6 Signal Correction for Reset Interval

```
Description Parameter:          Section 4.3.3
Processing Level:               SPD
Usage in processing:            Section 7.3.1
File Type:                      Binary FITS Table
File Names:                     PP1RESETI, PP2RESETI, PP3RESETI,
                                PC1RESETI, PC2RESETI
```

In Derive_SPD, each signal is transformed to the equivalent signal for a reference reset interval of 1/4 seconds. The Cal-G files provide the correction parameters A_0 and A_1 as defined in Section 7.3.1.

14.6.1 Product PP1RESETI: parameters for conversion to 1/4s reset interval for P1

Binary FITS table with record length 24. The record fields are:

Field	Offset	Number	Type	Description
PP1RESRI	0	1	I*4	Reset interval, n, with $t_{RI} = 2^{7-n}$ s
PP1RESDR	4	1	I*4	Data reduction factor
PP1RESA0	4	1	R*4	Offset correction, A_0 (V/s)
PP1RESA1	4	1	R*4	Slope correction, A_1
PP1RESE0	4	1	R*4	Error(standard deviation) in A_0 (V/s)
PP1RESE1	4	1	R*4	Error(standard deviation) in A_1

14.6.2 Product PP2RESETI: parameters for conversion to 1/4s reset interval for P2

Same as PP1RESETI, all field keywords start with PP2.

14.6.3 Product PP3RESETI: parameters for conversion to 1/4s reset interval for P3

Same as PP1RESETI, all field keywords start with PP3.

14.6.4 Product PC1RESETI: parameters for conversion to 1/4s reset interval for C100

Same as PP1RESETI, all field keywords start with PC1.

14.6.5 Product PC2RESETI: parameters for conversion to 1/4s reset interval for C200

Same as PP1RESETI, all field keywords start with PC2.

14.7 Detector Dark Signals

```
Description Parameter:          Section 4.2.6
Processing Level:               SPD
Usage in processing:            Section 7.3.2
File Type:                      FITS Image
Units:                          V/s
File Names:                     PSDARK, PPDARK, PC1DARK, PC2DARK
```

To derive the absolute power falling on the detector it is necessary to remove the detector dark signal. For chopped measurements where only the signal difference matters, the dark signal correction is in principle not required. In the Cal-G file the unit for the detector dark currents is V/s.

The dark signal depends on the orbital phase of the satellite during the observation like the detector responsivity, but is not influenced by the curing in the handover window.

All products have:
NAXIS = 3
TYPE = R*4

14.7.1 Product PSDARK: PHT-S dark signals

AXIS	Length	Description
1	100	Orbital phase: each element corresponds to a phase in the range from 0.01 to 1.0 in steps of 0.01
2	128	Pixels - PHT-SS (1–64) and PHT-SL (65–128)
3	2	Dark signal and uncertainty

14.7.2 Product PPDARK: dark signals for detectors P1, P2, and P3

AXIS	Length	Description

1	100	Orbital phase: each element corresponds to a phase in the range from 0.01 to 1.0 in steps of 0.01
2	3	PHT-P detectors, P1,P2,P3
3	2	Dark signal and uncertainty

14.7.3 Product PC1DARK: dark signals for detector C100

AXIS	Length	Description
1	100	Orbital phase: each element corresponds to a phase in the range from 0.01 to 1.0 in steps of 0.01
2	9	C100 pixels, in same order as SPD.
3	2	Dark signal and uncertainty

14.7.4 Product PC2DARK: dark signals for detector C200

AXIS	Length	Description
1	100	Orbital phase: each element corresponds to a phase in the range from 0.01 to 1.0 in steps of 0.01
2	4	C200 pixels, in same order as SPD.
3	2	Dark signal and uncertainty

14.8 Correction for Signal Non-Linearity

```
Description Parameter:      None
Processing Level:           SPD
Usage in processing:        Section 7.3.3
File Type:                  Binary FITS Table
Units:                      [V/s]
File Names:                 PP1SLINR, PP2SLINR, PP3SLINR,
                            PC1SLINR, PC2SLINR
```

The correction tables for signal linearisation are in essence look-up tables providing for a given input signal a corrected output signal. Because the linearisation tables were obtained from a limited range of (calibrated) signals, the upper and lower validity boundaries are listed in the header of the Cal-G file.

14.8.1 Product PP1SLINR: signal linearisation for PHT-P1

Binary FITS table with record length 16. The record fields are:

Field	Offset	Number	Type	Description
PP1SLFIL	0	1	I*4	Filter (CHW position)
PP1SLSIG	4	1	R*4	Uncorrected input signal (plateau average in [V/s])
PP1SLSCR	8	1	R*4	Corrected signal [V/s]

PP1SLSCU	12	1	R*4	Uncertainty of the corrected signal [V/s]

The header keywords defining the calibrated signal range

Field	Type	Description
FILTCWd	I	CHW3 filter position, d=(1,n), n=number of filters
LOSIGLd	R	lower validity limit of signal non-linearity correction [V/s]
HISIGLd	R	upper validity limit of signal non-linearity correction [V/s]

14.8.2 Product PP2SLINR: signal PHT-P2 linearisation

Same as PP1SLINR, see Section 14.8.1, all field keywords start with 'PP2'.

14.8.3 Product PP3SLINR: signal linearisation for PHT-P3

Same as PP1SLINR, see Section 14.8.1, all field keywords start with 'PP3'.

14.8.4 Product PC1SLINR: signal linearisation for PHT-C100

Binary FITS table with record length 20. The record fields are:

Field	Offset	Number	Type	Description
PC1SLFIL	0	1	I*4	Filter (CHW position)
PC1SLPIX	4	1	I*4	pixel number
PC1SLSIG	8	1	R*4	Uncorrected input signal (plateau average in [V/s])
PC1SLSCR	12	1	R*4	Corrected signal [V/s]
PC1SLSCU	16	1	R*4	Uncertainty of the corrected signal [V/s]

The header keywords defining the calibrated signal range

Field	Type	Description
FILTCWd	I	CHW2 filter position, d=(1,n), n=number of filters
LOSIGLd	R	lower validity limit of signal non-linearity correction [V/s]
HISIGLd	R	upper validity limit of signal non-linearity correction [V/s]

14.8.5 Product PC2SLINR: signal linearisation for PHT-C200

Same as PC1SLINR, see Section 14.8.4, all field keywords start with 'PC2'.

14.9 PHT-S Dynamic Calibration for Staring Observations

Description Parameter:	Section 5.2.6
Processing Level:	SPD
Usage in processing:	Section 7.4 in particular Section 7.4.2
File Type:	FITS Image
Units:	Jy for PSDYNAMIC, dimensionless for PSDYNWT
File names:	PSDYNAMIC, PSDYNWT

The dynamic calibration for staring observations with PHT-S is based on the assumption that point sources with similar flux densities will produce identical signal variations as a function of time for each PHT-S detector array element. With a sufficient number of calibration stars spanning a large range of flux densities for each detector pixel, it has been possible to construct two dimensional surfaces where for any signal $s(i,t)$ of detector pixel i at time t a flux density $F_\nu^t(i) = \varphi(i, s(i,t), t)$ in Jy can be assigned (see Section 5.2.6). The calibration data are tabulated in PSDYNAMIC.

The SPD processing subdivides a staring measurement into a number of $s(i,t)$ depending on the number of ramps in the measurement. For each value of t a value of $F_\nu^t(i)$ can be determined. For small t, the corrections are largest because of the steep initial rise of the signal transient curve. The flux calibration becomes more accurate by giving the signals at larger t a relatively higher weight when averaging the $f(t)$ to obtain the average flux density for a measurement. The weights are stored in a separate calibration file PSDYNWT.

Due to the high dynamic range in possible signals $s(i,t)$ and times t, the calibration tables use logarithmic axes for signal and time. The axes are tabulated as follows:

- signal axis:

$$s(j) = -dex[-3.0202 + (j-1)(\frac{3.0202 - 5.0}{28})] \quad \text{for} \quad 1 \le j \le 29 \tag{14.1}$$

$$s(j) = 0 \quad \text{for} \quad j = 30 \tag{14.2}$$

$$s(j) = dex[-5 + (j-31)(\frac{2.0 + 5.0}{99})] \quad \text{for} \quad 31 \le j \le 130, \tag{14.3}$$

  where j is the array index and signal $s(j)$ is in [V/s]. Note that negative signals can occur.

- time axis:

$$t(j) = 2^j \quad [\text{s}] \quad for \;\; 0 \le j \le 12. \tag{14.4}$$

  As a consequence, times smaller than 1 s (and larger than 4096 s) are not handled by the calibration.

For both PSDYNAMIC and PSDYNWT the following FITS keywords are common:

NAXIS = 3
TYPE = REAL*4

14.9.1 Product PSDYNAMIC: PHT-S dynamic calibration - flux correction

AXIS	Length	Description
1	130	signal

2	13	time in $\log_2(t)$
3	128	pixels

14.9.2 Product PSDYNWT: PHT-S dynamic calibration - weighting function

AXIS	Length	Description
1	130	signal
2	13	time in $\log_2(t)$
3	128	pixels

14.10 Correction for Signal Losses in Chopped Mode

```
Description Parameter:          none
Processing Level:               SPD, AAR
Usage in processing:            Section 7.5, 8.4.1
File Type:                      Binary FITS Table
Units:                          [V/s]
File Names:                     PP1CHOPSIG, PP2CHOPSIG, PP3CHOPSIG,
                                PC1CHOPSIG, PC2CHOPSIG
```

The signal difference between the on- and off-chopper plateaux is observed to be lower than the signal difference obtained from the same source-background position combination in staring or nodding mode. The effect is attributed to the detector transient responsivity behaviour of the detectors which underestimates the on-signal and overestimates the background signal. The calibration files contain for each detector the parameters necessary to correct the difference signal for the signal loss. The correction depends on the chopper dwell time and the value of the difference signal. The correction is implemented by a lookup table which for each chopper dwell time, lists the corrected signal as a function of the uncorrected signal.

14.10.1 Product PP1CHOPSIG: PHT-P1 chopped signal correction

Binary FITS table with record length 16. The record fields are:

Field	Offset	Number	Type	Description
PP1CSCPT	0	1	I*4	Chopper dwell time: n, where $t_{dwell} = 2^{(n-1)}$ s, n=1, 8
PP1CSOOU	4	1	R*4	Uncorrected on-off source signal [V/s]
PP1CSOOC	8	1	R*4	Corrected on-off source signal [V/s]
PP1CSUNC	12	1	R*4	Uncertainty of the corrected on-off signal [V/s]

14.10.2 Product PP2CHOPSIG: PHT-P2 chopped signal correction

Same as PP1CHOPSIG, with 'P1' in field keyword replaced by 'P2'.

14.10.3 Product PP3CHOPSIG: PHT-P3 chopped signal correction

Same as PP1CHOPSIG, with 'P1' in field keyword replaced by 'P3'.

14.10.4 Product PC1CHOPSIG: PHT-C100 chopped signal correction

Binary FITS table with record length 20. The record fields are:

Field	Offset	Number	Type	Description
PC1CSPIX	0	1	I*4	pixel
PC1CSCPT	4	1	I*4	Chopper dwell time: n, where $t_{dwell} = 2^{(n-1)}$ s, n=1, 8
PC1CSOOU	8	1	R*4	Uncorrected on-off source signal [V/s]
PC1CSOOC	12	1	R*4	Corrected on-off source signal [V/s]
PC1CSUNC	16	1	R*4	Uncertainty of the corrected on-off signal [V/s]

14.10.5 Product PC2CHOPSIG: PHT-C200 chopped signal correction

Same as PC1CHOPSIG, with 'C1' in field keyword replaced by 'C2'.

14.11 Vignetting Corrections

```
Description Parameter:          Section 4.5.1
Processing Level:               SPD
Usage in processing:
File Type:                      FITS Image
Units:                          dimensionless
File Names:                     PP1VIGN, PP2VIGN, PP3VIGN,
                                PC1VIGN, PC2VIGN
```

The light deflected by the chopper mirror can be vignetted. Since the chopper deflection can only take place along the spacecraft Y direction, the corrections are tabulated as a function of Y offset, detector, filter, and aperture, if any. The correction factors are multiplied with the mean and median signal per chopper plateau for a given chopper throw.

The vignetting Cal-G files contain no corrections for detectors P1, P2, and P3, i.e. all correction factors are unity for these detectors.

The present corrections for signal losses in pointed chopped observations implicitly include the chopper vignetting correction in the form of a different signal correction for the on- and off-target positions. Consequently, these observations require no additional vignetting corrections. The chopper vignetting corrections are used in the processing of PHT32 where no corrections for chopped signal losses are included.

All products have:
NAXIS = 3
TYPE = R*4

14.11.1 Product PP1VIGN: vignetting corrections for P1

AXIS	Length	Description
1	14	Apertures: CHWII position, see Section A.1
2	25	Chopper position: from $-180''$ to $+180''$ in 15 arcsec steps
3	10	Filters: CHWIII position, see Section A.1

14.11.2 Product PP2VIGN: vignetting corrections for P2

AXIS	Length	Description
1	14	Apertures: CHWII position, see Section A.1
2	25	Chopper position: from $-180''$ to $+180''$ in 15 arcsec steps
3	2	Filters: 20, 25 μm

14.11.3 Product PP3VIGN: vignetting corrections for P3

see Product PP2VIGN, with filters: 60 and 100 μm.

14.11.4 Product PC1VIGN: vignetting corrections for C100

AXIS	Length	Description
1	9	C100 Pixels: index 1= pixel [1,1], 2= [1,2], etc
2	25	Chopper position: from $-180''$ to $+180''$ in 15 arcsec steps
3	7	Filters: [CHWII position $-$ 1], see Section A.1

14.11.5 Product PC2VIGN: vignetting corrections for C200

AXIS	Length	Description
1	4	C200 Pixels: pixel 1= [1,1], 2= [1,2], etc
2	25	Chopper position: from $-180''$ to $+180''$ in 15 arcsec steps
3	5	Filters: CHWII position $-$ 8, see Section A.1

14.12 FCS Power Calibration

`Description Parameter:`	`Section 2.7, 5.2.4`
`Processing Level:`	`SPD`
`Usage in processing:`	`Section 7.10`
`File Type:`	`FITS Image`
`Units:`	`mW`
`File names:`	`PP1FCSPOW, PP2FCSPOW,`
	`PP3FCSPOW_01, PP3FCSPOW_02,`
	`PC1FCSPOW_01, PC1FCSPOW_02,`
	`PC2FCSPOW_01, PC2FCSPOW_02`

The FCS power calibration tables give the electrical power in mW applied to the FCS as a function of filter, TRS, FCS and the *index* in the table listing the in-band power on the detector in regular logarithmic intervals. For a given filter, TRS, and FCS combination the indices $i-1, i$ and $P_{FCS}(i-1)$, $P_{FCS}(i)$ are retrieved from the Cal-G file. $P_{FCS}(i)$ is the first FCS power in the table higher than the actual FCS power $P_{FCS,meas}$ used in the FCS measurement. Once the indices have been determined Table 14.4 is used to convert these to in-band powers on the detector P_{det}.

Table 14.4: *Conversion index of axis 1 to power in W for C100 and C200 or* W mm^{-2} *for P1, P2, and P3.*

index	P_{det}	index	P_{det}	index	P_{det}
1	1.78E−20	16	1.00E−16	31	5.62E−13
2	3.16E−20	17	1.78E−16	32	1.00E−12
3	5.62E−20	18	3.16E−16	33	1.78E−12
4	100.E−19	19	5.62E−16	34	3.16E−12
5	1.78E−19	20	1.00E−15	35	5.62E−12
6	3.16E−19	21	1.78E−15	36	1.00E−11
7	5.62E−19	22	3.16E−15	37	1.78E−11
8	1.00E−18	23	5.62E−15	38	3.16E−11
9	1.78E−18	24	1.00E−14	39	5.62E−11
10	3.16E−18	25	1.78E−14	40	1.00E−10
11	5.62E−18	26	3.16E−14	41	1.78E−10
12	1.00E−17	27	5.62E−14	42	3.16E−10
13	1.78E−17	28	1.00E−13	43	5.62E−10
14	3.16E−17	29	1.78E−13	44	1.00E−09
15	5.62E−17	30	3.16E−13	45	1.78E−09

The final in-band power obtained in OLP is derived from a linear interpolation in logarithmic space in between $log(P_{det}(i-1))$ and $log(P_{det}(i))$ based on $P_{FCS}(i-1)$, $P_{FCS}(i)$ and $P_{FCS,meas}$.

The properties (FCS1,TRS2) altered between rev 93 and 94 due to unknown reasons. This event changed the FCS calibration for those detectors for which the (FCS1,TRS2) combination is used namely: P3, C100, and C200. For these detectors two calibration files are available: one for FCS measurements obtained before rev 94 (suffix _01) and one for rev 94 and higher (suffix _02).

During the ISO mission only specific FCS/TRS combinations were used. Entries in the Cal-G files that do not refer to these settings have been set to zero:

- FCS1/TRS1: P1, P2
- FCS1/TRS2: P3, C100, C200
- FCS2/TRS1: P1, P2 chopped mode
- FCS2/TRS2: P3, C100, C200 chopped mode

Example: for detector P2, settings FCS1/TRS2 and FCS2/TRS2 are not allowed and therefore set to zero in the corresponding table.

For all FCS power calibration tables, the following FITS keywords are common:

NAXIS = 4
TYPE = REAL*4

14.12.1 Product PP1FCSPOW: PHT-P1 FCS power calibration table

AXIS	Length	Description
1	45	Index for in-band optical power on detector
2	10	Filters ordered according to (see Section A.1):

		3.3, 3.6, 4.8, 7.3, 7.7, 10, 11.3, 12.8, 15, 12 μm
3	2	Each TRS: TRS1, TRS2
4	2	Each FCS: FCS1, FCS2

14.12.2 Product PP2FCSPOW: PHT-P2 FCS power calibration table

AXIS	Length	Description
1	45	Index for in-band optical power on detector
2	2	Filters ordered according to: 20, 25 μm
3	2	Each TRS: TRS1, TRS2
4	2	Each FCS: FCS1, FCS2

14.12.3 Product PP3FCSPOW_01/02: PHT-P3 FCS power calibration table

AXIS	Length	Description
1	45	Index for in-band optical power on detector
2	2	Filters ordered according to: 60, 100 μm
3	2	Each TRS: TRS1, TRS2
4	2	Each FCS: FCS1, FCS2

14.12.4 Product PC1FCSPOW_01/02: PHT-C100 FCS power calibration table

AXIS	Length	Description
1	45	Index for in-band optical power on detector (see Section A.1)
2	7	Filters ordered according to (see Section A.1): 90(backup), 65, 60, 80, 100, 105, 90 μm
3	2	Each TRS: TRS1, TRS2
4	2	Each FCS: FCS1, FCS2

14.12.5 Product PC2FCSPOW_01/02: PHT-C200 FCS power calibration table

AXIS	Length	Description
1	45	Index for in-band optical power on detector
2	5	Filters ordered according to (see Section A.1): 170, 200, 180, 150, 120 μm
3	2	Each TRS: TRS1, TRS2
4	2	Each FCS: FCS1, FCS2

14.13 PHT-P and PHT-C Default Responsivities

```
Description Parameter:          Sections 4.2.1, 4.2.4
Processing Level:               SPD
Usage in processing:            Section 7.10
File Type:                      FITS Image
Units:                          A/W
File names:                     PPRESP_01, PPRESP_02,
                                PC1RESP_01, PC1RESP_02,
                                PC2RESP_01, PC2RESP_02
```

Default responsivities are used in case:

- no FCS measurements were collected during an observation (except for PHT40, see Section 14.19),

For staring mode observations with the PHT-P or PHT-C subsystems, default detector responsivities are not needed as long as at least one FCS measurement was obtained per detector. However, it can happen that no FCS measurements were collected (due to e.g. data dropouts from telemetry loss) or that the quality of the FCS measurement is insufficient (due to e.g. complete saturation). In those cases default responsivities will be applied in the conversion from signal in V/s to an in-band power on the detector in W.

The detector responsivity is a function of orbital phase. At the end of the science window the responsivities of all detectors are higher than at the beginning. For detectors P3, C100, and C200 two sets of orbital dependencies are provided: one set for observations before rev 150 (files have suffix _01), the other set for rev 150 and later (files have suffix _02). At rev 150 an additional detector curing procedure was introduced sometime after apogee passage which restores the responsivity to the same level as that at the beginning of the science window.

Since the responsivities are provided in A/W, the conversion from V/s to W can only be carried out if the integration capacities C_{int} associated with a detector are known, see also Section 4.2.1. The capacitances are listed in Table 14.5.

Table 14.5: *Integration capacities associated with detectors.*

Detector	Capacitance [As/V]
P1	9×10^{-14}
P2	9×10^{-14}
P3	9×10^{-14}
C100	9×10^{-14}
C200	14×10^{-14}
SS	5.26×10^{-14}
SL	6.3×10^{-14}

Notes

- 1 A/(V/s) = 1 Farad
- For the arrays, capacitances refer to individual pixels.

For all default responsivity tables, the following FITS keywords are common:

NAXIS = 3
TYPE = REAL*4

14.13.1 Product PPRESP_01/02: PHT default responsivities for P1, P2 and P3 detectors

AXIS	Length	Description
1	100	Orbital phase: each element corresponds to a phase in the range from 0.01 to 1.0 in steps of 0.01
2	3	PHT-P detectors, P1,P2,P3
3	2	Default responsivity and uncertainty

14.13.2 Product PC1RESP_01/02: PHT default responsivities for the C100 detector

AXIS	Length	Description
1	100	Orbital phase: each element corresponds to a phase in the range from 0.01 to 1.0 in steps of 0.01
2	9	C100 pixels, in same order as in SPD
3	2	Default responsivity and uncertainty

14.13.3 Product PC2RESP_01/02: PHT default responsivities for the C200 detector

AXIS	Length	Description
1	100	Orbital phase: each element corresponds to a phase in the range from 0.01 to 1.0 in steps of 0.01
2	4	C200 pixels, in same order as SPD
3	2	Default responsivity and uncertainty

Note:
• see Section 2.6.2 for definition of C-arrays pixel identifiers

14.14 Array Illumination by FCS

```
Description Parameter:      Section 4.5.4
Processing Level:           SPD
Usage in processing:        Section 7.10.4
File Type:                  Fits Image
Units:                      dimensionless
Number of Records:          1
File Names:                 PC1ILLUM_01, PC1ILLUM_02,
                            PC2ILLUM_01, PC2ILLUM_02,
```

The FCS illumination is not uniform. For the PHT-C arrays, the non-uniform illumination requires a pixel dependent correction to the FCS power calibration table which gives only the mean value over the pixel array. Note that the illumination correction products contain only 1 record.

The properties (FCS1,TRS2) altered between rev 93 and 94 due to unknown reasons. This event changed the FCS illumination pattern. Therefore two calibration files are available: one for before rev 94 (suffix _01) and one for rev 94 and higher (suffix _02).

All products have:
NAXIS = 4
TYPE = R*4

14.14.1 Product PC1ILLUM_01/02: FCS illumination correction for C100

AXIS	Length	Description
1	9	C100 Pixels, in same order as SPD
2	7	[CHWII position − 1] (see Section A.1)
3	2	each FCS
4	2	Correction and uncertainty

14.14.2 Product PC2ILLUM_01/02: FCS illumination correction for C200

AXIS	Length	Description
1	4	C200 Pixels, in same order as SPD
2	5	[CHWII position − 8] (see Section A.1)
3	2	each FCS
4	2	Correction and uncertainty

14.15 Inhomogeneous FCS illumination of PHT-P

```
Description Parameter:          Section 4.5.4
Processing Level:               SPD
Usage in processing:            Section 7.10.3
File Type:                      FITS Image
Units:                          dimensionless
File Names:                     PP1FCSAP, PP2FCSAP, PP3FCSAP,
```

As already implemented for PHT-C (FCS illumination matrices 'PC1ILLUM' in Section 14.14.1 and 'PC2ILLUM' in Section 14.14.2), the PHT-P calibration must also be corrected for inhomogenous FCS illumination. This implies that the power on the detector from the FCS does not scale directly with the aperture area (which whould be the case for a perfectly homogeneous illumination) but that an additional correction factor is necessary.

For all aperture correction Cal-G files the following FITS keywords are common:
NAXIS = 4
TYPE = REAL*4

14.15.1 Product PP1FCSAP: FCS aperture correction tables for P1

AXIS	Length	Description
1	14	apertures: CHWII position (see Section A.1)
2	10	filters: CHWIII position (see Section A.1)
3	2	Each FCS
4	2	Correction and uncertainty

14.15.2 Product PP2FCSAP: FCS aperture correction tables for P2

AXIS	Length	Description
1	14	apertures: CHWII position (see Section A.1)
2	2	filters: 20, 25 μm
3	2	Each FCS
4	2	Correction and uncertainty

14.15.3 Product PP3FCSAP: FCS aperture correction tables for P3

AXIS	Length	Description
1	14	Apertures: CHWII position (see Section A.1)
2	2	Filters: 60, 100 μm
3	2	Each FCS
4	2	Correction and uncertainty

14.16 PHT-P Filter-to-Filter Corrections

```
Description Parameter:          Section 7.10.3
Processing Level:               SPD
Usage in processing:            Section 7.10.3
File Type:                      FITS image
File names:                     PPFTOF
```

This calibration table lists for a given PHT-P detector the relative filter corrections in order to obtain the same detector responsivity for each filter of that detector, see Section 7.10.3. The corrections are normalised to the largest value in the filter sample.

The product has:
NAXIS = 2
TYPE = R*4

14.16.1 Product PPFTOF: PHT-P filter-to-filter correction

AXIS	Length	Description
1	14	Filters
2	2	Correction and uncertainty

Filters 1 to 10 correspond to PHT-P1, filters 11 and 12 correspond to PHT-P2, and filters 13 and 14 correspond to PHT-P3.

14.17 Wavelength Dependent Detector Flat-Fields

```
Description Parameter:          Section 4.2.7
Processing Level:               SPD
Usage in processing:            Section 7.10.4
File Type:                      FITS Image
Units:                          Dimensionless
File Names:                     PC1FLAT, PC2FLAT
```

The responsivity of the individual detector pixels in the C100 and the C200 arrays vary from one filter to the other. These variations are different for different pixels in the array. Consequently, the flat-field of the array differs from one filter to the other. The flat-field is in principle calibrated out by the FCS measurement, but for multi-filter measurements where only 1 FCS measurement is taken, the flat-field correction must be applied when determining the fluxes in the filters in which the FCS was not taken.

For both detector flat-field calibration files the following FITS keywords are common:
NAXIS = 3
TYPE = REAL*4

14.17.1 Product PC1FLAT: PHT C100 filter-to-filter flat-field correction

AXIS	Length	Description
1	9	C100 pixels, in same order as SPD.
2	7	filters: [CHWII position – 1] (see Section A.1)
3	2	Correction and uncertainty

14.17.2 Product PC2FLAT: PHT C200 filter-to-filter flat-field correction

AXIS	Length	Description
1	4	C200 pixels in the same order as in SPD
2	5	Filters: [CHWII position – 8] (see Section A.1)
3	2	Correction and uncertainty

14.18 Point Spread Function Corrections

```
Description Parameter:      Section 4.5.2
Processing Level:           AAR
Usage in processing:        Section 8.4.6, 8.4.7
File Type:                  FITS Image (PPPSF), Binary FITS table (PCPSF)
Units:                      dimensionless
File Names:                 PPPSF, PCPSF
```

This calibration product lists for each wavelength band of PHT-P the fraction of the point source power that passes a given aperture size. The correction factors are needed in the conversion from power on the detector in [W] to point source flux in [Jy].

For the C100 and C200 detector arrays a separate Cal-G file is available which contains the fraction of point source power falling (1) on the entire array and (2) on a single pixel.

14.18.1 Product PPPSF: PHT-P point spread function corrections

NAXIS = 2
TYPE = R*4

AXIS	Length	Description
1	14	Corrections: for 14 P-apertures
2	14	Filter wheel positions

14.18.2 Product PCPSF: PHT-C point spread function corrections

Binary FITS table with record length 12. The record fields are:

Field	Offset	Number	Type	Description
PCPSFFIL	0	1	I*4	Filter (CHW position)
PCPSFPIX	4	1	R*4	PSF correction per pixel
PCPSFARR	8	1	R*4	PSF correction for array

14.19 PHT-S Wavelength and Signal Calibration

```
Description Parameter:      Section 4.6.2, 5.2.6
Processing Level:           SPD and AAR
Usage in processing:        Section 7.6 for SPD usage and Section 8.6 for AAR usage
File Type:                  Binary Fits Table
Number of Records:          128
File Names:                 PSPECAL
```

For each pixel in the PHT-SS and PHT-SL array the corresponding central wavelengths and spectral response are listed. The spectral response is given in units of [V/s/Jy] for point sources and in

[V/s/(MJy/sr)] for extended sources. These numbers provide a direct conversion from a pixel signal to a point source flux (in [Jy]) or a surface brightness (in [MJy/sr]) on the sky. The conversion assumes (1) a constant responsivity for the PHT-S arrays with time and orbital position and (2) no positional dependence of the source with respect to the centre of the aperture.

For PHT-S chopped observations two correction coefficients A^0_{pixel} and A^1_{pixel} are included for each pixel. These coefficients provide a fist order correction to the average spectral response function for chopped observations.

The records are filled as follows: data of PHT-SS pixels 1–64 are stored in records 1–64, PHT-SL pixels 1–64 are stored in records 65–128.

14.19.1 Product PSPECAL: PHT-S wavelength and signal calibration

Binary FITS table with record length 56 bytes. The record fields are:

Field	Offset	Number	Type	Description
PSPELAMB	0	1	R*4	Wavelength in m (increasing)
PSPELUNC	4	1	R*4	Uncertainty
PSPESRFP	8	1	R*4	Point source srf $C^p_{ave}(i)$ [(V/s)/Jy]
PSPESRUP	12	1	R*4	Uncertainty
PSPESRFE	16	1	R*4	Extended source srf $C^e_{ave}(i)$ [(V/s)/(MJy/sr)]
PSPESRUE	20	1	R*4	Uncertainty
PSPECRFP	24	1	R*4	Average chopped point source srf [(V/sec)/Jy]
PSPECRUP	28	1	R*4	Uncertainty
PSPECRFE	32	1	R*4	Average chopped extended source srf [(V/s)/Jy]
PSPECRUE	36	1	R*4	Uncertainty
PSPECCC0	40	1	R*4	$A^0(i)$, see Equation 7.61
PSPECUC0	44	1	R*4	Uncertainty
PSPECCC1	48	1	R*4	$A^1(i)$, see Equation 7.61
PSPECUC1	52	1	R*4	Uncertainty

Note:
srf = spectral response function

14.20 Conversion from Power on Detector to Flux Density

```
Description Parameter:          Equations 5.10 and 5.11
Processing Level:               AAR
Usage in processing:            Section 8.4.6 and 8.4.7
File Type:                      FITS Header
File Names:                     PFLUXCONV
```

The transmission of the whole optical path for each filter is characterised by the parameter C1 in m^2Hz. The effective size of the primary mirror, reflections, filter transmission, spectral response of the detector, etc. are included. The C1 values for all filters are given in this calibration file. Also included are the reference wavelengths of the filter bands.

14.20.1 Product PFLUXCONV: PHT-P/C power calibration

PFLUXCONV is a FITS header *without* accompanying data. All entries listed here have unit: m^2Hz.

Keyword	Type	Description
FCP3P29	R	conversion for P1 3.3 μm filter
FCP3P6	R	conversion for P1 3.6 μm filter
FCP4P85	R	conversion for P1 4.8 μm filter
FCP7P3	R	conversion for P1 7.3 μm filter
FCP7P7	R	conversion for P1 7.7 μm filter
FCP10	R	conversion for P1 10 μm filter
FCP11P3	R	conversion for P1 11.3 μm filter
FCP11P5	R	conversion for P1 12 μm filter
FCP12P8	R	conversion for P1 12.8 μm filter
FCP16	R	conversion for P1 15 μm filter
FCP20	R	conversion for P2 20 μm filter
FCP25	R	conversion for P2 25 μm filter
FCP60	R	conversion for P3 60 μm filter
FCP100	R	conversion for P3 100 μm filter
FCC50	R	conversion for C100 65 μm filter
FCC60	R	conversion for C100 60 μm filter
FCC70	R	conversion for C100 80 μm filter
FCC90	R	conversion for C100 90 μm filter
FCC100	R	conversion for C100 100 μm filter
FCC105	R	conversion for C100 105 μm filter
FCC120	R	conversion for C200 120 μm filter
FCC135	R	conversion for C200 150 μm filter
FCC160	R	conversion for C200 170 μm filter
FCC180	R	conversion for C200 180 μm filter
FCC200	R	conversion for C200 200 μm filter

14.20.2 Product PFLUXCONV: PHT-P/C reference wavelengths

PFLUXCONV is a FITS header *without* accompanying data. All entries listed below have units: m.

Keyword	Type	Description
CWP3P29	R	reference wavelength of P1 3.3 μm filter (m)
CWP3P6	R	reference wavelength of P1 3.6 μm filter (m)
CWP4P85	R	reference wavelength of P1 4.8 μm filter (m)
CWP7P3	R	reference wavelength of P1 7.3 μm filter (m)
CWP7P7	R	reference wavelength of P1 7.7 μm filter (m)
CWP10	R	reference wavelength of P1 10 μm filter (m)
CWP11P3	R	reference wavelength of P1 11.3 μm filter (m)
CWP11P5	R	reference wavelength of P1 12 μm filter (m)
CWP12P8	R	reference wavelength of P1 12.8 μm filter (m)
CWP16	R	reference wavelength of P1 16 μm filter (m)
CWP20	R	reference wavelength of P2 20 μm filter (m)
CWP25	R	reference wavelength of P2 25 μm filter (m)
CWP60	R	reference wavelength of P3 60 μm filter (m)

CWP100	R	reference wavelength of P3 100 μm filter (m)
CWC50	R	reference wavelength of C100 65 μm filter (m)
CWC60	R	reference wavelength of C100 60 μm filter (m)
CWC70	R	reference wavelength of C100 80 μm filter (m)
CWC90	R	reference wavelength of C100 90 μm filter (m)
CWC100	R	reference wavelength of C100 100 μm filter (m)
CWC105	R	reference wavelength of C100 105 μm filter (m)
CWC120	R	reference wavelength of C200 120 μm filter (m)
CWC135	R	reference wavelength of C200 150 μm filter (m)
CWC160	R	reference wavelength of C200 170 μm filter (m)
CWC180	R	reference wavelength of C200 180 μm filter (m)
CWC200	R	reference wavelength of C200 200 μm filter (m)

14.21 Effective Solid Angles of Apertures and Pixels

```
Description Parameter:        Sections 4.5.1, 5.2.5 and 5.3
Processing Level:             AAR
Usage in processing:          Section 8.4.7
File Type:                    Binary FITS Table
File Names:                   PPOMEGA, PC1OMEGA, PC2OMEGA
```

In the conversion from flux per pixel or per aperture (in Jy/beam) to surface brightness (in MJy/sr) the effective solid angles Ω_{eff} are required. In the present set of Cal-G files, the effective solid angles were obtained from a model calculation which takes into account the ISO primary mirror, secondary mirror, tripod, and the linear sizes of the apertures and the detectors as measured pre-flight.

The Cal-G files also contain the dimensions of the apertures (in case of P1, P2, and P3) or the offsets and dimensions of the detector pixels (in case of C100 and C200) as projected on the sky in arcseconds. Fields for the uncertainties of all parameters are included.

The Cal-G files related contain the following limitations:

- all uncertainties have been set to zero,
- the effective solid angles of the PHT-P apertures are the physical dimensions of the apertures in the focal plane projected on the sky.

In case the PHT-P aperture areas (in mm^2) are required, OLP uses a hardcoded list of aperture versus focal plane area (parameter $A(a)$ in Section 5.2.5 and in Section 7.10.3). The values of the areas are listed in Section A.1.2.

14.21.1 Product PPOMEGA: aperture dimensions and solid angles for P1, P2, and P3

Binary FITS table with record length 32. The record fields are:

Field	Offset	Number	Type	Description
PPOMFILT	0	1	I*4	Filter (CHW position)
PPOMAPER	4	1	I*4	Aperture (CHW position)
PPOMDASY	8	1	R*4	Aperture diameter in Y in arcsec

PPOMDAYU	12	1	R*4	Uncertainty in aperture diameter in Y in arcsec
PPOMDASZ	16	1	R*4	Aperture diameter in Z in arcsec
PPOMDAZU	20	1	R*4	Uncertainty in aperture diameter in Z in arcsec
PPOMOMEG	24	1	R*4	Effective Omega (in 10^{-7}sr)
PPOMOMUN	28	1	R*4	Uncertainty in Omega (in 10^{-7}sr)

14.21.2 Product PC1OMEGA: dimensions and solid angles for C100 pixels

Binary FITS table with record length 48. The record fields are:

Field	Offset	Number	Type	Description
PC1OMFIL	0	1	I*4	Filter (CHW position)
PC1OMPIX	4	1	I*4	Pixel in SPD order
PC1OMOFY	8	1	R*4	Offset in y relative to centre of array in arcsec
PC1OMOYU	12	1	R*4	Uncertainty in offset in y in arcsec
PC1OMOFZ	16	1	R*4	Offset in z relative to centre of array in arcsec
PC1OMOZU	20	1	R*4	Uncertainty in offset in Z in arcsec
PC1OMDAY	24	1	R*4	Aperture dimension y in arcsec
PC1OMDYU	28	1	R*4	Uncertainty in aperture dimension y in arcsec
PC1OMDAZ	32	1	R*4	Aperture dimension z in arcsec
PC1OMDZU	36	1	R*4	Uncertainty in aperture dimension z in arcsec
PC1OMOME	40	1	R*4	Effective Omega (in 10^{-7}sr)
PC1OMOMU	44	1	R*4	Uncertainty in omega (in 10^{-7}sr)

14.21.3 Product PC2OMEGA: dimensions and solid angles for C200 pixels

Same file and record structure as PC1OMEGA (Section 14.21.2), however all keywords start with 'PC2' instead of PC1.

14.22 Colour Corrections

```
Description Parameter:          Appendix C
Processing Level:               none
Usage in processing:            N/A
File Type:                      Binary FITS Table
File Names:                     PCCBB, PCCMBBONE, PCCMBBTWO, PCCPOWER
```

The colour correction tables are not used in OLP. Since the colour corrections depend on source specific assumptions, no efforts were made for implementation in OLP. The Cal-G products give the observer the possibility to apply colour corrections. Colour corrections are provided for 4 different models of the infrared continuum: blackbody $B_\nu(T)$, modified blackbodies $\nu^\alpha \cdot B_\nu(T)$ with $\alpha = 1$ and 2, and power-law continua ν^α. A description of the derivation of the colour corrections is given in Appendix C.

The flux density value in OLP which refers to a source spectrum $F_\nu \propto \nu^{-1}$ has to be *divided* by the colour correction factor associated to the assumed source spectrum.

14.22.1 Product PCCBB: black body $B_\nu(T)$ colour correction

Binary FITS table with record length 104. The record fields are:

Field	Offset	Number	Type	Description
TEMP	0	1	R*4	Temperature in K
P1_3.29	4	1	R*4	P1 3.3 μm correction
P1_3.60	8	1	R*4	P1 3.6 μm correction
P1_4.85	12	1	R*4	P1 4.8 μm correction
P1_7.30	16	1	R*4	P1 7.3 μm correction
P1_7.70	20	1	R*4	P1 7.7 μm correction
P1_10.0	24	1	R*4	P1 10 μm correction
P1_11.3	28	1	R*4	P1 11.3 μm correction
P1_11.5	32	1	R*4	P1 12 μm correction
P1_12.8	36	1	R*4	P1 12.8 μm correction
P1_16.0	40	1	R*4	P1 15 μm correction
P2_20	44	1	R*4	P2 20 μm correction
P2_25	48	1	R*4	P2 25 μm correction
P3_60	52	1	R*4	P3 60 μm correction
P3_100	56	1	R*4	P3 100 μm correction
C1_50	60	1	R*4	C100 70 μm correction
C1_60	64	1	R*4	C100 60 μm correction
C1_70	68	1	R*4	C100 80 μm correction
C1_90	72	1	R*4	C100 90 μm correction
C1_100	76	1	R*4	C100 100 μm correction
C1_105	80	1	R*4	C100 105 μm correction
C2_120	84	1	R*4	C200 120 μm correction
C2_135	86	1	R*4	C200 150 μm correction
C2_160	92	1	R*4	C200 170 μm correction
C2_180	96	1	R*4	C200 180 μm correction
C2_200	100	1	R*4	C200 200 μm correction

14.22.2 Product PCCMBBONE: modified black body $\nu^1 \cdot B_\nu(T)$ colour correction

Same file structure as in Section 14.22.1

14.22.3 Product PCCMBBTWO: modified black body $\nu^2 \cdot B_\nu(T)$ colour correction

Same file structure as in Section 14.22.1

14.22.4 Product PCCPOWER: Power-law ν^α colour correction

Same file structure as in Section 14.22.1, but instead of temperature in field 1, the exponent α of the power-law is given.

14.23 Footprint Matrices for PHT-P and C

```
Description Parameter:          none
Processing Level:               none, service to observer
Usage in processing:            N/A
File Type:                      FITS Image
File names:                     PP2FOOTP, PP3FOOTP, PC1FOOTP, PC2FOOTP
```

Using a model for the primary mirror, secondary mirror and tripod, the theoretical point spread function (PSF) was obtained assuming a given wavelength. By convolving the PSF with the geometrical properties of the apertures and detectors, synthetic *footprints* or *beam profiles* were derived for each filter. The footprints are monochromatic assuming the reference wavelength of the filter. The footprint matrices give at each listed position the fraction of the total power in the PSF falling on the aperture or pixel if the geometrical centre of the aperture or pixel is placed at position (0,0). The matrices are aligned with the spacecraft Y and Z-directions.

The high degree of asymmetry found in the measured P1 beam profiles cannot be explained with the present model. It has been decided to postpone the release of synthetic P1 footprints until a refined understanding of the P1 beams is available.

The footprint matrices can be used for accurate photometry in maps, e.g. for extracting accurate point source fluxes from an underlying extended component or in crowded fields.

14.23.1 Product PP2FOOTP: PHT-P2 footprint matrices

NAXIS = 4
TYPE = R*4

AXIS	Length	Description
1	2	Filters (20, 25 μm
2	14	Apertures (Change Wheel position)
3	87	Y-direction - $2''$ steps for apertures $< 18''$
		$3''$ steps for apertures $\geq 18''$
4	87	Z-direction - $2''$ steps for apertures $< 18''$
		$3''$ steps for apertures $\geq 18''$

14.23.2 Product PP3FOOTP: PHT-P3 footprint matrices

NAXIS = 4
TYPE = R*4

AXIS	Length	Description
1	2	Filters (60, 100 μm
2	14	Apertures (Change Wheel position)
3	87	Y-direction - $2''$ steps for apertures $< 52''$
		$10''$ steps for apertures $\geq 18''$
4	87	Z-direction - $2''$ steps for apertures $< 18''$
		$10''$ steps for apertures $\geq 18''$

14.23.3 Product PC1FOOTP: PHT-C100 footprint matrices

NAXIS = 3
TYPE = R*4

AXIS	Length	Description
1	7	Filters (C100, in wheel position order)
2	35	Y-direction - 7.5″ steps
3	35	Z-direction - 7.5″ steps

14.23.4 Product PC2FOOTP: PHT-C200 footprint matrices

NAXIS = 3
TYPE = R*4

AXIS	Length	Description
1	5	Filters (C200, in wheel position order)
2	35	Y-direction - 15″ steps
3	35	Z-direction - 15″ steps

14.24 Relative System Responses

```
Description Parameter:          none
Processing Level:               none, service to observer
Usage in processing:            N/A
File Type:                      Binary FITS table
File names:                     PPFILTRAN, PCFILTRAN
```

These Cal-G products contain the relative system responses as a function of wavelength of the PHT-P and PHT-C subsystems. The tables can be used to perform dedicated colour corrections to the photometry of sources with spectral energy distributions different from those tabulated in the colour correction tables described in Section 14.22.

14.24.1 Product PPFILTRAN: PHT-P relative system response

Binary FITS table with record length 112 bytes. The record fields are:

Field	Offset	Number	Type	Description
LP3P29	0	1	R*4	Wavelength in micron for PHT-P1 3.3 micron filter
SRP3P29	4	1	R*4	Spectral response for PHT-P1 3.3 micron filter
LP3P6	8	1	R*4	Wavelength in micron for PHT-P1 3.6 micron filter
SRP3P6	12	1	R*4	Spectral response for PHT-P1 3.6 micron filter
LP4P85	16	1	R*4	Wavelength in micron for PHT-P1 4.8 micron filter
SRP4P85	20	1	R*4	Spectral response for PHT-P1 4.85 micron filter

LP7P3	24	1	R*4	Wavelength in micron for PHT-P1 7.3 micron filter
SRP7P3	28	1	R*4	Spectral response for PHT-P1 7.3 micron filter
LP7P7	32	1	R*4	Wavelength in micron for PHT-P1 7.7 micron filter
SRP7P7	36	1	R*4	Spectral response for PHT-P1 7.7 micron filter
LP10	40	1	R*4	Wavelength in micron for PHT-P1 10 micron filter
SRP10	44	1	R*4	Spectral response for PHT-P1 10 micron filter
LP11P3	48	1	R*4	Wavelength in micron for PHT-P1 11.3 micron filter
SRP11P3	52	1	R*4	Spectral response for PHT-P1 11.3 micron filter
LP11P5	56	1	R*4	Wavelength in micron for PHT-P1 12 micron filter
SRP11P5	60	1	R*4	Spectral response for PHT-P1 12 micron filter
LP12P8	64	1	R*4	Wavelength in micron for PHT-P1 12.8 micron filter
SRP12P8	68	1	R*4	Spectral response for PHT-P1 12.8 micron filter
LP16	72	1	R*4	Wavelength in micron for PHT-P1 15 micron filter
SRP16	76	1	R*4	Spectral response for PHT-P1 15 micron filter
LP20	80	1	R*4	Wavelength in micron for PHT-P2 20 micron filter
SRP20	84	1	R*4	Spectral response for PHT-P2 20 micron filter
LP25	88	1	R*4	Wavelength in micron for PHT-P2 25 micron filter
SRP25	92	1	R*4	Spectral response for PHT-P2 25 micron filter
LP60	96	1	R*4	Wavelength in micron for PHT-P3 60 micron filter
SRP60	100	1	R*4	Spectral response for PHT-P3 60 micron filter
LP100	104	1	R*4	Wavelength in micron for PHT-P3 100 micron filter
SRP100	108	1	R*4	Spectral response for PHT-P3 100 micron filter

14.24.2 Product PCFILTRAN: PHT-C relative system response

Binary FITS table with record length 56 bytes. The record fields are:

Field	Offset	Number	Type	Description
LC50	0	1	R*4	Wavelength in micron for C100 65 micron filter
SRC50	4	1	R*4	Spectral response for C100 65 micron filter
LC60	8	1	R*4	Wavelength in micron for C100 60 micron filter
SRC60	12	1	R*4	Spectral response for C100 60 micron filter
LC70	16	1	R*4	Wavelength in micron for C100 80 micron filter
SRC70	20	1	R*4	Spectral response for C100 80 micron filter
LC90	24	1	R*4	Wavelength in micron for C100 90 micron filter
SRC90	28	1	R*4	Spectral response for C100 90 micron filter
LC100	32	1	R*4	Wavelength in micron for C100 100 micron filter
SRC100	36	1	R*4	Spectral response for C100 100 micron filter
LC105	40	1	R*4	Wavelength in micron for C100 105 micron filter
SRC105	44	1	R*4	Spectral response for C100 105 micron filter
LC120	48	1	R*4	Wavelength in micron for C200 120 micron filter
SRC120	52	1	R*4	Spectral response for C200 120 micron filter
LC135	56	1	R*4	Wavelength in micron for C200 150 micron filter
SRC135	60	1	R*4	Spectral response for C200 150 micron filter
LC160	64	1	R*4	Wavelength in micron for C200 170 micron filter
SRC160	68	1	R*4	Spectral response for C200 170 micron filter
LC180	72	1	R*4	Wavelength in micron for C200 180 micron filter
SRC180	76	1	R*4	Spectral response for C200 180 micron filter
LC200	80	1	R*4	Wavelength in micron for C200 200 micron filter
SRC200	84	1	R*4	Spectral response for C200 200 micron filter

Appendix A

Instrument Tables

A.1 Mean Filter/Aperture Specifications

A.1.1 PHT-P filters

The PHT-P filters were located on Change Wheel III (CHW3). Each wheel position is indicated by an integer. In Table A.1 the filter specifications corresponding to a Change Wheel III position have been listed. The values for the spectral resolution ($\lambda_c/\Delta\lambda$) and airy diameter (d_{Airy}) were measured in the laboratory. The system responses (R_{mean}) were derived from in-flight data. The reference central wavelength (λ_{ref}) is defined as a wavelength close to the isophotal centre of the filter, and where possible, matching values given for filters corresponding to other ISO and IRAS instruments (see Moneti, Metcalfe & Schulz 1997, [39]).

Table A.1: *Description of the PHT-P filters on CHWIII.*

Wheel position	Filter ID	λ_{ref} [μm]	$\lambda_c/\Delta\lambda$	R_{mean}	d_{Airy} [$''$]	description
1	P1_3p29_UM	3.3	15.16	0.103	2.8	PAH
2	P1_3p6_UM	3.6	3.62	0.136	3.0	Cosmological gap, see ISOCAM
3	P1_4p85_UM	4.8	3.14	0.159	4.1	Continuum
4	P1_7p3_UM	7.3	2.19	0.275	6.2	Continuum
5	P1_7p7_UM	7.7	9.32	0.249	6.4	PAH
6	P1_10_UM	10.0	5.55	0.345	8.4	sillicate feature
7	P1_11p3_UM	11.3	14.07	0.293	9.5	PAH
8	P1_12p8_UM	12.8	5.55	0.517	10.8	Continuum
9	P1_16p0_UM	15.0	5.33	0.354	13.8	Continuum
10	P1_11p5_UM	12.0	1.82	0.483	10.0	IRAS 12 μm see ISOCAM
11	P2_20_UM	20.0	2.33	0.321	17.7	Close to Q band
12	P2_25_UM	25.0	2.61	0.375	20.0	IRAS 25 μm
13	P3_60_UM	60.0	2.35	0.112	50.3	IRAS 60
14	P3_100_UM	100.0	2.59	0.305	83.9	IRAS 100

A.1.2 PHT-P apertures

The PHT-P apertures were located on the inner circle of Change Wheel II (CHW2). Each wheel position is indicated by an integer. In Table A.2 the aperture specifications corresponding to a Change Wheel II position have been listed.

Table A.2: *Description of the PHT-P apertures located on CHWII.*

Wheel position	Aperture ID	Diameter [″]	Area [mm^2]	Solid Angle [10^{-8} sr]	description
1	52_SEC	52	4.1548	5.13	circular 2.3 mm
2	79_SEC	79	9.0792	11.21	circular 3.4 mm
3	99_SEC	99	14.522	17.93	circular
4	120_SEC	120	21.237	26.22	circular
5	127×127_SEC	127×127	30.250	37.3	square
6	180_SEC	180	48.398	59.8	circular
7	180_SEC_XBLK				not used
8	5_SEC	5	0.0314	0.039	circular
9	7p6_SEC	7.6	0.1001	0.124	circular
10	10_SEC	10	0.1735	0.214	circular
11	13p8_SEC	13.8	0.2827	0.349	circular
12	18_SEC	18	0.5281	0.625	circular
13	20×32_SEC	20×32	1.1288	1.39	rectangular
14	23_SEC	23	0.7854	0.97	circular

A.1.3 PHT-C filters

The PHT-C filters were located in the outer circle of Change Wheel II (CHW2). In Table A.3 the filter specifications corresponding to a Change Wheel II position have been listed. The values for the spectral resolution ($\lambda_c/\Delta\lambda$) were measured in the laboratory. The point spread function factor for the fraction of the psf falling on the entire array (f_{PSF}^{array}, Laureijs 1999, [32]) and the system responses (R_{mean}) were derived from in-flight data. The values of f_{PSF}^{array} and those of f_{PSF} (Tables 2.3 and 2.8) are included in Cal G files PPPSF and PCPSF (Section 14.18). The reference wavelength (λ_{ref}) is defined as a wavelength close to the isophotal centre of the filter, and where possible, matching values are given for filters corresponding to other ISO and IRAS instruments (see Moneti, Metcalfe & Schulz 1997, [39]).

The point spread function factor represents the fraction of the power in the beam falling on the whole detector array if the beam is centred on the array (the values have been derived from in-flight data, see Chapter 10 for an explanation). The geometrical solid angles of the pixels are slightly filter dependent, their averages are:

$\Omega_{C100} = 0.0688{\times}10^{-6}$ sr
$\Omega_{C200} = 0.281{\times}10^{-6}$ sr

A.1.4 Other filterwheel components

Change Wheel I (CHW1) is either used to redirect the light to the next optical component such as PHT-S, the inner Change Wheel II and the outer Change Wheel II, or is used to put a polariser in the beam. In Table A.4 the specifications corresponding to a Change Wheel I position have been listed.

Table A.3: *Description of the PHT-C filters on CHWII.*

Wheel position	Filter ID	λ_{ref} [μm]	$\lambda_c/\Delta\lambda$	R_{mean}	f_{psf} [$''$]	description
1	C100_OPEN					not used
2	C100_90_RED	90	1.73	0.759	N/A	wide band cont.(backup)
3	C100_50_UM	65	1.13	0.044	0.799±0.006	continuum
4	C100_60_UM	60	2.51	0.130	0.782±0.004	continuum IRAS 60 μm
5	C100_70_UM	80	1.67	0.122	0.831±0.007	continuum
6	C100_100_UM	100	2.18	0.268	0.757±0.008	continuum IRAS 100 μm
7	C100_105_UM	105	2.79	0.236	0.764±0.010	continuum
8	C100_90_UM	90	1.69	0.296	0.759±0.008	wide band continuum
9	C200_160_UM	170	1.94	0.425	0.512±0.020	wide band continuum
10	C200_200_UM	200	3.55	0.219	0.667±0.019	continuum
11	C200_180_UM	180	2.63	0.327	0.601±0.045	continuum
12	C200_135_UM	150	1.91	0.259	0.552±0.028	continuum
13	C200_120_UM	120	2.40	0.131	0.489±0.028	continuum
14	C200_RETICLE	0.00	0.00	0.00	0.00	not used

Table A.4: *Description of CHWI.*

Wheel position	Element ID	description
1	PHT_P_POL000	PHT P Polariser 0deg
2	PHT_P_POL120	PHT P Polariser 120deg
3	PHT_P_POL240	PHT P Polariser 240deg
4	PHT_P_NO_POL	PHT P Flat mirror
5	PHT_S	PHT S Flat mirror
6	PHT_C_RETICL	PHT C C-cut Quartz
7	PHT_C_FREE1	PHT C Free aperture
8	PHT_C_FREE2	PHT C Free aperture
9	PHT_C_FREE3	PHT C Free aperture
10	PHT_S_REDUND	PHT S Flat mirror (redundant)
11	PHT_C_POL000	PHT C Polariser 0deg
12	PHT_C_POL120	PHT C Polariser 120deg
13	PHT_C_POL240	PHT C Polariser 240deg
14	PHT_C_NO_POL	PHT C Free aperture

A.2 Filter Transmission Data

See Figures A.1 to A.8.

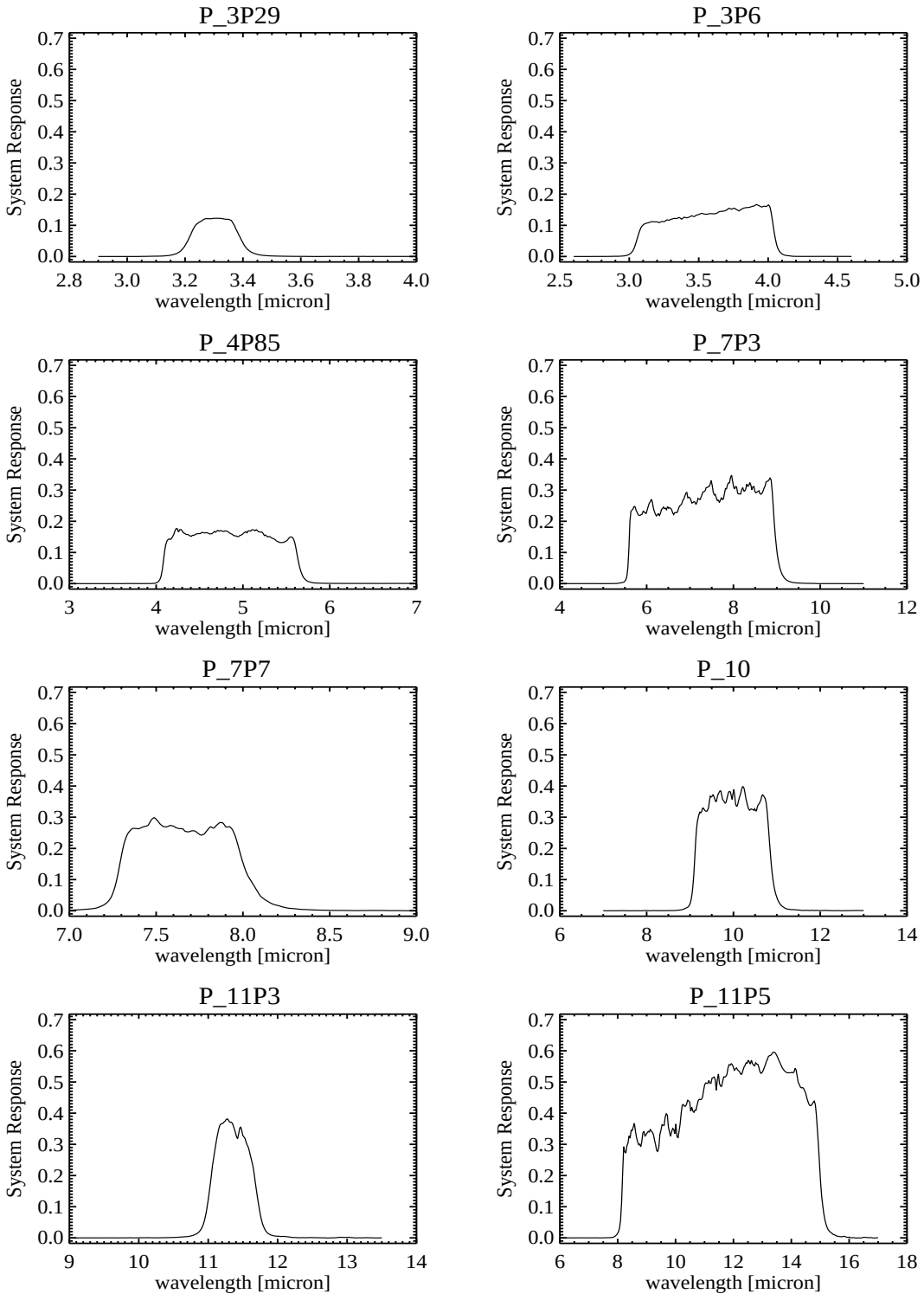

Figure A.1: *P1 filters, first part.*

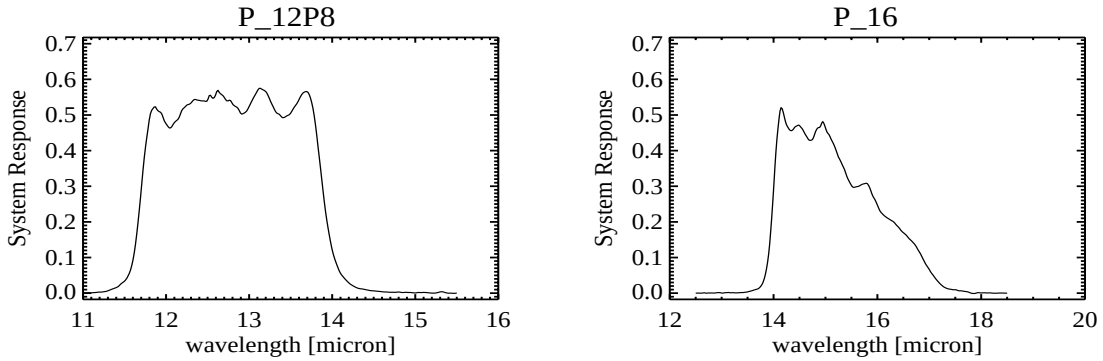

Figure A.2: *P1 filters, second part.*

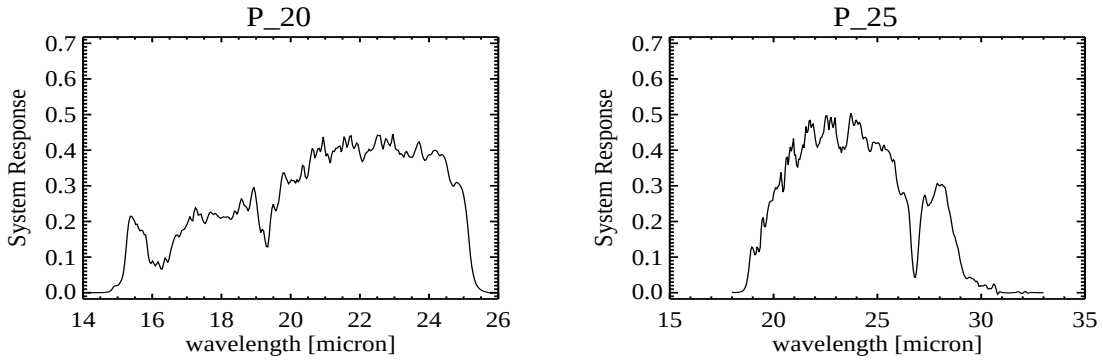

Figure A.3: *P2 filters.*

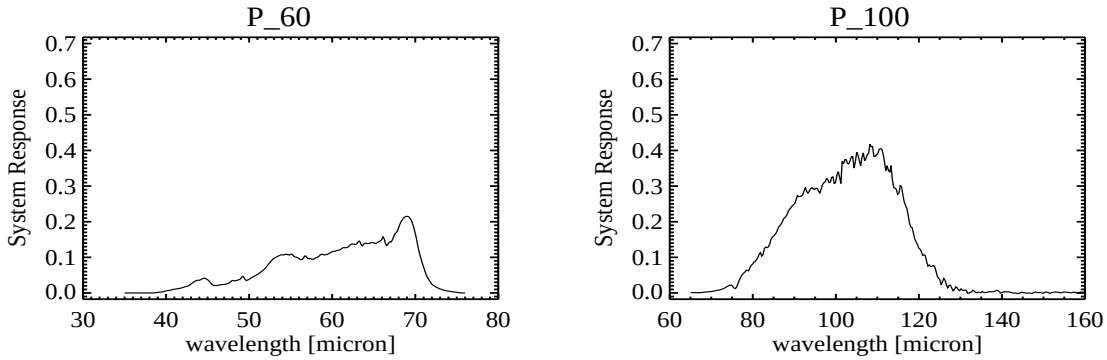

Figure A.4: *P3 filters.*

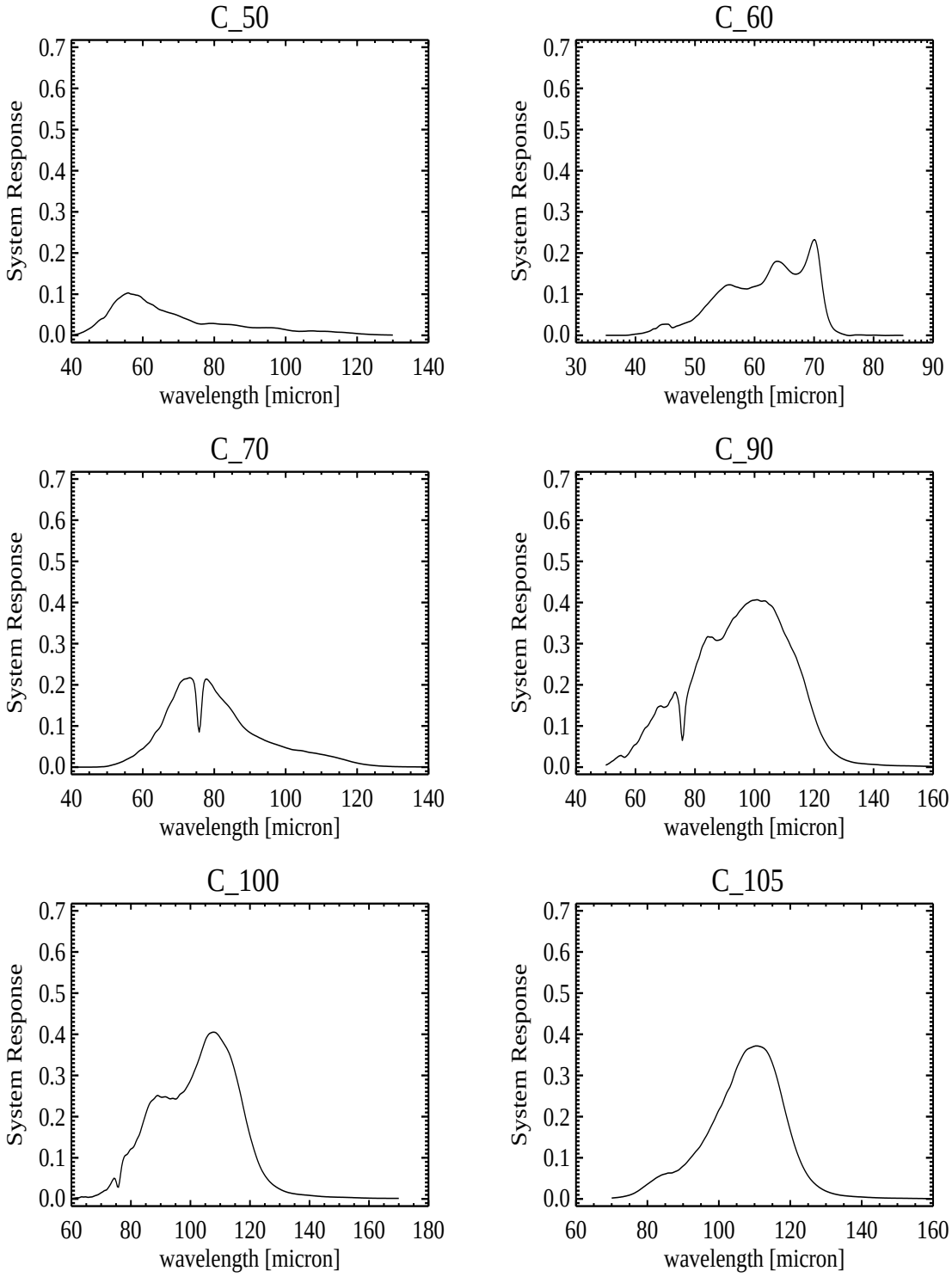

Figure A.5: *C100 filters.*

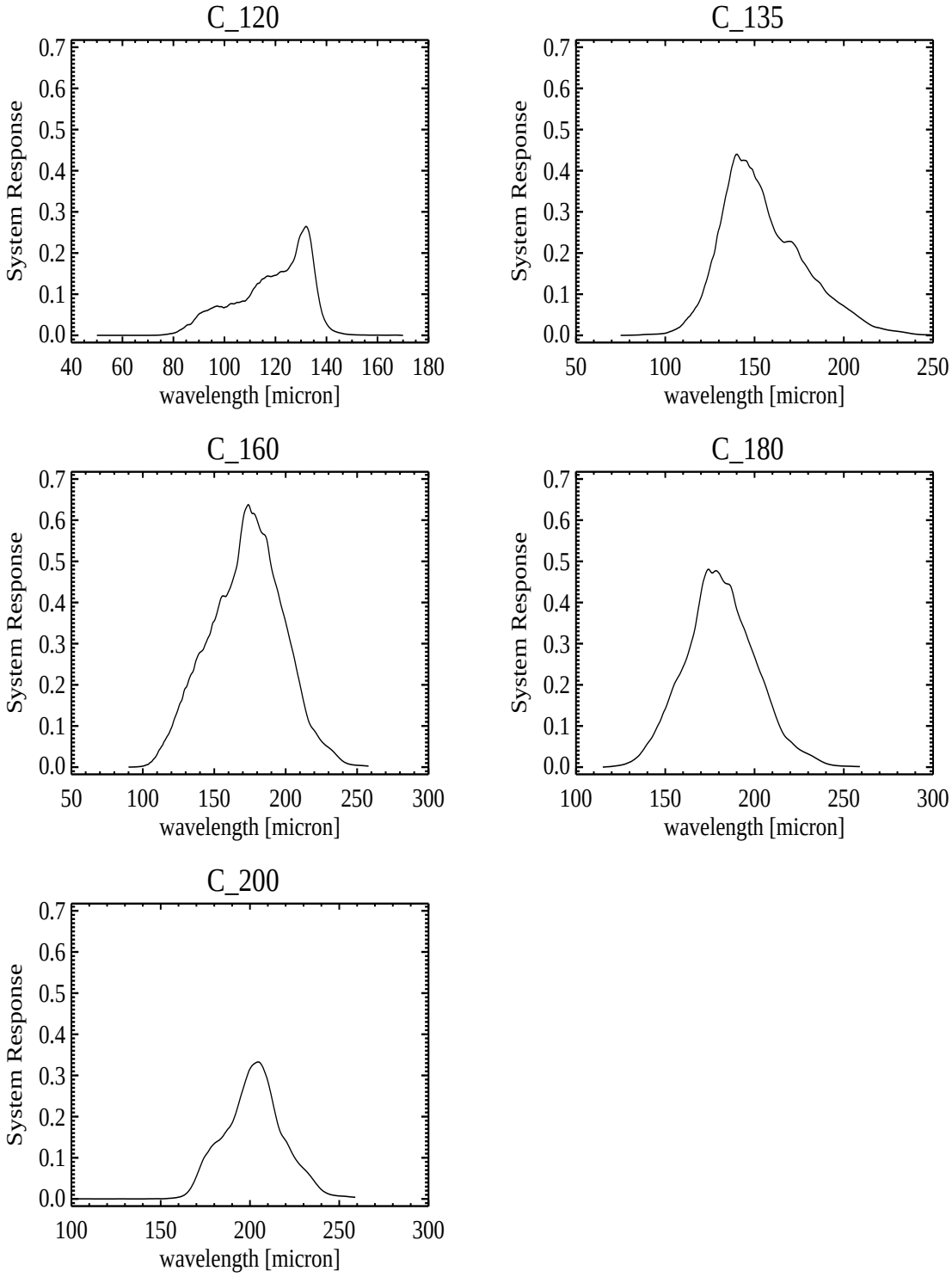

Figure A.6: *C200 filters.*

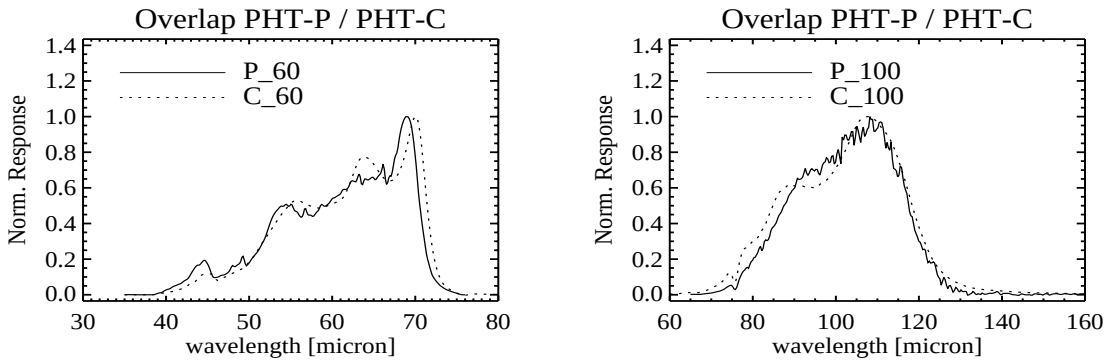

Figure A.7: *Comparison PHT-P/PHT-C.*

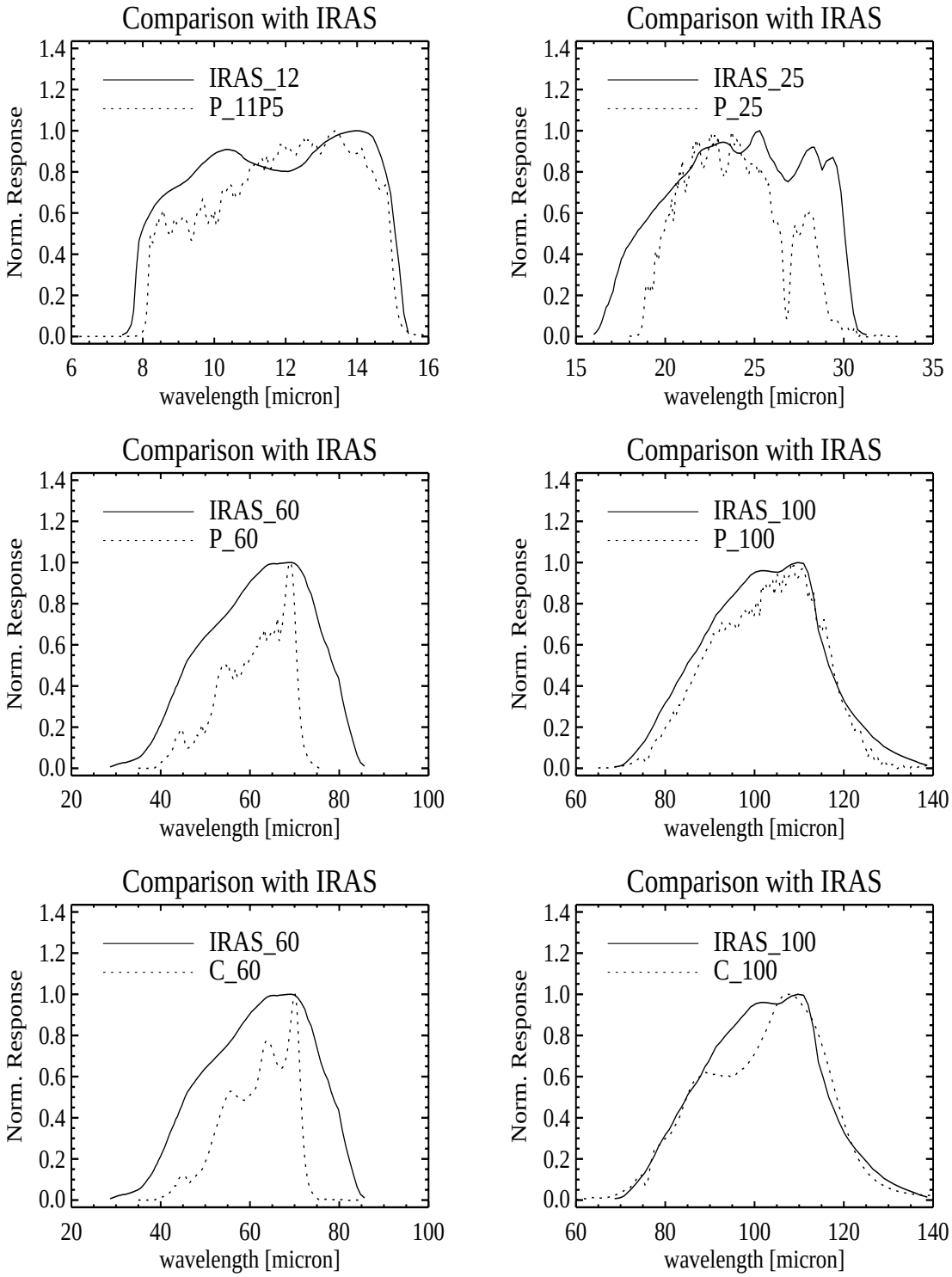

Figure A.8: *Comparison IRAS/PHT.*

Appendix B

Conversion Algorithms for ERD

B.1 Temperature Sensors

Detector temperature

To convert ERD voltage to actual detector temperature one should apply the following relationship:

$$T = B\frac{1}{{}^{10}\log(R_s) + \frac{K}{{}^{10}\log(R_s)} - A} \qquad [\mathrm{K}] \tag{B.1}$$

where:

A, B, K = constants, different for each sensor
R_s = sensor resistance in Ω, according to

$$\frac{\mathrm{R_s}}{1000} = \frac{1}{\frac{1}{\mathrm{C_1 \times tmd - C_2}} - \frac{1}{\mathrm{R_p}}} - \mathrm{R_k} \qquad [\Omega] \tag{B.2}$$

Where:

tmd = telemetry data value
C_1, C_2 = constants
R_k = harness resistance in kΩ
R_p = EEU shunt resistor in parallel to sensor in kΩ

EEU temperature

$$T = \frac{B}{A + ln(R_s)} \qquad [\mathrm{K}] \tag{B.3}$$

with

$$R_s = \frac{tmd - 2048}{4096 - tmd} \times 7500 \qquad [\Omega] \tag{B.4}$$

where

Table B.1: *Constants for PHT temperature sensors.*

Sensor	A	B	K
FCS1	6.54	2.90	10.67
FCS2	6.54	2.90	10.67
C100	5.44	3.05	7.34
C200	4.51	3.12	4.92
P1	6.02	3.61	8.77
P2	7.59	3.13	14.40
P3	5.11	3.49	6.29
S1	6.54	2.94	10.66
S2	6.54	2.90	10.67

Table B.2: *Resistances for PHT temperature sensors.*

Sensor	C_1 [kΩ]	C_2 [kΩ]	R_k [kΩ]	R_p [kΩ]
FCS1	0.259	495.83	1.12	1000
FCS2	0.256	495.83	1.12	1000
C100	0.099	146.38	1.34	infinite
C200	0.048	−78.32	0.67	infinite
P1	0.174	344.55	1.12	499
P2	0.210	388.13	1.34	499
P3	0.182	288.11	1.34	infinite
S1	0.173	341.63	1.12	499
S2	0.170	336.88	1.12	499

A = 3.9489
B = 3442 K
R_s = sensor resistance in Ω
T = EEU Temperature in K
tmd = telemetry data value

B.2 Selected FCS Power

Conversion from telemetered FCS power data in PSTA to a real power in mW

$$P_{fcs} = \frac{P_{max} \times tmd}{tmd_{max}} \qquad \text{[mW]} \tag{B.5}$$

where

tmd = telemetry data value = PSTA1TS or PSTA2TS
tmd_{max} = maximum value of telemetry word = 4095
P_{max} = maximum commandable power = 50 mW

B.3 Focal Plane Chopper Deflection

The telemetry contains the actual (measured) chopper position. The value represents a voltage which is non-linear to the chopper angle on the sky, and non-synchronous to IR readout data. The conversion depends on the chopper mode.

The initial step is the conversion of the data word (X^{raw}_{FPC} = RAW_FPC_POSN) to a voltage (V_{ini}) according to:

$$V_{ini} = C(\frac{X^{raw}_{FPC} \times Q}{P} - R) \qquad [\text{mV}], \tag{B.6}$$

where

C = 1000, the conversion to mV
Q = 20 V
P = 4096
R = 10.0 V

At this stage a crude first approximation to the chopper angle (α) is calculated from a simple linear model:

$$\alpha_{linear} = -\frac{V_{ini} + b}{a} \qquad [\text{arcsec}] \tag{B.7}$$

Since there are several chopping modes (see Table 13.2), the software has to sort out the conversion based on the chopper mode to be processed. In case of rectangular chopper mode

$$\alpha_{approx} = \alpha_{linear} - \frac{\Delta U_{DC}(\alpha_{linear})}{a} \qquad [\text{arcsec}] \tag{B.8}$$

where $\Delta U_{DC}(\alpha)$ is a correction obtained from linear interpolation in a hardcoded table given in Table B.3. An additional correction for hysteresis is computed according to:

$$\alpha_{sky} = \alpha_{approx} - (\frac{\Delta U_{ACI}(-3.6)}{a})(\frac{|\alpha_{approx}|}{150}) \quad [\text{arcsec}] \text{ if } \alpha_{approx} > 0, \tag{B.9}$$

$$\alpha_{sky} = \alpha_{approx} - (\frac{\Delta U_{ACD}(0)}{a})(\frac{|\alpha_{approx}|}{150}) \quad [\text{arcsec}] \text{ if } \alpha_{approx} < 0, \tag{B.10}$$

For scanning modes (such as used in AOT PHT32) the chopper amplitude (α_{amp}) is required. In case of sawtooth and triangular chopper mode, α_{amp} is determined from:

$$\alpha_{amp} = N_{step} \times \alpha_{inc}, \tag{B.11}$$

where N_{step} is the number of chopper steps and α_{inc} the increment in arcsec as given in the compact status (product PSTA, keywords PSTACSTE and PSTACINC, see Section 13.2.7). For the other modes α_{amp} is equal to the value of PSTACAMP, provided in the compact status.

The approximation is then corrected for deviations from the line approximation:

$$\alpha_{approx} = \alpha_{linear} - \frac{\Delta U_{DC}(\alpha_{amp})}{a} \qquad [\text{arcsec}] \tag{B.12}$$

Next, corrections must be made for hysteresis effects:

- For saw-tooth profile SUBMODE(0)

$$\alpha_{sky} = \alpha_{approx} - \alpha_{amp}\frac{\Delta U_{ACI}(\alpha_{approx}/\alpha_{amp})}{150\times a} \quad \text{[arcsec]} \tag{B.13}$$

- for triangular-tooth profile SUBMODE(1)

$$\alpha_{sky} = \alpha_{approx} - \alpha_{amp}\frac{\Delta U_{ACI}(\alpha_{approx}/\alpha_{amp})}{150\times a} \quad \text{[arcsec] for increasing angle,} \tag{B.14}$$

$$\alpha_{sky} = \alpha_{approx} - \alpha_{amp}\frac{\Delta U_{ACD}(\alpha_{approx}/\alpha_{amp})}{150\times a} \quad \text{[arcsec] for decreasing angle.} \tag{B.15}$$

In the correction the ratio $\alpha_{approx}/\alpha_{amp}$ is equivalent to α_{NORM} in interpolation Table B.3.

For chopper modes 12 and 13 (central field of view, see Table 13.2) the chopper deflection is still computed according to Equation B.12.

Values of the different parameters:

$A = 9.862622$
$B = -20.0057$
$U_{ACF1} = 4238.0$
$U_{DCF1} = 4238.0$
$U_{OF1} = 131.0$
$U_{OF2} = 239.0$
$TOL = 6.0$

B.4 Description of the Pixel Status Flag PIXF in ERD Products

See Table B.4.

Table B.3: *Parameters for deriving the chopper deflection.*

α_{NORM}	α	$\Delta U_{DC}(\alpha)$	$\Delta U_{ACD}(\alpha)$	$\Delta U_{ACI}(\alpha)$
−1.0	−180.0	−11.4	0.0	0.0
−0.9	−162.0	−10.4	−2.8	−7.4
−0.8	−144.0	−11.5	−5.7	−14.8
−0.7	−126.0	−12.5	−8.7	−21.5
−0.6	−108.0	−13.6	−11.7	−28.2
−0.5	−90.0	−15.1	−13.6	−32.8
−0.4	−72.0	−15.2	−15.5	−37.4
−0.3	−54.0	−14.2	−15.2	−39.4
−0.2	−36.0	−11.5	−14.8	−41.4
−0.1	−18.0	−8.1	−12.6	−41.0
0.0	0.0	−2.9	−10.3	−40.5
0.1	18.0	−1.0	−7.8	−37.3
0.2	36.0	−2.9	−5.4	−34.1
0.3	54.0	−2.4	−3.1	−30.2
0.4	72.0	−1.6	−0.9	−26.3
0.5	90.0	−0.8	0.6	−22.6
0.6	108.0	0.3	2.1	−18.9
0.7	126.0	1.7	1.6	−15.5
0.8	144.0	3.9	1.0	−12.0
0.9	162.0	6.1	−1.3	−7.8
1.0	180.0	9.1	−3.6	−3.6

Table B.4: *Description of 16 bits ERD bit flag variable* PPERPIXF. *LSB = 0, MSB = 15.*

bit range	item	decimal value	meaning
0	auto data reduction	0	not active; all telemetry (TM) blocks can be transferred
		1	active; one or more TM blocks of the measurement could not be transmitted. science data shall not be used, they may be corrupted.
1–2	not used	–	none
3–4	selected TRS of FCS1	0	both TRSs not connected
		1	only TRS1 connected
		2	only TRS2 connected
5–6	selected TRS of FCS2	0	both TRSs not connected
		1	only TRS1 connected
		2	only TRS2 connected
7	SW override	0	not active
		1	active; no operational but purely diagnostic set-up
8–11	TM data structure	0	P1 data structure
		1	P2 data structure
		2	P3 data structure
		3	PHT-S data structure
		4,5	not used
		6	C100 data structure
		7	C200 data structure
		8..12	not used
		13	diagnostic data structure
		14	extended housekeeping (HK) data structure
		15	not used
12–15	integration time	0..15	selected fundamental integration time (reset interval) exponent n in $2^{(7-n)}$ [s] $0 \leq n \leq 15$

Appendix C

Colour Corrections

C.1 Application of Tabulated Colour Correction Factors

The flux densities quoted in the ISOPHOT AAR results have been derived from the detector in-band powers assuming an energy distribution of the source which is constant in the flux per logarithmic frequency interval; i.e., the flux density with frequency ν goes as $f_\nu \propto \nu^{-1}$. This is the same convention as used for IRAS data.

In order to derive the flux density for any other spectral energy distribution (SED) a 'colour correction' must be applied to the background subtracted source flux density in the following way:

$$F_{\nu_{\rm ref}}(SED) = F_{\nu_{\rm ref}}(\nu^{-1}) \ / \ K_{\rm cc}(SED) \tag{C.1}$$

where:

$F_{\nu_{\rm ref}}(SED)$ = flux density for applied SED
$F_{\nu_{\rm ref}}(\nu^{-1})$ = quoted flux density in AAR
$K_{\rm cc}(SED)$ = tabulated colour correction factor for applied SED

Tabulated colour correction factors are available for

1) power-laws $F(\nu^\alpha), -3 \ \leq \ \alpha \ \leq \ +3$
   → Cal-G file PCCPOWER

2) black bodies $F(B(\nu,T))$
   → Cal-G file PCCBB

3) modified black bodies $F(\nu^{+1} \cdot B(\nu,T))$ and $F(\nu^{+2} \cdot B(\nu,T))$
   → Cal-G files PCCMBBONE and PCCMBBTWO

C.2 Computation of Colour Correction Factors

C.2.1 Derivation of flux density values from in-band power values

In order to derive flux density values (monochromatic fluxes) from measured in-band powers the following corrections and calibrations have to be done:

a) correction for effective telescope area

b) correction for reflection losses on all optical elements in the beam from the primary mirror to the detector

c) correction for the beam profile related to the selected aperture or array

d) correction for the bandpass transmission, determined by the filter and field lens transmission and the relative detector response. The product of these factors is called the relative system response.

The latter correction contains the determination of the relative contribution of the flux density at the central wavelength of the band to the total flux in the band, depending on the assumed spectral shape of the source. Doing this calculation for a variety of source spectra and computing the ratios provides the colour correction factors between the various SEDs.

The flux conversion can be written in the following form:

$$IBP = T_{\mathrm{refl}} \cdot A \cdot \int f_{\mathrm{beam}}(\lambda) \cdot F(\lambda) \cdot R(\lambda)\, d\lambda \tag{C.2}$$

where:

IBP = in-band power (unit: W)
T_{refl} = reflection losses on optical elements
A = primary mirror area
$f_{\mathrm{beam}}(\lambda)$ = wavelength dependent beam profile function
$F(\lambda)$ = flux density of source at specific wavelength λ
$R(\lambda)$ = system response at specific wavelength λ

Currently the in-band power calculation contains some simplification, in particular related to the beam profiles.

For point source fluxes the following calculation is done:

$$IBP = T_{\mathrm{refl}} \cdot A \cdot f_{\mathrm{psf}}(\lambda_{\mathrm{ref}}) \cdot \int F(\lambda) \cdot R(\lambda)\, d\lambda \tag{C.3}$$

where:

$f_{\mathrm{psf}}(\lambda_{\mathrm{ref}})$ = fraction of the point spread function at the reference wavelength λ_{ref} inside the aperture or pixel → Cal-G file PPPSF

For extended source fluxes the corresponding calculation is done:

$$IBP = T_{\mathrm{refl}} \cdot A \cdot (1 - \varepsilon^2) \cdot \Omega \cdot \int F(\lambda) \cdot R(\lambda)\, d\lambda \tag{C.4}$$

where:

ε = central obscuration factor by the secondary mirror
Ω = solid angle of selected aperture or pixel

In order to derive the flux density for the central wavelength, or more general a reference wavelength, of the bandpass the spectral energy distribution function is normalised with respect to the flux density at this wavelength:

$$F(\lambda) = F(\lambda_{\rm ref}) \cdot \frac{SED(\lambda)}{SED(\lambda_{\rm ref})} \tag{C.5}$$

where:

$F(\lambda)$ = flux density at any wavelength λ
$F(\lambda_{\rm ref})$ = flux density at reference wavelength $\lambda_{\rm ref}$
$SED(\lambda)$ = functional dependence of spectral energy distribution of source with wavelength

Furthermore, for conversion between frequency range and wavelength range the following convention is used:

$$\lambda \cdot F(\lambda) = \nu \cdot F(\nu) \tag{C.6}$$

where:

$F(\lambda)$ = flux density in wavelength range (unit: $\mathrm{W\,m^{-2}\,\mu m^{-1}}$)
$F(\nu)$ = flux density in frequency range (unit: $\mathrm{W\,m^{-2}\,Hz^{-1}}$ or Jy)

Solving this equation for $F(\nu)$ yields:

$$F(\nu) = \frac{\lambda^2}{c_{\rm light}} \cdot F(\lambda) \tag{C.7}$$

where:

$c_{\rm light}$ = speed of light

Using the normalisation with respect to the flux density value at the reference wavelength and the convention for conversion of $F(\lambda)$ into $F(\nu)$ the above formula of the in-band power can be solved for $F(\nu)$ for a general source energy distribution $SED(\lambda)$:

$$F(\nu_{\rm ref}) = \frac{1}{b \cdot c_{\rm light}} \cdot \lambda_{\rm ref}^2 \cdot SED(\lambda_{\rm ref}) \cdot \frac{IBP}{\int SED(\lambda) \cdot R(\lambda)\, d\lambda} \tag{C.8}$$

where:

b = $A \cdot T_{\rm refl} \cdot f_{\rm psf}(\lambda_{\rm ref})$

C.2.2 Flux density conversion factors for different spectral energy distributions

In the formula for the flux density $F(\nu)$ the term, which is dependent on the shape of the spectral energy distribution of the source, is called the flux density conversion factor $a(SED)$

$$a(SED) = \frac{\lambda_{\rm ref}^2 \cdot SED(\lambda_{\rm ref})}{c_{\rm light} \cdot \int SED(\lambda) \cdot R(\lambda)\, d\lambda} \tag{C.9}$$

In the following the conversion factors for specific SEDs are listed:

1) flux density $\propto \nu^{\alpha}, SED(\nu) = \nu^{\alpha} \rightarrow SED(\lambda) = \frac{c_{\rm light}}{\lambda^2} \cdot \frac{c_{\rm light}^{\alpha}}{\lambda^{\alpha}} = \frac{c_{\rm light}^{1+\alpha}}{\lambda^{2+\alpha}}$

$$a(\nu^{\alpha}) = \frac{1}{c_{\rm light} \cdot \lambda_{\rm ref}^{\alpha} \cdot \int \frac{R(\lambda)}{\lambda^{2+\alpha}}\, d\lambda} \tag{C.10}$$

2) flux density is a modified black body function with emissivity $\propto \nu^{\beta}, SED(\nu) = \nu^{\beta} \cdot B(\nu, T)$
$\rightarrow SED(\lambda) = \frac{c_{\rm light}^{\beta}}{\lambda^{\beta}} \cdot B(\lambda, T)$ ($\beta = 0$: pure black body)

$$a(\nu^{\beta} \cdot B(\nu, T)) = \frac{B(\lambda_{\rm ref}, T)}{c_{\rm light} \cdot \lambda_{\rm ref}^{\beta-2} \cdot \int \frac{B(\lambda,T)}{\lambda^{\beta}} \cdot R(\lambda)\, d\lambda} \tag{C.11}$$

Note that:

$$B(\lambda, T) = \frac{2 \cdot h \cdot c_{\rm light}^2}{\lambda^5} \cdot \frac{1}{e^{\frac{h \cdot c_{\rm light}}{k \cdot \lambda \cdot T}} - 1} \tag{C.12}$$

where:

h = Planck constant
k = Boltzmann constant
B(λ,T) contains the $\frac{c_{\rm light}}{\lambda^2}$ correction factor from the frequency to wavelength conversion !

C.2.3 Derivation of colour correction factors from flux density conversion factors

From the general formula of the colour correction in Appendix C.1 it follows that

$$K_{\rm cc}(SED) = F_{\nu_{\rm ref}}(\nu^{-1}) \;/\; F_{\nu_{\rm ref}}(SED) \tag{C.13}$$

and with the formulae from Appendix C.2.1 for $F(\nu_{\rm ref})$

$$K_{\rm cc}(SED) = a(\nu^{-1}) \;/\; a(SED) \tag{C.14}$$

the colour correction factor is the ratio of the flux density conversion factors.
Inserting the formulae from Appendix C.2.2 for both flux density conversion factors this yields

$$K_{\rm cc}(SED) = \frac{1}{\lambda_{\rm ref} \cdot SED(\lambda_{\rm ref})} \cdot \frac{\int SED(\lambda) \cdot R(\lambda)\, d\lambda}{\int \frac{R(\lambda)}{\lambda}\, d\lambda} \tag{C.15}$$

In order to calculate the colour correction factors this needs a numerical solution of the two integrals using the tabulated relative system response $R(\lambda_{\rm i})$.

C.3 Colour Correction Values

The following tables are extracted from the published Cal-G files with colour correction factors: PCCPOWER, PCCBB, PCCMBBONE and PCCMBBTWO. They have been computed using a minimum threshold of the bandpass transmission (Cal-G FITS files PCFILTRAN and PPFILTRAN) of 10^{-4} in the numerical integrations. Tests using thresholds of 10^{-3} and 10^{-5}, respectively, showed that the results

were pretty stable. The tabulated colour correction values are related to the reference central wavelength (λ_{ref}), which is defined as a wavelength close to the isophotal centre of the filter, and where possible, matching values given for filters corresponding to other ISO and IRAS instruments (see Moneti, Metcalfe & Schulz 1997, [39]).

For the following spectral energy distributions the colour correction factors have been computed:

- power-laws $F(\nu^{\alpha}), -3 \leq \alpha \leq +3$ (Table C.1)
- black bodies $F(B(\nu, T))$ (Table C.2 and C.3)
- modified black bodies $F(\nu^{+1} \cdot B(\nu, T))$ (Table C.4 and C.5) and $F(\nu^{+2} \cdot B(\nu, T))$ (Table C.6 and C.7)

Remarks:

1) Colour correction values between 2 and 10 have to be taken with care, the colour correction will dominate the final photometric accuracy.

2) Colour correction values of 10 indicate that no reliable photometry of this source is possible in the given filter.

Table C.1: *Colour correction factors for different power-law spectra:* $SED(\nu) = \nu^{\alpha}$.

α	−3.0	−2.0	−1.0	0.0	1.0	2.0	3.0
P1_3.29	1.06	1.02	1.00	1.00	1.02	1.05	1.10
P1_3.60	1.03	1.00	1.00	1.02	1.05	1.12	1.21
P1_4.85	1.04	1.01	1.00	1.01	1.03	1.07	1.13
P1_7.30	1.02	1.00	1.00	1.02	1.07	1.15	1.26
P1_7.70	1.00	1.00	1.00	1.01	1.02	1.03	1.05
P1_10.0	1.00	1.00	1.00	1.01	1.02	1.03	1.05
P1_11.3	1.01	1.01	1.00	1.00	0.99	0.99	1.00
P1_11.5	0.96	0.97	1.00	1.07	1.17	1.33	1.56
P1_12.8	1.00	1.00	1.00	1.00	1.01	1.02	1.04
P1_16.0	1.02	1.01	1.00	1.00	0.99	1.00	1.00
P2_20	1.09	1.03	1.00	0.98	0.99	1.01	1.06
P2_25	0.90	0.94	1.00	1.08	1.17	1.29	1.44
P3_60	1.01	1.00	1.00	1.02	1.07	1.14	1.24
P3_100	1.04	1.01	1.00	1.00	1.02	1.05	1.10
C1_50	1.06	1.00	1.00	1.05	1.15	1.29	1.50
C1_60	1.04	1.01	1.00	1.00	1.02	1.06	1.13
C1_70	0.99	0.98	1.00	1.05	1.12	1.23	1.38
C1_90	1.09	1.02	1.00	1.01	1.06	1.17	1.34
C1_100	1.03	1.01	1.00	1.01	1.05	1.10	1.19
C1_105	1.03	1.01	1.00	1.00	1.02	1.05	1.10
C2_120	0.96	0.97	1.00	1.05	1.12	1.22	1.36
C2_135	1.05	1.01	1.00	1.01	1.04	1.10	1.18
C2_160	1.00	0.99	1.00	1.04	1.10	1.20	1.35
C2_180	1.00	0.99	1.00	1.02	1.05	1.10	1.17
C2_200	1.02	1.00	1.00	1.00	1.01	1.03	1.06

Table C.2: *Colour correction factors for black body spectra (part I): $SED(\nu) = F(B(\nu, T))$.*

Temp.	10000	5000	4000	3000	2000	1000	800	600	500	400	300	250	220
P1_3.29	1.00	1.00	1.00	1.00	1.00	1.00	1.00	1.01	1.01	1.02	1.03	1.05	1.08
P1_3.60	1.06	1.05	1.05	1.04	1.03	1.00	0.99	0.99	1.00	1.04	1.17	1.33	1.51
P1_4.85	1.04	1.03	1.03	1.03	1.02	0.99	0.99	0.98	0.99	1.01	1.10	1.21	1.34
P1_7.30	1.13	1.12	1.11	1.10	1.09	1.04	1.01	0.98	0.97	0.95	0.97	1.01	1.07
P1_7.70	1.02	1.02	1.02	1.02	1.02	1.01	1.01	1.00	1.00	0.99	0.99	0.98	0.98
P1_10.0	1.02	1.02	1.02	1.02	1.02	1.01	1.01	1.00	1.00	0.99	0.99	0.98	0.98
P1_11.3	0.99	0.99	0.99	0.99	0.99	0.99	0.99	0.99	0.99	1.00	1.00	1.00	1.01
P1_11.5	1.31	1.30	1.29	1.28	1.26	1.19	1.15	1.10	1.06	1.01	0.94	0.91	0.89
P1_12.8	1.02	1.02	1.02	1.02	1.02	1.01	1.01	1.01	1.00	1.00	1.00	0.99	0.99
P1_16.0	0.99	0.99	0.99	0.99	0.99	0.99	0.99	0.99	0.99	0.99	0.99	0.99	1.00
P2_20	1.01	1.01	1.01	1.01	1.00	1.00	0.99	0.99	0.98	0.97	0.96	0.96	0.96
P2_25	1.28	1.28	1.28	1.27	1.27	1.25	1.23	1.21	1.20	1.17	1.13	1.10	1.07
P3_60	1.13	1.13	1.13	1.13	1.13	1.12	1.12	1.11	1.11	1.10	1.09	1.08	1.08
P3_100	1.05	1.05	1.05	1.05	1.05	1.05	1.05	1.05	1.05	1.04	1.04	1.04	1.04
C1_50	1.29	1.29	1.29	1.29	1.28	1.27	1.27	1.26	1.25	1.24	1.21	1.20	1.18
C1_60	1.06	1.06	1.06	1.06	1.06	1.05	1.05	1.05	1.05	1.04	1.04	1.03	1.03
C1_70	1.23	1.23	1.23	1.23	1.22	1.22	1.21	1.21	1.20	1.20	1.18	1.17	1.17
C1_90	1.17	1.17	1.16	1.16	1.16	1.15	1.15	1.15	1.14	1.13	1.12	1.11	1.11
C1_100	1.10	1.10	1.10	1.10	1.10	1.10	1.09	1.09	1.09	1.09	1.08	1.08	1.07
C1_105	1.05	1.05	1.05	1.05	1.05	1.05	1.05	1.05	1.05	1.04	1.04	1.04	1.04
C2_120	1.22	1.21	1.21	1.21	1.21	1.21	1.21	1.20	1.20	1.20	1.19	1.18	1.18
C2_135	1.10	1.10	1.10	1.10	1.09	1.09	1.09	1.09	1.09	1.09	1.08	1.08	1.08
C2_160	1.20	1.20	1.20	1.20	1.20	1.20	1.20	1.19	1.19	1.19	1.18	1.18	1.18
C2_180	1.10	1.10	1.10	1.10	1.10	1.10	1.10	1.10	1.10	1.09	1.09	1.09	1.09
C2_200	1.03	1.03	1.03	1.03	1.03	1.03	1.03	1.03	1.03	1.03	1.03	1.03	1.03

Table C.3: *Colour correction factors for black body spectra (part II): $SED(\nu) = F(B(\nu, T))$.*

Temp.	200	180	160	140	120	100	80	60	50	40	30	20	15	10
P1_3.29	1.10	1.13	1.19	1.29	1.53	2.32	7.12	10	10	10	10	10	10	10
P1_3.60	1.69	1.97	2.43	3.25	4.95	9.39	10	10	10	10	10	10	10	10
P1_4.85	1.47	1.67	2.01	2.61	3.89	7.56	10	10	10	10	10	10	10	10
P1_7.30	1.13	1.22	1.37	1.62	2.10	3.15	6.18	10	10	10	10	10	10	10
P1_7.70	0.98	0.98	0.98	0.98	0.99	1.01	1.06	1.20	1.38	1.91	10	10	10	10
P1_10.0	0.99	0.99	0.99	1.00	1.03	1.07	1.17	1.45	1.93	2.95	10	10	10	10
P1_11.3	1.01	1.01	1.02	1.02	1.03	1.05	1.08	1.14	1.21	1.34	10	10	10	10
P1_11.5	0.89	0.89	0.90	0.94	1.02	1.20	1.62	3.02	5.69	10	10	10	10	10
P1_12.8	0.99	0.99	0.99	1.00	1.01	1.03	1.09	1.23	1.42	1.77	10	10	10	10
P1_16.0	1.00	1.00	1.01	1.02	1.03	1.06	1.12	1.27	1.48	1.86	10	10	10	10
P2_20	0.96	0.97	0.97	0.99	1.03	1.09	1.25	1.65	2.24	3.44	10	10	10	10
P2_25	1.05	1.02	1.00	0.96	0.92	0.87	0.82	0.79	0.80	0.85	10	10	10	10
P3_60	1.07	1.06	1.05	1.04	1.03	1.01	0.99	0.97	0.96	0.97	1.03	1.32	1.86	4.42
P3_100	1.03	1.03	1.03	1.03	1.02	1.02	1.01	0.99	0.98	0.98	0.98	1.03	1.17	1.73
C1_50	1.17	1.16	1.14	1.12	1.09	1.05	1.00	0.94	0.90	0.89	0.85	1.75	4.80	10
C1_60	1.02	1.02	1.01	1.01	1.00	0.99	0.98	0.97	0.98	1.00	1.09	1.44	2.10	5.34
C1_70	1.16	1.15	1.14	1.13	1.11	1.09	1.05	1.00	0.97	0.93	0.92	1.04	1.44	4.51
C1_90	1.10	1.09	1.08	1.07	1.05	1.03	1.01	0.97	0.95	0.94	0.96	1.16	1.59	3.87
C1_100	1.07	1.07	1.06	1.06	1.05	1.04	1.02	1.00	0.99	0.97	0.96	1.02	1.17	1.89
C1_105	1.03	1.03	1.03	1.03	1.02	1.02	1.01	1.00	0.99	0.98	0.98	1.02	1.11	1.50
C2_120	1.17	1.17	1.16	1.15	1.14	1.13	1.11	1.07	1.04	1.01	0.96	0.92	0.94	1.10
C2_135	1.08	1.07	1.07	1.07	1.06	1.06	1.05	1.03	1.02	1.00	0.98	0.96	0.99	1.22
C2_160	1.17	1.17	1.16	1.16	1.15	1.14	1.12	1.09	1.07	1.04	1.00	0.95	0.94	1.04
C2_180	1.09	1.09	1.08	1.08	1.08	1.07	1.07	1.05	1.04	1.03	1.01	0.98	0.96	1.00
C2_200	1.03	1.02	1.02	1.02	1.02	1.02	1.02	1.01	1.01	1.01	1.00	0.99	0.99	1.01

Table C.4: *Colour correction factors for modified black body spectra (part I):* $SED(\nu) = F(\nu^{+1} \cdot B(\nu, T))$.

Temp.	10000	5000	4000	3000	2500	2000	1000	800	600	500	400	300	250	220
P1_3.29	1.00	1.00	1.00	1.00	1.00	1.00	1.00	1.00	1.00	1.00	1.01	1.03	1.05	1.07
P1_3.6	1.10	1.09	1.08	1.07	1.07	1.05	1.00	0.98	0.97	0.97	0.99	1.07	1.19	1.32
P1_4.85	1.07	1.06	1.06	1.05	1.05	1.04	1.00	0.99	0.98	0.98	0.99	1.06	1.15	1.26
P1_7.3	1.22	1.21	1.20	1.19	1.18	1.16	1.09	1.06	1.01	0.99	0.96	0.94	0.97	1.01
P1_7.7	1.03	1.03	1.03	1.03	1.03	1.03	1.02	1.02	1.01	1.01	1.00	0.99	0.98	0.98
P1_10	1.04	1.04	1.04	1.03	1.03	1.03	1.02	1.02	1.01	1.01	1.00	0.99	0.99	0.99
P1_11.3	0.99	0.99	0.99	0.99	0.99	0.99	0.99	0.99	0.99	0.99	0.99	1.00	1.00	1.00
P1_11.5	1.52	1.50	1.50	1.48	1.47	1.45	1.35	1.30	1.22	1.16	1.09	0.99	0.94	0.91
P1_12.8	1.03	1.03	1.03	1.03	1.03	1.03	1.02	1.02	1.02	1.01	1.01	1.00	1.00	0.99
P1_16	1.00	1.00	1.00	1.00	1.00	1.00	0.99	0.99	0.99	0.99	0.99	0.99	0.99	0.99
P2_20	1.06	1.05	1.05	1.05	1.05	1.05	1.03	1.03	1.01	1.00	0.99	0.97	0.96	0.96
P2_25	1.43	1.42	1.42	1.42	1.41	1.41	1.38	1.37	1.34	1.32	1.29	1.24	1.20	1.16
P3_60	1.24	1.24	1.23	1.23	1.23	1.23	1.22	1.22	1.21	1.20	1.19	1.18	1.16	1.15
P3_100	1.10	1.10	1.10	1.10	1.10	1.10	1.10	1.10	1.09	1.09	1.09	1.09	1.08	1.08
C1_50	1.50	1.50	1.49	1.49	1.49	1.49	1.47	1.46	1.45	1.44	1.42	1.39	1.37	1.35
C1_60	1.13	1.12	1.12	1.12	1.12	1.12	1.12	1.11	1.11	1.10	1.10	1.09	1.08	1.07
C1_70	1.38	1.38	1.38	1.38	1.38	1.37	1.36	1.36	1.35	1.35	1.34	1.32	1.30	1.29
C1_90	1.34	1.33	1.33	1.33	1.33	1.33	1.32	1.31	1.30	1.29	1.28	1.27	1.25	1.24
C1_100	1.18	1.18	1.18	1.18	1.18	1.18	1.18	1.17	1.17	1.17	1.16	1.16	1.15	1.14
C1_105	1.10	1.10	1.10	1.10	1.10	1.10	1.10	1.10	1.09	1.09	1.09	1.08	1.08	1.08
C2_120	1.35	1.35	1.35	1.35	1.35	1.35	1.34	1.34	1.33	1.33	1.32	1.31	1.31	1.30
C2_135	1.18	1.18	1.18	1.18	1.18	1.17	1.17	1.17	1.17	1.17	1.16	1.16	1.15	1.15
C2_160	1.35	1.35	1.35	1.35	1.35	1.35	1.35	1.34	1.34	1.34	1.33	1.32	1.32	1.31
C2_180	1.17	1.16	1.16	1.16	1.16	1.16	1.16	1.16	1.16	1.16	1.16	1.15	1.15	1.15
C2_200	1.06	1.06	1.06	1.06	1.06	1.05	1.05	1.05	1.05	1.05	1.05	1.05	1.05	1.05

Table C.5: *Colour correction factors for modified black body spectra (part II):* $SED(\nu) = F(\nu^{+1} \cdot B(\nu, T))$.

Temp.	200	180	160	140	120	100	80	60	50	40	30	20	15	10
P1_3.29	1.09	1.12	1.17	1.26	1.46	2.07	10	10	10	10	10	10	10	10
P1_3.6	1.46	1.66	2.00	2.59	3.78	6.79	10	10	10	10	10	10	10	10
P1_4.85	1.37	1.55	1.84	2.38	3.50	6.69	10	10	10	10	10	10	10	10
P1_7.3	1.05	1.13	1.26	1.47	1.89	2.81	5.48	10	10	10	10	10	10	10
P1_7.7	0.98	0.98	0.97	0.98	0.98	1.00	1.04	1.17	1.34	10	10	10	10	10
P1_10	0.99	0.99	0.99	1.00	1.02	1.07	1.16	1.44	1.82	10	10	10	10	10
P1_11.3	1.00	1.01	1.01	1.02	1.03	1.04	1.07	1.13	1.19	10	10	10	10	10
P1_11.5	0.89	0.88	0.88	0.90	0.97	1.11	1.49	2.74	4.83	10	10	10	10	10
P1_12.8	0.99	0.99	0.99	0.99	1.00	1.02	1.07	1.20	1.36	1.72	2.84	10	10	10
P1_16	0.99	1.00	1.00	1.01	1.02	1.04	1.10	1.24	1.41	1.80	3.08	10	10	10
P2_20	0.95	0.95	0.95	0.96	0.98	1.03	1.16	1.51	1.96	3.09	7.33	10	10	10
P2_25	1.14	1.11	1.07	1.02	0.97	0.91	0.85	0.79	0.78	0.83	1.06	10	10	10
P3_60	1.14	1.13	1.12	1.11	1.08	1.06	1.02	0.98	0.96	0.95	0.99	1.22	1.68	3.90
P3_100	1.08	1.07	1.07	1.06	1.06	1.05	1.03	1.01	1.00	0.98	0.97	1.00	1.09	1.55
C1_50	1.33	1.31	1.29	1.26	1.22	1.16	1.09	0.99	0.93	0.88	0.88	1.35	3.29	10
C1_60	1.07	1.06	1.05	1.04	1.03	1.01	0.99	0.97	0.96	0.97	1.03	1.32	1.88	4.66
C1_70	1.28	1.27	1.26	1.24	1.22	1.18	1.13	1.06	1.01	0.96	0.91	0.96	1.24	3.46
C1_90	1.23	1.22	1.20	1.18	1.16	1.12	1.08	1.01	0.98	0.94	0.92	1.04	1.37	3.12
C1_100	1.14	1.14	1.13	1.12	1.11	1.09	1.07	1.04	1.01	0.99	0.96	0.98	1.09	1.66
C1_105	1.08	1.07	1.07	1.06	1.06	1.05	1.04	1.02	1.00	0.99	0.97	0.99	1.06	1.38
C2_120	1.29	1.29	1.28	1.27	1.25	1.23	1.20	1.15	1.11	1.06	1.00	0.93	0.92	1.04
C2_135	1.15	1.15	1.14	1.14	1.13	1.12	1.11	1.08	1.06	1.03	1.00	0.95	0.96	1.11
C2_160	1.31	1.30	1.30	1.29	1.28	1.26	1.24	1.19	1.16	1.12	1.05	0.97	0.93	0.98
C2_180	1.15	1.15	1.14	1.14	1.13	1.13	1.12	1.10	1.09	1.07	1.04	0.99	0.96	0.97
C2_200	1.05	1.05	1.05	1.05	1.04	1.04	1.04	1.03	1.03	1.02	1.01	0.99	0.98	1.00

Table C.6: *Colour correction factors for modified black body spectra (part I):* $SED(\nu) = F(\nu^{+2} \cdot B(\nu, T))$.

Temp.	10000	5000	4000	3000	2500	2000	1000	800	600	500	400	300	250	220
P1_3.29	1.00	1.00	1.00	1.00	1.00	1.00	1.00	1.00	1.00	1.00	1.01	1.02	1.04	1.06
P1_3.6	1.15	1.13	1.12	1.11	1.10	1.09	1.02	1.00	0.97	0.96	0.97	1.04	1.14	1.25
P1_4.85	1.11	1.10	1.10	1.09	1.08	1.07	1.03	1.01	0.98	0.98	0.98	1.02	1.09	1.18
P1_7.3	1.34	1.32	1.32	1.30	1.29	1.27	1.18	1.13	1.07	1.02	0.98	0.94	0.94	0.96
P1_7.7	1.04	1.04	1.04	1.04	1.04	1.04	1.03	1.03	1.02	1.01	1.01	1.00	0.99	0.98
P1_10	1.05	1.05	1.05	1.05	1.05	1.05	1.04	1.03	1.03	1.02	1.01	1.00	0.99	0.99
P1_11.3	0.99	0.99	0.99	0.99	0.99	0.99	0.99	0.99	0.99	0.99	0.99	0.99	1.00	1.00
P1_11.5	1.82	1.79	1.78	1.76	1.74	1.71	1.58	1.51	1.40	1.32	1.21	1.07	0.99	0.94
P1_12.8	1.05	1.05	1.05	1.04	1.04	1.04	1.04	1.03	1.03	1.02	1.02	1.01	1.00	1.00
P1_16	1.00	1.00	1.00	1.00	1.00	1.00	1.00	1.00	1.00	0.99	0.99	0.99	0.99	0.99
P2_20	1.13	1.12	1.12	1.12	1.12	1.11	1.09	1.08	1.07	1.05	1.03	1.00	0.98	0.97
P2_25	1.61	1.60	1.60	1.59	1.59	1.58	1.55	1.53	1.50	1.47	1.43	1.37	1.32	1.28
P3_60	1.38	1.38	1.38	1.38	1.38	1.37	1.36	1.35	1.34	1.33	1.32	1.30	1.28	1.27
P3_100	1.17	1.17	1.17	1.17	1.17	1.17	1.17	1.16	1.16	1.16	1.16	1.15	1.14	1.14
C1_50	1.78	1.77	1.77	1.77	1.77	1.76	1.74	1.73	1.71	1.70	1.67	1.63	1.60	1.58
C1_60	1.22	1.22	1.22	1.22	1.22	1.21	1.21	1.20	1.19	1.19	1.18	1.17	1.15	1.14
C1_70	1.58	1.58	1.58	1.58	1.58	1.57	1.56	1.55	1.54	1.54	1.52	1.50	1.48	1.47
C1_90	1.60	1.60	1.59	1.59	1.59	1.59	1.57	1.56	1.55	1.54	1.52	1.49	1.47	1.45
C1_100	1.30	1.30	1.30	1.30	1.30	1.30	1.29	1.29	1.28	1.28	1.27	1.26	1.25	1.25
C1_105	1.17	1.17	1.17	1.17	1.17	1.17	1.16	1.16	1.16	1.16	1.15	1.15	1.14	1.14
C2_120	1.54	1.54	1.54	1.53	1.53	1.53	1.52	1.52	1.51	1.51	1.50	1.49	1.48	1.47
C2_135	1.29	1.29	1.29	1.29	1.29	1.29	1.28	1.28	1.28	1.28	1.27	1.27	1.26	1.26
C2_160	1.57	1.57	1.57	1.56	1.56	1.56	1.56	1.55	1.55	1.54	1.54	1.52	1.52	1.51
C2_180	1.25	1.25	1.25	1.25	1.25	1.25	1.25	1.25	1.25	1.24	1.24	1.24	1.23	1.23
C2_200	1.09	1.09	1.09	1.09	1.09	1.09	1.09	1.09	1.09	1.09	1.09	1.09	1.09	1.08

Table C.7: *Colour correction factors for modified black body spectra (part II):* $SED(\nu) = F(\nu^{+2} \cdot B(\nu, T))$.

Temp.	200	180	160	140	120	100	80	60	50	40	30	20	15	10
P1_3.29	1.08	1.11	1.15	1.23	1.41	1.94	10	10	10	10	10	10	10	10
P1_3.6	1.37	1.56	1.86	2.39	3.46	6.16	10	10	10	10	10	10	10	10
P1_4.85	1.28	1.43	1.68	2.14	3.09	5.73	10	10	10	10	10	10	10	10
P1_7.3	1.00	1.05	1.15	1.33	1.67	2.45	4.70	10	10	10	10	10	10	10
P1_7.7	0.98	0.98	0.97	0.97	0.98	0.99	1.03	1.14	1.31	10	10	10	10	10
P1_10	0.99	0.99	0.99	0.99	1.01	1.04	1.13	1.38	1.72	10	10	10	10	10
P1_11.3	1.00	1.00	1.01	1.01	1.02	1.03	1.06	1.12	1.17	10	10	10	10	10
P1_11.5	0.91	0.89	0.87	0.87	0.91	1.02	1.32	2.37	4.12	10	10	10	10	10
P1_12.8	0.99	0.99	0.99	0.99	0.99	1.01	1.05	1.16	1.31	1.64	2.67	10	10	10
P1_16	0.99	0.99	0.99	1.00	1.01	1.03	1.07	1.19	1.35	1.70	2.84	10	10	10
P2_20	0.96	0.95	0.94	0.94	0.95	0.98	1.07	1.36	1.73	2.68	6.22	10	10	10
P2_25	1.25	1.21	1.16	1.11	1.04	0.97	0.88	0.80	0.78	0.80	0.99	10	10	10
P3_60	1.25	1.24	1.22	1.20	1.17	1.13	1.08	1.01	0.98	0.95	0.95	1.13	1.53	3.45
P3_100	1.14	1.13	1.13	1.12	1.11	1.10	1.08	1.05	1.03	1.00	0.97	0.97	1.04	1.41
C1_50	1.56	1.53	1.50	1.46	1.40	1.33	1.23	1.09	1.00	0.91	0.85	1.10	2.34	10
C1_60	1.14	1.13	1.12	1.10	1.08	1.06	1.02	0.98	0.96	0.95	0.99	1.22	1.70	4.09
C1_70	1.46	1.44	1.42	1.40	1.36	1.32	1.25	1.16	1.09	1.01	0.93	0.91	1.09	2.71
C1_90	1.44	1.42	1.39	1.37	1.33	1.28	1.21	1.10	1.04	0.97	0.91	0.96	1.20	2.56
C1_100	1.24	1.24	1.23	1.21	1.20	1.18	1.15	1.10	1.06	1.02	0.97	0.95	1.02	1.47
C1_105	1.14	1.13	1.13	1.12	1.11	1.10	1.08	1.05	1.03	1.01	0.98	0.97	1.02	1.28
C2_120	1.46	1.45	1.44	1.42	1.40	1.38	1.33	1.27	1.22	1.15	1.05	0.94	0.91	0.99
C2_135	1.25	1.25	1.24	1.24	1.23	1.21	1.19	1.16	1.13	1.09	1.04	0.97	0.94	1.02
C2_160	1.50	1.50	1.49	1.47	1.46	1.43	1.40	1.34	1.30	1.24	1.14	1.01	0.94	0.93
C2_180	1.23	1.23	1.22	1.22	1.21	1.20	1.19	1.17	1.15	1.13	1.09	1.02	0.98	0.95
C2_200	1.08	1.08	1.08	1.08	1.08	1.07	1.07	1.06	1.05	1.04	1.03	1.00	0.99	0.98

Appendix D

Magnitude System in ISOPHOT

The zero magnitude of a given ISOPHOT filter is defined as the signal of the 'ideal' (i.e. model) Vega which would have been measured in that filter with an infinitely large aperture.

The ideal spectrum of Vega was derived from a Kurucz model with T_{eff} = 9400 K , log(g) = 3.900, metal poor, $V_{turb} = 0.0$ km s^{-1} and no infrared excess due to circumstellar dust, extended to 300 μm and absolutely calibrated as described by Cohen et al. 1992, [6], and Walker & Cohen 1992, [55].

The magnitude m_{filter} can be obtained from the PHT auto analysis data product by applying the relation:

$$m_{filter} = -2.5 \log [\frac{F_\nu(measured)}{F_{\nu,0}}] \quad , \tag{D.1}$$

where $F_\nu(measured)$ is the AAR flux density. The values for $F_{\nu,0}$ with filter identifier and reference wavelength λ_{ref} are listed in Table D.1.

For completeness, we have included in Table D.1 the corresponding powers on the detector $P_0(\lambda_{ref})$, the ideal Vega flux density at the reference wavelength $F_\nu(\lambda_{ref})$, and the colour correction k.

$P_0(\lambda_{ref})$ can be applied to the SPD products, thereby taking into account the point spread function correction, see Equations 5.8 and 5.9. The values of k are very close to the ones which have been derived for a 10000 K blackbody, see Table C.2.

Table D.1: *Zero magnitude flux densities of ISOPHOT filter bands.*

filter ID	λ_{ref} [μm]	$P_0(\lambda_{ref})$ [W]	$F_{\nu,0}(\lambda_{ref})$ [Jy]	$F_\nu(\lambda_{ref})$ [Jy]	k [ ]
P_3.29	3.3	4.60E−13	312.0	318.2	0.981
P_3.6	3.6	2.15E−12	284.7	270.9	1.051
P_4.85	4.8	1.24E−12	163.2	152.1	1.072
P_7.3	7.3	1.01E−12	79.96	71.09	1.125
P_7.7	7.7	1.61E−13	65.14	64.23	1.014
P_10	10	1.77E−13	39.40	38.60	1.021
P_11.3	11.3	3.94E−14	29.96	30.40	0.985
P_12.8	12.8	5.71E−13	35.47	26.97	1.315
P_16	15	1.26E−13	24.21	23.79	1.018
P_11.5	12	5.46E−14	17.25	17.40	0.991
P_20	20	5.17E−14	9.940	9.840	1.010
P_25	25	3.47E−14	8.109	6.307	1.286
P_60	60	7.29E−16	1.233	1.087	1.135
P_100	100	3.55E−16	0.4068	0.3866	1.052
C_50	65	5.76E−16	1.197	0.9245	1.295
C_60	60	7.60E−16	1.153	1.087	1.061
C_70	80	5.22E−16	0.7489	0.6075	1.233
C_90	90	8.45E−16	0.5597	0.4787	1.169
C_100	100	4.03E−16	0.4261	0.3866	1.102
C_105	105	2.25E−16	0.3683	0.3503	1.052
C_120	120	1.15E−16	0.3253	0.2672	1.217
C_135	150	1.32E−16	0.1862	0.1698	1.096
C_160	170	1.60E−16	0.1587	0.1316	1.205
C_180	180	6.92E−17	0.1288	0.1172	1.099
C_200	200	2.27E−17	0.0972	0.0945	1.028

Appendix E

List of Acronyms

AAR	auto-analysis results
AD	analogue to digital
ADD	architectural design document
AOCS	attitude and orbit control system
AOT	astronomical observation template
APART	Arizona's Program for the Analysis of Radiation Transfer
APH	aperture pointing history
CCSH	continuous compact status history
CFOV	centre field of view
CHW	change wheel
CMOS	complementary metal-oxide semiconductor
CRE	cold readout electronics
CSH	compact status history
C1 or C100	C100 detector array
C2 or C200	C200 detector array
DIE	detector interface electronics
DN	digitised numbers
DR	destructive readout
DUM	data users manual
EEU	external electronic unit
EOH	executed observation history
ERD	edited raw data
FCS	fine calibration source
FIR	far-infrared
FITS	flexible image transfer system
FL	first look
flpht	first look tool for PHT
FOV	field of view
FPC	focal plane chopper
FPG	focal plane geometry
FPU	focal plane unit
FWHM	full width at half maximum
HTML	hyper-text mark-up language
ID	identifier
IDA	ISO Data Archive
IDPD	ISO data product document

IDUM	ISOPHOT data users manual
IR	infrared
IRAS	Infrared Astronomical Satellite
IRPH	instrument reference pointing history
ISDM	ISO satellite and data manual
ITK	instrument time key ($=2^{-14}$ sec)
LSB	least significant bit
MSB	most significant bit
MUX	multiplexer
NDR	non-destructive readout
OBDH	on-board data handling
OLP	off-line processing
OPF	on-position flag
OTF	on-target flag
PAH	polycyclic aromatic hydrocarbons
PGA	proposal generation aids
PHT	ISOPHOT
PV	performance verification
P1	P1 detector
P2	P2 detector
P3	P3 detector
RI	reset interval
ROT	readout timing
RPID	raster point identification
RPQ	raster point quaternion
SED	spectral energy distribution
S&H	sample and hold
SL or S1	long wavelength part of PHT-S
SPD	standard processed data
srf	spectral response function
SS or S2	short wavelength part of PHT-S
TDF	telemetry data file
TDT	target dedicated time
TM	telemetry
TRS	thermal radiation source
ZL	zodiacal light

Appendix F

List of Symbols

F.1 Roman Symbols

Symbol		Explanation
A		area
	A	area of primary mirror
	$A(a)$	area of aperture a
	a	aperture
A		generic constant
	$A_0(t_1, t_2)$	offset of linear regression in the reset interval correction
	$A_1(t_1, t_2)$	slope of linear regression in the reset interval correction
	A_0, A_1	first order correction on point source spectral response function
	A_0, A_1	first order signal corrections for PHT-S chopped observations
	$A_0(i)$, $A_1(i)$	coefficients for signal dependent PHT-S correction
	$a(SED)$	flux density conversion factor
	A_{chop}	empirical asymmetry factor for chopper offset
	$A_0, A_1, A_2, A_3, A_4, A_5$	coefficients for chopper offset correction
B		surface brightness
	$B(i, j)$	mean brightness
	B_{back}	background surface brightness
	$B_n(i, j)$	accumulated sum of first n sky measurements to mean brightness
B		generic constant
c_{light}		speed of light c= 299792500 $\mathrm{m\,s^{-1}}$ in OLP
c		generic constant
C		generic constant
	C_1, C_2	constants
$C()$		statistic
C_{int}		detector capacitance
	C_{int}^{det}	idem for detector *det*
$\mathrm{C1}^f$		constant for transmission of the whole optical path for a given filter assuming $\nu f_\nu = const$ as reference spectrum.The effective size of the primary mirror; reflection losses, filter transmission, spectral response of the detector, etc. are included
$C(i)$		spectral response function for pixel i
	$C_{avg}^{c,p}(i)$	average spectral response function for a point source
	$C^{c,p}(i)$	spectral response of pixel i for a point source p corrected for chopped c signal losses
	$C_{avg}^{c,s}(i)$	average spectral response function for PHT-S staring observations
	$C^{c,p}(i)$	spectral response function for pixel i corrected for chopped signal loss
	$C_{ave}^{c,p}(i)$	PHT-S averaged chopped spectral response function for a point source
	C_{int}^{det}	integration capacitance associated with detector P1, P2 or P3,
	$C_{phts,pixel}$	point source responsivity for PHT-S pixel
	$C_{phts,pixel}^{E}$	extended source responsivity for PHT-S pixel

d		height of source peak (background subtracted)
d_{airy}		diameter of Airy disk
D_A		diameter of aperture for PHT-P, side length of the array for PHT-C
Dec		declination
DI		selected offset data word (0...4095)
D_0		fixed voltage offset for CRE
e		exposure time
	e_n(i,j)	contribution from nth sky sample to exposure time
E		accumulated exposure time
	E_n(i,j)	sum of first n sky pointings
	E_{total}(i,j)	total exposure time of image
f		filter
f_ν		flux density
f_{PSF}^f		point spread function fraction for filter f entering the field aperture in case of PHT-P or falling onto the array in case of PHT-C
	f_{PSF}	intensity function of a point source entering the aperture
	$f_{PSF}(\lambda_c, aperture)$	fraction of the telescope point spread function falling into a given aperture for PHT-P or onto the full array for PHT-C
	$f_{psf}^{aperture}$	idem for a given aperture
	f_{psf}^{array}	idem for the entire detector array
	f_{psf}^{pixel}	idem for a given pixel
	$f_{psf}(\lambda_{ref})$	fraction of point spread function at the reference wavelength λ_{ref}
$f_{beam}(\lambda)$		wavelength dependent beam profile inside the aperture or pixel
f_{cov}		coverage factor
ff(i)		flat-field correction for pixel i
F		flux density in frequency units unless explicitly specified
	F_ν(i,k)	flux for pixel i at raster point k
	$F_{scr+back}$	source+background flux
	F_{on}	source+background flux
	F_{back}	background flux
	F_{off}	background flux
	F_{scr}	source flux with psf correction for point source
	F_λ(i)	flux density in wavelength units for pixel i
	$F(\lambda)$	flux density of source at specific wavelength λ
	F_ν^f	source flux density for an assumed spectral energy distribution $\nu f_\nu = const$ (flux density at reference wavelength)
	$F_\nu(\lambda_c)$	flux density at centre wavelength of filter
	$F_{\nu_{ref}}(SED)$	flux density for applied SED
	$F_{\nu_{ref}}(\nu^{-1})$	flux density quoted in AAR
	$F(\nu)$	flux density in frequency range
	$F(\lambda)$	flux density in wavelength range
	F_ν^f	source flux density for an assumed spectral energy distribution $\nu f_\nu = const$ at reference wavelength
$g(i, S(i,t), t)$		weighting function for correction ϕ
	$g(i, S, t)$	weight factors related to correction φ(i,S,t)
g_{fit}		goodness of fit
G		gain
	G_{off}	offset gain
	G_{signal}	signal gain
h		Planck constant
h		heating power of FCS
$H(S)$		linearisation correction for signal S
	$H^{f,i}(s)$	idem, for filter f, detector pixel i, and signal s
i		pixel index, integer counter
I		Surface brightness in wavelength units unless explicitly stated
	$I_\nu(\lambda_c)$	surface brightness based on monochromatic point source flux density
	I_ν^f	surface brightness of (extended) source in filter f, assuming $\nu F_\nu = const$
	I_λ(i)	surface brightness of a given detector array element i (of PHT-S)
IBP		in-band power in W
I_{step}		step flag, for chopper position within a chopper cycle

k		integer counter
	k	chopper cycle number
	k	raster point number in one direction
k		Boltzmann's constant
	k_f	colour correction
K		constant
K_{CC}(SED)		colour correction factors for applied SED
l		length or integer counter
	l	raster point number in one direction
L		length
	L_α	map size in RA
	L_δ	map size in Dec
	m_{pix}	mean pixel value used to convert into the correct units
	M	number of raster steps along a raster leg
	$m(u)$	median of s_{diff} per chopper unit
	M	number of columns of raster
n		integer counter
	n_α	minimum number of image pixels in RA to cover raster area
	n_δ	minimum number of image pixels in Dec to cover raster area
	n_d	index representing the dwell time in the calibration files
	n_{pix}	number of detector pixels
N		integer counter
	N_{it}	number of iterations for ramp deglitching
	N_{min}	minimum number of readouts per ramp
	N_σ	sigma value to identify outliers in ramp deglitching
	N_u	number of chopper units
	N_r	number of ramps per chopper plateau
	N_{read}	total number of readouts
	N'_r	actual number of ramps per chopper plateau in the telemetry, is derived from N'$_r$ = N$_r$/DAT_RED where N$_r$ is the commanded number of ramps per chopper plateau and DAT_RED is the applied data reduction factor
	N_{fg}	number of fine grid positions that fall within the detector footprint
	N_{total}	total number of fine grid positions that fall within a pixel
N_{cc}		cirrus confusion noise
N_{gc}		galaxy confusion noise
P		power in W
	$P^{f'}_{fcs}(h)$	in-band power for filter f' and FCS heating power h in mW as obtained from FCS power tables, for PHT-P in W mm^{-2}, for PHT-C in W/pixel
	P_{src}	source power
	P_C	power measured on pixel if line is centred
	P^1_C	power measured on adjacent pixel if line is centred
	P_M	power measured on pixel if line is centred between pixels
	P^f_{fcs}(h)	in-band power for filter f and FCS heating power h
	P^f_{cal}	in-band power of celestial calibrator
	$P^f_{scr}(a)$	in-band power for filter f in aperture a
	$P^f_{scr}(i)$	in-band power for filter f and pixel i
	P_{max}	maximum commandable power on FCS
	$P(s+b)$	in-band power of on-source position
	$P(b)$	in-band power of off-source position
	$P(s)$	in-band power of source only
	$P_{gauss}(s)$	peak (source) power value
	$P_{gauss}(b)$	background power value
	$P_{fcs}(f,h)$	in-band power on the detector from the FCS due to heating power h
	$P_{target}(f')$	in-band power obtained from the source
	$P_{fcs}(f,h)$	in-band power for given FCS heating power h
	P	constant
q		detection limit in multiples of σ
Q		quaternion
	Q_{raster}	quarternion that defines the position of the PHT central field of view for a given raster point in the J2000 inertial frame
	Q_{str}	defines the J2000 pointing of the ISO star tracker
	Q_r	defines the raster point relative to the raster centre of the scan

	$Q_{str/qss}$	describes misalignment between the star tracker and the quadrant star sensor (QSS)
	$Q_{qss/pht}$	describes the QSS to instrument aperture alignment
	Q_{cor}	gives the fine pointing correction to the star tracker calibration
	$Q1, Q2$	quarternions representing the rotations of the detector origin with respect to a given raster point, assuming perfect alignment between chopper and spacecraft y-axis
	Q_{chop}	chopper quaternion
Q		constant
R		responsivity
	R_c	average relative system response derived from a bandpass
	R_{det}	detector responsivity
	R_{det}(i)	detector responsivity of pixel i
	$R_{default}$	default detector responsivity
	$R(i)$	responsivity for each pixel of a C detector
	$R_{FCS}(i)$	responsivity of pixel i obtained from FCS
$R(\lambda)$		system response at specific wavelength
R_s		sensor resistance
	R	constant in resistance
	R_k	harness resistance
	R_p	EEU shunt resistor in parallel to sensor
$r(i)$		measured responsivity of pixel i relative to default responsivity
s		signal in V/s
	s_{src}	source signal
	$s(t)$	signal at time t
	$s(k)$	pairwise differences between V(k) and V(k+1)
	$s(j)$	slope for ramp j
	$s(RI, DAT\_RED)$	signal taken with reset interval RI and data reduction rate DAT_RED
	$s'(\phi(t))$	signal after orbital dependent dark correction
	$s(\phi(t))$	initial signal
	$s_{dark}(\phi$(t))	orbit dependent dark correction
	s_{old}	signal before signal linearisation
	s_{new}	signal after signal linearisation
	$s(k)$	signal
	$< s >$	average of valid signals per chopper plateau
	s_{diff}	difference signals of consecutive readouts
	$s(i)$	generic pattern
	s_{scr}	source signal determined via generic pattern
	s^c_{scr}	source signal determined via generic pattern, corrected for losses due to chopper modulation
	s_k(x)	source signal for chopper cycle k
	s_k(X)	given set of powers
	$< s_{fcs}(f) >$	weighted mean signal for FCS measurement
	$< s_{fcs}(i, f) >$	FCS signal per chopper plateau
s_{pixel}		image pixel size
	s	nominal uncertainty of fit
	s'	uncertainty of fit
S		signal
	S_{src}	linearised difference signal (from chopped measurement)
	S'_{src}	linearised difference signal, corrected for losses due to chopper modulations
	S_{on}, S_{off}	on- and off-source signals
	$S(i, k)$	signal for pixel i at raster point k
	S^f_{cal}	measured signal of calibrator
	S^f_{str}	measured dark FCS signal (stray light)
	$S^{f'}_{fcs}$	signal of FCS measurement in filter f'
	$S_{scr}(a)$	linearised source signal (PHT-P) after dark signal subtraction
	$S_{scr}(i)$	linearised source signal (PHT-C) after dark signal subtraction
	$S(i, t)$	signal transient of pixel i at time t
	S^{det}_{dark}	orbit dependent dark signals
S		size
	$S_{finegrid}$	side length of (square) fine grid image pixel
	S_{pixel}	side length of square detector pixel
t		time in s

	t_{mid}	time at midpoint of a given ramp
	t_0	time at first readout of a given ramp
	t_{dwell}	chopper dwell time
	t_m	measurement time
	t_r	reset interval time
	t_{plat}	chopper plateau time
	t_n	dwell time
T		temperature in K
	T	EEU temperature
T_{refl}		reflection losses on optical elements
tmd		telemetry data value
	tmd_{max}	maximum value of telemetry word (=4096)
	TOL	voltage for chopper deflection calibration
	RA	right ascension
u		chopper unit
u		uncertainty
	u_n(i,j)	mean brightness uncertainty contribution from nth sky sample
U		voltage in V
	U_{ACF_1}	voltage for chopper deflection calibration
	U_{DCF_1}	voltage for chopper deflection calibration
	U_{OF_1}	voltage for chopper deflection calibration
	U_{OF_2}	voltage for chopper deflection calibration
	U_{CRE}	CRE output voltage
	U_{off}	$GAIN_1$ dependent offset voltage
U		uncertainty
	U_n(i,j)	accumulated mean brightness uncertainty
	U_{rms}(i,j)	brightness uncertainty from rms
V		voltage in V
	$V(k)$	voltage corresponding to readout k
	V_{ini}	voltage
w		weight
	$w(i,t)$	weight function for PHT-S chopped measurements
	w_j	statistical weight of each signal obtained from its associated statistical uncertainty
x		distance or coordinate
	x_m	margin around raster in m direction
	x_n	margin around raster in n direction
	x_0	angular x coordinate of the image pixel origin
X^{raw}_{FPC}		data word for focal plane chopper position
y		distance or coordinate
	y_{det}	chopper deflection
	y_0	angular y coordinate of the image pixel origin
z		distance or coordinate
	z_{det}	spacecraft z-offset

F.2 Greek Symbols

Symbol		Explanation
α		angle, right ascension
	α	chopper angle
	α	x-axis offset of the peak from the centre of the array
	α_c	right ascension for raster centre
	$\alpha_{m,n}$	right ascension of raster point (m,n)
	α_{amp}	chopper amplitude
	α_{approx}	approximation to chopper angle
	α_{linear}	first approximation to chopper angle from linear model,
	α_{sky}	approximation to chopper angle
α		probability that null hypothesis is rejected
α(f,a)		correction for inhomogeneous illumination in aperture a by FCS
	α^f(a)	inhomogeneous FCS illumination for PHT-P
β		y-axis offset of the peak from the centre of the array
β		power of the dust emissivity
Γ(i,f)		FCS illumination matrix
	Γ^f(i)	idem
δ		declination
	δ_c	declination of raster centre
	$\delta_{m,n}$	declination of raster point (m,n)
δ		degrees of freedom
Δ		Increment, difference, or uncertainty
	Δl	physical pixel size in Z-direction
	ΔM, ΔN	raster step size in M and N
	Δx	physical distance between pixels
	$\Delta\lambda$	width of filter bandpass
	$\Delta\lambda_{pix}$	PHT-S pixel width in wavelength
ϵ		central obscuration factor by the secondary mirror
ζ(S)		signal correction function for losses due to chopper modulation
	$\zeta(s_{scr}, det, t_{dwell})$	idem
	$\zeta(S_{src}, det, t_{dwell})$	idem
ι		number of interpolations,
θ_{chop}		maximum chopper deflection while mapping (PHT32 only)
κ		threshold
	κ_1, κ_2	first and second threshold in deglitch method
λ		wavelength
	λ_c	central wavelength of filter bandpass
	λ_{ref}	reference wavelength of filter bandpass
	$\lambda(i)$	centre wavelength of a pixel
σ		uncertainty or rms
	$\sigma(P)$	uncertainty of detector in-band power in the selected filter band
	σ_{FWHM}	uncertainty of FWHM
Φ		rotation angle
	Φ_{raster}	raster rotation angle (ATTRROTA)
	Φ	spacecraft roll angle
φ(i,s(i,t),t)		transfer function converting PHT-S signals s(i,t) to flux densities
ϕ(t)		orbital phase
χ(i,f)		relative filter-to-filter responsivity correction for detector pixel i
	χ^f(i)	idem
	χ(f)	idem for a given P detector
χ^2		goodness of fit
Ω		solid angle
	Ω^f_{eff}	effective solid angle for filter f,

Appendix G

Glossary

auto analysis results	(AAR) are the products from the auto-analysis processing
chopper	Movable mirror positioned in the beam to enable differential sky measurements or to deflect the beam to one of the FCSs
chopper dwell time	The commanded time for a given position of the chopper.
chopper plateau	The period during a fixed position of a chopper. In the case of a staring measurement the chopper plateau is equal to the whole measurement period.
data reduction	The ISO telemetry fully supported only a maximum readout rate, higher readout rates were achieved by transmitting parts of the data flow. The ratio between the amount of data read and the amount transmitted is called data reduction.
default aperture	(Also standard aperture) the ISOPHOT photometric calibration against celestial standards of a given PHT-P filter is only performed in one selected aperture, the default or standard aperture.
default responsivity	A mean detector responsivity value which is a function of orbital phase. The default responsivity is used in case the FCS calibration of an observation cannot be used.
destructive readout	Last readout of an integration ramp.
generic pattern	A sequence of 8 signals (4 off- and 4 on-source signals) representing the repeated signal pattern of the chopper cycles in a chopped measurement.
glitch	A *glitch* is a short duration anomaly in the data stream, usually caused by an ionising particle.
illumination matrix	A table which lists the relative illumination of an FCS to the individual detector pixels of the PHT-C arrays.
in-band power	The power (in W) falling on the detector for a filter, aperture, and polariser combination
integration time	The period a detector sees a specific position on the sky during a measurement.
measurement	See definition Section 2.5
meaurement time	The period of a measurement
non-destructive readout	Any CRE voltage sample along an integration ramp except for the last one.
performance verification	The *performance verification* (PV) phase comprises the first 80 days of the ISO mission and was exclusively

	reserved for instruments check-out, calibrations, and AOT commissioning.
product	(Or *FITS product*) is a FITS file with defined contents and contains ISO data for official distribution.
observation	An *observation* refers to the acquisition of the scientifically useful data during one AOT by the prime instrument requested by the proposer. The term 'observation' also loosely refers to the data products created from the acquired data.
ramp	A *ramp* is formed by the readouts collected during one and the same reset interval
raster	Regular and rectangular grid of pointings on the sky where the distance between the pointings is the same in each of the grid directions.
raster point	A pointing in a raster.
raster point dwell time	The commanded time the spacecraft spent while pointing on a given raster point.
reset interval	The time between two reset pulses while reading out the detector, also referred to as fundamental integration time.
responsivity	The detector *responsivity* (in A/W) is the ratio between electrical current (in [A]) through a detector and the illuminating power (in [W]) falling on the detector.
signal	The rate of voltage increase of the CRE output, this is in general equivalent to the slope of an integration ramp in V/s. The signal is proportional to the photocurrent or power on the detector.
sparse map	A map obtained with the sparse map AOTs.
standard aperture	See default aperture
standard processed data	(SPD) are products from the standard processing or Derive_SPD step, Chapter 7
straylight	Unwanted light from sources outside the central field of view contributing to the detector signal.
target dedicated time	A *target dedicated time* (TDT) is the entire contiguous time period scheduled for performing the N observations of a concatenated group. (N = 1 if no concatenation). All overheads, including slewing, are included (TDT = observation time plus overheads time). The start of a TDT is defined as the time of the first AOCS command to point at the new target. The end of the TDT is defined as the time at which all instrument activities connected with the (N) observation(s) have been completed. Note that the above restrictions on concatenation imply that one TDT can belong to only one proposer.
telemetry	Data send by the spacecraft to the ground station
transient	A systematic variation of the detector output signal in time after an illumination change.

Bibliography

[1] Ábrahám P., Acosta-Pulido J.A., Klaas U. et al. 1997, *ISOPHOT-S measurements of the zodiacal light: a calibration tool*, in 'First ISO workshop on analytical spectroscopy', Eds. A.M. Heras, K. Leech, N.R. Trams & M. Perry, ESA SP-419, 119

[2] Ábrahám P., Leinert C., Acosta-Pulido J.A., Schmidtobreick L. & Lemke D. 1998, *Zodiacal light observations with ISOPHOT*, in 'The Universe as Seen by ISO', Eds. P. Cox & M.F. Kessler, ESA SP-427, 145

[3] Acosta-Pulido J.A., Gabriel C., Catañeda H. 2000, *Transient effects in ISOPHOT data: status of modelling and correction procedures*, ExA 10, 333

[4] Blommaert J.A.D.L, Boulanger F. & Okumura K. 2001, *ISOCAM CVF photometry report*, IDC Report, SAI/2001-034/Rp

[5] Castañeda H. & Klaas U. 2000, *Recognition of space weather impact on the ISOPHOT detectors*, ExA 10, 369

[6] Cohen M., Walker R.G., Barlow M.J. & Deakon J.R. 1992, *Spectral irradiance calibration in the infrared. I. Ground-based and IRAS broadband calibrations*, AJ 104, 1650

[7] Cohen M., Witteborn F.C., Walker R.G., Bregman J.D. & Wooden D.H. 1995, *Spectral irradiance calibration in the infrared. IV. 1.2-35 μm spectra of six standard stars*, AJ 110, 275

[8] Gabriel C. & Acosta-Pulido J. 2000, *Deglitching methods by the ISOPHOT interactive analysis procedures*, ExA 10, 319

[9] Gabriel C. 2000, *PHT Interactive Users Manual* Version 9.0, 27 June 2000 (see ISOPHOT documentation under: `http://www.iso.vilspa.esa.es`)

[10] Gautier T.N., Boulanger F., Pérault M. & Puget J.-L. 1992, *A calculation of confusion noise due to infrared cirrus*, AJ 103, 1313

[11] Griffin M. & Orton G. 1993, *The near-Millimiter brightness temperature spectra of Uranus and Neptune*, Icarus 105, 537.

[12] Gry C., Swinyard B., Harwood A. et al. 2002, *The ISO Handbook: Volume III, LWS – The Long Wavelength Spectrometer*, ESA SP-1262, SAI-99-077/Dc, Version 2.0

[13] Guest S. 1993, *Deglitching of ISOPHOT data*, ISOPHOT internal report, 13 July 1993 (see ISOPHOT documentation at `http://www.iso.vilspa.esa.es`)

[14] Hammersley P.L., Jourdain de Muizon M., Kessler M.F. et al. 1998, *Infrared standards for ISO. I. A new calibration of mid infrared photometry*, A&AS 128, 207

[15] Hartung J. 1991, *Statistik - Lehr und Handbuch der angewandten Statistik*, R. Oldenburg Verlag

[16] Heinrichsen I., Walker H.J. & Klaas U. 1998, *Infrared mapping of the dust disc around Vega*, MNRAS 293, L78

[17] Helou G. & Beichman C.A. 1990, *The confusion limits to the sensitivity of submillimeter telescopes*, in 'From ground-based to space borne sub-mm astronomy', ESA SP-314, 117

[18] Herbstmeier U., Ábrahám P., Lemke D. et al. 1998, *Small-scale structures in the far-infrared background*, A&A 332, 793

[19] Jourdain de Muizon M. & Habing H. 1992, *The ISO Groundbased Preparatory Programme Working Group ISO-GBPPWG*, in 'Infrared Astronomy with ISO', Eds. Th. Encrenaz & M.F. Kessler, 129

[20] Kessler M.F., Müller T.G., Leech K. et al. 2002, *The ISO Handbook: Volume I, ISO – Mission & Satellite Overview*, ESA SP-1262, SAI-2000-035/Dc, Version 2.0

[21] Klaas U., Krüger H., Heinrichsen I., Heske A. & Laureijs R.J. (Eds.) 1994, *ISOPHOT Observer's Manual*, Version 3.1.1, 9 May 1994 (see ISOPHOT documentation under: `http://www.iso.vilspa.esa.es`)

[22] Klaas U., Ábrahám P., Haas M., Herbstmeier U. & Laureijs R.J. 1997, *General ISOPHOT observing strategies for faint sources*, Version 1.3, SAI/97-013/Wb, 28 Feb 1997

[23] Klaas U., Acosta-Pulido J.A., Ábrahám P. et al. 1997, *ISOPHOT-S: Capabilities and calibration*, in 'Proceedings of the first ISO workshop on Analytical Spectroscopy', Eds: A.M. Heras, K. Leech, N.R. Trams & M. Perry, ESA SP-419, 113

[24] Klaas U., Lemke D., Kranz T. et al. 1998, *Infrared straylight measurements of the ISO telescope*, in 'Infrared astronomical instrumentation', Proc. SPIE 3354, 996.

[25] Klaas U., Laureijs R.J., Müller T.G., Kreysa E. & Krätschmer W. 1999, *Data reduction, calibration and performance of the ISOPHOT polarization modes*, in 'Workshop on ISO polarisation observations', Eds. R.J. Laureijs & R. Siebenmorgen, ESA SP-435, 19

[26] Klaas U., Ábráham P., Laureijs R.J., Radovich M., Schulz B. & Wilke K. 2002, *ISOPHOT calibration accuracies*, IDC Report SAI/98-092/Dc, Version 5.0, May 2002

[27] Klaas U. & Richards P.J., with contributions by: Wilke K., Kiss C., Ábráham P. and Radovich M. 2002, *Report on the scientific validation of PHT OLP Version 10.0*, Version 1.0 issued 9 April 2002 (see PHT documentation under `http://www.iso.vilspa.esa.es`)

[28] Klaas U., Laureijs R.J., Schulz B. et al. 2001, *ISOPHOT calibration strategy*, in 'The Calibration Legacy of the ISO Mission', Eds. L. Metcalfe & M.F. Kessler, ESA SP-481 (in press)

[29] Kranz T. 1998, *Messung des Streulichts von Sonne, Mond und Erde im ISO Weltraumteleskop*, Diplomarbeit (Ruprecht-Karls-Universität Heidelberg)

[30] Lagache G. & Puget J.-L. 2000, *Detection of the extra-Galactic background fluctuations at 170 μm*, A&A 355, 17

[31] Laureijs R.J. & Klaas U. 1999, *ISOPHOT error budgets*, IDC Report SAI/98-091/Dc, Version 1.0, 21 April 1999

[32] Laureijs R.J. 1999, *Point spread function fractions related to the ISOPHOT C100 and C200 arrays*, IDC Report, Version 1.0, 29 June 1999 (see ISOPHOT documentation under: `http://www.iso.vilspa.esa.es`)

[33] Laureijs R.J. & Klaas U. 1999, *Processing steps and signal analysis of ISOPHOT polarisation observations at 170 μm*, in 'Workshop on ISO polarisation observations', Eds. R.J. Laureijs & R. Siebenmorgen, ESA SP-435, 27

[34] Leech K., Kester D., Shipman R., et al. *The ISO Handbook: Volume V, SWS – The Short Wavelength Spectrometer* ESA SP-1262, SAI/2000-008/Dc, Version 2.0

[35] Lemke D., Lützow-Wentzky P., Fricke W. & Bollinger W. 1993, *Cryogenic aspects of ISOPHOT, the photometer for the ISO satellite*, Cryogenics 33, 395

[36] Lemke D., Garzón F., Grözinger U. et al. 1994, *Far-infrared imaging, polarimetry, and spectrophotometry on the Infrared Space Observatory*, Optical Engineering 33, 20

[37] Lemke D., Klaas U., Abolins J. et al. 1996, *ISOPHOT - capabilities and performance*, A&A 315, L64

[38] Lemke D., Kranz Th., Klaas U. et al. 2001, *Straylight in ISOPHOT?*, in 'The Calibration Legacy of the ISO Mission', Eds. L. Metcalfe & M.F. Kessler, ESA SP-481 (in press)

[39] Moneti A., Metcalfe L. & Schulz B. 1997, *Reference wavelengths for ISO: CAM and PHOT filters*, IDC Report SAI/97-002/Dc, 17 Jan 1997

[40] Müller T. & Lagerros J. 1998, *Asteroids as far-infrared photometric standards for ISOPHOT*, A&A 338, 340

[41] Müller T. 2000a, *ISOPHOT aperture profiles and background measurements*, in 'ISO Beyond Point Sources: Studies of Extended Infrared Emission', Eds. R.J. Laureijs, K. Leech & M.F. Kessler, ESA SP-455, 33

[42] Müller T. 2000b, *ISOPHOT aperture sequences on point- and extended sources*, in 'ISO Beyond Point Sources: Studies of Extended Infrared Emission', Eds. R.J. Laureijs, K. Leech, M.F. Kessler, ESA SP-455, 41

[43] Müller T. & Lagerros J. 2002, *Asteroids as calibration standards in the thermal infrared for space observatories*, A&A 381, 324.

[44] Okumura K. 2000, *The ISO point spread function and CAM beam profiles*, in 'ISO Beyond Point Sources: Studies of Extended Infrared Emission', Eds. R.J. Laureijs, K. Leech & M.F. Kessler, ESA SP-455, 47

[45] Oliver S.J. 2001, *FIRST extragalactic surveys: practical considerations*, in 'The Promise of the Herschel Space Observatory', Eds. G. Pilbratt et al., ESA SP-460, 105

[46] Richards P.J., Klaas U., Laureijs R.J. et al. 2001, *The ISOPHOT pipeline data processing*, in 'The Calibration Legacy of the ISO Mission', Eds. L. Metcalfe & M.F. Kessler, ESA SP-481 (in press)

[47] Salama A., Beintema D., Lloyd C. et al. 2001, *Beam Profiles and Pointing Working Group Final Report*, IDC report, SAI/2001-027/Dc

[48] Schlötelburg M. 1992, *Polarimetry with ISOPHOT*, ISOPHOT Internal Report, MPIA Heidelberg

[49] Schubert J., Fouks B.I., Lemke D. & Wolf J. 1995, *Transient response of ISOPHOT Si:Ga infrared photodetectors: experimental results and application of the theory of non-stationary processes*, in 'Infrared Spaceborne Remote Sensing III', Proc. SPIE 2553, 42

[50] Schulz B. 1993, *Bodencalibration des Infrarotmeters im Satellitenexperiment ISOPHOT*, Dissertation (Ruprecht-Karls-Universität Heidelberg)

[51] Schulz B. 1999, *Linearisation of ISOPHOT-P and C detector signals in OLP8*, IDC report, Version 1.0, 29 September 1999 (see ISOPHOT documentation under: `http://www.iso.vilspa.esa.es`)

[52] Schulz B. 1999, *Long term responsivity stability of ISOPHOT-S*, IDC report, Version 1.0, 28 May 1999 (see ISOPHOT documentation under: `http://www.iso.vilspa.esa.es`)

[53] Schulz B., Huth S., Laureijs R.J. et al. 2002, *ISOPHOT - Photometric Calibration of point sources*, A&A 381, 1110

[54] van der Bliek N.S., Bouchet P., Habing H.J. et al. 1992, *Standard stars for the Infrared Space Observatory ISO*, The Messenger 70, 28

[55] Walker R.G. & Cohen M. 1992, *An Atlas of selected calibrated stellar spectra*, NASA Contractor's Report CR-177604

[56] Wilke K. 1995, *Untersuchung von Detektordriften des C200-Detectors im Satellitenexperiment ISOPHOT und deren Kalibration*, Diplomarbeit (Ruprecht-Karls-Universität, Heidelberg)

[57] Wolf J. 1994, *Low background far-infrared detectors and arrays*, Optical Engineering 33, 1492

[58] Wolf J., Grözinger U. & Lemke D. 1995, *Cryogenic readout electronics for the Infrared Space Observatory ISO*, in 'Third Symposium on Low Temperature Electronics and High Temperature Superconductivity', Eds. C. Claeys, S. Raider, R. Kirschman & W. Brown, 95-9, 355. The Electrochemical Society, Inc., Pennington, NJ

Index